TECHNICAL REPORTS SERIES NO. 423

Radiotracer Applications in Industry – A Guidebook

IAEA
International Atomic Energy Agency

RADIOTRACER APPLICATIONS IN INDUSTRY — A GUIDEBOOK

The following States are Members of the International Atomic Energy Agency:

AFGHANISTAN
ALBANIA
ALGERIA
ANGOLA
ARGENTINA
ARMENIA
AUSTRALIA
AUSTRIA
AZERBAIJAN
BANGLADESH
BELARUS
BELGIUM
BENIN
BOLIVIA
BOSNIA AND HERZEGOVINA
BOTSWANA
BRAZIL
BULGARIA
BURKINA FASO
CAMEROON
CANADA
CENTRAL AFRICAN REPUBLIC
CHILE
CHINA
COLOMBIA
COSTA RICA
CÔTE D'IVOIRE
CROATIA
CUBA
CYPRUS
CZECH REPUBLIC
DEMOCRATIC REPUBLIC OF THE CONGO
DENMARK
DOMINICAN REPUBLIC
ECUADOR
EGYPT
EL SALVADOR
ERITREA
ESTONIA
ETHIOPIA
FINLAND
FRANCE
GABON
GEORGIA
GERMANY
GHANA
GREECE
GUATEMALA
HAITI
HOLY SEE
HONDURAS
HUNGARY
ICELAND
INDIA
INDONESIA
IRAN, ISLAMIC REPUBLIC OF
IRAQ
IRELAND
ISRAEL
ITALY
JAMAICA
JAPAN
JORDAN
KAZAKHSTAN
KENYA
KOREA, REPUBLIC OF
KUWAIT
KYRGYZSTAN
LATVIA
LEBANON
LIBERIA
LIBYAN ARAB JAMAHIRIYA
LIECHTENSTEIN
LITHUANIA
LUXEMBOURG
MADAGASCAR
MALAYSIA
MALI
MALTA
MARSHALL ISLANDS
MAURITIUS
MEXICO
MONACO
MONGOLIA
MOROCCO
MYANMAR
NAMIBIA
NETHERLANDS
NEW ZEALAND
NICARAGUA
NIGER
NIGERIA
NORWAY
PAKISTAN
PANAMA
PARAGUAY
PERU
PHILIPPINES
POLAND
PORTUGAL
QATAR
REPUBLIC OF MOLDOVA
ROMANIA
RUSSIAN FEDERATION
SAUDI ARABIA
SENEGAL
SERBIA AND MONTENEGRO
SEYCHELLES
SIERRA LEONE
SINGAPORE
SLOVAKIA
SLOVENIA
SOUTH AFRICA
SPAIN
SRI LANKA
SUDAN
SWEDEN
SWITZERLAND
SYRIAN ARAB REPUBLIC
TAJIKISTAN
THAILAND
THE FORMER YUGOSLAV REPUBLIC OF MACEDONIA
TUNISIA
TURKEY
UGANDA
UKRAINE
UNITED ARAB EMIRATES
UNITED KINGDOM OF GREAT BRITAIN AND NORTHERN IRELAND
UNITED REPUBLIC OF TANZANIA
UNITED STATES OF AMERICA
URUGUAY
UZBEKISTAN
VENEZUELA
VIETNAM
YEMEN
ZAMBIA
ZIMBABWE

The Agency's Statute was approved on 23 October 1956 by the Conference on the Statute of the IAEA held at United Nations Headquarters, New York; it entered into force on 29 July 1957. The Headquarters of the Agency are situated in Vienna. Its principal objective is "to accelerate and enlarge the contribution of atomic energy to peace, health and prosperity throughout the world".

© IAEA, 2004

Permission to reproduce or translate the information contained in this publication may be obtained by writing to the International Atomic Energy Agency, Wagramer Strasse 5, P.O. Box 100, A-1400 Vienna, Austria.

Printed by the IAEA in Austria
June 2004
STI/DOC/010/423

SAFETY REPORTS SERIES No. 423

RADIOTRACER APPLICATIONS IN INDUSTRY – A GUIDEBOOK

INTERNATIONAL ATOMIC ENERGY AGENCY
VIENNA, 2004

IAEA Library Cataloguing in Publication Data

Radiotracer applications in industry : a guidebook. — Vienna : International Atomic Energy Agency, 2004.
p. ; 24 cm. — (Technical reports series, ISSN 0074–1914 ; no. 423)
STI/DOC/010/423
ISBN 92–0–114503–9
Includes bibliographical references.

1. Radioactive tracers. I. International Atomic Energy Agency. II. Technical reports series (International Atomic Energy Agency) ; 423.

IAEAL 04–00364

FOREWORD

Radioactive tracers were first applied to industrial problem solving around the middle of the last century. Since then their use has increased steadily so that, at the time of writing, radiotracer techniques are used extensively throughout the world for troubleshooting and process optimization in industry.

The economic benefits that may be derived from the use of this technology are great, a fact that is recognized by the governments of developing countries. Among the Member States of the International Atomic Energy Agency (IAEA), nearly fifty developing countries have radiotracer applications groups.

The IAEA plays a major role in facilitating the transfer of the technology, and an important part of this process is the provision of relevant literature that may be used for reference purposes or as an aid to teaching. In this respect, over the past decade, the IAEA has distributed widely throughout the developing world the Guidebook on Radioisotope Tracers in Industry, Technical Reports Series No. 316 (1990). This guidebook is still in common use for reference and as a teaching aid, since much of the information it contains has retained its value and relevance. However, in the fifteen years or so since that guidebook was conceived, many important technological developments have taken place, resulting in a perceived need at present for a modern guidebook that covers both the theoretical and the practical aspects of the industrial applications of radiotracers.

This new guidebook aims to fill the gap by providing not only an extensive description of what can be achieved by the application of radiotracer techniques but also sound, experience based, guidance on all aspects of the design, implementation and interpretation of the results of industrial applications. It describes the principles and the state of the art of radiotracer methodology and technology as applied to oil and geothermal reservoirs and industrial processing.

This guidebook has been prepared with contributions from outstanding specialists from around the world. Also included are the major achievements of the IAEA Co-ordinated Research Project (CRP) on Radiotracer Technology for Engineering Unit Operation Studies and Unit Process Optimization, and the CRP on Integration of Residence Time Distribution (RTD) Tracing with Computational Fluid Dynamics (CFD) Simulation for Industrial Process Visualization and Optimization. Novel developments in radiotracer methodology and technology are reflected as well. The guidebook covers for the first time the methodology of radiotracers for all kinds of industrial applications.

Although written primarily for the radioisotope practitioner, this new guidebook is also intended to promote the benefits of the technology to governments, the general public and industrial end users.

The IAEA wishes to thank the CRP participants and all the contributors for their co-operation. The IAEA officers responsible for this publication were J. Thereska and Z. Pang of the Division of Physical and Chemical Sciences.

EDITORIAL NOTE

Although great care has been taken to maintain the accuracy of information contained in this publication, neither the IAEA nor its Member States assume any responsibility for consequences which may arise from its use.

The use of particular designations of countries or territories does not imply any judgement by the publisher, the IAEA, as to the legal status of such countries or territories, of their authorities and institutions or of the delimitation of their boundaries.

The mention of names of specific companies or products (whether or not indicated as registered) does not imply any intention to infringe proprietary rights, nor should it be construed as an endorsement or recommendation on the part of the IAEA.

CONTENTS

1. INTRODUCTION

The objective of this guidebook is to provide the radiotracer practitioner with practical, experience based information about all the facets of an investigation: design, planning, implementation, data treatment and interpretation of results. It is aimed at clearly identifying the questions that need to be asked at each stage of the investigation and, as comprehensively as possible, to either provide the answers to those questions or identify appropriate works of reference. The primary focus is on the methodology of radiotracing. If the methodology is fully understood it becomes possible, conceptually, to design an experiment fully from beginning to end, taking into account both the desired objectives and the practical limitations imposed by the system being studied.

Radiation protection, a subject that is of paramount importance in using radioactive materials, is not given detailed consideration in this report. The rationale is that the radioisotope practitioner, to whom the book is directed, will already be well versed in this subject. However, for the sake of completeness, a review of radiation safety considerations is provided immediately after this introduction.

After a brief discussion of the scientific and technological background, different aspects of the methodology are discussed:

(a) Tracer selection and optimization;
(b) Methods of tracer injection;
(c) Detection and measurement of radiation;
(d) Data treatment and filtering, including identification of available software;
(e) Data analysis, interpretation and modelling.

An early consideration in designing an investigation is selection of the tracer. The criteria of critical importance are that (1) the tracer must be compatible with the stream to be traced and (2) its behaviour must be representative of that stream. The first decision to make is whether to use a radioactive tracer or some alternative type. Generally, if the objectives of the investigation can be achieved using a non-radioactive tracer and without incurring disproportionate costs, then that tracer should be used. However, as will become apparent from the case studies presented, there are many problems that can be investigated only by using a radiotracer. In these cases it is necessary to choose a tracer based on the following selection criteria:

— Type of radiation emitted: alpha particle, beta particle or gamma ray.

— Half-life of the radionuclide.
— Energy of the emitted radiation.
— Optimization of the activity injected.

The methodology reviewed considers the most commonly used radioisotopes for tracing solid materials, aqueous solutions, organic liquids and gaseous phases. The main emphasis is on the practical aspects of the technology. Various types of injection system are described and examples of devices used for liquid, solid and gaseous tracers are given. The special design features of injectors that must operate under difficult conditions, for example at high pressure or in flammable atmospheres, are presented.

Radiation detection and measurement are then discussed, with particular emphasis on how the collected data are influenced by factors such as experimental design, type and energy of radiation, type of detector and its collimator.

The treatment of raw experimental data is presented in detail. Various steps towards obtaining the residence time distribution (RTD) are described and illustrated by examples. A selection of available software is indicated.

Data analysis and modelling are considered after a specific section dedicated to the convolution/deconvolution procedure. Examples of applications are presented, from the simplest treatment (determination of time characteristics) to more complex model adjustments (peak decomposition, networks of elementary flow models — so-called systemic analysis). Flow models are only briefly described since abundant literature is available on the subject. Links between tracer data, systemic analysis and computational fluid dynamics (CFD) are then explored.

The examples presented are given emphasis, since the main objective of this guidebook is a practical one. Four field studies have been selected and fully detailed, as being illustrative of radiotracer methodology:

(1) Dispersion in a packed column. This very generic application is analysed in detail, including the design of the experiment, data acquisition, data modelling by adjustment with a simple flow model and a discussion of the reliability of measured parameters.
(2) Room air ventilation characterization. Radioisotopes are not normally used for this kind of application since in most cases alternative tracers do exist (helium or SF_6). This case is, however, a very didactic example of the methodology, involving RTD, local RTD, system analysis and CFD calculations. This approach can be extended to many industrial situations.
(3) Tracer experiments in a wastewater treatment plant (WWTP). The efficiency of several devices in a WWTP (primary and secondary clarifiers, aeration tank) is investigated by means of radiotracers.

Modelling allows characterization of the flow patterns (bypassing, stagnant zones) in these devices.

(4) Radioactive tracers in oil and geothermal fields. This section describes tracer preparation, injection, sampling and measurement, as well as several case applications for interwell communications and flow parameter determination.

2. RADIATION SAFETY CONSIDERATIONS

Radiotracers emit ionizing radiations, which are potentially hazardous to health so that radiation protection measures are necessary throughout all aspects of operations.

The relevant radiation safety standards are the International Basic Safety Standards for Protection against Ionizing Radiation and for the Safety of Radiation Sources (the BSS) [1], which were jointly sponsored by the Food and Agriculture Organization of the United Nations, the IAEA, the International Labour Organisation, the OECD Nuclear Energy Agency, the Pan American Health Organization and the World Health Organization. These standards are based on the work of the United Nations Scientific Committee on the Effects of Atomic Radiation (UNSCEAR) and the recommendations of the International Commission on Radiological Protection. Their aim is to enable the safe and secure use of radiation sources without unduly limiting the benefits or incurring disproportionate costs in interventions.

Operations with radiation sources constitute practices, and the requirements for such practices are set out in a Safety Fundamentals publication [2] and the BSS [1]. These publications are supported by a number of Safety Guides, such as that on occupational exposure [3], and Safety Reports, such as that on training [4], which give more specific advice on practices. Many IAEA Member States have incorporated these international standards into national legislation, regulations and codes of practice, which users should follow rigorously.

The key radiation protection principles are:

(a) A practice shall be justified on the grounds that it produces sufficient benefits to the exposed individual(s) and to society to offset the radiation detriment that it may cause.

(b) For justified practices, other than those involving medical exposures, restrictions on the dose that an individual may incur (dose limits) shall be

imposed to ensure that no person be subject to an unacceptable risk attributable to radiation exposure. Dose limits for both public and occupational exposure are set out in the BSS [1].

(c) For exposures from any source, except for therapeutic medical exposure, the doses, the number of people exposed and the likelihood of incurring exposures shall all be kept as low as reasonably achievable.

2.1. NATIONAL REGULATIONS AND AUTHORIZATION OF PRACTICES

An effective national infrastructure is a fundamental requirement for safety and security of sources. Principle 10 in Ref. [2] states that: *"The government shall establish a legal framework for the regulation of practices and interventions, with a clear allocation of responsibilities, including those of a Regulatory Authority."*

The preamble to the BSS defines the elements of a national infrastructure to be: legislation and regulations; a regulatory authority empowered to authorize and inspect regulated activities and to enforce the legislation and regulations; sufficient resources and an adequate number of trained personnel. The regulatory authority must also be independent of the registrants, licensees and the designers and constructors of the radiation sources used in practices. Further information on the legal and governmental infrastructure can be found in an IAEA Safety Requirements publication [5].

Hence users of radiotracers, unless the activity is below the exemption level for that radiotracer, should have an authorization from the appropriate regulatory authority. Exemption levels are defined in the BSS.

The BSS in para. 2.13(c) of Ref. [5] requires that "any legal person applying for an authorization shall make an assessment of the nature, magnitude and likelihood of the exposures attributed to the source and take all necessary steps for the protection and safety of both workers and the public"; and para. 2.13(d) requires of any person legally applying for an authorization that "if the potential for an exposure is greater than any level specified by the Regulatory Authority, have a safety assessment made and submitted to the Regulatory Authority as part of the application."

The user should, therefore, provide all relevant information to the Regulatory Authority, including details of the proposed practice, the safety assessment (considering both potential occupational and public exposures) and information on the training and any necessary qualification of personnel using the tracers.

A useful IAEA publication for preparing safety assessments for radiation sources is IAEA-TECDOC-1113 [6]. This book provides practice specific checklists with items to be considered during the performance of safety assessments that will be included in authorization applications and during the performance of inspections by the regulatory authority.

Safety assessments should be made for each application of the tracer having an activity above the exemption level, since circumstances and the application environment will differ. Each application should consider both occupational and public exposures and ensure that all exposures are as low as reasonably achievable. The level of the assessment should be commensurate with the hazard posed by the source. Hence detailed assessments should not be required where the risk is small, as is the case with many tracer experiments.

The BSS require that all sources be kept secure to avoid theft or damage or unauthorized use. This involves ensuring that sources are not relinquished without compliance with the authorization, not transferred unless the receiver holds a valid authorization, and a periodic inventory be conducted of their locations to ensure they are secure.

Sources should be transported in conformance with the transport regulations [7].

2.2. OCCUPATIONAL AND PUBLIC PROTECTION

A radiation protection programme should be established that addresses each stage of the process, for both exposure and contamination control, and optimizes the protection of the workers and the public (Ref. [1], para. I.4). This radiation protection programme should also consider employees of any third party organization. Optimization of protection begins at the design stage, where there is greatest flexibility to introduce changes, and continues into the operational phase, with the capability to respond to unexpected situations.

Users should consider classifying areas whenever there is occupational exposure to radiation. The classifications should be based on the prior safety assessment. Controlled areas should be foreseen where specific protective measures or safety provisions are, or could be, required, while supervised areas should be planned for where exposures need to be kept under review. Local rules, describing the processes to be followed in controlled areas, should be developed and written down prior to the application. The Radiation Protection Officer should take part in the planning of activities involving significant exposures and advise on the conditions under which work can be undertaken in controlled areas. These conditions should specify the type and nature of the protective equipment that may be needed.

Monitoring of exposures should be part of the radiation protection programme. The BSS require those who are occupationally exposed to have their doses assessed — if they work in controlled areas, then the assessment should be by individual monitoring; if in a supervised area, then either individual monitoring or monitoring of the workplace is acceptable. Workplace monitoring may also be required in controlled areas to evaluate the radiological conditions, enable exposure assessment and facilitate review of controlled or supervised areas.

The procedures for monitoring workers, including the type of dosimeter, should be chosen in consultation with a qualified expert, such as the Radiation Protection Officer, or as specified by the regulatory authority. Depending on the situation, both direct reading dosimeters and thermoluminescent dosimeters (TLDs) or film badges may be needed. For non-uniform exposures, it may be necessary to wear additional dosimeters, for example for the hands or fingers. Dose records should be kept of each application, where possible, and be available to the regulatory authority if requested.

Individual and workplace monitoring should consider the potential for internal exposure through inhalation or ingestion, for example through spills of material. All doses should be recorded. Further advice on occupational exposure control can be found in Ref. [3].

Appropriate equipment, safety systems and procedures should be provided to reduce the possibility for human error; provide a means for detecting human errors and for correcting or compensating for them; and facilitate intervention in the event of failure of safety systems. Given the high dependence on appropriate human actions, personnel should be adequately trained and understand their responsibilities, both for routine operation and in the event of an abnormal or emergency situation. With the use of unsealed sources, special attention should be paid to storage and handling of sources and to the potential for contamination of workers and equipment.

The safety assessment should consider the potential for exposures of the public and appropriate protection and workplace monitoring established for the application, commensurate with the magnitude and likelihood of the exposure. The requirements and guidance of the standards [1–3] should be applied. Calculations should also be made of the impacts of any possible discharge into the environment to ensure that any dose constraints and authorized limits, established by the regulatory authority, are met.

All parties should promote the concept of a strong safety culture, where every action is undertaken with safety as the highest priority.

2.3. EMERGENCY PLANNING

Emergency plans should be developed and written down to allow a coherent response to abnormal incidents. These plans should describe the responsibilities of the various parties and the need for summoning assistance. Such plans should be developed on the basis of safety assessment for each application of radiotracing, since the circumstances will change. Special consideration and procedures will be needed to deal with spills or other loss of the radiotracer. General advice on establishing emergency plans for radiological incidents can be found in Refs [8, 9].

2.4. RECORD KEEPING

Records should be kept of each application and the experiment should be reviewed to look for opportunities for improving the practice and for reducing exposures. Information on tracers used, their activities and form, together with the outcomes of the experiment, should be recorded. All exposures should be recorded consistently with the requirements of the regulatory authority.

3. METHODOLOGY

3.1. INTRODUCTION

Radiotracer methodology is described extensively in the literature. Here, we will focus on specific aspects of the technology to amplify and complement material from other sources.

Though radioisotopes have been applied to the solution of problems in industry for over 50 years, research and development of the technology continues unabated. There are two main reasons for the continuing interest.

Firstly, it is industry driven. Because of their unique properties, radioactive isotopes can be used to obtain information about plants and processes that cannot be obtained in any other way. Often, the information is obtained with the plant on-stream and without disrupting the process in any way. This can lead to substantial economic benefits, from shutdown avoidance to process optimization.

Secondly, the methodology is derived from many fields of science and technology including radioisotope production, radiation detection, data acquisition, treatment and analysis, and mathematical modelling (Fig. 1). Advances in any and all of these areas act as further stimuli for the development of radiotracer methodology.

This presents an on-going challenge to the radioisotope practitioner, who must not only have a sound knowledge of these disciplines but must also keep abreast of developments in them to ensure that the technology being used remains up to date.

The baseline background knowledge is to be found in several works of reference. The following books are recommended reading:

(a) Guidebook on Radioisotope Tracers in Industry, IAEA Technical Reports Series No. 316 [10]. This book describes the main concept of tracer methodology and focuses on different applications (flow rates, mass balances, mixing efficiency, trouble shooting, particle size distribution, diffusion, corrosion, two phase flow measurements, process control and kinetic processes) over a large spectrum of industries (chemical, paper, petroleum, cement, metallurgical, energy, electronics, automotive, environmental and mineral processing).

(b) Chemical Reaction Engineering [11] and Génie de la réaction chimique [12]. Both books are dedicated to the successful design and operation of chemical reactors, with particular emphasis on RTD and systemic analyses.

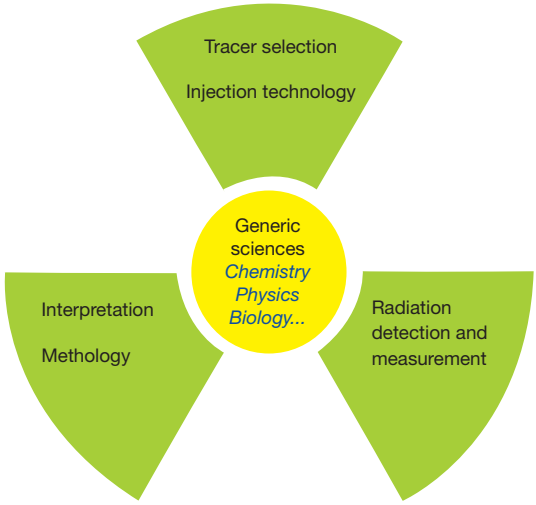

FIG. 1. Radiotracer methodology and interrelated aspects.

(c) Radioisotope Techniques for Problem Solving in Industrial Process Plants [13]. This book is intended for chemical engineers, describing the technological background and the types of technique employed. There are numerous case histories covering a variety of applications such as measurement of flow, measurement of RTD and detection of leaks. The applications of sealed sources of radiation are also discussed.

(d) Radiation Detection and Measurement [14]. This may serve as a textbook for those new to the field of radiation and measurement, but is also sufficiently comprehensive to function as a reference for those actively involved in radiation measurements.

(e) Analysis and Diagnostics of Industrial Processes by Radiotracers and Radioisotope Sealed Sources [15]. This book presents an extensive amount of work and experience dealing specifically with radioactive tracer tests throughout a very large range of applications and test cases. Full details of interpretation and modelling of RTD are given from a chemical engineering point of view.

Apart from these books, there is also software to assist in the planning and interpretation of radiotracer studies, and the radioisotope practitioner should be aware of what is available.

There is a large variety of commercial software for data acquisition and data treatment, for example smoothing, filtering, normalization, convolution, deconvolution, peak decomposition and curve fitting. Many programs are readily available, but, as they are being continuously refined and often replaced by superior programs, it is not our intention to list them here. However, there are a number of programs that have been written specifically for radiotracer methodology and RTD analysis. The reader's attention is drawn to J. Thyn's RTD suite [16] and PROGEPI's software DTSPro V. 4.2 Instruction Manual [17].

Other software deals with the simulation of radiation interactions with matter by Monte Carlo codes. Tola [18] has built a unique software package (JANU, MACALU, ECRIN and SPEEDY) based on an original accelerated Monte Carlo simulation module. These software packages calculate, for simple geometries, the expected counting rate as a function of the characteristics of an experiment (walls, shielding, collimator, crystal and counting chain efficiency) in several configurations of practical interest (gamma emitting point or a distributed source as a tracer within a flow). These software packages are now of prime importance for training, scaling up, dose rate estimation and sometimes tracer data interpretation. Since they have not yet been discussed elsewhere, ample use will be made of these tools within this book, either for didactic reasons or in order to focus on particular points of the methodology.

One very important question in tracer methodology concerns what a detector really measures. A detector actually does not perform a local measurement but collects a certain amount of information within a solid angle. The weight of each item of information inside that so-called detection volume is not the same for each point. This aspect is very important from a methodological point of view and should be taken into account in the interpretation of radiotracer data. It is also important from a quality insurance point of view in that it determines the level of uncertainty of measured parameters. One of the objectives of this guidebook is to focus on this aspect of the methodology. Let us take as an example the situation shown in Fig. 2.

Gas tracing in the riser of a fluidized catalyst cracking (FCC) unit was performed using two different gamma emitting tracers, ^{79}Kr (maximum energy 830 keV) and ^{41}Ar (energy 1.3 MeV). The curves for these two tracers are fairly close but their shapes are slightly different. Shapes contain information related to dispersion. What is seen inside the riser is different in these cases because of the difference in gamma energies: ^{41}Ar is more energetic and allows an investigation deeper inside the reactor. Since the flows are different at the wall and in the centre of the riser (because of the velocity profile and possible recirculation along the wall), accurate interpretations in terms of velocity and dispersion have to take into account the detection volume of the detectors.

A very important prerequisite for high quality radiotracer work is for the radiotracer team to be expert and professional, and to work in unison with the needs and requirements of chemical engineers. Planning a radiotracer experiment and interpreting its results requires a complete understanding of the system, process and problem under survey. This includes the properties of the process material (phase, density and viscosity), process parameters (e.g. flow rate, volume, pressure, temperature, expected residence time and stability of the operating conditions during the tracer experiment), the flow diagram of the process material, the expected degree of mixing and the injection conditions. This understanding of the process has to be coupled with a field feasibility assessment, which includes a visit to the plant, selection of injection and detection locations, measurement of background radiation level, and waste disposal. The example presented in Fig. 3 stresses the importance of co-operation with the process engineer and shows how good knowledge of the process conditions, obtained on-site, is a key requirement for successful interpretation.

Two detectors were positioned on opposite sides below the fountain of the riser in an FCC plant, a few metres below the catalyst bed level. The objective was to try to identify a suspected intrusion of the gas phase inside the catalyst bed. No counts were recorded by detector B, but detector A recorded a

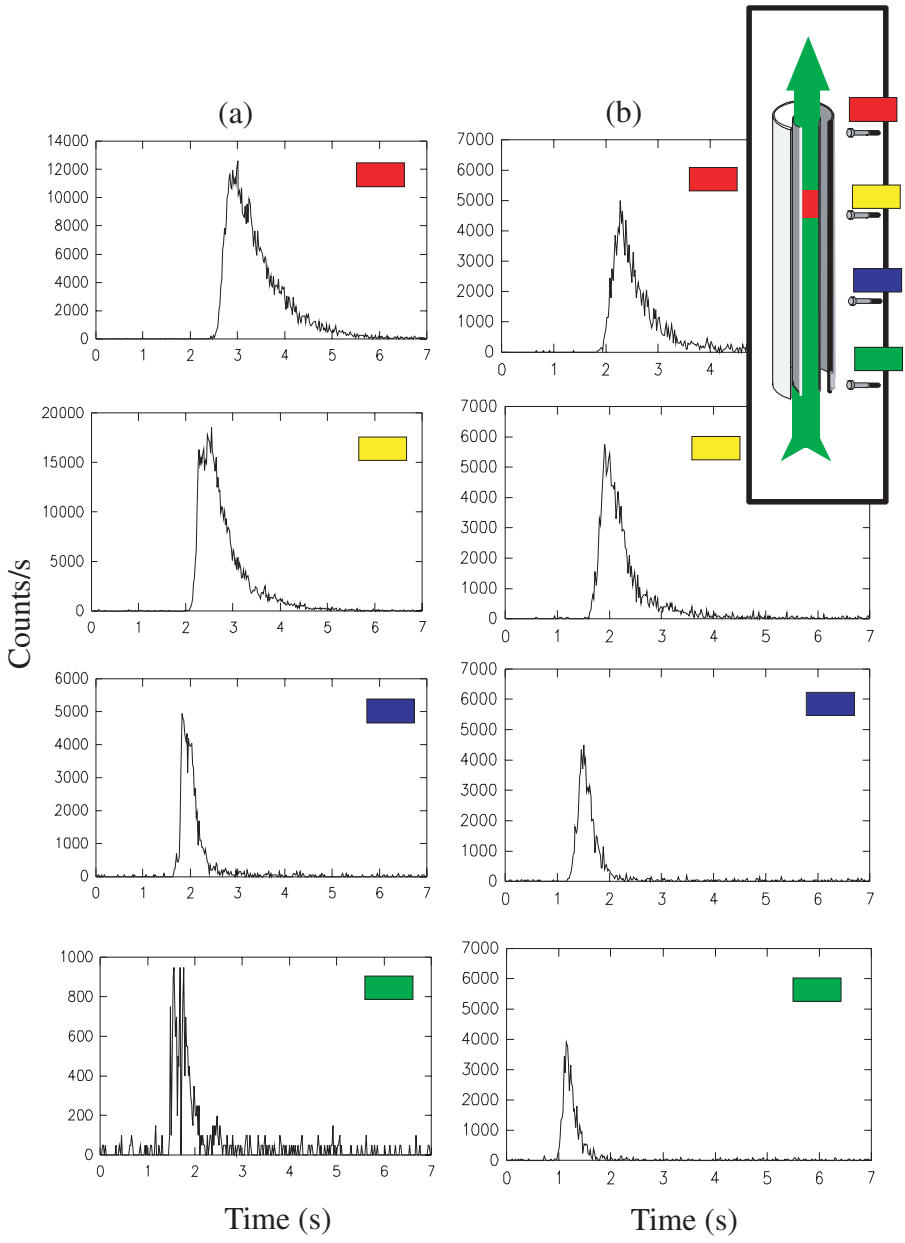

FIG. 2. Fluidized catalyst cracking riser gas tracing with (a) ^{79}Kr and (b) ^{41}Ar.

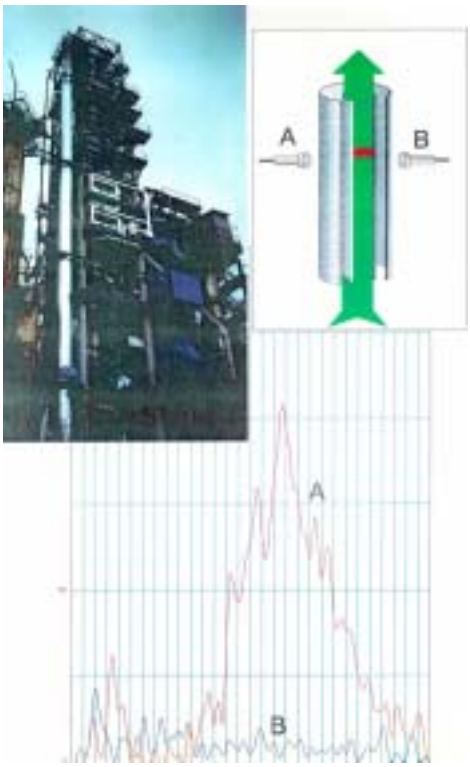

FIG. 3. Gas tracer survey below the end of the riser in an FCC plant.

very weak signal. This could mean that a very small amount of the gas phase was projected inside the catalyst and taken along, with an unsymmetrical behaviour since it was noticeable only on one side of the reactor. Such an interpretation proved wrong: detector A actually recorded the signal due to the transit of the tracer from the top of the FCC unit to the distillation column. Such a situation is often encountered when dealing with small peaks (such as 'leakage' peaks) that are difficult to interpret. Good knowledge of radiation detection, of plant and process conditions, and of how to correlate logically the responses of each detector, is necessary to overcome ambiguities and achieve a correct analysis.

As the last part of this introductory section, it is thought necessary to recall the basic fundamentals of RTD analysis, a key theory for the exploitation of tracer experiments.

There are many ways to describe the flow of matter in a system. In the case of a gas, for example, it is possible to study the flow at the molecular scale, and to establish the rules that govern the movement of the molecules. This is

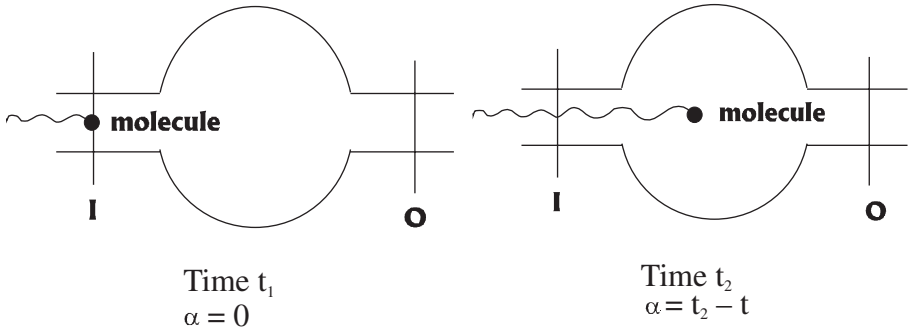

FIG. 4. Definition of the age of a molecule.

basically what is done in lattice gas simulations. Alternatively, one can also consider the gas as a continuum, and write macroscopic balance equations (e.g. the Navier–Stokes equations) that rule its flow. Both approaches are useful, but they involve great mathematical or numerical complexity and the description they provide is far more refined than that actually required for many applications.

A third possibility is to describe flows in a much more global way through the use of the RTD concept. This approach, first proposed by Danckwerts [19], has been developed and expanded by many authors, for example, by Levenspiel [11] and Villermaux [12] in the above mentioned books on chemical reaction engineering.

The basic concept is the following: consider a system, i.e. a definite portion of space through which parcels of matter (of whatever form) are moving. Let I be the inlet section and O the outlet section of this system. Consider a molecule moving inside the system. Its age α is defined as the time that has elapsed since it has entered the system through Section I (Fig. 4).

The RTD $E(t_s)$ is such that $E(t_s)\mathrm{d}t_s$ is the fraction of the outlet flow rate that contains molecules of age between t_s and $t_s + \mathrm{d}t_s$. In the same way,

$$\int_0^{t_s} E(\theta)\mathrm{d}\theta$$

is the fraction of outlet flow rate that contains molecules the age of which is less than t_s. Since the age of outgoing molecules obviously lies between 0 and infinity, $E(t_s)$ is area normalized by construction:

$$\int_0^{\infty} E(\theta)\mathrm{d}\theta = 1. \qquad (1)$$

This RTD concept has close links with tracing. Suppose the molecules entering the system at time 0 can be tagged in some way, i.e. provided with some distinguishable property that other molecules do not possess, without disturbing the flow. Suppose it is possible to measure continuously the concentration $C(t)$ of marked molecules that leave the system. $C(t)$ is proportional to the number of molecules leaving the system at time t, and therefore to the number of particles aged t leaving the system. Intuitively, it appears that $C(t)$ is an image of the RTD. $C(t)$ and $E(t)$ are, however, not identical, since there is no reason why the area of $C(t)$ should be 1. Therefore:

$$E(t) = \frac{C(t)}{\int_0^\infty C(t)\mathrm{d}t}. \tag{2}$$

This equivalence can be proved rigorously within certain assumptions. The RTD can be accessed by an impulse injection of tracer at the system inlet. If the system can be considered as linear (meaning that the response to a sum of stimuli is equal to the sum of the individual responses — not a very stringent assumption), this conclusion can be extended to any shape of tracer signal at the inlet. In that case, system response is the convolution of this signal with $E(t)$. Alternatively, the latter can be obtained by deconvolution of the system response by input stimulus. The techniques of convolution and deconvolution are described in more detail in Section 3.6.1.

In theory, measurement of the RTD by a tracer experiment requires many conditions (homokinetic injection, flat velocity profile and no backmixing at the outlet section). These conditions are reasonably satisfied in systems with high velocity (and turbulence) of inlet and outlet flows, through small cross-section pipes. In the opposite case, the tracer experiments only provide the concentration transfer function, which is of less general import.

RTD allows, first of all, diagnosis of the functioning of a system, and characterization of malfunctioning. RTD also allows the computation of a system response to any stimulus, given the assumption of linearity. This is valuable to devise control/command models. Finally, RTDs are an important part of a well established general method for the design of complex systems, especially where mass transfers are involved. The reader is once again referred to the works of Levenspiel [11] or Villermaux [12] for more information on this point.

3.2. SELECTION AND OPTIMIZATION OF THE RADIOACTIVE TRACER

3.2.1. Radioactive tracer characteristics

The selection of a suitable radiotracer is of prime importance for a radiotracer experiment. The tracer should represent the stream it is tracing. Often, it is possible to select a representative tracer on the basis of experience, from published references or from a physical and chemical evaluation of its compatibility with the stream to be traced. If necessary, however, the suitability of the tracer must be confirmed by validation tests in the laboratory.

Under certain circumstances, the tracer has to be chemically identical with the traced substances. This is the case when studying, for example, chemical reactions, kinetics, solubilities, vapour pressure and processes dominated by atomic or molecular diffusion. Radioactive isotopes of the traced elements and labelled molecules may be used as tracers, for example: H^3HO (or HTO) for water, $^{24}NaOH$ for NaOH and $^{14}CO_2$ for CO_2.

These tracers are called chemical radioactive tracers, intrinsic tracers or internal tracers. Use of an intrinsic tracer is of course preferable because it suppresses all questions about representativity, but is unfortunately not always possible. To take the example of CO_2 again, neither carbon nor oxygen possesses reasonably long lived gamma emitting isotopes (for instance, ^{10}C and ^{15}C are gamma emitters, but their half-lives are 19.1 and 2.3 s, respectively). This means that the intrinsic tracers of CO_2 will have to be beta emitters, like the above mentioned $^{14}CO_2$, and that through-the-wall measurements will not be possible, an unacceptable constraint in many cases.

Whenever chemical identity of the tracer with the traced material is not required (or when no suitable intrinsic tracer is available), a physical radioactive tracer, extrinsic tracer or external tracer can be used that has to fulfil a limited set of not so strict physical and physicochemical conditions. For example, it should be miscible in the traced material, or it should not be absorbed by the walls of the system or dissolved into another phase. In most cases, physical rather than chemical radioactive tracers have to be used.

If several radioisotopes are suitable for a tracer investigation, a choice will be made on the basis of occupational hazard, waste disposal, availability and cost.

Since radiation detectors are extremely sensitive, radioisotope tracers can be used at very low concentrations. In this range of concentrations, adsorption losses can be high. It is therefore essential to have some material that will act as a ‘carrier’, injected into the system together with the radioactive tracer. For instance, the carrier for ^{198}Au as gold chloride would be stable ^{197}Au also under

this chemical form. The total concentration in gold chloride will therefore be high enough for adsorption effects to be negligible. In many situations, carrier material is already present in the system. An example is the use of $^{82}Br^-$ (bromide anions) as a tracer for the investigation of water systems. Water already contains a few ten or hundred parts per million of chloride, the properties of which are similar to those of bromide. No carrier has to be used in that case — a welcome conclusion, since the addition of a carrier could be prohibitive when studying large reservoirs.

3.2.2. Potential radiotracers for typical applications

3.2.2.1. Radioisotope generators

Radioisotope generators are very important in tracer work in developing countries without nuclear reactors. There are three available types of radioisotope generator for tracer experiments: Mo/^{99m}Tc, Sn/^{113m}In and Cs/^{137m}Ba.

Mo/^{99m}Tc has a relatively short half-life and low gamma ray energy. However, it is relatively cheap and universally available. For these reasons, it accounts for approximately 20% of reported tracer studies.

Sn/^{113m}In can be purchased from only a few suppliers. It has a longer half-life and higher gamma energy than Mo/^{99m}Tc, but is 2–3 times more expensive. However, it can be used in situations in which the Mo/^{99m}Tc generator is ineffective, for example, in carrying out studies on vessels with relatively thick walls.

The Cs/^{137m}Ba generator produces a very short lived radiotracer but the generator has a very long useful life (several years, in practice). This is a very suitable radiotracer generator for routine service work, in particular for liquid flow rate measurement and flow meter calibration. Its high gamma energy renders the tracer easily detectable through pipes and vessels, and its short half-life ensures that there are no problems associated with the disposal of residual activity. The Cs/^{137m}Ba generator is no longer available commercially. However, ^{137}Cs may be readily purchased and so, with the aid of a competent radiochemist, it is possible to construct the generator using methods described in the literature.

These three generators are particularly recommended for practitioners in developing countries who may not have access to other radioisotope production facilities. By using them it is possible to carry out a wide range of liquid and solid phase tracer studies.

3.2.3. Estimation of radiotracer amount

After selecting a suitable radiotracer for a particular application, the amount of tracer required is the second important step in designing a radiotracer study. Measurement sensitivity, desired accuracy, tracer dilution and background radiation intensity determine the minimum usable amount of tracer. The upper limit is set by radiological safety considerations.

Ideally, the smallest amount possible of radioactive material should be used, consistent with achieving the objectives of the measurement.

In all cases, care must be taken to ensure that the amount of tracer used does not saturate the detector response. This is, perhaps, less important in studies such as velocity measurement, in which it is the timing, rather than the shape, of the pulse that matters. However, in other cases, such as RTD investigations, detector saturation will lead to erroneous results (approximate means for correcting detector saturation effects are, however, presented in Section 3.5).

The amount of radiotracer required for a given application depends on the following factors:

— Accuracy required,
— Expected level of dilution/dispersion,
— Efficiency of measurement or calibration factor of detection system,
— Half-life of radiotracer used,
— Background radiation level,
— Expected losses of tracer from the system,
— Number of repeat measurements to be made,
— Mode of injection and detection.

These factors are discussed in detail below.

3.2.3.1. Accuracy required

An important consideration in tracer experiments is the maximum tolerable error, which is statistically related to the minimum signal to noise ratio of the detector. This factor determines the minimum number of events that must be measured.

Suppose, for example, that a standard deviation σ_{net} of 2% of the net signal value after background subtraction is an acceptable error. Further suppose that the counting time per measurement is 10 min and that the background radiation intensity is 200 counts/min (cpm in equations below).

Radioactive disintegration has the well known property that σ_n, the standard deviation on count number n, is given by:

$$\sigma_n = \sqrt{n}. \tag{3}$$

Applying this equation to count rate $\dot{n}$ measured over counting time Δt gives:

$$\sigma_{\dot{n}} = \sqrt{\frac{\dot{n}}{\Delta t}}. \tag{4}$$

The net count rate x is obviously:

$$x = \text{Gross cpm} - \text{Background cpm}. \tag{5}$$

The standard deviation for x can then be deduced from the standard deviations of gross count and background count rates (applying the so-called variance propagation law):

$$\sigma_x = \left(\sigma^2_{\text{gross}} + \sigma^2_{\text{background}}\right)^{1/2} = \left(\frac{\text{Gross cpm}}{\text{Counting time}} + \frac{\text{Background cpm}}{\text{Counting time}}\right)^{1/2} \tag{6}$$

or

$$\frac{2x}{100} = \left(\frac{x+200}{10} + \frac{200}{10}\right)^{1/2}. \tag{7}$$

Hence, x is equal to 465 counts/min (minimum count rate required), and the gross counting rate to 665 counts/min.

Ratemeter measurements are subject to similar considerations. The effective count accumulation time for a ratemeter is equal to twice the time constant T_c ($=RC$ for a resistor/capacitance integrating circuit). The appropriate expression for standard deviation is then:

$$\sigma = \sqrt{\frac{\dot{n}}{2T_c}}, \tag{8}$$

where $\dot{n}$ the count rate.

3.2.3.2. Dilution/dispersion

Industrial processes work in either batch or continuous operation. A common occurrence in all tracer experiments is the dilution of tracer between injection and detection points in the system being investigated. It is important to make some estimate of this dilution in designing a tracer study.

The processes of dilution in batch and continuous processes are different. In a batch process, dilution occurs simply because of mixing of the tracer in the fixed batch volume, while in continuous processes it is due to axial dispersion.

In a batch process studied by sampling, the dilution is the ratio of the total volume (or weight) to the sample volume (or weight). In continuous process systems, the dilution of tracer depends on the type of flow pattern; it is described by suitable mathematical models based on the physical nature of the system. Examples are given in Section 3.6.5.

This subject is also discussed in the IAEA Guidebook on Radioisotope Tracers in Industry [10].

3.2.3.3. Efficiency of measurement or calibration factor

Efficiency of measurement is defined as the response of the detector to a known amount of radioactivity and specific detection geometry. It is given in terms of count rate per activity per unit volume of the fluid flowing through the pipe to which the detector is attached, or into which it is submerged. Efficiency of measurement is, for example, expressed in units of counts·s^{-1}·Bq^{-1}·m^3.

The efficiency of measurement depends upon the following factors:

— Geometrical factor, f_g;
— Intrinsic efficiency of the detector, f_e;
— Radiation absorption in material between the source and detector, f_a;
— Yield of detectable radiation per disintegration of radioisotope, f_d;
— Buildup factor, f_b;
— Radiation field, i.e. volume v seen by the detector.

Therefore the efficiency of measurement is given as:

$$k = f_g f_e f_a f_d f_b v. \quad (9)$$

The geometrical factor f_g is the ratio of gamma rays entering the detector to the total number of gamma rays emitted.

For a specific detection geometry, the geometrical factor is given by the following relation:

$$f_g = \frac{1}{2}\left(1 - \frac{r}{\sqrt{r^2 + \frac{d_d^4}{4}}}\right), \tag{10}$$

where

r is the distance between the detector face and the centre of the cross-section of the pipe, and
d_d is the diameter of the detector used.

For ease of calculation it is assumed that the tracer is concentrated at the centre of the pipe.

The intrinsic efficiency f_e of the detector is defined as the ratio of the number of gamma rays detected to the number entering the detector, and depends upon the size of the sensitive area of the detector and upon the radiation energy.

NaI(Tl) scintillation detectors are commonly used for industrial tracer applications because of their high efficiency for gamma ray detection. The intrinsic efficiencies of a 1 in. (2.54 cm) thick NaI(Tl) detector crystal for 100 keV, 500 keV and 1 MeV energy photons are about 100, 59 and 42%, respectively.

The attenuation f_a of radiation in materials between source (tracer solution) and detector can be calculated from the thickness and attenuation coefficient of the intervening material.

The number of gamma radiations emitted per disintegration f_d is different for different radioisotopes and is available in the literature.

The buildup factor f_b for narrow beam geometries is unity. For other geometries, it can be determined experimentally.

The volume v seen by the detector is equal to the cross-sectional area of the pipe on which the detector is mounted, multiplied by the length of the visual field. The volume seen by the detector depends upon the detection geometry that is used, i.e. collimator and pipe diameter. The following relation estimates the volume seen by the detector:

$$v = 0.5\left(\frac{d^2}{4\pi}\right)d_{co}, \tag{11}$$

where d is the pipe diameter and d_{co} is the collimator diameter.

In practice, it is difficult to calculate the calibration factor of experimental arrangements from the theory. In order to estimate the amount of tracer required for an investigation, the calibration factor should be known beforehand. The calibration factor of the detection system for a particular radiotracer and detection geometry can be measured experimentally by simulating the field experimental arrangement in the laboratory under static conditions. A short length of pipe (about 2 m) satisfying the infinite–infinite detection geometry condition, with a small injection port (opening) on the pipe surface, is plugged at both ends. The pipe is laid down horizontally with the opening facing upwards, and a small quantity of radiotracer with specific activity A_s is diluted by a factor f and mixed thoroughly. The homogeneously mixed tracer solution is transferred into the calibration pipe until the pipe is completely filled. The detection system that is to be used in the actual field experiment is mounted on the pipe with the identical detection geometry. The tracer concentration is recorded in terms of count rate. If n counts are recorded in time t, then $n \propto A_s t/f$ or $n = kA_s t/f$, where k is the calibration factor of the detector. Thus:

$$k = \frac{nf}{A_s t} \tag{12}$$

(in counts·s^{-1}·Bq^{-1}·m^3 for example). It is also possible to use Monte Carlo simulations to determine the factor k. This point is illustrated in Section 3.4.1.

3.2.3.4. Half-life

The half-life of a radiotracer is an important factor to be considered while designing a radiotracer investigation. The half-life should be sufficiently long to allow time to transport the tracer from the nuclear reactor to the experimental site, prepare the tracer for use and complete the measurement. In order to reduce the level of residual tracer in the exit streams, a short half-life tracer is, however, desirable. In addition to radiological safety considerations, a short half-life is also useful if a series of similar experiments is to be repeated, particularly in a closed recycling system.

3.2.3.5. Background radiation level

It is necessary to know the background radiation level prior to the tracer test to estimate the amount of activity required. In general, the maximum count rate should be at least 5–10 times the background radiation count rate at the

measuring points. However, for high accuracy, the maximum count rate should be about 100 times that of the background radiation count rate.

If a series of radiotracer tests is carried out in a closed recycling system then the background radiation level should be measured after each experiment, and the amount of radiotracer to be used for the next test should be adjusted accordingly.

3.2.3.6. Expected losses

Any expected losses due to splitting of tracer stream, adsorption, evaporation, etc., should be taken into consideration while estimating the amount of activity for a particular radiotracer experiment.

3.3. INJECTION

The theoretical requirements for tracer injection have been discussed in Section 3.1 from a methodological point of view: fundamentally, the tracer should have the same behaviour as the bulk flow. This emphasizes the importance of the way in which the tracer is injected into the system and the importance of the mixing with the bulk flow.

Good mixing is essential in order to make the direct correlation between the behaviour of the tracer and that of the bulk flow. If such conditions are not reached, modelling and simulation are the only ways in which the correlation can be made.

This section is divided into two parts. The first (3.3.1) deals with how good mixing can be achieved in practice while the second (3.3.2) describes a number of effective injection devices.

3.3.1. Methodology: Good mixing length estimation

3.3.1.1. Practical equations and tools

The following information is taken from the French National Standards on pipe flow rate measurement, Standard No. NF X 10-131 [20]. It provides basic guidelines for the estimation of good mixing length in duct flow and suggests several means to reduce it.

Good mixing length is defined as the distance beyond which the variation in the duct cross-section of c, in the case of continuous injection, or

$$c_\infty = \int_0^\infty c(t)\,\mathrm{d}t$$

in the case of pulse injection (where c denotes the tracer concentration and t is time) is smaller than some previously chosen value.

(a) Injection at the centre of the pipe

The following equations can be used to calculate good mixing length, in terms of length to diameter (L/D) ratio (or equivalently in the number of pipe diameters), as a function of the admissible variation of tracer concentration in the cross-section of the pipe, of flow Reynolds number Re and of wall friction. The Reynolds number in the pipe flow is defined as

$$\mathrm{Re} = \frac{UD}{\nu}, \tag{13}$$

where U is the fluid velocity and ν is the fluid kinematic viscosity (in m^2/s).

Equation (14) is derived on the assumption of a constant radial diffusion coefficient and a flat velocity profile, Eq. (15) on the assumption of a parabolic radial diffusion coefficient profile and flat velocity profile, and Eq. (16) on the assumption of a parabolic radial diffusion coefficient profile and a logarithmic velocity profile:

$$\frac{L}{D} = 1.18\sqrt{\frac{8}{\lambda}}\left(2.94 - \frac{\ln x}{2.3}\right), \tag{14}$$

$$\frac{L}{D} = \left(2.95 - \frac{\ln x}{2.4}\right)\sqrt{\frac{8}{\lambda}}, \tag{15}$$

$$\frac{L}{D} = (20.5 - 2.85\ln x)\,\mathrm{Re}^{0.1}\left(\frac{\lambda_{\mathrm{smooth}}}{\lambda_{\mathrm{pipe}}}\right)^{0.5}, \tag{16}$$

where

x is the maximum percentage of variation of tracer concentration over the cross-section of the pipe in the case of constant flow rate injection, or of the quantity

$$\int_0^\infty C(t)\,\mathrm{d}t$$

in the case of pulse injection;

λ is the pipe friction coefficient (λ_{smooth} being the value for a smooth pipe);

λ_{pipe} is the value for the real pipe.

Many correlations for λ as a function of Reynolds number and pipe roughness can be found in handbooks on pressure loss calculations [21]. A simple one, valid for smooth pipes at 'moderate' Reynolds numbers (say 10^4–10^5), is the well known Blasius correlation:

$$\lambda = \frac{0.3164}{\mathrm{Re}^{0.25}}. \tag{17}$$

In turbulent pipe flow, it is reasonable to assume a parabolic radial diffusion profile with either a flat or a logarithmic velocity profile.

These equations are plotted in Fig. 5 (the Blasius correlation for λ is used). They show that for Reynolds numbers equal to 10^5 and a smooth pipe, the good mixing length (predictably) decreases when x increases. Good mixing length is predicted to be larger for flat velocity and diffusion coefficient profiles.

The Reynolds number has little influence on good mixing length (see, e.g., Eq. (16)). For $x = 1\%$, good mixing length only increases by about 25% when the Reynolds number is increased from 10^5 to 10^6.

(b) Annular injection

Uniform injection by means of a ring with a diameter r equal to 0.63 times the diameter R of the pipe reduces good mixing length by a factor of about three compared with the values calculated for central injection.

(c) Experimental determination of good mixing length

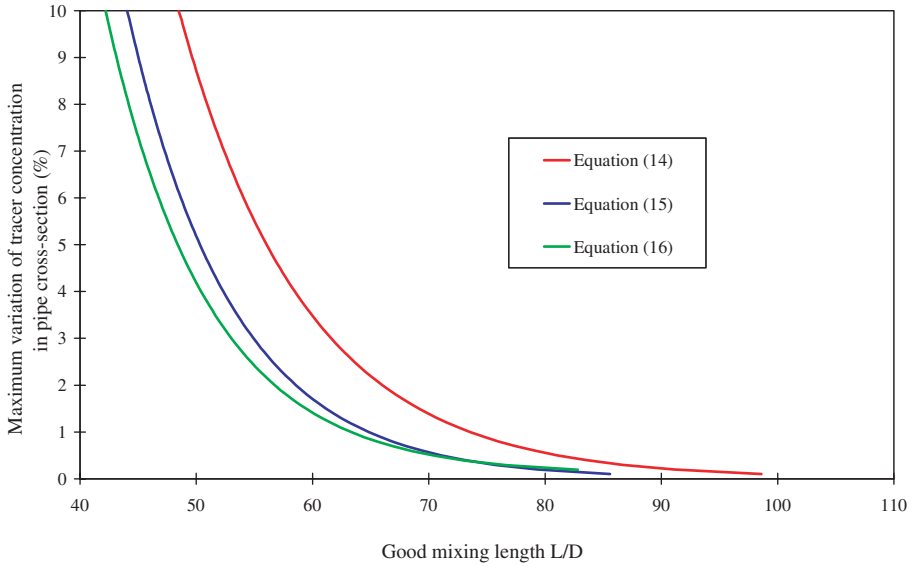

FIG. 5. Good mixing length (L/D) versus maximum variation of tracer concentration.

Values for good mixing length determined experimentally in a straight pipe of circular cross-section, with central tracer injection are about twice as large as theoretical values. The main reason for this discrepancy is the difference between actual and postulated flow conditions. Theoretical results should therefore be used with some caution.

Figure 6 shows an example of the measured variation in good mixing length as a function of x, in the case of four types of injection. It should also be noted that the level of turbulence has an influence on these results.

(d) Examples of methods for reducing good mixing length

The previous examples have shown that good mixing may require as many as 200 pipe diameters to be achieved. It is often not possible to inject the tracer at such a distance upstream of the measurement section. It is therefore very useful to be able to reduce that length by using appropriate devices.

(e) Multiple orifice injectors

A substantial reduction of mixing length can be obtained by injecting the tracer through multiple orifices uniformly distributed on the pipe wall or (if possible) inside the pipe, as illustrated in Fig. 6.

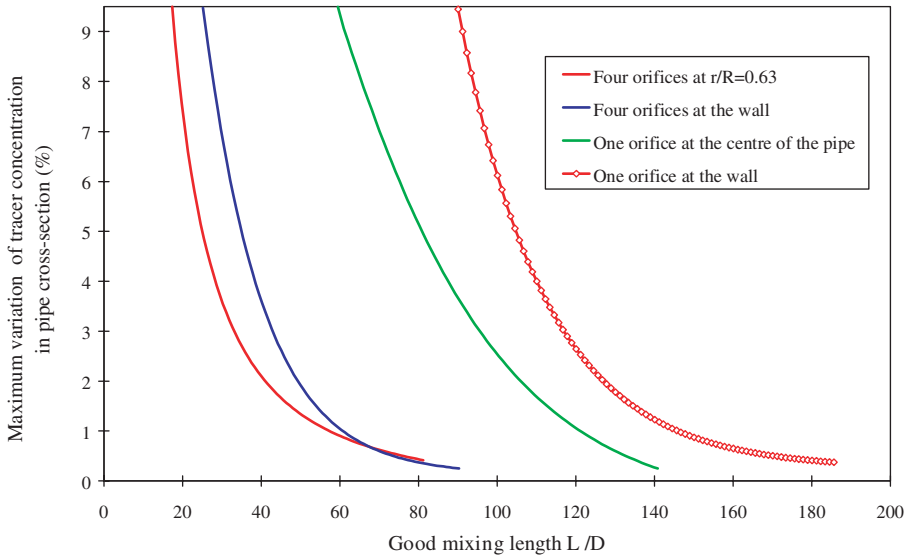

FIG. 6. Good mixing length (L/D) versus maximum variation of tracer injection with four types of injection.

(f) High velocity jets

Injecting the tracer countercurrently at a velocity much larger than the bulk flow velocity induces high mixing at the end of the jet. The reduction in good mixing length depends on the number and momentum of the jets and on their angle with respect to the main flow direction.

Few quantitative data are available on these effects. However, a simple jet arrangement can bring a 30% reduction compared with a single central injection point.

(g) Vortex generators

Incorporating obstacles within the pipe, in the vicinity of where the tracer is injected, produces turbulence that enhances mixing and reduces good mixing length.

As an example, injecting the tracer through three triangular plates, at an angle of 40° to the main flow direction, reduces mixing length by one third with respect to a central single injection point.

(h) Pumps and turbines

If the tracer is injected upstream of a pump or a turbine, mixing length is considerably reduced. Available information indicates that centrifugal pumps reduce mixing length by about 100 pipe diameters.

(i) Bends, valves and other obstacles

Every singularity in the pipe promotes turbulence, which tends to decrease good mixing length. Although no quantitative data are available, measurement sections where such kinds of devices are present should be preferred. However, it is advisable to use straight lengths of pipe without obstacles whenever transit times are to be measured.

3.3.1.2. Numerical simulations

To obtain a better understanding of the process of mixing, it is also suggested to examine the results of CFD simulations, modelling both the bulk flow and the tracer injection. In this section, we present a few results obtained with this kind of tool [22].

The geometry of injection devices is usually rather complex (for instance, a small pipe protruding into a large one, possibly with bends and counter-current flow). Here, no attempt has been made at precise representation of the geometry. These simulations should be considered as illustrative only.

A finite element code is used here since such codes can quite easily model complex shapes by means of unstructured mesh grids. This code is CASTEM2000, developed by the French Atomic Energy Commission (CEA) [23]. The application is concerned with turbulent pipe flow of incompressible Newtonian fluids. The Navier–Stokes equations are solved in two or three dimensions, turbulence being represented by the standard k–ε model. Boundary layers are handled by a logarithmic wall function.

Since the use of a CFD code is not yet quite foolproof, the need for some kind of validation may be felt. A step by step procedure is proposed.

Firstly, turbulent flows in a straight pipe are simulated for a wide range of Reynolds numbers (5×10^4–10^6) with a two dimensional grid. The influence of mesh size and shape is also investigated. Computed velocity and turbulent viscosity profiles are found to be in very good agreement with theoretical and experimental results. This gives some confidence in the ability of the code to reproduce the hydrodynamics of pipe flow.

In the previous section a few formulas for the prediction of good mixing length in certain configurations were given. The CFD code was found to be able

to reproduce these theoretical results, provided it was supplied with adequate hydrodynamic profiles. Results were once more quite satisfactory, as shown in Table 1. They were slightly improved when a three dimensional mesh grid was used, even though these configurations are basically two dimensional. Here good mixing lengths are once again expressed in number of pipe diameters.

It is then possible to build a realistic three dimensional model for the injection of a squirt of tracer into a duct flow from an injection tube perpendicular to the axis of the duct. The parameters are duct diameter, bulk and injection flow rates and duration. To keep computer time as short as possible, calculations are divided into three phases:

(1) Injection phase (both bulk and injection flows are calculated);
(2) Perturbed flow phase (injection is turned off but the bulk flow is still perturbed);
(3) Diffusion phase (the bulk flow has returned to the developed pipe flow and only the transport diffusion equation needs to be solved).

This calculation has been tested for numerical and physical consistency, but it has not been validated against experimental results in this example. Figure 7 illustrates typical computed concentration maps as a function of time. The

TABLE 1. COMPARISON OF EXPERIMENTAL AND SIMULATED MIXING LENGTHS*

Injection	Reynolds number	Theory	2-D simulations	3-D simulations	Experiment
Central	2×10^4	61	70	63	
	10^5	71	82	77	135
	10^6	89.5	100		
	2×10^4	40.5	46		
Annular	10^5	47.5	47.5		70
	10^6	60	60		
	2×10^4			260	
At the wall	10^5			321.5	160
	10^6			>350	

* Expressed in number of pipe diameters.

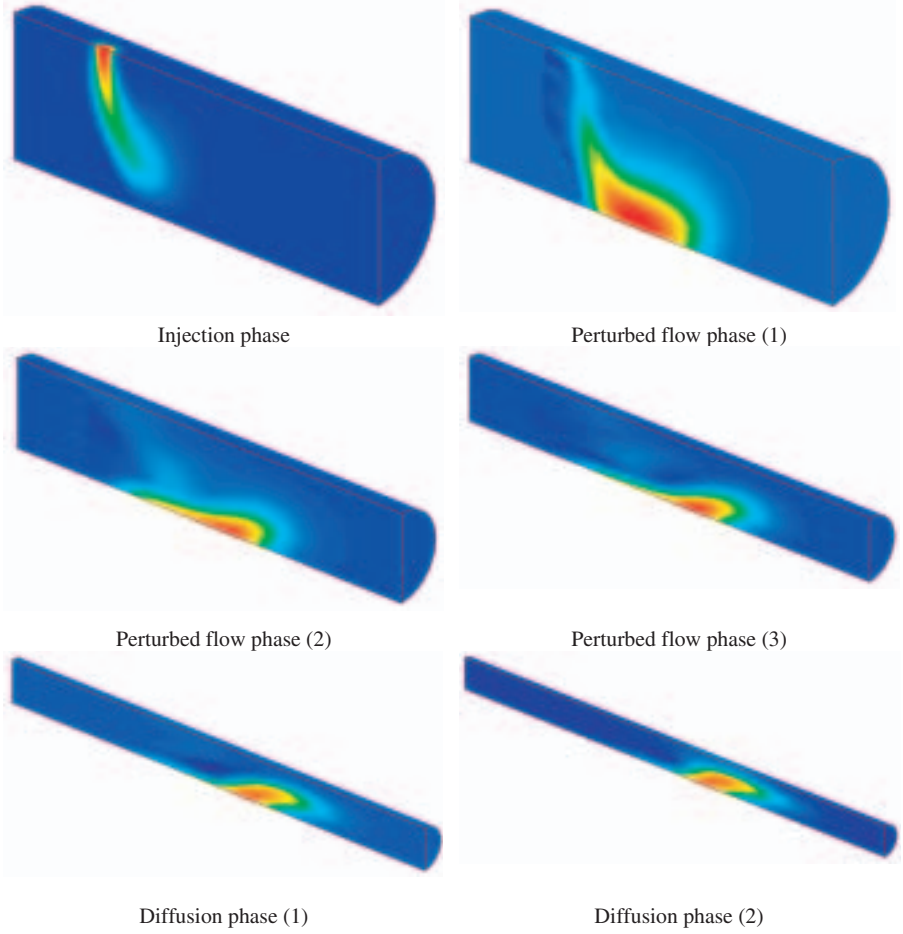

FIG. 7. Different phases of the mixing of tracer in a flow of water.

initial tracer jet, its deviation by the main flow, its impact against the tube wall and its subsequent dispersion are clearly visible (the computational domain gets longer and longer as the tracer cloud moves inside the duct, hence the more elongated aspect of the figures).

3.3.2. Examples of injectors

Injection systems are generally home made, built and adapted for specific applications. They vary considerably in design, from the simplest (a syringe, or a reservoir with a peristaltic pump) to the most complex (devices for remote injection into pressure vessels).

Firstly, a multipurpose device for pulse injection is presented. This injection device, shown in Fig. 8, is constructed so as to be usable in explosive environments, for example in hydrogen environments.

This system injects the radiotracer as a pulse (Dirac type) signal into the flow under investigation. It is worth noting that other types of injection (continuous flow rate, sinusoidal and random) can be of great interest in the understanding of certain complex processes. Nevertheless, most industrial processes can be perfectly characterized using the above proposed injection device, provided that the time duration of the injected signal is about a hundredth the mean residence time (MRT) of the flow studied (if that condition is not fulfilled, deconvolution of signals has to be carried out, as explained in Section 3.6.1).

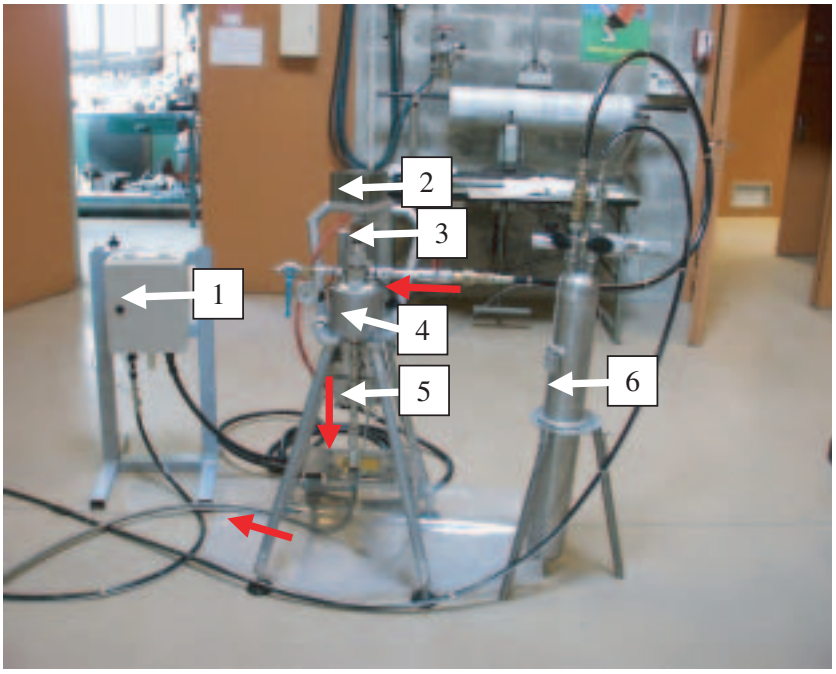

FIG. 8. Photograph of a multipurpose injection device: 1, tracer injection and air release pneumatic controls (linked to an N_2 cylinder at 6 bar pressure); 2, pneumatic actuator; 3, hammer; 4, dilution chamber with lead shielding for radiological protection; 5, pneumatic three way valve; 6, pressurized fluid (liquid or gas) container (up to 80 bar). The red arrows indicate the fluid flow inside this system from the pressurized fluid container to the industrial reactor.

In the system shown in Fig. 8, the tracer is initially contained in a quartz ampoule, which is placed in an internal steel cylinder inside the dilution chamber (4). This chamber is then filled with the fluid being traced (gas, liquid or solid). If required, this volume is connected to a pressurized container (6). The pneumatic actuator (2) releases a hammer (3). Its initial top position in the chamber and running length can be adjusted in order to efficiently break the quartz ampoule into pieces that are retained by a grid. The tracer is then diluted by the pressurized fluid contained in the chamber. The pneumatic three way valve (5) facilitates the injection of the labelled volume of fluid into the industrial reactor. Once the tracer has been injected it is possible to extract the internal cylinder containing the broken quartz ampoule.

After the tracer ampoule has been placed in the dilution chamber, every operation is controlled remotely so as to minimize exposure to radiation. Only pneumatic devices are used, hence the explosive environment capability of this injection device.

Figure 9 depicts a conventional injection device.

3.4. RADIATION DETECTION AND MEASUREMENT IN A TRACER TEST CONFIGURATION

3.4.1. Influence of the test configuration

Three conditions have to be fulfilled to achieve a good tracer experiment:

(1) Time resolution should be sufficient to track the transient radiotracer wave,
(2) Count numbers should be sufficient,
(3) Space resolution should also be sufficient.

The first condition is self-explanatory. Imagine the radiotracer wave lasts 1 s at a particular location; if the shape of this wave is to be accurately monitored, count time should obviously not be more than a few hundredths of a second, so as to have a few tens of significant data points. This sets a maximum value for the counting time.

The second condition is firstly imposed by the statistical nature of nuclear radiation. The standard deviation on count number n is theoretically equal to $\sqrt{n}$. If an accuracy of 10% is required, the number of recorded counts should be more than 100 during one counting period, at least at the peak of the radiotracer wave. Another consideration is that the tracer signal should

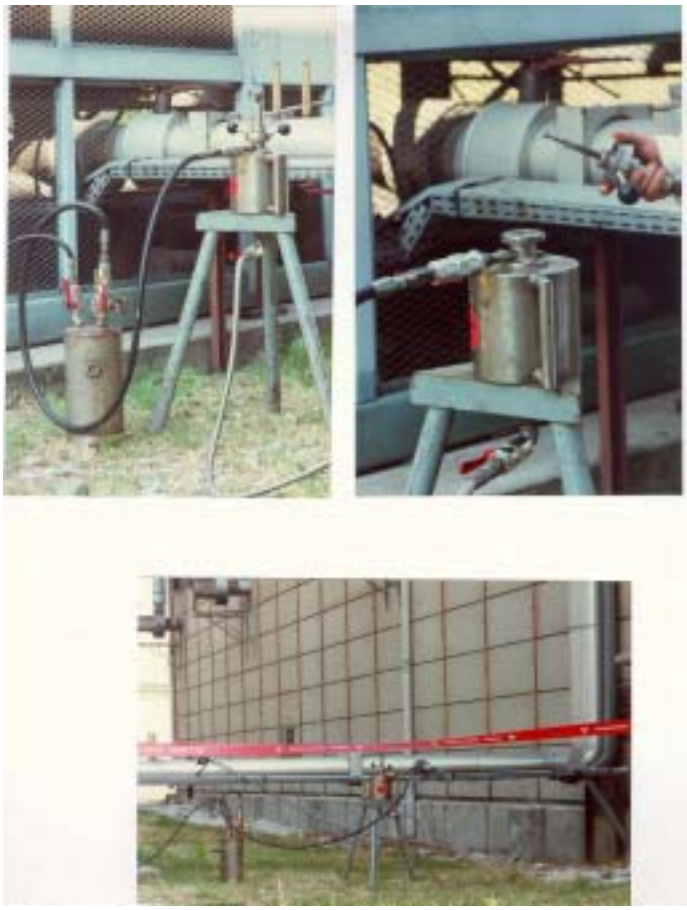

FIG. 9. Details of a conventional injection device for chemical industry applications.

supersede the background level of the radiation. These points have already been discussed in Section 3.2.3.

The last condition is usually not so important. High spatial resolution is often not required in industrial conditions. Otherwise, it would imply precise collimation, which is not favourable to high count rates, and it is often preferable to have higher count rates at the cost of some spatial resolution. However, it can be a requirement in high quality measurements at a laboratory or on the pilot scale.

A maximum value for the counting time and a minimum value for the count number are therefore imposed; the combination of both gives a minimum value for the count rate. This constraint is very important for the

choice of tracer, of the injected activity and of the configuration of the detectors.

This section illustrates the influence on the count rate of (a) the radiotracer, (b) the detector and (c) the collimator by means of Monte Carlo simulations, on both the pilot scale and in industrial cases. The objective of this section is to focus on the relative importance of all the parameters involved. Most of the Monte Carlo simulations are presented here for didactic reasons and have been validated by laboratory experiments. They have been made with the codes ECRIN and SPEEDY of Tola [18], which are dedicated to Monte Carlo simulations for radioactive tracer experiment design, scaling up and interpretation.

3.4.2. Example 1: A radiotracer experiment in pipe flow

This example is based on a test rig for two-phase pipe flow experiments. The main part is a 32 m long, 60 mm diameter glass pipe in which co-current air–water flows can be created. The pipe thickness is 5 mm. Flow regimes range from bubble flow to slug flow and annular flow. Radiotracer experiments have been made in this test rig in one-phase air flow, with ^{133}Xe as a tracer [24]. First, we shall describe how to estimate the necessary activity in a given configuration (tracer and detection). Then we shall show the influence of all the parameters on the count rate and therefore on the necessary activity.

3.4.2.1. Results from Monte Carlo simulations: Determination of the required activity

Suppose tracing of the gas phase is repeated under the following conditions: void fraction 10% in bubble flow regime, gas velocity 5 m/s (liquid velocity should also be close to 5 m/s, since the bubble flow regime is assumed). Argon-41, which is a classical tracer for the gas phase with a relatively high emission energy (1.29 MeV), can be used. Available detectors have 1.5 in. (3.81 cm) by 2 in. (5.12 cm) NaI(Tl) scintillators, with a 1 mm thick steel window. The detector is shielded by a 3 cm thick lead cylinder (Fig. 10).

Under these conditions, a Monte Carlo simulation (with the ECRIN 2 software) allows the calculation of many parameters:

(a) The count rate that would be obtained if the tube was filled with an air–water mixture uniformly tagged with 3.7×10^{10} Bq of ^{41}Ar: $\dot{n} = 6.8 \times 10^{-6}$ counts·s^{-1}·Bq^{-1}·m^3. This value is very important since it allows comparison of the efficiency of two different tracers, and prediction of the total

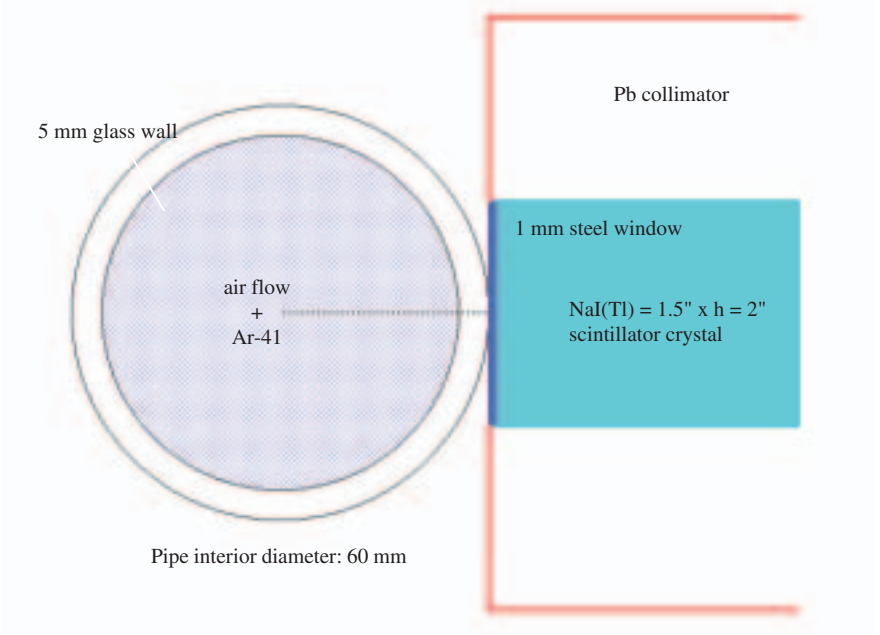

FIG. 10. Test case configuration: air flow measurement in a pipe with ^{41}Ar.

number of counts N that would be recorded by a detector if activity A of ^{41}Ar was injected into the pipe in a real tracer experiment. N is given by $N = A\dot{n}/Q$, where Q is the mixture volumetric flow rate. In the present case, N is equal to about 17 500 counts for a 3.7×10^{10} Bq injection. If the tracer wave is supposed to last ten seconds at a particular location, the average count rate will be about 1750 counts/s, which corresponds to a 2.5% statistical error. This is a first useful indication for the selection of the injected activity. This point is further developed later. The simulation also indicates the efficiency of the detector and the buildup factor (39% and 1.4 in our case, respectively). This provides guidelines for the selection of the detector and its geometry.

(b) The detected spectrum (which can be corrected by an energy resolution to mimic the output of a multichannel analyser: the 'convoluted spectrum' in Fig. 11). This is a useful indication for the choice of the thresholds of the detection chain. In our case, the gamma emission peak and Compton plateau can be clearly seen.

(c) If the tracer is supposed to be uniformly distributed in each cross-section of the tube, the simulation also gives the contribution of each tracer cross-sectional slice to the total count (Fig. 12). This gives a clear image of the

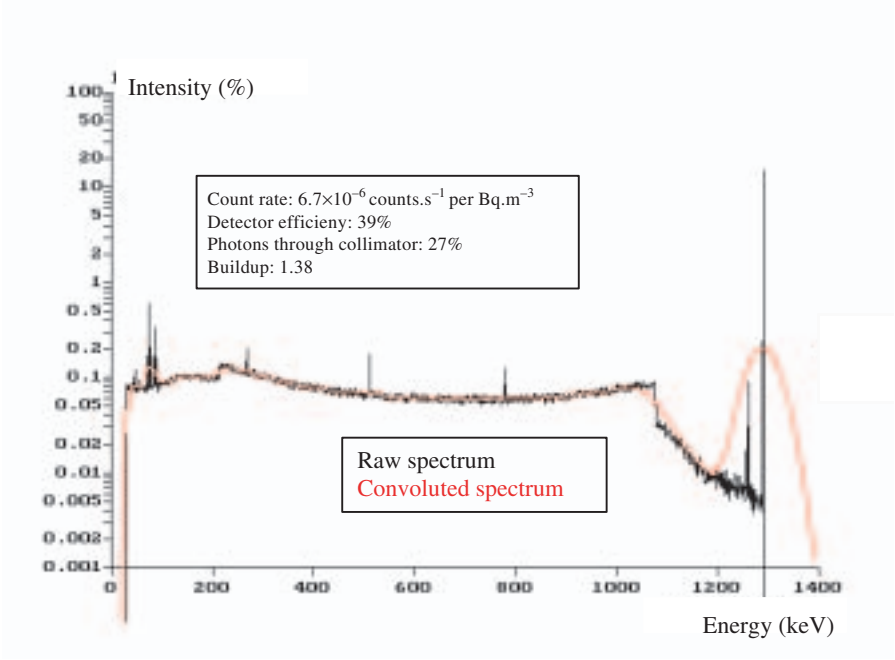

FIG. 11. Argon-41 test case: raw and convoluted spectra.

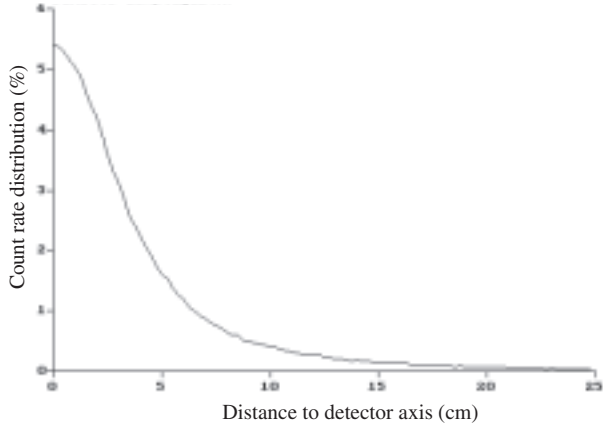

FIG. 12. Argon-41 case: count rate distribution versus distance to detector axis.

spatial resolution of the detection chain. In our case, the detector 'sees' about 10 cm of tube on each side of its axis (i.e. much more than the opening of the lead shielding; this is due to the high emission energy of the tracer). If the tracer distribution is known to be non-uniform, it is also possible to have the detail of the contribution of each point inside the tube, as shown in the example shown in Fig. 13. This kind of result, however, requires long and tedious calculations and is usually not necessary for a classical tracer experiment.

(d) Finally, the results from the Monte Carlo simulation make it possible to predict the output of the tracer experiment, provided that the flow can be approximated by axial dispersive plug flow with velocity U (m/s) and dispersion coefficient D (m^2/s). A calculation has been made with the SPEEDY code by Tola. The result is given here for $U = 5$ m/s and $D = 0.064$ m^2/s, which is the theoretical value for water pipe flow in the conditions of our experiment (according to Ref. [25]). The count rate versus time curves are shown in Fig. 14, for three detector locations: 10, 20 and 30 m from the injection point. A ^{41}Ar tracer of 3.7×10^{10} Bq is assumed to be injected instantaneously.

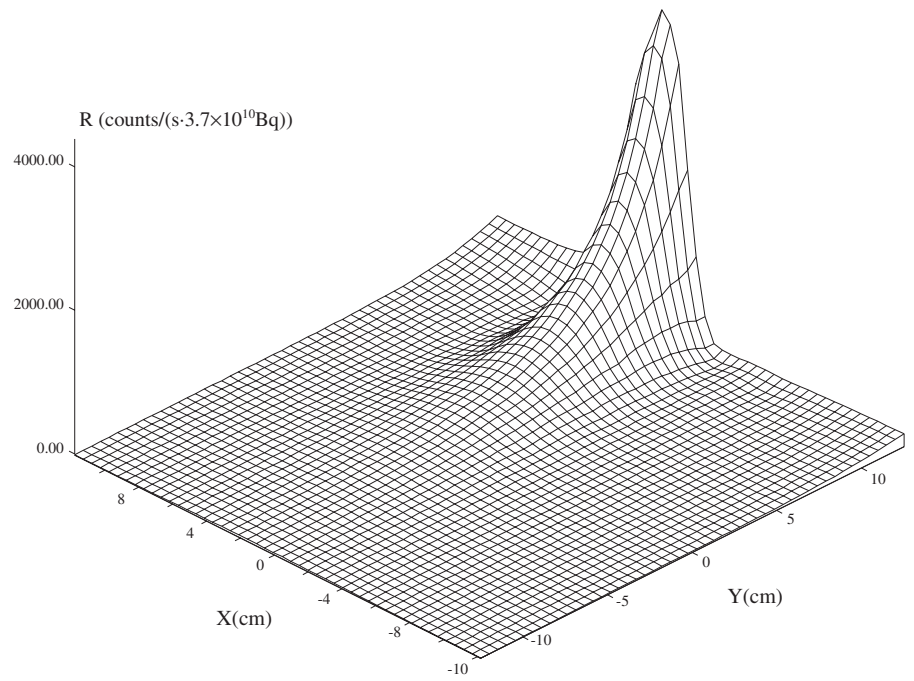

FIG. 13. Example of the distribution of contributions to count rate as a function of position.

In this figure we see that the maximum count rates are 6.8×10^7, 4.9×10^7 and 4.0×10^7 counts/s, respectively, for a 3.7×10^{10} Bq injection of ^{41}Ar. Therefore, if a 1% accuracy that corresponds to 10^4 counts/s is required at all the points, only 0.25 mCi (or 9.25 MBq) is required. Figure 14 also gives an indication of the transit time of the radioactive wave (about 1 s here). It should be noted that if injection is not instantaneous, the transit time will be longer and the maximum count rate lower (total count will be conserved). It would therefore be wise to increase this 0.25 mCi activity by some factor to be on the safe side.

This approach allows the amount of activity needed to achieve a certain accuracy to be predicted. It may, however, look rather paradoxical since it requires values for the velocity and the dispersion coefficient, which are precisely the quantities that can be measured in a tracer experiment. Yet the count rate versus time calculation is very simple, so that a parametric study can easily be made. As for the velocity, its order of magnitude is usually known; hence it is easy to calculate a range of likely values. In a few simple cases (such as the tube flow considered) it is possible to find in the literature correlations or probable values for the dispersion coefficient. Otherwise, one can try values corresponding to a low (2–5), average (10–20) or high (over 50) Péclet number, the dimensionless number defined as UL/D, where L is the distance from the injection. Although higher values are possible, they will result in sharper peaks, and consequently higher count rates, so that they do not need to be taken into account for a conservative estimate of the required activity.

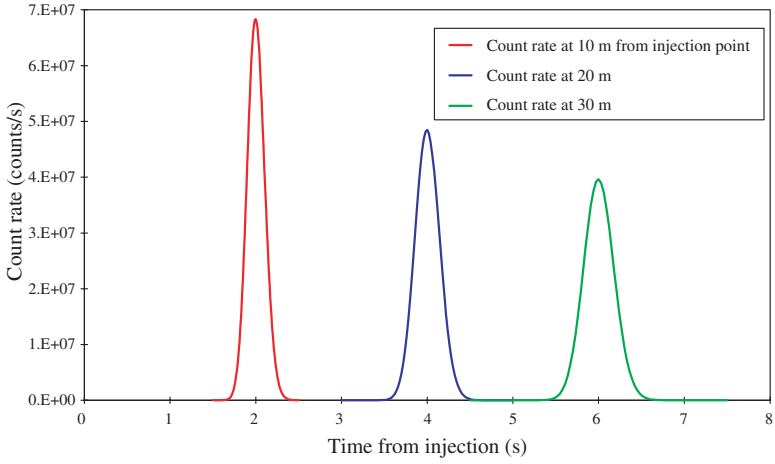

FIG. 14. Argon-41 test case: count rate versus distance from injection.

All these estimates rely on Monte Carlo simulations, but there is good evidence that they can be trusted in the conditions of a radiotracer experiment [22].

3.4.2.2. Influence of various parameters

In the previous section we have seen how to use Monte Carlo simulations to estimate the required activity for a given tracer and detector configuration. In this section, we illustrate (also through the use of Monte Carlo calculations) the influence of several parameters:

(a) Influence of the radiotracer

Suppose we want to trace the liquid and gas phases in our pipe flow experiment. For each phase various radioisotopes can be used. It is important to determine which ones are acceptable and what amount of activity is necessary.

Figures 15(a) and (b) illustrate the count rate per 3.7×10^{10} Bq/m^3 ($\dot{n}$ in the previous section) and the detector efficiency for a selection of radiotracers for gas and liquid phases from Ref. [10].

For the gas phase, ^{85}Kr is clearly not acceptable in spite of medium emission energy (514 keV) and reasonably good detector efficiency; this is due to the very low emission percentage (0.44%). Results for the other radioisotopes range from 2.3×10^{-6} (^{133}Xe) to 2.3×10^{-5} counts·s^{-1}·Bq^{-1}·m^3 (^{82}Br), mainly because of the differences in emission energy (81 and 550–1400 keV). Tracing the air phase with ^{133}Xe would therefore require about ten times as much activity as with ^{82}Br, while still remaining in the (acceptable) millicurie range. This is due to low attenuation in the fluid and the pipe walls (^{133}Xe is definitely not advisable in most industrial cases, as will be shown in the next example). High emission energy (^{41}Ar, 1.29 MeV) is not favourable for detector efficiency, because of the relatively small thickness of the scintillator.

Other considerations such as price, availability and physicochemical properties of the radioisotopes should of course be taken into account (e.g. ^{133}Xe is at the same time highly advantageous for its low price and low radiotoxicity but not quite suitable for our experiment since it is soluble in water). These considerations are not related to radiation detection and measurement and will therefore not be expounded here.

As regards the liquid phase, ^{51}Cr is handicapped by its low emission percentage (10%). Results for other isotopes are in the range 2×10^5 (^{38}Cl) to 3.3×10^{-5} counts·s^{-1}·Bq^{-1}·m^3 (^{82}Br), which would result in acceptable values for injected activity. Once again, low energy radioisotopes (^{99m}Tc, 141 keV) can be

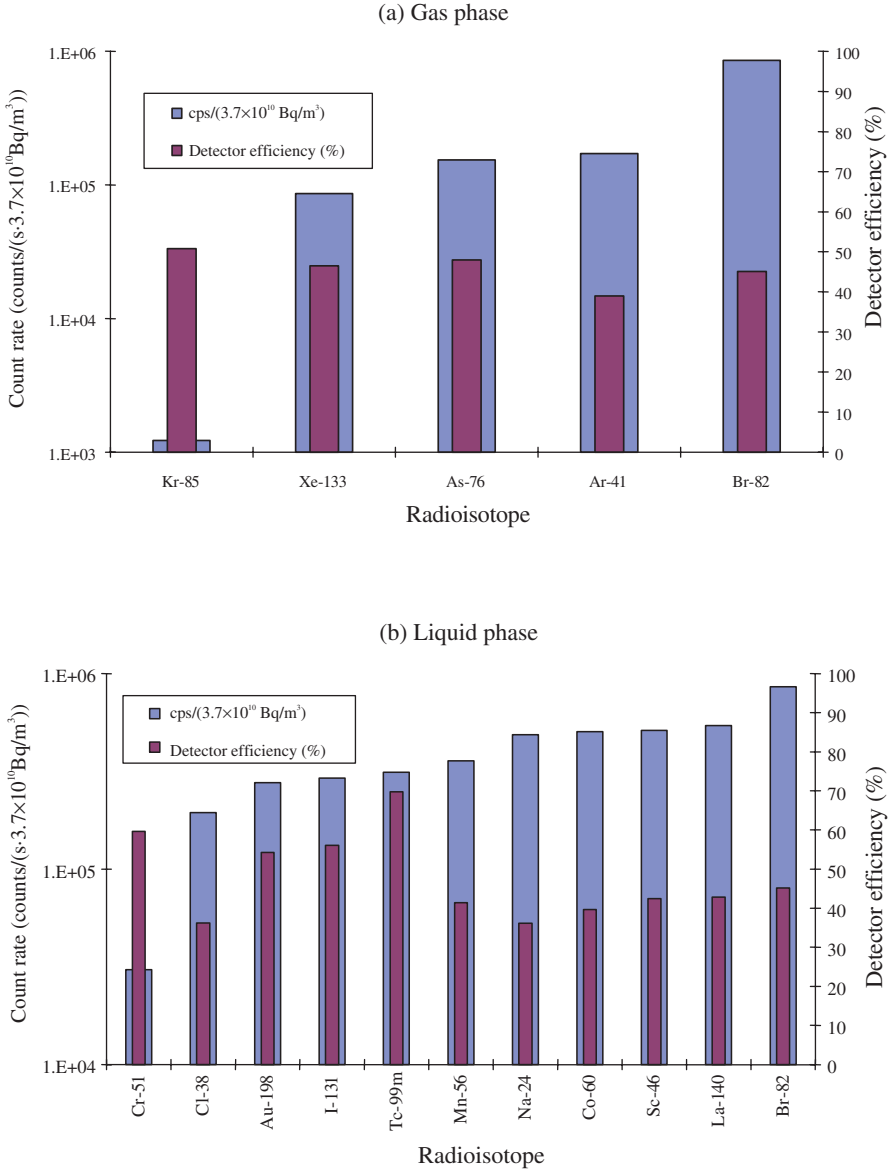

FIG. 15. Two phase flow measurement test cases ((a) gas phase, (b) liquid phase): influence of radioisotope selection.

used while high energy isotopes (e.g. ^{24}Na) result in degraded detector efficiency.

Tracer selection also has some impact on the space resolution of the detection chain, as illustrated in Fig. 16 in the case of low energy ^{133}Xe and high energy ^{41}Ar. This, however, has no visible consequence on the shape of the recorded signals, as shown in Fig. 17 (count rates are, predictably, much higher with ^{41}Ar) for a 3.7×10^{10} Bq injection.

(b) Influence of scintillator crystal nature and dimensions

In the same way, the influence of the nature and the dimensions (diameter and thickness) of the scintillator crystal on the count rate per 3.7×10^{10} Bq/m^3 and on the efficiency of the detection is illustrated in Fig. 18. The radioisotope is ^{41}Ar, with the scintillator crystal being either 1.5 in. (3.81 cm) in diameter by 2 in. (5.08 cm) in thickness or half that size, and either NaI(Tl) or bismuth germanium oxide (BGO).

Not surprisingly with this high energy tracer, efficiency is significantly better with thick crystals and BGO always performs better than NaI(Tl).

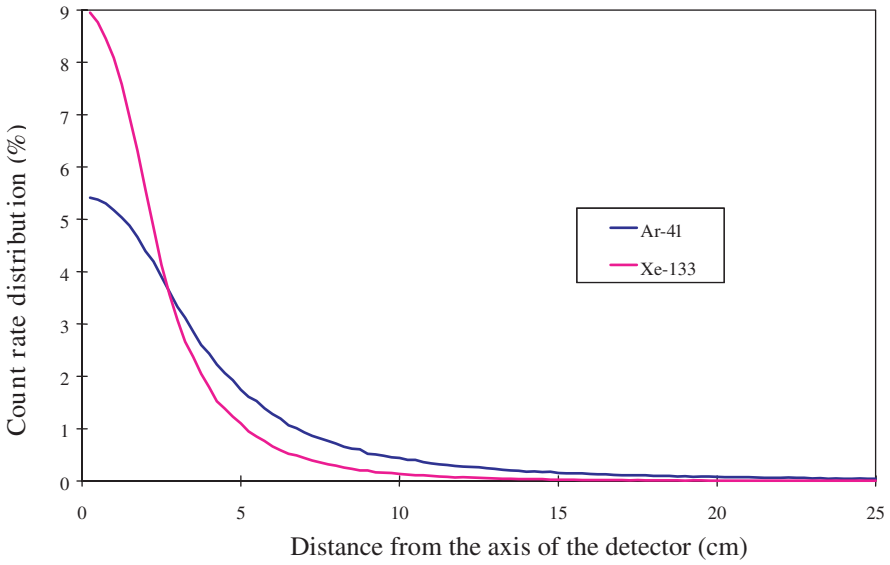

FIG. 16. Flow measurement test case: count rate distribution versus distance from the axis of the detector, for ^{41}Ar and ^{133}Xe.

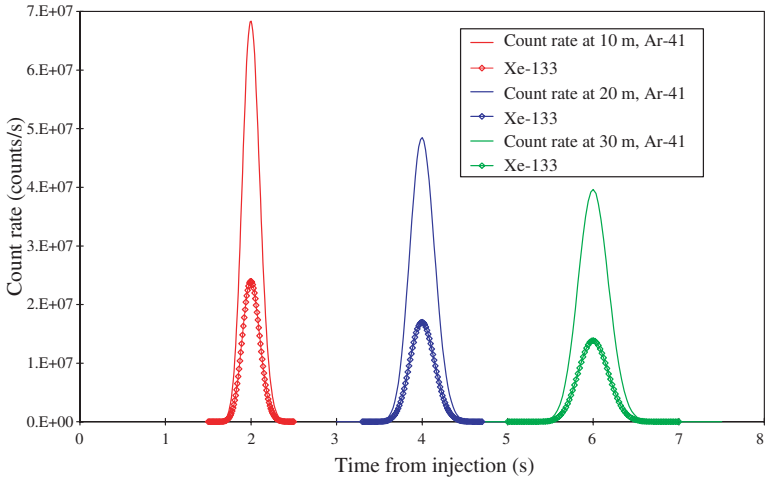

FIG. 17. Flow measurement test case: count rate versus time from injection for ^{41}Ar and ^{133}Xe.

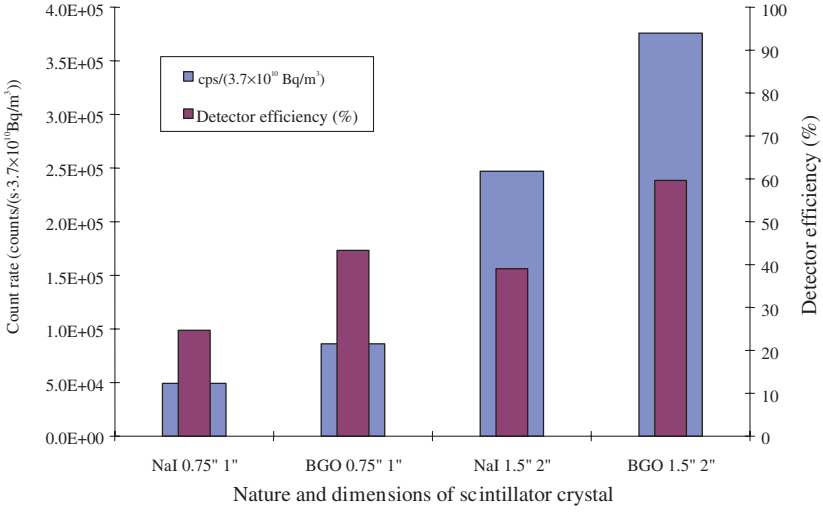

FIG. 18. Flow measurement test case: influence of scintillator crystal characteristics.

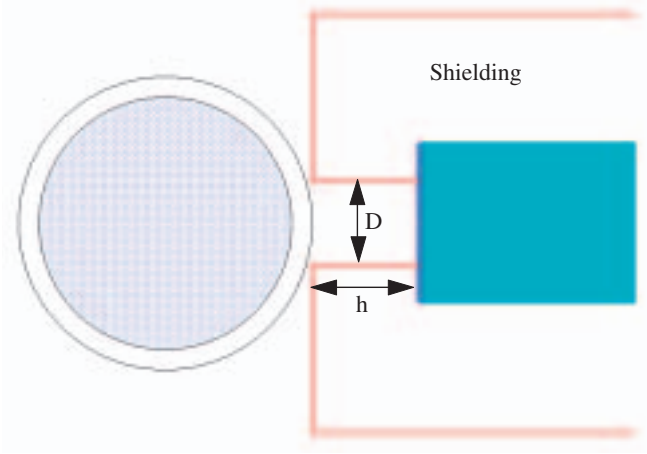

FIG. 19. Flow measurement test case: influence of shielding.

(c) Influence of shielding and collimating

We now investigate the effect of variations in collimating depth h and diameter D (Fig. 19; h was set to zero and D was equal to the diameter of the scintillator crystal). Increasing h or decreasing D improves the spatial resolution of the detector.

As illustrated in Fig. 20, increasing h (here from 0 to 2.5 and 5 cm) obviously decreases the count rate, for both low and high energy tracers (^{133}Xe and ^{41}Ar, respectively). In the case of ^{133}Xe, a depth of 5 cm leads to a very low count rate, about 2.4×10^{-6} counts·s^{-1}·Bq^{-1}·m^3, resulting in unacceptably high activity requirements. Detector efficiency is not reported here because it depends only marginally on collimating parameters.

The impact of collimating depth on spatial resolution is shown in Figs 21(a) and (b).

An increase in h does improve the sharpness of the count distribution in the case of low energy ^{133}Xe. This effect is more dubious in the case of ^{41}Ar, the photons of which are so energetic that they can reach the crystal through the lead shield, hence the long (and undesirable) tailing in the count distribution curves.

Finally, collimating depth is set at 2.5 cm and collimating diameter varied from 3.8 cm (or 1.5 in., i.e. the diameter of the scintillator crystal) to 2 cm and 1 cm. The effect on count rate is shown in Fig. 22.

In the case of ^{41}Ar, count rates are not very sensitive to collimator opening (the count rate at 1 cm is about one half of the count rate at full

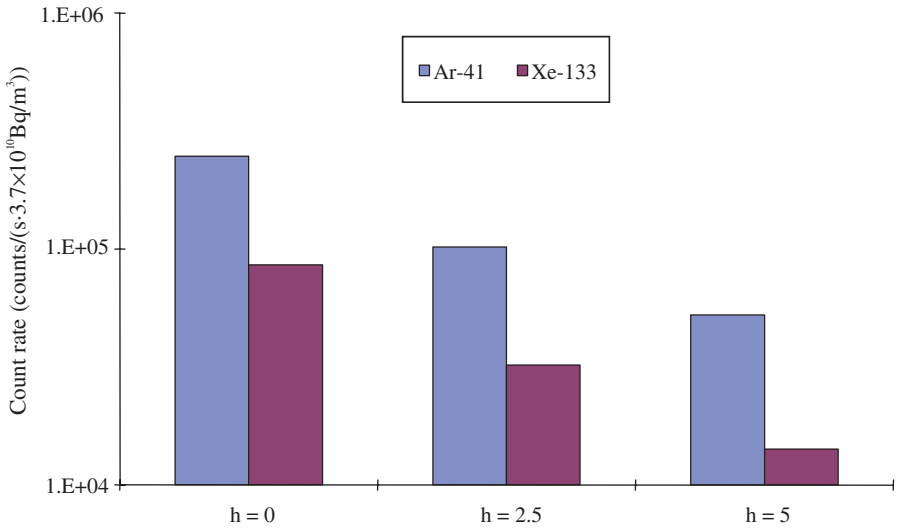

FIG. 20. Flow measurement test case: influence of collimating depth.

opening). This is due to the fact that a large proportion of the high energy photons reach the scintillator crystal through the lead shielding, which would have to be much thicker to be efficient. This results in a spatial distribution curve with even more spread than in the previous cases.

Low energy photons emitted by ^{133}Xe are effectively stopped by the shielding, resulting in good spatial resolution, as shown in Fig. 23. The drawback is a drastic drop in count rates, with a minimum of about 400 counts·s^{-1}·Ci^{-1}·m^3 with the sharpest collimation, resulting in large and impractical activity requirements.

3.4.3. Example 2: A radiotracer experiment in the industrial case

This example is based on a tracer experiment that was conducted on the quenching tower of an incinerator. Hot flue gasses enter the top of the tower at a temperature of about 1000°C. Cold water is supplied at some point along the tower to reduce mean gas temperature to 200°C. The problem was to monitor the flow of gas inside the tower. The height is about 10 m and the internal diameter 2.5 m. There is a 4–6 mm thick steel wall, thermally insulated by means of 24–30 cm of concrete. The flow rate is about 10^4 N·m^3/h. As in the pipe flow experiment, it will be shown how to estimate the necessary activity with a given tracer and detector configuration, and the influence of a few parameters on the count rate will be illustrated.

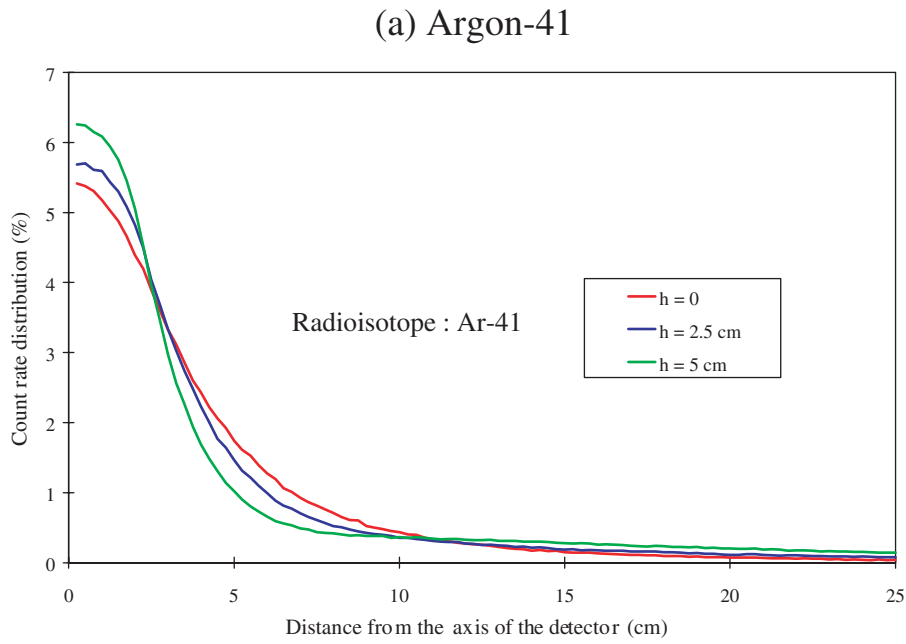

FIG. 21. Flow measurement: influence of collimating depth for (a) ^{41}Ar and (b) ^{133}Xe.

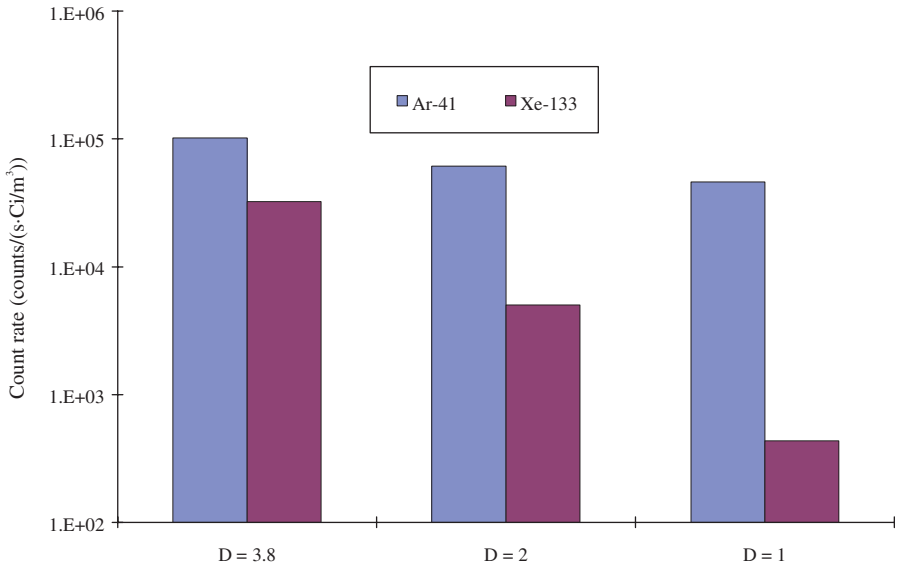

FIG. 22. Flow measurement test case: influence of collimating diameter.

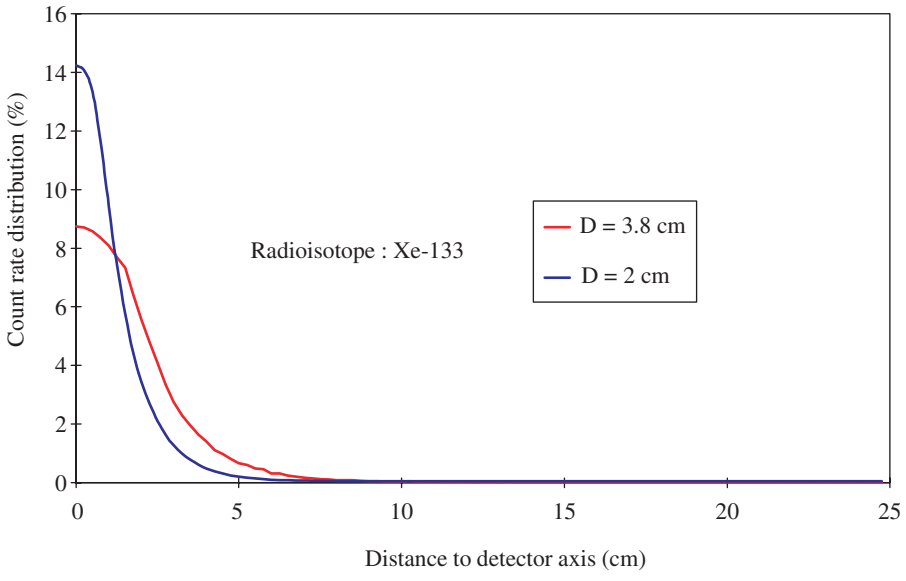

FIG. 23. Flow measurement test case: influence of collimating diameter for ^{133}Xe.

3.4.3.1. Required activity with ^{41}Ar

A reasonable choice for the radiotracer is ^{41}Ar, because it can be expected to remain inert in high temperature conditions and its radiation is energetic enough to be detected through thick concrete and steel walls. Once again we use 1.5 in. (3.81 cm) by 2 in. (5.08 cm) NaI(Tl) scintillators with 1 mm thick steel windows and 3 cm thick lead shielding (Fig. 24).

From the Monte Carlo simulation we obtain the following results:

(a) The count rate per curies per cubic metre is $\dot{n} = 2.5 \times 10^{-5}$ counts·s^{-1}·Bq^{-1}·m^3, which results in 67 000 counts for a 3.7×10^{10} Bq injection or a scant, but manageable, count of 670 for 370 MBq, the activity that was actually used. The detector efficiency is 53%, much higher than that in the pipe flow experiment, because most photons reach the detector after undergoing multiple interactions and therefore with low energies. This last point is visible on the detected spectrum (Fig. 25), where the 1.29 MeV ^{41}Ar peak is still visible, but the contribution from the lower energy part is more important than in the previous case.

(b) The spatial resolution is very poor, as shown in Fig. 26. This is due to the detection geometry and to the high proportion of indirect photons that reach the scintillator crystal. However, the spatial resolution could only

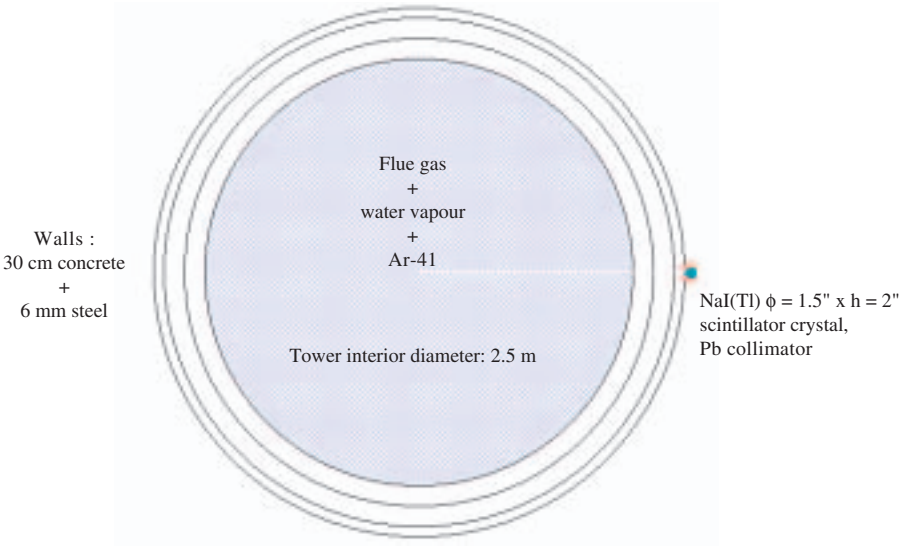

FIG. 24. Incinerator test case: configuration of the tracer test with ^{41}Ar.

be improved by heavy collimation, resulting in lower count rates that hardly seem practical.

(c) The count rate as a function of time can be predicted at given distances from the injection point, as shown in Fig. 27 (here at 5 and 10 m with velocity estimated at 3 m/s and with the Péclet number being taken as 10 and 20, respectively). Maximum count rates for a 370 MBq injection are acceptable though rather low (approximately 320 and 230, respectively). This order of magnitude is indeed close to the values recorded in the actual experiment.

3.4.3.2. Influence of various parameters

(a) Influence of the radiotracer

The count rate per 3.7×10^{10} Bq/m^3 and the detector efficiency for the same radiotracers as in the previous section (irrespective of their suitability for a high temperature experiment) are investigated here. The results are shown in Fig. 28.

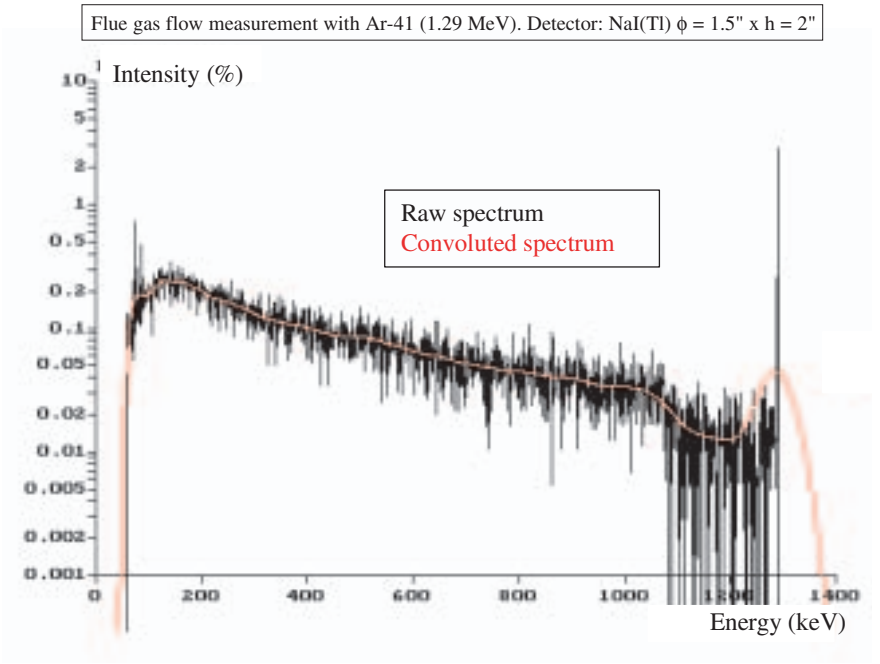

FIG. 25. Incinerator test case: raw and convoluted spectra.

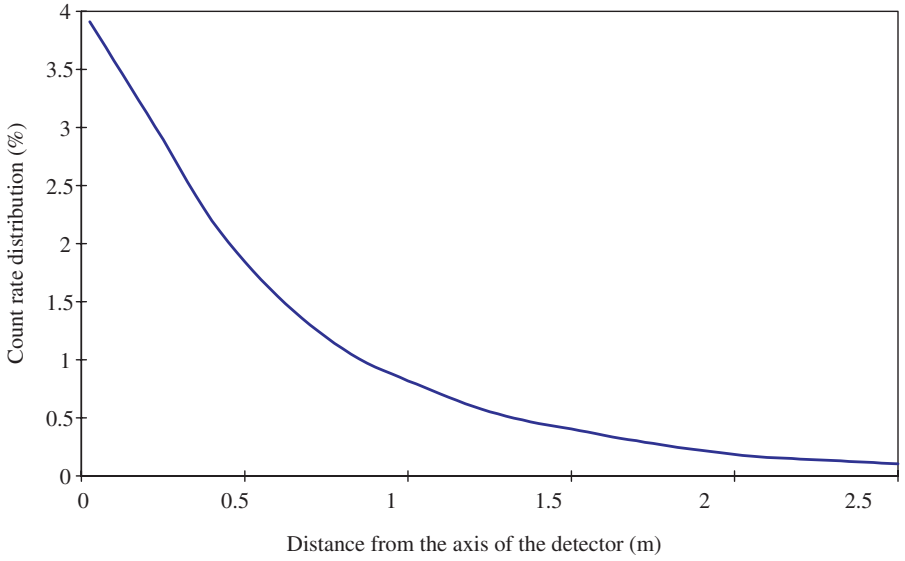

FIG. 26. Incinerator test case: count rate versus distance from the axis of the detector.

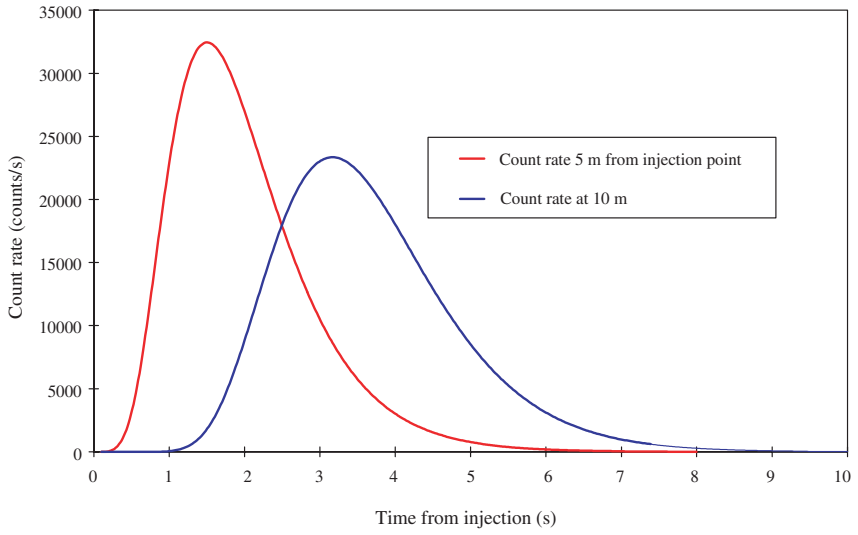

FIG. 27. Incinerator test case: count rate versus time from injection.

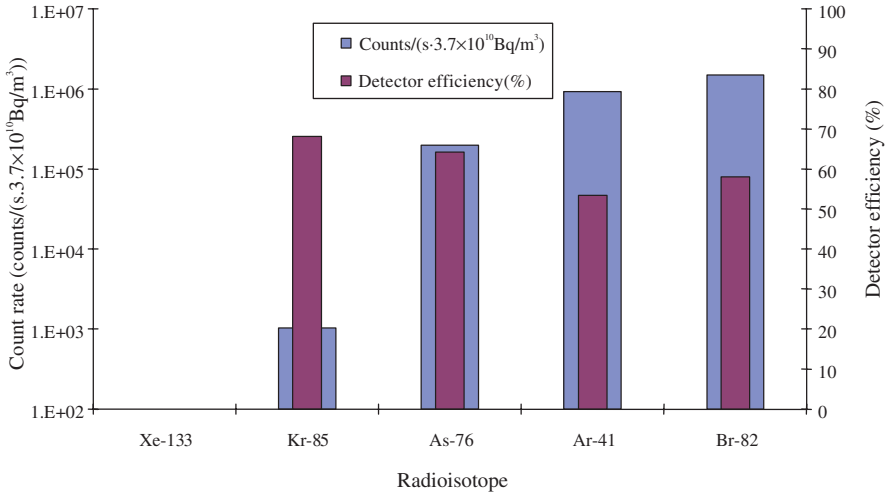

FIG. 28. Incinerator test case: influence of radioisotope.

Xenon-133 fails to produce any significant count rate, because of its low emission energy. Krypton-85, though better, has to be ruled out because of its low emission percentage. Argon-41 and ^{82}Br give the best count rates; ^{76}As would require about ten times as much activity to produce the same number of counts. As mentioned before, detector efficiency is fairly high in spite of the small scintillator thickness, owing to the wide energy spectrum of the incident photons.

(b) Influence of scintillator crystal nature and dimensions

Comparison is made again between NaI(Tl) and BGO crystals, with dimensions 1.5 in. (3.81 cm) by 2 in. (5.08 cm) or 0.75 in. (1.9 cm) by 1 in. (2.54 cm) (Fig. 29). The tracer used was ^{41}Ar.

A difference of almost one order of magnitude is observed between the small NaI and the large BGO scintillator crystals.

(c) Influence of wall thickness

The walls of the quenching tower vary in thickness as the temperature of the flue gases is reduced; the concrete shielding is first 30 cm, then 27 and 24 cm in thickness. The steel skin also gradually reduces to 4 mm in thickness. The effect is illustrated in Fig. 30, where an unrealistic 40% decrease is also

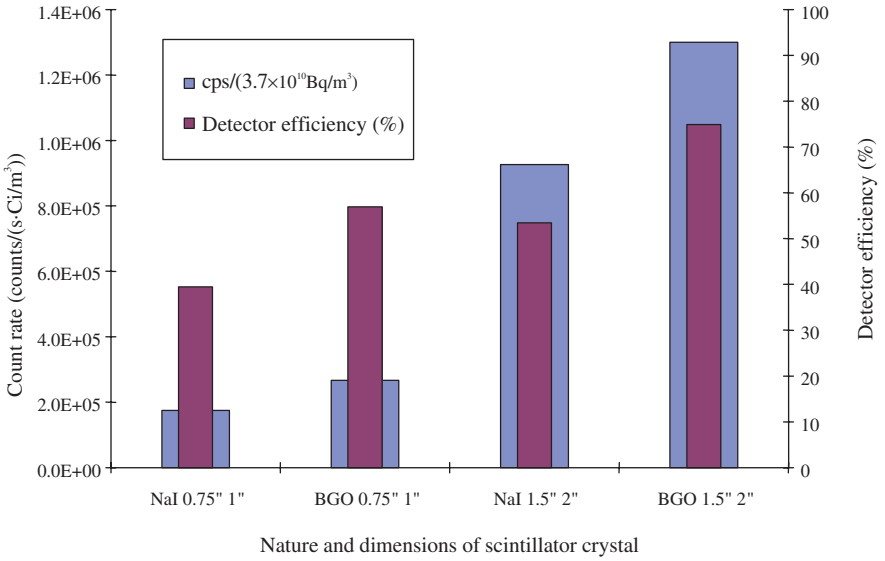

FIG. 29. Incinerator test case: influence of nature and dimensions of the scintillator crystal.

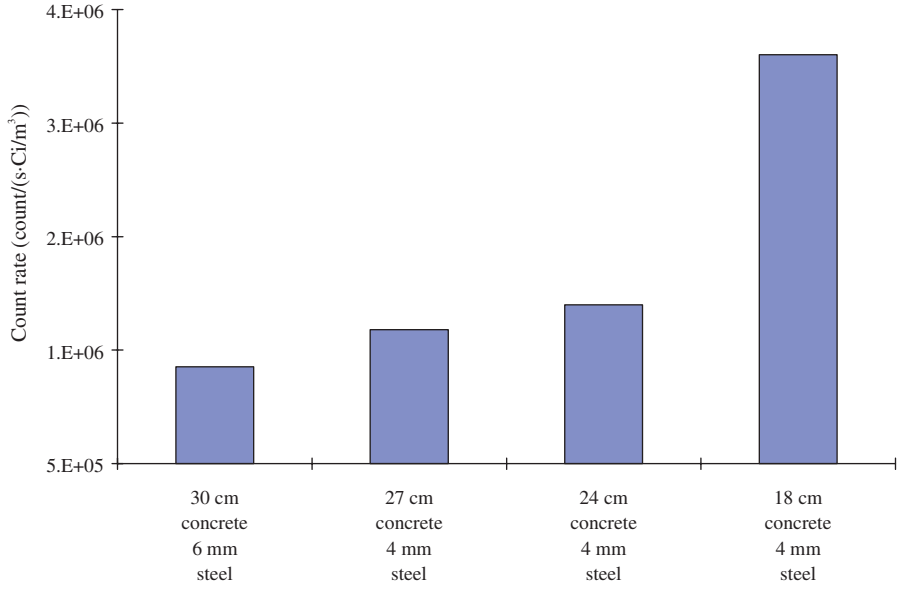

FIG. 30. Incinerator test case: influence of wall thickness.

included for the sake of illustration. It clearly appears that only the latter has a significant impact on the expected count rate. The tracer was again ^{41}Ar.

3.4.4. Detector positioning and protection

Figure 31 describes the general arrangement of detectors in the case of an FCC unit. Position, location and distance between the detectors depend on data requirements; they have to be optimized and discussed with process

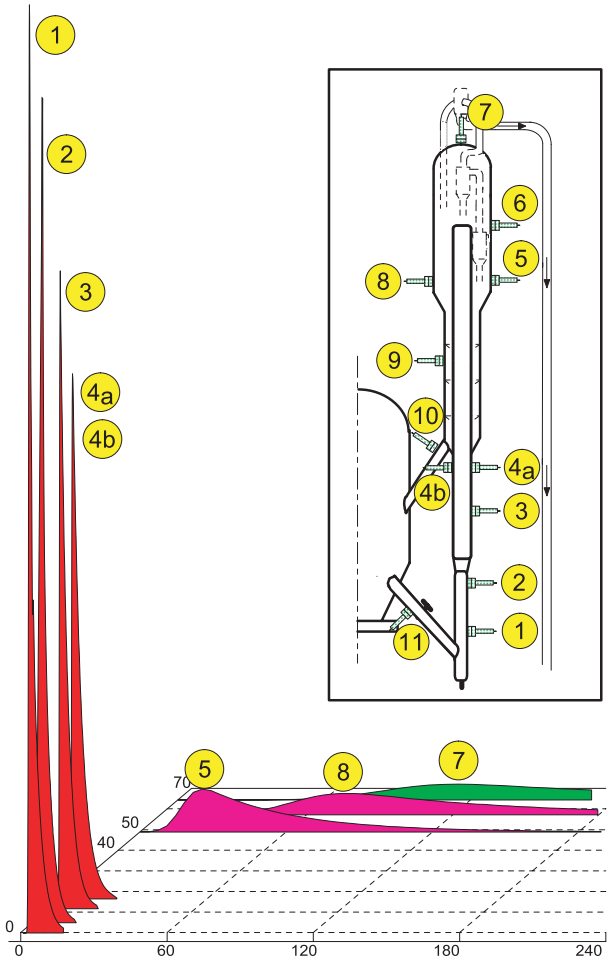

FIG. 31. General arrangement of detectors in an FCC plant tracer test. Results of a gas phase tracing with ^{41}Ar.

engineers. In this case, for instance, the experiment is designed for gas and catalyst tracer tests: the riser is surveyed with five detectors (detectors 1–5). Detectors 1–4 record the velocity and dispersion evolutions (which are directly correlated to reaction efficiency) in the first part of the riser. Detectors 4a and 4b are at the same level but on opposite sides: the aim is to survey any axial asymmetry in the velocity profile. Detectors 6 and 7 survey the gas behaviour from the end of the riser to the outlet of the FCC unit, while detectors 5–11 survey catalyst recycling. The FCC unit is thus divided into sections of interest. The readings from each detector can be seen as the inlet signal of a section and the outlet signal of the preceding one, when describing the unit from a systemic methodological point of view.

In Fig. 32 photographs are shown of a detector (NaI scintillator), with its collimator and heat insulator, positioned on the riser wall, and the data

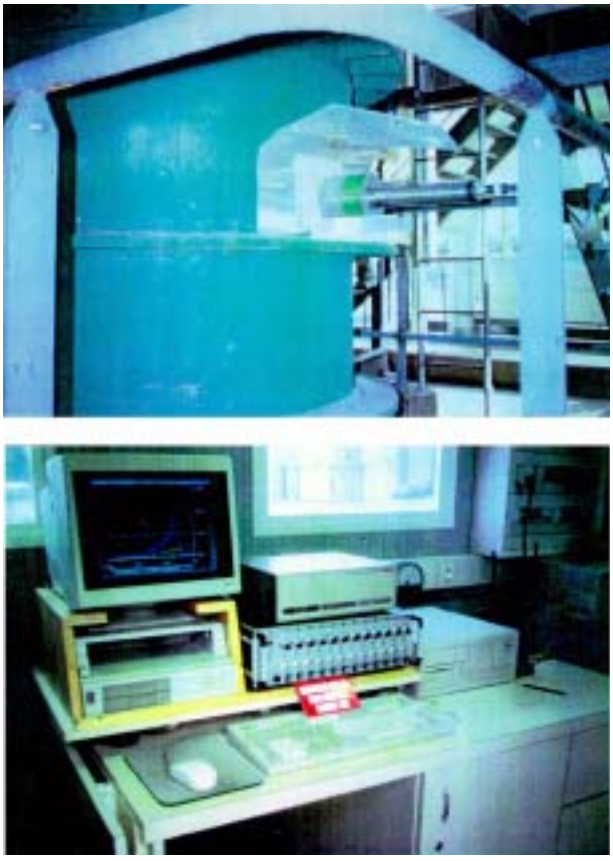

FIG. 32. Detector positioning and data acquisition in an FCC tracer test.

acquisition monitoring station. When dealing with high temperature conditions along a wall, as in the case of rotary kilns in the cement or mineral industry, the detectors are placed at minimum distances from the walls: the sensitive part of the detector is protected by heat insulation (Fig. 33), which is a modern alternative to conventional cooling by water circulation.

FIG. 33. Tracer test in a rotary kiln in the minerals industry. Heat protection of detectors.

3.4.5. Data acquisition

Owing to the widespread use of data acquisition systems in numerous fields (automation, electronics, etc.), it is possible to find up to date commercial applications of great quality (LabView from National Instruments, Austin, Texas; TestPoint from Keithley, Cleveland, Ohio). In this section some of the basic characteristics of a radiotracer data acquisition system are described.

It is advisable, in order to cover the largest number of situations (i.e. at least 90% of what is really required for conventional industrial applications), that this system should offer the possibility to treat a minimum of 12 measurement channels.

The measurements (counting) have to be simultaneous and the software should have three different blocks:

(1) For control of the good operational functioning of the probes.
(2) For data acquisition during the tracing experiment. For each probe it should be possible to define several (for example five) measurement phases. Each measurement phase is defined by its duration, and by the counting time ranging between 1 ms and 1 h. It should be emphasized that the measurements have to be simultaneous for all active channels. The software has to ensure archiving, basic treatment and visualization of the data. The dead time between two measurements should be less than 1 μs. The visualization of data should be as close as possible to 'real time' refreshment of the graphical window.
(3) For allowing the user to read and display archived data.

3.4.5.1. Data acquisition frequency

A compromise between a sufficiently high counting rate (statistical accuracy) and the necessity not to alter the fast flow dynamics by too much time averaging of the data results in the time between two consecutive measurements that defines the acquisition frequency. The characteristic time response of the data acquisition device is about 1 μs.

Quite often, signals rise sharply after the injection, then decay more slowly. A good strategy is therefore to perform acquisition in a series of phases:

(a) With high frequency acquisition (each 10 ms for example) during a small period of time (say 120 s), to capture the swift rise;
(b) With medium frequency acquisition (ranging from each 0.1 s to 5 s for instance) over a few minutes (up to 15 min for instance), to follow the gentler tailing;

(c) With low frequency acquisition (each 5 s to 2 min) during a long period (from 15 min to 48 h for instance), to make sure that the signal goes back to the baseline.

The system must be as user friendly as possible. Programming must be easy and upgradeable, as is now the case with object oriented languages.

3.5. DATA TREATMENT AND FILTERING

3.5.1. Basic principles and tools

Even in a carefully planned and executed tracer experiment some amount of treatment must be applied to the recorded signals before further analysis or modelling. The first obvious reason is that no signal is ever quite noise free. Another reason lies in the statistical character of radioactive detection: if the number of counts n is too small (because, for example, injected activity is too small, or counting time too short), the $1/\sqrt{n}$ statistical noise will blur out the useful signal. The 'see through' nature of gamma ray measurement is another potential source of trouble: unforeseen perturbations may be caused by the proximity of the injecting device or of the storage of spent fluid.

The aim of this section is therefore to present the basic procedures for preliminary data treatment. A general outline will be provided. Available tools will be listed. Real examples will then be given to illustrate the application of these procedures.

A proper treatment of radioactive tracer data can require up to nine successive stages, as illustrated in the flow chart (Fig. 34). The starting point is the data acquisition stage, the result of which is basically a set of count rate versus time values. At the end of the data treatment procedure these values are transformed into an area-normalized tracer restitution curve that can be processed by the methods presented in Section 3.6.

The order of the operations should be as logical as possible. There are, however, so many possible cases with radioactive tracing that it is perhaps not possible to give a procedure of universal validity. Rather, the aim is to make the reader understand the reasons for such and such treatments and their basic principles. Application to particular cases is then a matter of common sense. For example, it will be preferable to perform filtering before background corrections in the case of very noisy signals. As a matter of fact, only area normalization (step 9) is truly unavoidable prior to tracer response analysis and modelling. Some of the other steps may be omitted according to circumstances.

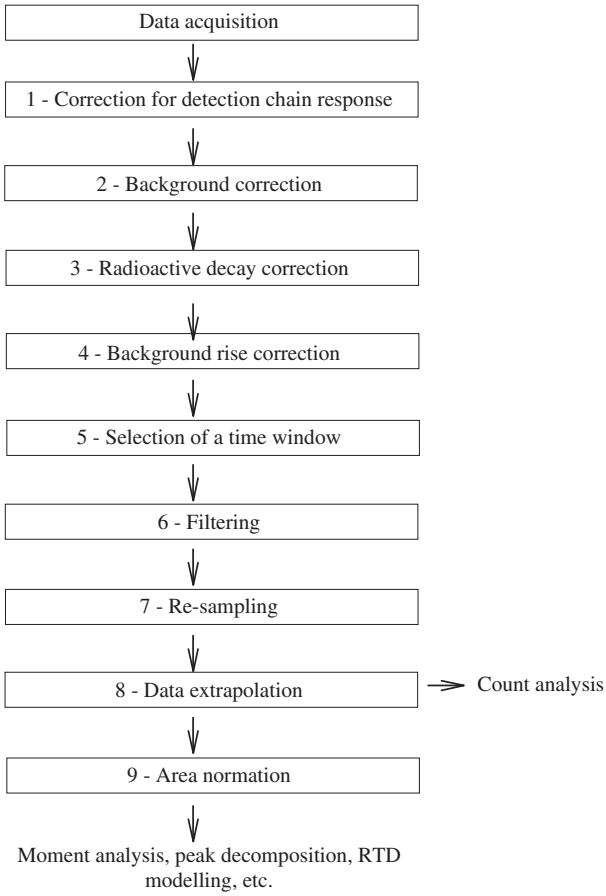

FIG. 34. Typical flow chart for data treatment.

Radiotracer practitioners have several software packages at their disposal. Many treatments can be performed with a spreadsheet program such as Microsoft Excel. More specialized software includes Peakfit [26] and RTD0 [15]. DTSPro [17] also offers some limited data treatment capabilities. Mathematical packages such as Mathematica [27] or Matlab [28] can also be useful, but their application to radiotracer data needs some programming and will not be discussed further. In Table 2 an attempt has been made to summarize the possibilities of these software programs.

TABLE 2. AVAILABLE SOFTWARE FOR DATA TREATMENT
(crosses indicate functions that software can carry out)

Treatment	Spreadsheet	RTD0	Peakfit	DTSPro
Detection chain response		×		
Background correction	×	×	×	×
Radioactive decay correction	×	×	×	×
Background rise correction		×	×	×
Selection of a time window	×	×	×	×
Filtering			×	
Resampling		×	×	
Data extrapolation	×	×		×
Area normalization	×	×	×	×

3.5.2. Application to selected examples

3.5.2.1. Correction for detection chain response

This step accounts for two different phenomena:

(1) Time constant correction

When analogue devices, such as count ratemeters which involve an integrating circuit with a resistor R and a capacitance C, are used for the measurement of tracer concentration, some loss of count may occur due to the time response of the integrating circuit. Therefore, a correction has to be applied. The relationship between net count rate $\dot{n}_{\mathrm{N}}(t)$ and measured count rate $\dot{n}_{\mathrm{m}}(t)$ is given by the following differential equation:

$$\dot{n}_{\mathrm{N}}(t) = \dot{n}_{\mathrm{m}}(t) + RC\frac{\mathrm{d}\dot{n}_{\mathrm{m}}(t)}{\mathrm{d}t}, \tag{18}$$

where the product RC is the time constant of the integrating device.

This operation amounts to deconvolving the measured signal $\dot{n}_{\mathrm{m}}(t)$ from a decaying exponential with time constant RC. It can be done through numerical evaluation of the time derivative $\mathrm{d}\dot{n}_{\mathrm{m}}(t)/\mathrm{d}t$ and direct application of Eq. (18) or by the methods presented in Section 3.6.1.

(2) Dead time correction

Nearly all detector systems have a minimum amount of time that must separate two gamma photons in order that they be recorded as two separate pulses. This minimum time delay may be due either to the physical detection process itself or to associated electronic devices. It is called the dead time of the counting system [14]. This phenomenon results in detector 'saturation', already mentioned in Section 3.2.3.

Two models for dead time behaviour are commonly used: paralysable and non-paralysable responses. In both cases, detection of one photon is followed by a dead time t in which no new event can be recorded. In the non-paralysable case, the detector is always apt to record a new photon after time t. In the paralysable case, the dead time is prolonged by t by each photon interaction occurring during the dead time period.

The relationship between the true photon interaction rate $\dot{n}_{\mathrm{t}}(t)$ and the recorded count rate $\dot{n}_{\mathrm{m}}(t)$ in the non-paralysable case is as follows:

$$\dot{n}_{\mathrm{t}}(t) = \frac{\dot{n}_{\mathrm{m}}(t)}{1 - \tau\, \dot{n}_{\mathrm{m}}(t)} \tag{19}$$

and in the paralysable case:

$$\dot{n}_{\mathrm{m}}(t) = \dot{n}_{\mathrm{t}}(t) \exp\left[-\tau\, \dot{n}_{\mathrm{t}}(t)\right]. \tag{20}$$

The latter expression is implicit with respect to $\dot{n}_{\mathrm{t}}(t)$, the quantity to be computed, and has therefore to be inverted numerically (mathematical packages like Mathematica are more than adequate).

These relations are illustrated in Fig. 35 for typical dead time values of 1 and 10 μs. Very high true count rates imply an actual decrease in recorded count rates in the case of a paralysable detector. With a dead time of 10 μs, the error is less than 10% up to the fairly large value of 10^4 counts/s.

The reader is referred to Ref. [14] for practical methods for measuring dead time.

Tools

RTD0 [15] accounts for time constant correction. The second case (dead time correction) can either be treated with a simple spreadsheet (non-

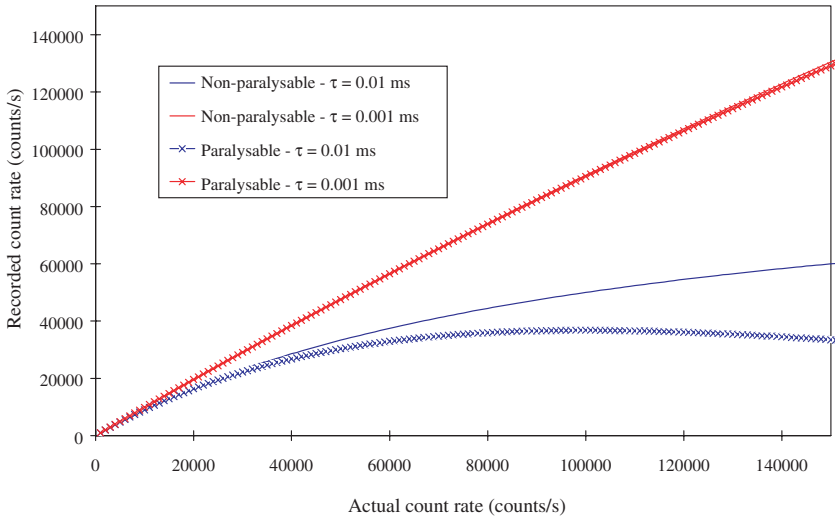

FIG. 35. Measured count rate versus actual count rate, non-paralysable and paralysable cases.

paralysable case) or requires the use of a mathematical package for the inversion of the paralysable detector response function.

3.5.2.2. Background correction

(a) Principle

This section refers to the background radiation level that exists independently of the tracer experiment (due, for example, to sources in nuclear gauges permanently mounted on the installation). Prior to the injection of tracer into the system, it is necessary to measure the background radiation level at the detection points under the same conditions as in the actual experiment.

It should be noted that correction for background level due to the tracer itself (if, for example, some tracer is stored in the vicinity of a detector) should be made after the correction for radioactive decay (Section 3.5.2.3), since that part of the background radiation obviously decays with the same rate as the net signal.

It is desirable to have 20–30 readings for the determination of background radiation level. The measured background radiation levels are subtracted from the experimental data. The net count rate $\dot{n}_{\mathrm{N}}(t)$ is given as:

$$\dot{n}_{\mathrm{N}}(t) = \dot{n}_{\mathrm{m}}(t) - \dot{n}_{\mathrm{bg}}, \tag{21}$$

where $\dot{n}_m(t)$ is the measured count rate and $\dot{n}_{bg}$ is the background count rate.

(b) Example

In the following example (Fig. 36), the first 35 readings are used to evaluate background level prior to the experiment (about 65 counts/s). The curve is shifted downwards accordingly. It can be seen that after the experiment the level of ambient radiation has increased considerably. This is in fact because spent fluid is stored in a tank near the detector. This problem will be accounted for later.

3.5.2.3. Radioactive decay correction

(a) Principle

Since radioisotope tracers decay exponentially with time, it is necessary to apply decay correction to the measured data (otherwise, more weight would unduly be given to early measurements). The decay corrected count rate $\dot{n}_c(t)$ is given as:

$$\dot{n}_c(t) = \dot{n}_m(t)\exp(\lambda t) = \dot{n}_m(t)\exp\left(\frac{0.693t}{T_{1/2}}\right), \quad (22)$$

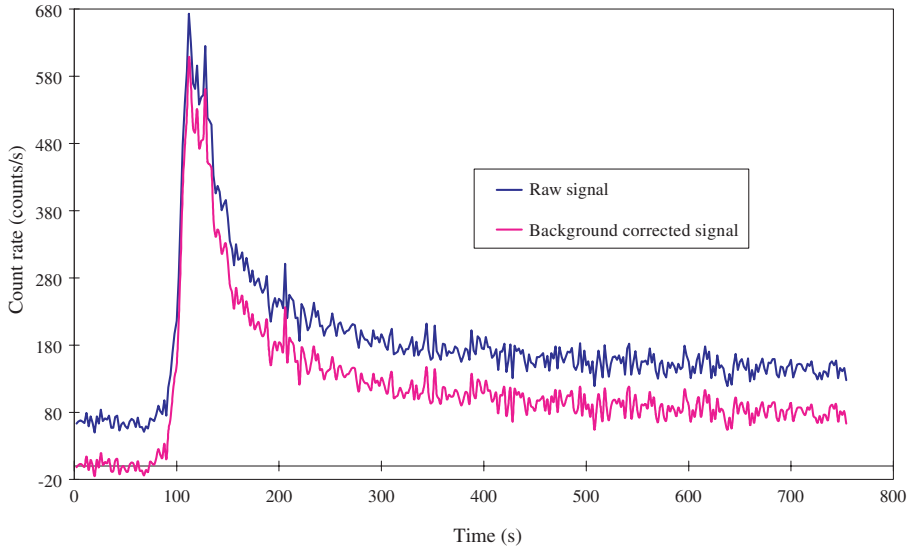

FIG. 36. Raw signal and background corrected signal.

TABLE 3. ERROR DUE TO RADIOACTIVE DECAY

Error $\left(\frac{\dot{n}_c}{\dot{n}_m} - 1\right)$ (%)	$\frac{t}{T_{1/2}}$ (%)
1	1.4
5	7.0
10	13.8

where λ is the decay constant, t is time and $T_{1/2}$ is the half-life of the radioisotope.

As an example, Table 3 indicates which percentage of $T_{1/2}$ error due to decay is 1, 5 or 10%.

(b) Example

In Fig. 37, the results of radioactive tracing with ^{113m}In (half-life 5970 s) are presented. Fluid is continuously recirculating in the system, which causes tracer to be homogeneously mixed after some time. The strong initial radiation

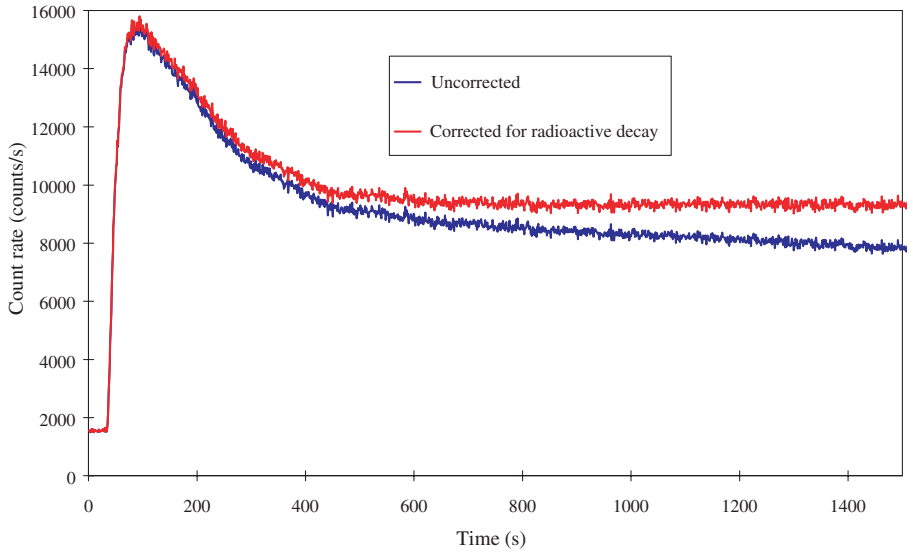

FIG. 37. Effect of the correction for radioactive decay with ^{113m}In.

level is due to tracer from a previous experiment (as explained in Section 3.5.2.2, it has not been subtracted before applying the decay correction). Before the decay correction is applied, one gets the wrong impression that the tracer concentration is decreasing at the end of the experiment, which might suggest some fresh fluid is somehow brought into the system. Applying a decay correction shows that the tracer concentration actually reaches a constant level.

3.5.2.4. Background rise correction

This section deals with the case when the count rate does not go back to zero at the end of the experiment (at this stage, i.e. after the correction for radioactive decay, initial count rate should have been set to zero). Two cases are possible:

(1) The shift in the baseline is due to cumulation of the tracer in the neighbourhood of the detector, as illustrated in Fig. 38. The relationship between measured signal $\dot{n}_{\mathrm{m}}(t)$ and unperturbed signal $\dot{n}_{\mathrm{t}}(t)$ is the following:

$$\dot{n}_{\mathrm{m}}(t) = \dot{n}_{\mathrm{t}}(t) + k\int_0^t \dot{n}_{\mathrm{t}}(u)\,\mathrm{d}u, \tag{23}$$

where the proportionality constant k expresses the strength of the coupling between accumulated tracer and detector.

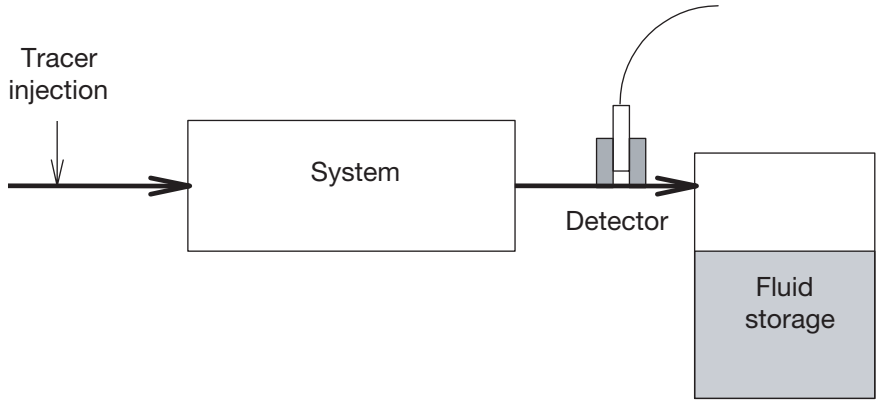

FIG. 38. Perturbation due to the storage of spent fluid.

Thyn [16] proposed an elegant analytical solution for this problem, of the form:

$$\dot{n}_t(t) = \dot{n}_m(t) - k\dot{n}_m(t) * \exp(-kt), \tag{24}$$

where asterisks denote the convolution product (defined in Section 3.6.1).

(2) The second case is when the reason for the background rise is not precisely known (drift in electronics or some other reason) or when no model is available. In that case, different shapes for the baseline (linear, quadratic, exponential, etc.) should be tried to see which gives the best fit with those points that are supposed to correspond to zero count rate.

(a) Examples

In the first example (Fig. 39), the rise in background level was known to be due to the accumulation of tracer near a detector and Thyn's correction was applied. Figure 39 shows original data and the effect of the parameter *k* on the shape of the baseline (large *k* means the influence of accumulated tracer on the detector is strong).

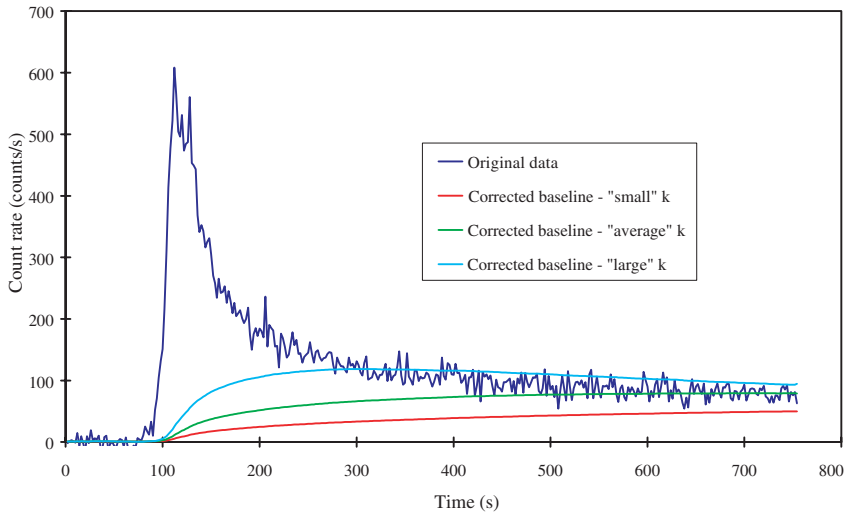

FIG. 39. Correction for background rise.

Therefore, a criterion has to be chosen for k. The one suggested by Thyn et al. [15] seems to be a good choice:

$$k = \frac{\dot{n}_{\mathrm{m}}^{\infty}}{\int_0^{t_{\max}} \dot{n}_{\mathrm{m}}(u)\,\mathrm{d}u}, \tag{25}$$

where $\dot{n}_{\mathrm{m}}^{\infty}$ is the steady state count rate measured at the end of the experiment and $t_{\max}$ is the duration of the experiment. The corrected curve is shown in Fig. 40.

In the second example (Fig. 41) the drift in background radiation level was due to some tracer becoming trapped inside the injection line and influencing the neighbouring detectors. The shape of the baseline could therefore be assumed to be very steep at the beginning, and then almost flat. This shape could be approximately reconstructed using Peakfit's logarithmic baseline option.

(b) Tools

Spreadsheets can be used for some baseline fitting although they are not very practical. DTSPro can do some simple (linear) baseline corrections. Peakfit allows a user friendly choice of the baseline points and offers many

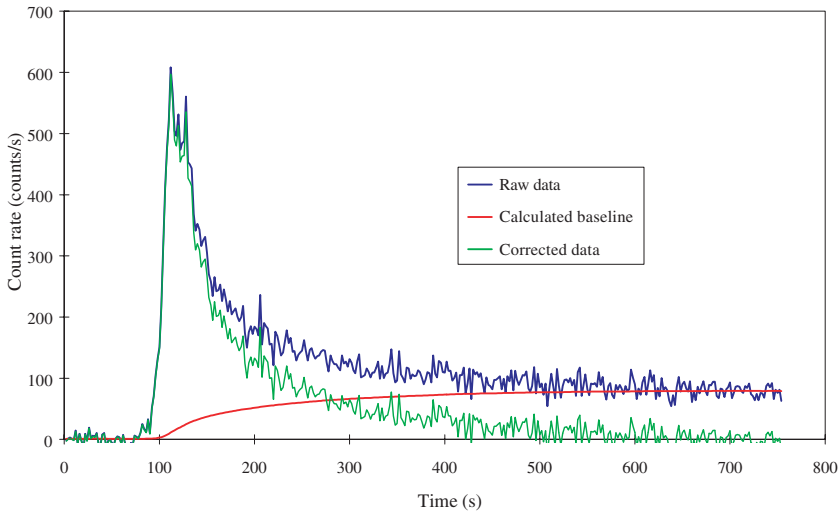

FIG. 40. Correction for background rise (first example).

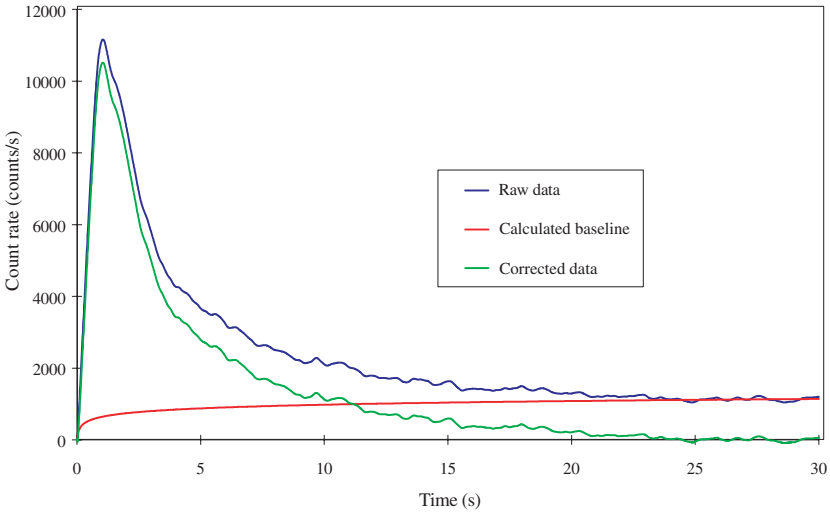

FIG. 41. Correction for background rise (second example).

options. RTD0 is the only software package with an 'accumulated tracer' correction capability.

At this stage, all effects linked to background radiation should have been eliminated, i.e. the signal should start from zero count rate and return to zero count rate (except in the case when the end of the signal has not been measured, which is treated in Section 3.5.2.8). Because of fluctuations, negative count rates always appear at the beginning and end of the curves. It is often tempting to set these negative count rates to zero, on the reasonable grounds that count rate is basically a positive quantity. We believe that this temptation should be resisted because suppressing negative counts will alter the frequency spectrum of the signal and therefore may cause undesired effects if a Fourier transform is to be applied. In addition, this will artificially give increased weight to the tail of the curve, which may be a problem when computing statistical moments.

3.5.2.5. Selection of a time window

(a) Principle

The duration of a tracer wave at a particular location is in general not precisely known. The operator will, with good reason, tend to overestimate that duration when programming the data acquisition system. On the other hand,

some delay may occur between launching of data acquisition and actual injection of tracer. For both reasons a number of useless data points will result at the beginning or at the end of data acquisition. Selection of the time window consists in discarding these points, that is to say in selecting only the period of time in which significant results are obtained. Sometimes it is also desirable to shift the time origin to the beginning of the new data set.

This operation will reduce computer workload for further data treatment. Suppression of useless data points at large times may also improve precision in the computation of the first and second moments.

If several data sets are to be treated in pairs (e.g. because one wants to deconvolve one data set by another), care should be taken to select a common time window for the two sets. This operation can be renewed at different stages in the data treatment procedure: some points can be eliminated at the very beginning, while keeping a certain number of baseline points to process background correction. These baseline points can be discarded after that correction has been made.

(b) Tools

Peakfit allows interactive selection of the data points and is very convenient for that operation. Otherwise, any spreadsheet program (or even any text editor if ASCII data files are used) will suffice.

3.5.2.6. Filtering

(a) Principle

The aim of filtering is to eliminate, or at least decrease, fluctuations due to counting statistics or electronic noise. In some cases, filtering allows useful data to be extracted from statistical noise, as will be illustrated later.

Several methods are available. First and foremost, the Fourier transform can be used to compute the signal frequency spectrum and undesired (usually high frequency) components can be eliminated. This method is very effective; Fourier transformation, however, requires that the data be sampled at regular time intervals, i.e. that counting time be constant. Other algorithms (e.g. the Loess algorithm) allow a variable counting time.

Radioactive measurements also offer the simple and attractive possibility to cumulate counts. Consider a series of N count rates $\dot{n}_i$ with constant counting time Δt:

Time	Count rate	Count
$t_1 = \Delta t$	$\dot{n}_1$	$\dot{n}_1 \Delta t$
$t_2 = 2\Delta t$	$\dot{n}_2$	$\dot{n}_2 \Delta t$
⋮	⋮	⋮
$t_N = N\Delta t$	$\dot{n}_N$	$\dot{n}_N \Delta t.$

It is possible to accumulate counts by series of p values, that is to say to replace the original data set by the following (for simplicity, N is assumed to be a multiple of p):

Time	Count rate	Count
$T_1 = p\Delta t$	$\dfrac{\dot{n}_1 + \dot{n}_2 + \ldots + \dot{n}_p}{p}$	$\dot{n}_1 \Delta t + \dot{n}_2 \Delta t + \ldots + \dot{n}_p \Delta t$
$T_2 = 2p\Delta t$	$\dfrac{\dot{n}_{p+1} + \dot{n}_{p+2} + \ldots + \dot{n}_{2p}}{p}$	$\dot{n}_{p+1} \Delta t + \dot{n}_{p+2} \Delta t + \ldots + \dot{n}_{2p} \Delta t$
⋮	⋮	⋮
$T_{N'} = N\Delta t$	$\dfrac{\dot{n}_{N-p+1} + \dot{n}_{N-p+2} + \ldots + \dot{n}_N}{p}$	$\dot{n}_{N-p+1} \Delta t + \dot{n}_{N-p+2} \Delta t + \ldots + \dot{n}_N \Delta t.$

This transformation strictly amounts to changing the counting time from Δt to $p\Delta t$, thereby decreasing relative uncertainty by a factor of $\sqrt{p}$ (this result can be proved in a rigorous way by calculating the variances of the initial and processed data using Poisson statistics).

Whatever method is chosen for data filtering, care should be taken not to distort the essential features of the signal, as illustrated below.

(b) Examples

The first example (Fig. 42) shows filtering of reasonably 'clean' data by the use of a Fourier transform. More components (50, 80, 90, 95 and 97.5%) are

eliminated from the frequency spectrum, starting from the high frequency end. The results are shown by the graphs in Fig. 42.

Fourier transform filtering is quite efficient; many high frequency components can be filtered away without altering the general shape of the data curve. However, some kind of compromise has to be found so as not to alter the significant features in the data. For example, if the indentation at the top of the peak is thought important in these data, at least 20% of the frequency components should be kept.

The second example (Fig. 43) shows how seemingly unusable data can be exploited by count cumulation. It should be noted that the original data set is too noisy to allow for background level correction, which can only be done after some amount of filtering. Points are cumulated in groups of 5, 25 and 100.

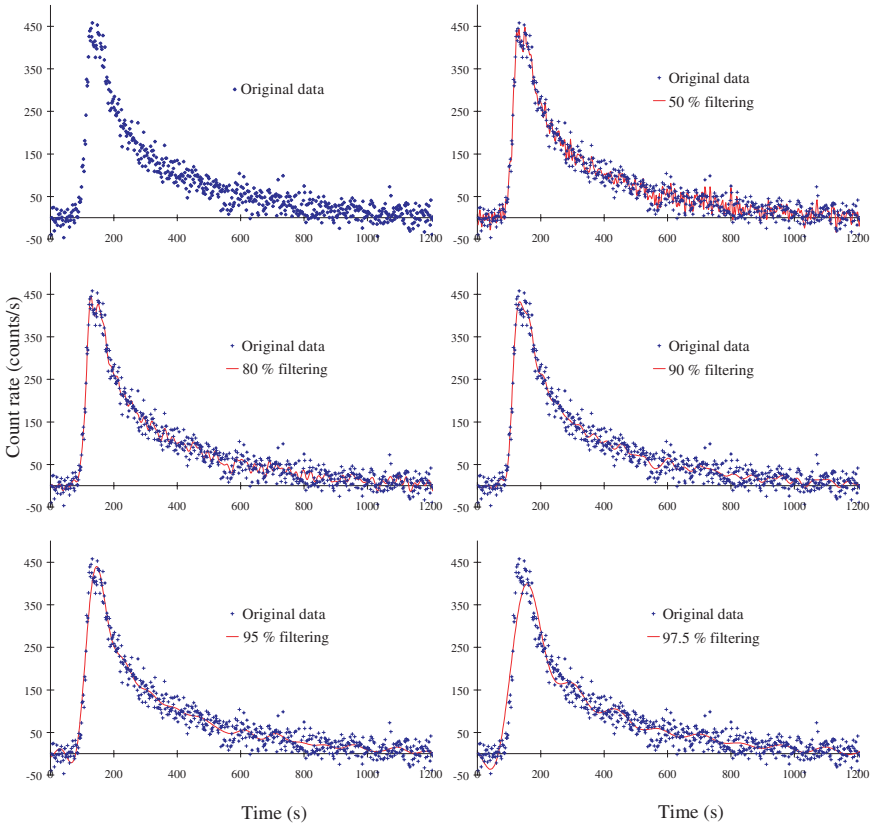

FIG. 42. Effect of Fourier transform filtering.

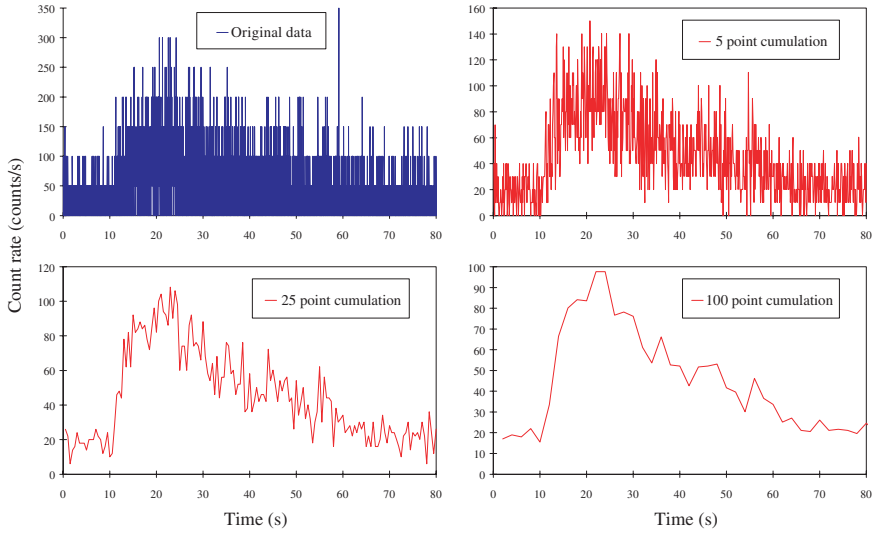

FIG. 43. Filtering by count cumulation.

Once again, the optimum between smoothness and time resolution of filtered data has to be found.

The same kind of result could also be obtained by Fourier transform filtering.

(c) Tools

The use of Peakfit for data filtering is very efficient and user friendly. Peakfit allows interactive Fourier transform filtering and has several other efficient algorithms, with the possibility to work with unequally spaced data (Loess), as shown in Fig. 44.

3.5.2.7. Resampling

There can be two main reasons why data should be resampled:

(1) The data set is too large to be comfortably processed and there is therefore a need to reduce the number of points.
(2) The counting time is not constant, which is not allowed with certain data treatment or modelling software (e.g. DTSPro).

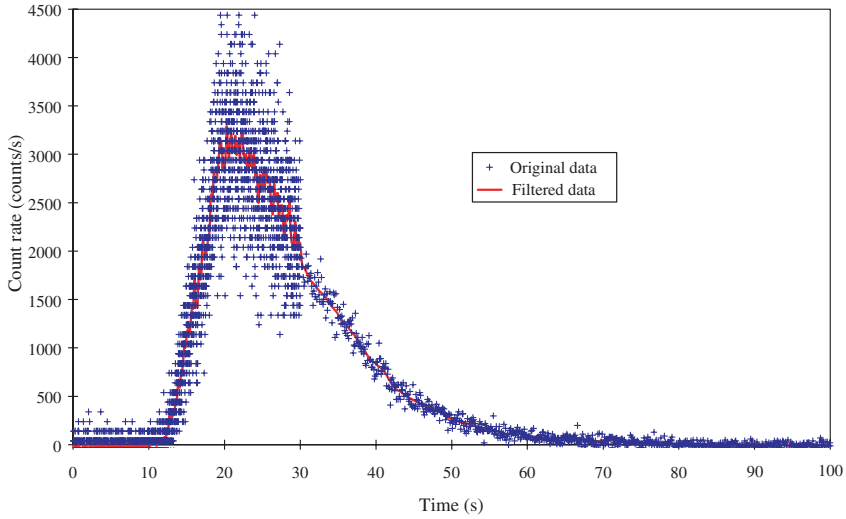

FIG. 44. Filtering of unequally spaced data.

Another reason might be that one needs to have 2^n (128, 256, 512) points, because one wants to use an old fashioned fast Fourier transform (FFT) algorithm, like the one in older versions of the DTS program (DTS 3.2 and earlier).

Resampling can be done by any adequate interpolation method. Peakfit, for example, offers linear and quadratic interpolation routines. Mathematical packages also propose many options. If the number of points is to be downsized, care should once again be taken to preserve the main features of the data (e.g. the peak heights).

The count cumulation technique, presented in Section 3.5.2.6, is also a simple and effective method to reduce the number of data points, or to set the counting time constant. In the following example, the counting time was set to 10 ms for the first 30 s of the experiment, and to 100 ms later. The idea was to have a higher time resolution to capture the beginning of the tracer wave, but this proved to be useless. Cumulating the 3000 first data points in groups of ten amounts to increasing the counting time to a uniform value of 10 ms and diminishes statistical fluctuations, as shown in Fig. 45.

3.5.2.8. Data extrapolation

(a) Principle

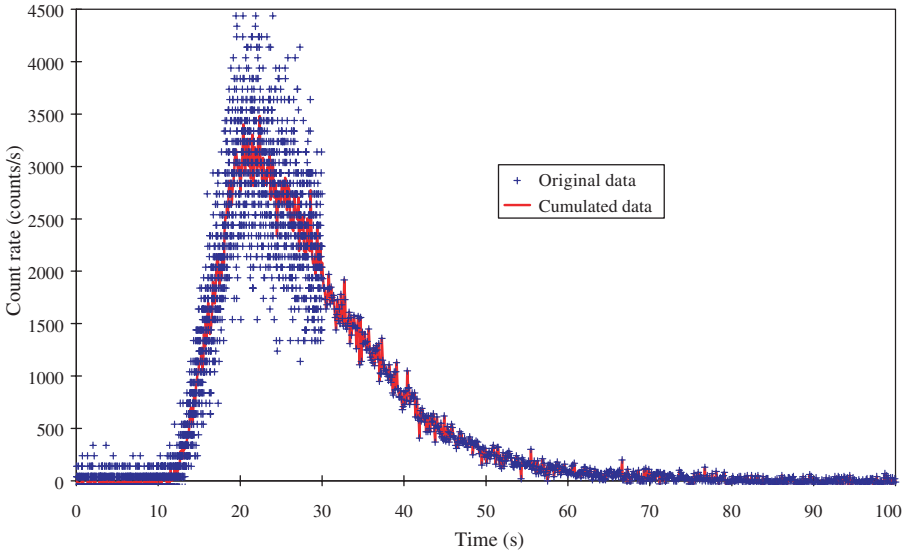

FIG. 45. Resampling by count cumulation.

Data extrapolation is needed when the end of the tracer wave is missed, or, in other words, count rates go back to zero after the end of the data acquisition sequence, as illustrated in Fig. 46.

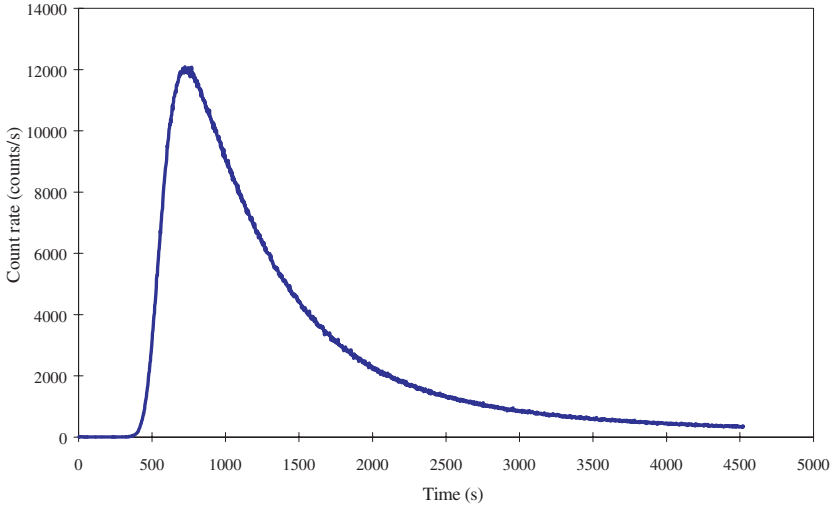

FIG. 46. Incomplete curve from a tracer experiment.

Before extrapolating, one should be sure that non-zero values at the end of the curve are actually due to an early termination of data acquisition and not to some interference with spent tracer (in this example, count rates were monitored some time after the end of data acquisition and found to be back to zero).

The aim of data extrapolation is to extend the tracer curve in some plausible way. The most common procedure is to check that the count rates decrease exponentially at the end of the experiment; this is easily done by plotting the logarithm of count rate versus time, which should exhibit a linear behaviour towards the end (Fig. 47).

A decaying exponential function should then be adjusted on that part of the curve, and the data extended with this function until the count rates are small enough to be neglected (Fig. 48).

The number of extrapolated points should obviously be reasonable (the meaning of 'reasonable' depends very much on the data available and the level of precision desired). From a practical point of view, the contributions of the extrapolated part to the zero, first and second order moments are given in Table 4.

In our example, the contributions in terms of total count number (zero order moment), first order moment (MRT) and variance (centred second order moment) are given in Table 5.

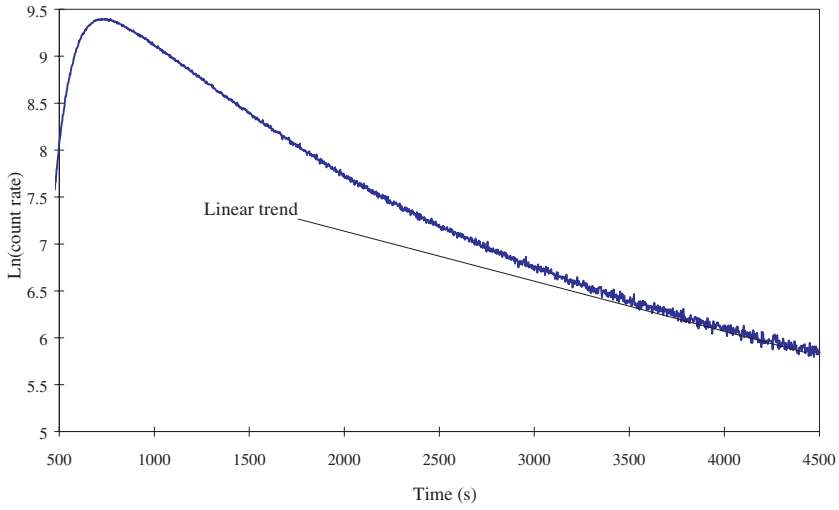

FIG. 47. Exponential decay of a tracer curve.

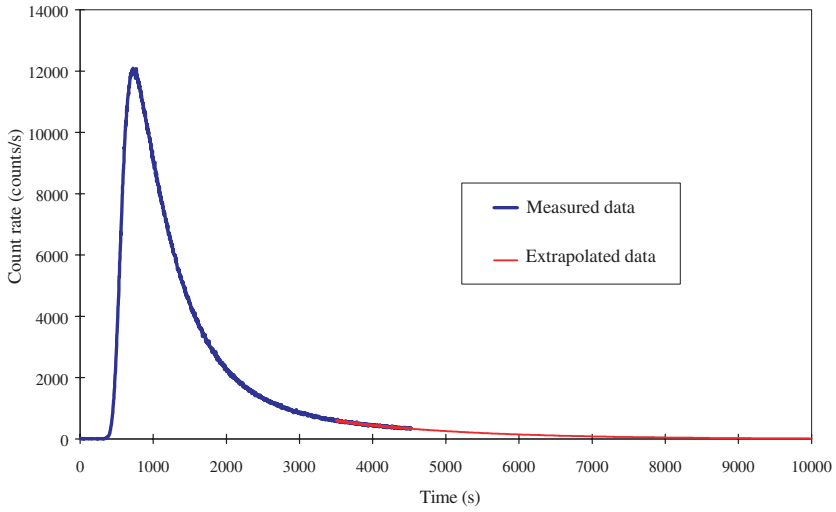

FIG. 48. Extrapolation of a tracer curve with decaying exponential.

The contribution of extrapolated data to the second moment, and to a fortiori higher order moments, can be very high. The values for these high order moments should therefore be taken very cautiously.

TABLE 4. CONTRIBUTION OF EXTRAPOLATED CURVE TAIL TO MOMENTS

Extrapolation function	$C_1 \exp\left(-\frac{t}{\tau}\right)$, from $t = t_1$ to $t = \infty$
Zero order moment	$\int_{t_1}^{\infty} C_1 \exp\left(-\frac{t}{\tau}\right) \mathrm{d}t = C_1 \tau \exp\left(-\frac{t_1}{\tau}\right)$
First order moment	$\int_{t_1}^{\infty} t C_1 \exp\left(-\frac{t}{\tau}\right) \mathrm{d}t = C_1 \tau \left(t_1 + \tau\right) \exp\left(-\frac{t_1}{\tau}\right)$
Second order moment	$\int_{t_1}^{\infty} t^2 C_1 \exp\left(-\frac{t}{\tau}\right) \mathrm{d}t = C_1 \tau \left(t_1^2 + 2t_1\tau + 2\tau^2\right) \exp\left(-\frac{t_1}{\tau}\right)$

TABLE 5. ERROR PERCENTAGES IN EXAMPLE CONSIDERED

Quantity	Without extrapolation	With extrapolation	Percentage difference
Total count	1.22×10^7	1.28×10^7	4.7
MRT (s)	1392	1624	17
Variance (s^2)	6.86×10^5	1.89×10^6	180

(b) Tools

Data extrapolation can easily be done with a spreadsheet program. DTSPro allows extrapolation with a decaying exponential. RTD0 offers the extra possibility of a $1/t^3$ prolongation, which is the exact solution for the RTD pipe flow with a laminar velocity profile.

3.5.2.9. Area normalization

After all the previous corrections have been made, it is possible to exploit the data by time analysis or count numbers analysis. These methods provide valuable information on, for example, arrival time, modal time and transit time, on the one hand, and dilution, flow rates, flow maldistributions and tracer mass balance on the other.

One final operation, area normalization, can then be performed. This operation has several benefits. Firstly, the influence of all the factors that affect the area of the curves but not their shape (injected activity and radiation attenuation by walls) is eliminated. It is then possible to compare the readings from two experiments with different injected activities or at two points with different wall thicknesses. Secondly, the calculation of moments is simpler with area normalized data. Thirdly, area normalized curves are in certain cases RTD curves, which have a precise meaning in terms of fluid population balance.

Area normalization is compulsory when adjusting a model with software such as DTSPro (models in DTSPro are area normalized by construction).

The tracer concentration curve is normalized by dividing each data point by the area under the curve (i.e. the total count number):

$$E(t) = \frac{\dot{n}_c(t)}{\int_0^\infty \dot{n}_c(t)\,\mathrm{d}t}, \tag{26}$$

where $\dot{n}_c(t)$ is the corrected count rate (i.e. the result of all the previous operations) and $E(t)$ is the normalized data function.

Since count rates are actually known at discrete intervals Δt, values of the function $E(t)$ can only be calculated at the same intervals:

$$E_i = \frac{\dot{n}_{c,i}}{\sum_1^N \dot{n}_{c,i}\Delta t}, \tag{27}$$

where $\dot{n}_{c,i}$ is the corrected count rate at time $i\Delta t$.

The area under the new curves is therefore unity. If the tracer injection can be considered as a Dirac pulse, the function $E(t)$ is the RTD at the measurement point. If not, some deconvolution or modelling has to be performed to obtain access to the RTD function, as explained in Section 3.6.1.2.

It is also customary to define the cumulative RTD function $F(t)$ and the washout function $W(t)$:

$$F(t) = \int_0^t E(u)\mathrm{d}u, \tag{28}$$

$$W(t) = 1 - F(t) \tag{29}$$

and the intensity function $\lambda(t)$:

$$\lambda(t) = \frac{E(t)}{1-F(t)} = \frac{E(t)}{W(t)}. \tag{30}$$

These functions can be useful when analysing the behaviour of a system. They can all be derived from area normalized tracer count rate curves.

3.6. DATA ANALYSIS AND MODELLING

3.6.1. Convolution and deconvolution procedures

3.6.1.1. Convolution

(a) Principle

Consider a radioisotope tracer experiment in a system in which a tracer is injected at the entrance and detected at the outlet. Let $C_0(t)$ and $C(t)$ be the tracer concentration histories at these two points.

Many systems have, to some approximation, the following properties:

(1) They are stationary, meaning that they do not change with time. In other words, two successive injections with the same concentration history will produce identical signals.
(2) They are linear, meaning that the multiplication of $C_0(t)$ by some factor will cause the signal $C(t)$ to be multiplied by the same factor and that the response to the sum of two tracer injections will be the sum of the responses to each individual injection.

Let us assume these properties are verified in our system. Let $E(t)$ be the response at the outlet to the injection of a very short unit pulse (Dirac pulse injection), $\delta(t)$, at the inlet.

Convolution is a mathematical transformation that allows the response to any injection history $C_0(t)$ to be predicted from knowledge of $E(t)$.

Any function $C_0(t)$ can be broken into a sum of steps of duration δu. If δu is short enough, each step is close to a Dirac pulse of magnitude $C_0(t)\delta u$. Consider the step injected at time u; provided the system is stationary and linear, response to this injection step at the outlet will be given by the function $E(t)$ shifted by time u and multiplied by magnitude $C_0(u)\delta u$. Taking advantage once again of the linearity of the system, it is possible to express the response to the whole injection sequence $C_0(t)$ as the sum of the responses to each individual injection step. In other words, the signal at the outlet can be written as:

$$C(t) = \int_0^t C_0(u)E(t-u)\mathrm{d}u, \tag{31}$$

which expresses $C(t)$ as the convolution product of $C_0(t)$ and $E(t)$, often denoted as $C_0 * E$. These operations (decomposition of $C_0(t)$ into multiple steps, calculation of the response to each step and summation of the responses) are illustrated in Fig. 49.

The convolution product can also be defined as:

$$C(t) = \int_0^\infty C_0(u)E(t-u)\mathrm{d}u \tag{32}$$

with infinity as the upper limit for the integral. Both formulations are equivalent, since $E(t)$ is zero at negative times (in other words, the tracer concentration is obviously zero before the tracer is injected). Another property worth noting is that convolution is commutative, i.e.:

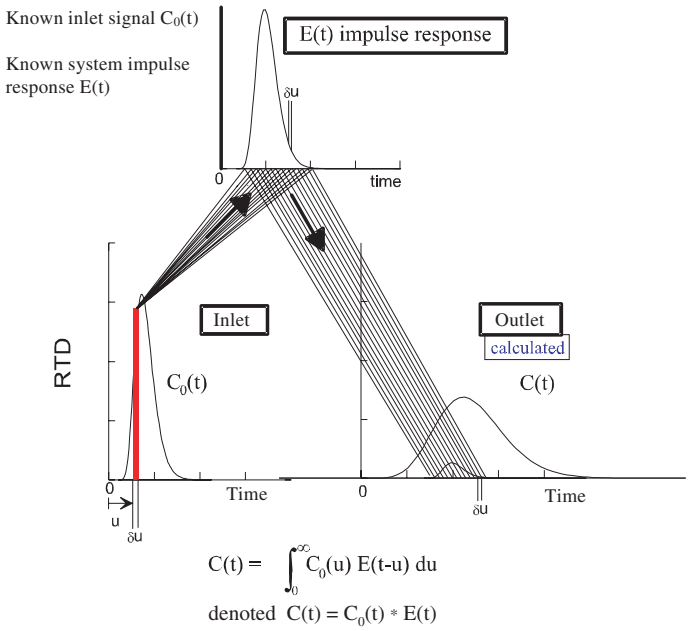

FIG. 49. The convolution procedure.

$$C_0 * E = E * C_0. \tag{33}$$

In a few cases, the convolution integral can be calculated analytically. Continuous functions are, however, rarely dealt with in practice, but rather sets of values at discrete time intervals. The functions $C_0(t)$, $E(t)$ and $C(t)$ should therefore be replaced by the values C_0^1, C_0^2, ..., C_0^n, E_1, E_2, ..., E_n, and C_1, C_2, ..., C_n, at times t_1, t_2, ..., t_n. We shall assume that the times t_1, t_2, ..., t_n are equally spaced, with time step Δt. The convolution product can then be approximated as:

$$C_j = \sum_{i=1}^{j} C_0^i E_{j-i+1} \Delta t \tag{34}$$

or

$$\begin{aligned} C_1 &= C_0^1 E_1 \Delta t \\ C_2 &= \left(C_0^1 E_2 + C_0^2 E_1\right) \Delta t \\ C_3 &= \left(C_0^1 E_3 + C_0^2 E_2 + C_0^3 E_1\right) \Delta t \\ C_4 &= \left(C_0^1 E_4 + C_0^2 E_3 + C_0^3 E_2 + C_0^4 E_1\right) \Delta t \ldots, \end{aligned} \tag{35}$$

which can be expressed in matrix form as:

$$\begin{pmatrix} C_1 \\ \vdots \\ C_i \\ \vdots \\ C_n \end{pmatrix} = \begin{pmatrix} C_0^1 & 0 & \cdots & \cdots & 0 \\ \vdots & C_0^1 & 0 & \cdots & 0 \\ C_0^i & \cdots & C_0^1 & 0 & 0 \\ \vdots & \vdots & \vdots & C_0^1 & 0 \\ C_0^n & \cdots & C_0^i & \cdots & C_0^1 \end{pmatrix} \begin{pmatrix} E_1 \\ \vdots \\ E_i \\ \vdots \\ E_n \end{pmatrix} \Delta t. \tag{36}$$

One interesting property of the convolution operation is that the area of the resulting function is equal to the product of the areas of the original functions:

$$\int_0^\infty C(t)\mathrm{d}t = \int_0^\infty C_0(t)\mathrm{d}t \int_0^\infty E(t)\mathrm{d}t \tag{37}$$

or

$$\sum_{i=1}^{n} C_i \Delta t = \sum_{i=1}^{n} C_0^i \Delta t \sum_{i=1}^{n} E_i \Delta t. \tag{38}$$

This latter formulation is easily deduced from the matrix expression of C_i.

(b) Practical methods

From a practical point of view, convolution products are easily calculated through the use of Eq. (36). Convolution can also be very easily performed with any standard mathematical analysis package.

An efficient alternative is the use of the Fourier transform. In the continuous formulation, one definition [29] of the Fourier transform of function $E(t)$ is:

$$\tilde{E}(f) = \int_{-\infty}^{\infty} E(t)\exp(2\pi i f t)\mathrm{d}t, \tag{39}$$

where the variable f is a frequency and i is the square root of –1. In discrete form, this equation becomes:

$$\tilde{E}_j = \sum_{k=1}^{n} E_k \exp\left[2\pi \mathrm{i}(k-1)\, j/n\right]. \tag{40}$$

In the continuous case, $\tilde{E}(f)$ is a complex function; in the discrete case, the $\tilde{E}_j$s are a set of complex numbers. The Fourier transform is easily inverted:

$$E(t) = \int_{-\infty}^{\infty} \tilde{E}(f) \exp(-2\pi \mathrm{i} f t)\, \mathrm{d}f \tag{41}$$

or

$$E_j = \frac{1}{n} \sum_{k=1}^{n} \tilde{E}_k \exp\left[-2\pi \mathrm{i}(k-1)\, j/n\right]. \tag{42}$$

These expressions for the discrete Fourier transform assume that the E_j be sampled at equal time intervals.

The Fourier transform of the convolution of two functions is the product of the Fourier transforms of each function:

$$\tilde{C} = \tilde{C}_0 \tilde{E}. \tag{43}$$

The convolution product of functions $C_0(t)$ and $E(t)$ can therefore be calculated in the following way:

(a) Calculate the Fourier transforms of C_0 and E.
(b) Multiply the results (in discrete form, this means simply calculating the products $\tilde{C}_0^j \tilde{E}_j$).
(c) Calculate the inverse Fourier transform of the product.

The functions $C_0(t)$ and $E(t)$ should, of course, be sampled at the same time intervals.

In discrete form, the direct and inverse Fourier transforms can be obtained with an FFT algorithm. The computing effort to calculate the FFT of n data points is approximately $n\log_2 n$. The computation of a convolution product with n data points involves three direct or inverse Fourier transforms and n multiplications, i.e. it still remains about proportional to $n\log_2 n$. On the other hand, the direct matrix calculation (Eq. (36)) involves approximately $n^2/2$ calculations, which is a much faster growing function of n. For large data sets

(say, more than a few thousand points), it is therefore advisable to use Fourier transforms instead of direct calculations.

Both methods (matrix equation (36) and Fourier transform) are foolproof as far as convolution is concerned. When using Fourier transforms, attention should, however, be paid to the area of the calculated convolution product; some kind of normalization is usually necessary. If one of the signals does not return to zero at large times, Fourier transforms can also cause undesirable aliasing. This problem can be avoided by adding zeros to the incomplete data set.

The FFT source code can be found in the literature [29] or in standard numerical packages. One constraint with the older versions of FFT is that the number of points should be some power of 2 (e.g. 128, 256 or 512). This constraint can easily be met by resampling the data or adding zeros.

(c) Example

To illustrate the convolution procedure, we use the following example:

$$C_0(t) = \frac{a_0}{\sqrt{2\pi}\,a_2}\exp\left(-\frac{(t-a_1)^2}{2a_2}\right), \tag{44}$$

where $C_0(t)$ is a Gaussian distribution function, a_0 is the area, a_1 is the mean time, a_2 is the standard deviation and $E(t)$ is a decaying exponential function with time constant a_3:

$$E(t) = \frac{1}{a_3}\exp\left(-\frac{t}{a_3}\right). \tag{45}$$

In this case, the convolution integral can be calculated analytically, the solution being the so-called exponentially modified Gaussian (EMG) function, which is also going to be used in Section 3.6.4 (peak decomposition):

$$C(t) = \frac{a_0}{2a_3}\exp\left(\frac{a_2^2}{2a_3^2}+\frac{a_1-t}{a_3}\right)\left[\operatorname{erf}\left(\frac{t-a_1}{\sqrt{2}\,a_2}-\frac{a_2}{\sqrt{2}\,a_3}\right)+1\right]. \tag{46}$$

Calculations are made in this example with area normalized functions ($a_0 = 1$), with mean time $a_1 = 100$ s, standard deviation $a_2 = 25$ s and time constant $a_3 = 50$ s, as illustrated in Fig. 50.

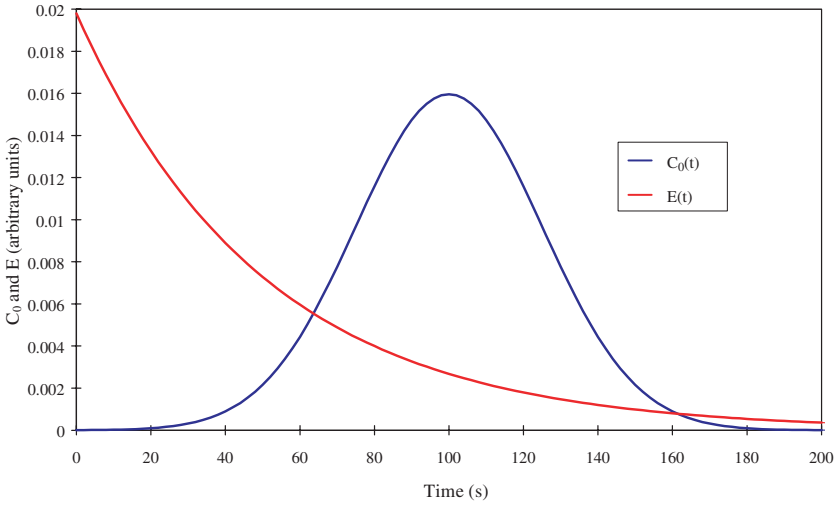

FIG. 50. The functions $C_0(t)$ and $E(t)$.

The functions $C_0(t)$ and $E(t)$ are sampled at regular 1 s intervals between 0 and 512 s. Some area normalization has to be performed because the relatively small number of points causes some error on the numerical integral of both functions. The resulting samples are then numerically convolved using Eq. (36). The result is shown in Fig. 51 and compared with the analytical EMG function.

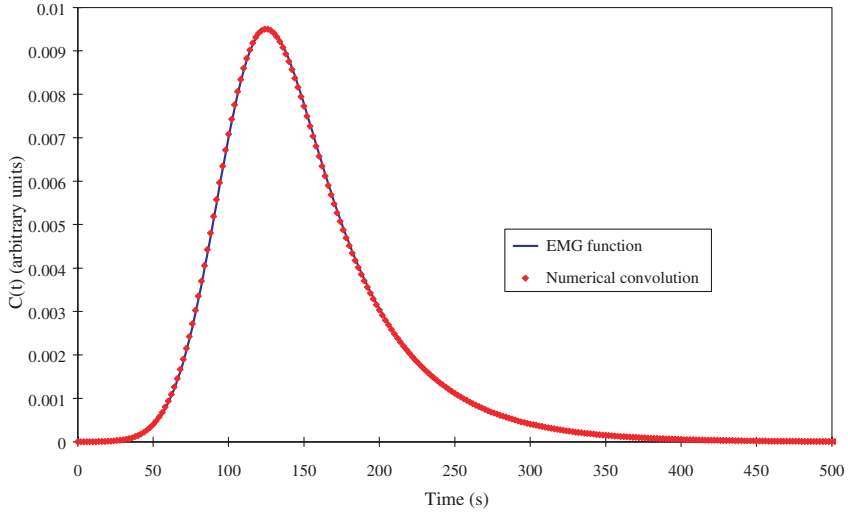

FIG. 51. Numerical convolution product and EMG function.

Both results fit well. To illustrate the above mentioned problems with aliasing, the same calculation is shown with a 256 s sample. The end of the $E(t)$ curve is therefore missing. In the convolution product calculated by an FFT, the tail of the $C(t)$ curve is folded back to the beginning while the matrix equation (36) gives the correct result (Fig. 52).

(d) Tools

Both RTD1 and DTSPro can be used to calculate the convolution product of two signals. As an alternative, convolution can easily be programmed with standard mathematical packages.

3.6.1.2. Deconvolution

(a) Principle

Convolution consists in calculating $C(t)$ when $C_0(t)$ and $E(t)$ are known. Deconvolution is the inverse procedure, i.e. calculation of $E(t)$ when $C_0(t)$ and $C(t)$ are known, or of $C_0(t)$ when $E(t)$ and $C(t)$ are known (the first case, where the responses at two measurement stations are known, being the most common one in tracer applications). We choose to denote the deconvolution of $C(t)$ and

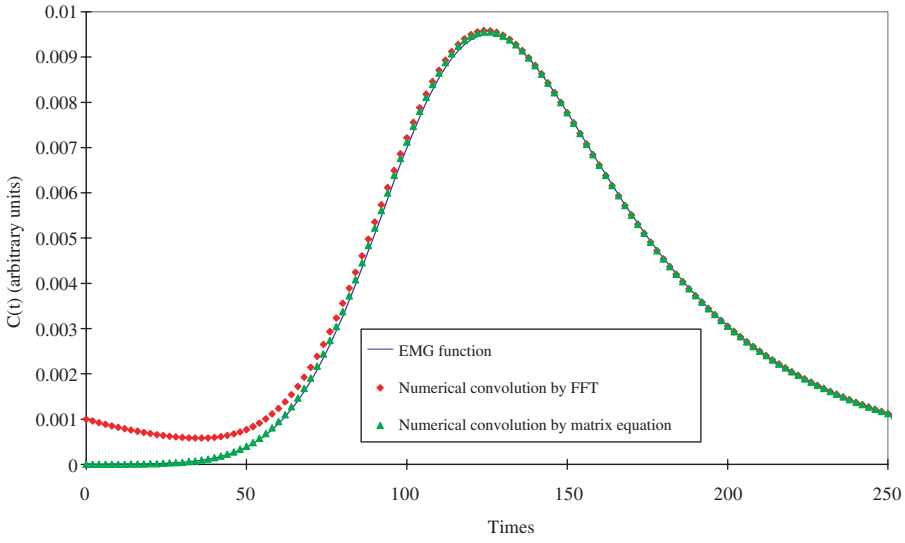

FIG. 52. Convolution by FFT and matrix equation (36).

$C_0(t)$ by $C \div C_0$, keeping in mind that if convolution is commutative, deconvolution is not.

There are several reasons why signals need to be deconvolved. As explained in Section 3.1, and again in Section 3.6.1, RTD system analysis of any stationary and linear system is unambiguously characterized by its impulse response function, or its response to a Dirac pulse stimulus. This response can, in most practical cases, be considered as the RTD of the traced material. Knowledge of that impulse response function is therefore desirable for predicting system response to any stimulus or for analysing system behaviour in terms of RTD.

Unfortunately, injection of a true Dirac tracer pulse is not always achievable. Besides, it is quite common to have several detectors at different stages of complex systems. Even if tracer is injected as a perfect Dirac pulse, only readings from the first detector can be considered as the impulse response function of that part of the system; one has to deconvolve the signals from the second and first detectors (i.e. calculate $C_2 \div C_1$) to obtain the impulse response function of the second part of the system, and so forth with the next detectors. This case is illustrated by an example in Section 3.6.4.

(b) Practical methods

Deconvolution seems a simple matter at first glance. The first method is by inversion of the matrix equation (36), which is a simple triangular sytem, the result of which would be, assuming that we want to compute $E = C \div C_0$, as follows:

$$
\begin{aligned}
E_1 &= \frac{C_1}{C_0^1 \Delta t} \\
E_2 &= \frac{1}{C_0^1}\left(\frac{C_2}{\Delta t} - C_0^2 E_1\right) \\
E_3 &= \frac{1}{C_0^1}\left(\frac{C_3}{\Delta t} - C_0^2 E_2 - C_0^3 E_1\right)
\end{aligned}
\qquad (47)
$$

… etc.

A problem appears at this stage if C_0^1 is zero so that the system is singular and cannot be solved. If it is not zero but very small compared with other values in the C_0 data set, the system to be inverted will anyway be ill conditioned (with small diagonal terms and large non-diagonal ones) and therefore difficult to solve. Unfortunately, C_0^1 is very often small because the tracer wave needs some time to reach the detector. One may then try particular methods for solving nearly singular systems. A description of these numerical

techniques is quite beyond the scope of this book. Reference [30] is a good introduction to this subject.

Another obvious method would be the use of a Fourier transform. If convolution is equivalent to multiplication in the Fourier domain, deconvolution should be achieved by the simple division of Fourier transforms. Hence, with our notation:

$$\tilde{E} = \frac{\tilde{C}}{\tilde{C}_0}. \tag{48}$$

This method will not work in most cases. A typical Fourier spectrum will usually exhibit a signal peak at low frequencies and a noise tail at high frequencies. Division will give undue weight to the noise tail in $\tilde{C}_0$, which results in a very noisy estimation of $\tilde{E}$ and the need for some drastic filtering. In some cases, good results can be achieved by simply chopping off some part of the high frequency spectrum of $\tilde{E}$. Methods do exist for more sophisticated filtering (Wiener optimal filtering), but once again they are beyond the scope of this book. The reader is also referred to the RTD1 manual [16] for more information on direct numerical deconvolution by FFT and other techniques.

The final method consists of parametric adjustment. This method involves the following steps:

(a) Choose a suitable model for the deconvolved function with a reasonable number of parameters.
(b) Estimate the initial values for these parameters.
(c) Convolve the input function with the theoretical function.
(d) Compare the results.
(e) If the result is satisfactory, the problem is solved; if not, estimate a new (and hopefully better) set of parameter values and start from the beginning again.

This method is usually very effective. The main difficulty lies in a judicious choice for the model. This model should be as simple as possible, while being able to reproduce the main expected features for the experimental RTD curve (e.g. tailing and multiple peaks). It is often advisable to start with a simple model (e.g. a two parameter axial dispersed plug flow model, as described in Section 3.6.3) and to refine it gradually, by adding parallel branches and recycling.

(c) Examples

The same case is used here as for the convolution procedure: $C_0(t)$ is a Gaussian function, $E(t)$ a decaying exponential and $C(t)$ an EMG function, with parameters $a_0 = 1$, $a_1 = 100$ s, $a_2 = 25$ s and $a_3 = 50$ s. All three methods for deconvolution, i.e. matrix system inversion, Fourier transform and parametric adjustment, are illustrated here.

Matrix system inversion (Eq. (36)) is effective in the calculation of $C(t) \div E(t)$ because the first value of $E(t)$ happens also to be the largest one. In this particular case, the system is strongly diagonal dominant and is therefore easily inverted. The result is shown in Fig. 53. Calculation of $C(t) \div C_0(t)$ is not worth attempting with this method (failure is guaranteed).

Fourier transform deconvolution also gives good results for the calculation of $C(t) \div E(t)$, one reason being that the frequency spectrum of $E(t)$ contains very little noise, so that little or no filtering is required.

For the same reason the inverse case (calculation of $C(t) \div C_0(t)$) cannot be properly handled by a cut-off for the high frequency components of the estimated deconvolved function. The best compromise is to keep only ten low frequency components; only a very crude estimate of $E(t)$ is obtained (Fig. 54).

This result could certainly be improved with some more adequate filtering. It is not intended to pursue this point any further, our purpose being mainly to illustrate that direct numerical deconvolution is, in general, a difficult and tedious affair.

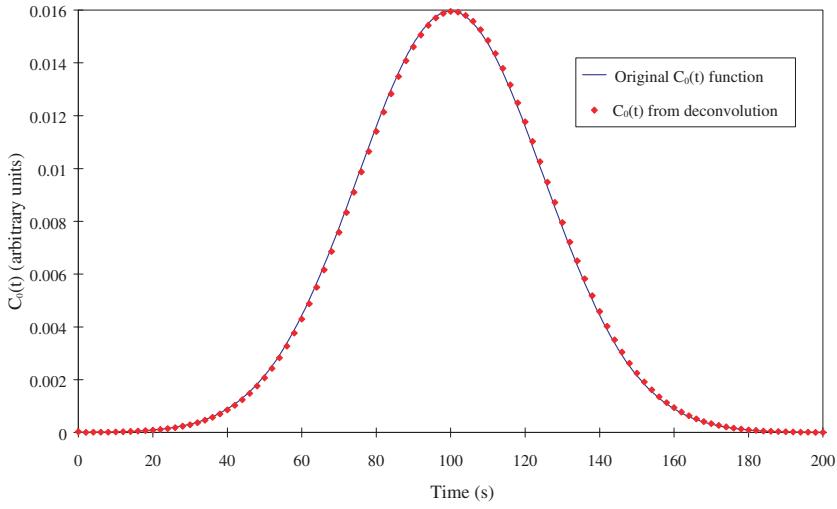

FIG. 53. Deconvolution by inversion of matrix equation (36).

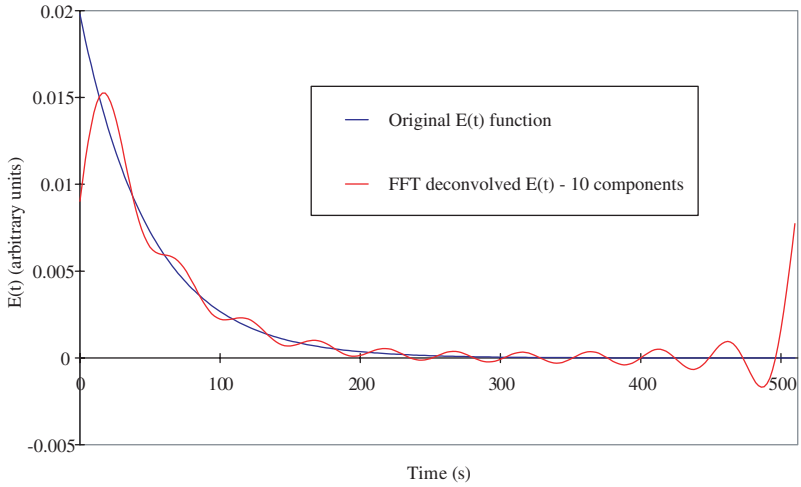

FIG. 54. Deconvolution by FFT.

The problem of computing $E(t) = C(t) * C_0(t)$ is properly solved by parametric adjustment. Let us suppose, in the first place, that it is somehow suspected that $E(t)$ is a decaying exponential — the reason being, for example, that the system under scrutiny should obviously behave like a perfect mixer (Section 3.6.5.1). In this case, the problem is simply to optimize the time constant a_3 in $E(t)$ so that $C_0(t) * E(t)$ is as close as possible to $C(t)$. By simple moment calculations (Section 3.6.2), it is possible to make a reasonable estimate for a_3, say 40 s (a poor estimate). Optimization of a one parameter model can then be made by a simple trial and error method. Figure 55 compares $C_0(t) * E(t)$ with $C(t)$ for several values of time constant a_3.

Plotting the root mean square (RMS) error:

$$e = \frac{1}{n}\sum_{i=1}^{n}\left[C_i - \left(C_0 * E\right)_i\right]^2 \tag{49}$$

as a function of a_3 readily shows that the best value is indeed equal to 50 s, as shown in Fig. 56.

Optimizing a model with two or more parameters requires further refined methods. Once again the reader is referred to the literature for more information on this particular point.

In this example, the true mathematical nature of the model to be adjusted was known. Such is not the general case. Inadequate choice of the model will

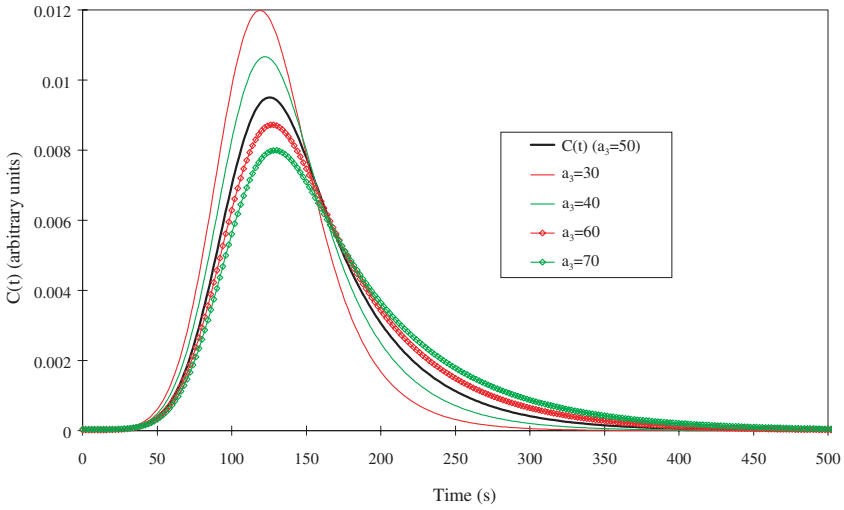

FIG. 55. Comparison of model with the EMG function for various values of the parameter a_3.

result in poor fitting and dubious values for the parameters. This point is illustrated in Fig. 57, where the fitting of the $E(t)$ function has been attempted with the axial dispersed plug flow model described in Section 3.6.3. The optimized time constant of this model is 58.2 s, quite far from the actual value of 50 s (the Péclet number is correctly estimated at the low value of 1.3).

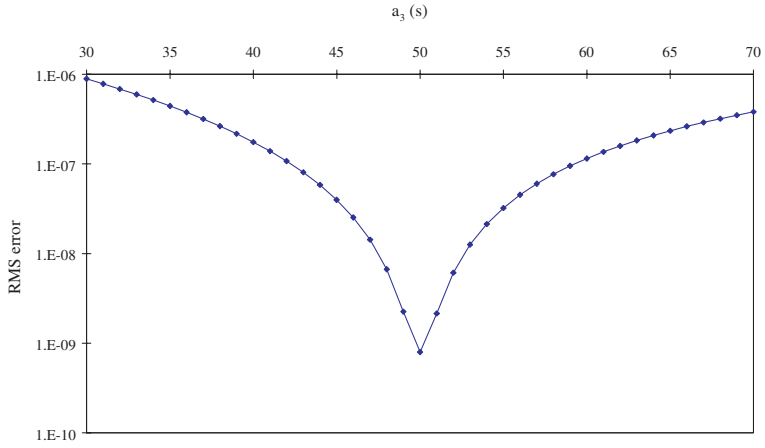

FIG. 56. RMS error as a function of the parameter a_3.

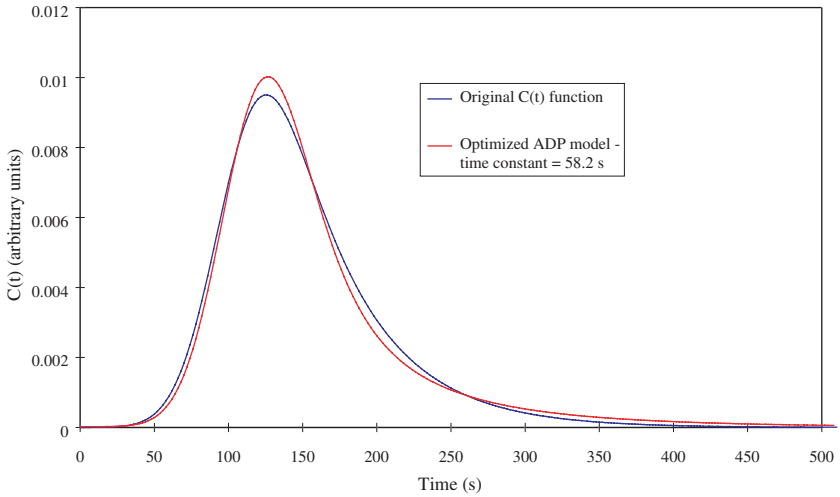

FIG. 57. Optimization of axial dispersed plug flow model.

(d) Tools

Direct numerical deconvolution can be attempted with packages for numerical analysis or data treatment. It can also be done with RTD1. Several algorithms are proposed in RTD1 for this problem, referred to as a black box analysis in Ref. [16].

Parametric adjustment (grey box analysis) is the basic function of RTD2 and DTSPro.

3.6.1.3. Example of application: Cascade of reactors in series

The use of the deconvolution procedure is illustrated in a typical example from the mineral processing industry (Fig. 58). The process under investigation is a part of the conversion process of aluminium hydroxide in ore to sodium aluminate. Process improvements, either by increasing flow rates or by improving the productivity of the liquors, require knowledge of the hydrodynamics of digesters and mud settlers in an operating plant, in order to analyse the process and to identify its limitations, if any. Information collected may be both devoted to correction, in optimizing process operating conditions or in performing technological adjustments, and to modelling for process analysis or for the design of new plants. As an in situ, non-intrusive and non-process

FIG. 58. Input/output survey of reactors in series (mineral industry process).

disrupting method, the radioactive tracer technique can provide accurate information about the hydrodynamic characteristics of flows in the reactors.

Figure 59 illustrates the overall design of the radiotracer experiment, its scale and the location of each collimated detector. The digestion line is composed of eight digesters in series. The feed consists of aluminium ore, soda and flocculent. Collimated detectors are positioned between reactors. Thus, the information collected represents the inlet signal of one digester and the outlet signal of the preceding one. Concerning the four mud settlers, only three are operational, one always being closed for maintenance.

Numerous difficulties raised by the choice of the correct tracer in such a process are discussed in Ref. [30]. The liquor tracers recommended are halogenic derivatives of carboxylic acids. The selection of an appropriate tracer is also governed by considerations of simplicity in the implementation and detection. Bromine-82 in the form of $BrNH_4$, liquor soluble, has been chosen as the best compromise.

Digesters in series are analysed individually since the tracer test provides both the inlet function $I(t)$ and the outlet function $O(t)$ of each vessel (both functions are area normalized prior to further treatment). The MRT $\overline{t}$ and

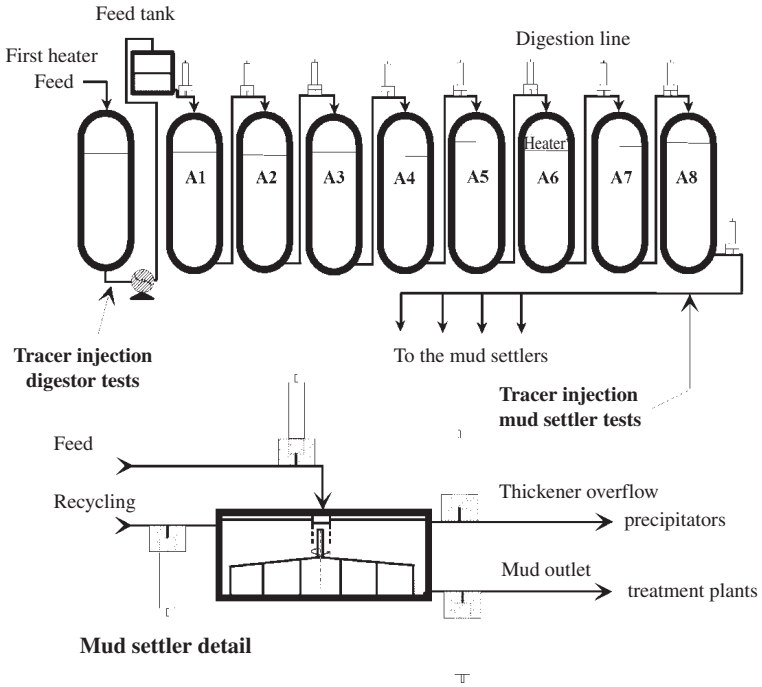

FIG. 59. Overall arrangement of the collimated detectors on the digestion line and on each mud settler.

standard deviation σ are calculated by numerical methods. Such an analysis allows determination of the MRT of the liquor in each vessel and, taking advantage of the additive properties of $\bar{t}$ and σ^2, the MRT of the liquors since their entry into the digestion line. Figure 60 presents the MRT of the liquors in

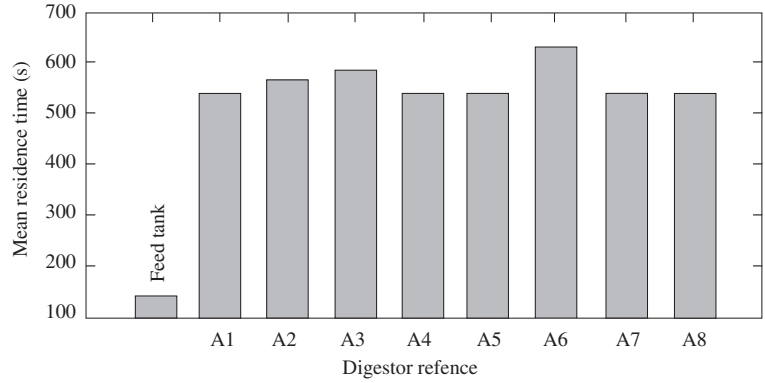

FIG. 60. Mean residence time of liquors in each digester of the digestion line.

each unit of the digestion line. Dead volumes are deduced, taking into account the geometric volumes of the apparatus and the flow rate through the system. In this case, this leads to a filling capacity ranging from 90 to 100%, depending on the reactor.

The second piece of information which can be extracted from an RTD analysis are the mixing efficiencies of the digesters. This information is found by determining the impulse response of each vessel and modelling. The data available are the input $I(t)$ and output $O(t)$ functions of each digester. The impulse response $E(t)$ is obtained by parametric adjustment of an axial dispersed plug flow function (described in more detail in Section 3.6.3). This function has two parameters, time constant τ and Péclet number Pe. Pe is an indication of the degree of mixing (small Pe values indicate vigorous mixing).

As indicated in Section 3.6.1.2, deconvolution is performed by iterative adjustment of the model parameters. Figure 61 presents, as an example, the results of such a procedure when dealing with digester A5, and Fig. 62 depicts the complete results for all the vessels in the digestion line. The quality of the fits can be observed, since the output curves cannot be discriminated from the

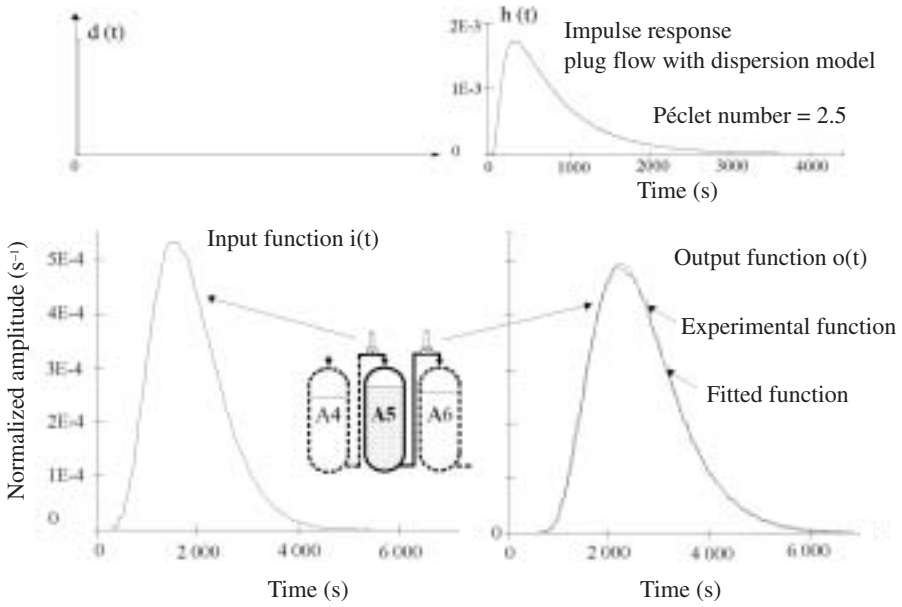

FIG. 61. Impulse response of digester A5 obtained by deconvolution.

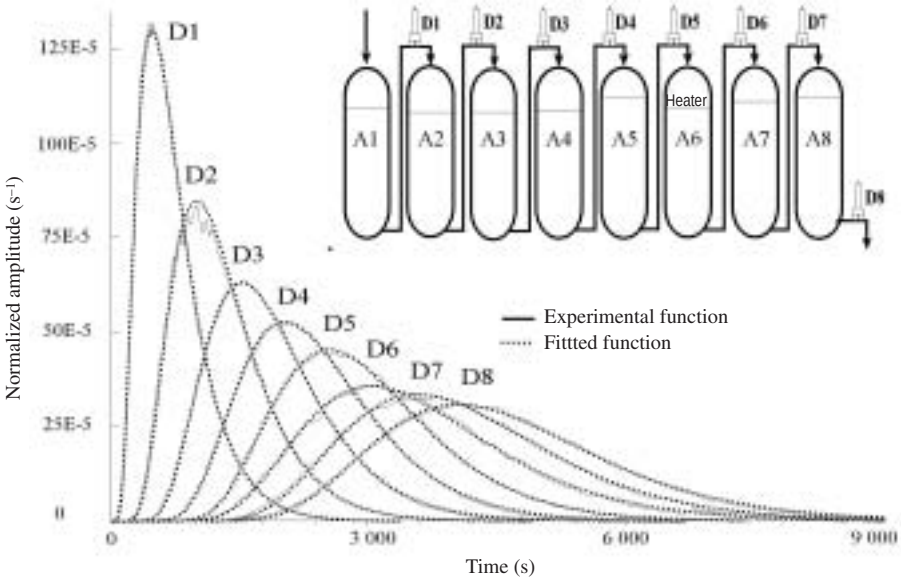

FIG. 62. Comparison between the experimental output curves and the results of convolutions of the input functions by the optimized impulse responses of the digestors.

calculated ones which are obtained by convolution of the input function by the optimized impulse response of the digester.

The Péclet number of the flow in each reactor is deduced from the modelling. Figure 63 shows the evolution of the Péclet number throughout the digestion line. The flow in each digestor is close to axial dispersed plug flow with a gradual increase of the mixing effect until the seventh digestor. The sixth

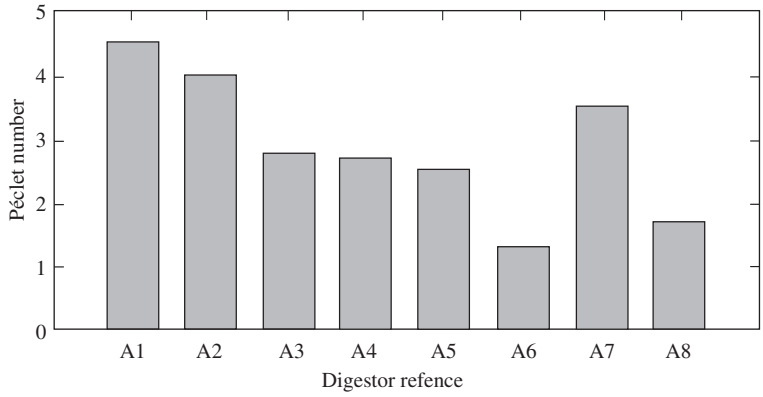

FIG. 63. Evolution of the Péclet number throughout the digestion line.

digestor is the first one that is heated by live steam. The slurry temperature increase is the highest in the digestion line.

3.6.2. Time analysis and moment extraction

The analysis of the measured RTD depends upon the specific purpose for which the experiment has been carried out. Some of the common applications are discussed here. Moments are used to characterize the RTD functions in terms of statistical parameters such as MRT, variance and skewness. The moments around the origin are defined as:

$$M_i = \int_0^\infty t^i E(t)\,\mathrm{d}t, \tag{50}$$

where $i = 1, 2, 3, \ldots$ The zeroth moment of the normalized RTD gives the area under the distribution, which is equal to unity:

$$M_0 = \int_0^\infty E(t)\,\mathrm{d}t = 1. \tag{51}$$

The MRT is equal to the first moment:

$$M_1 = \bar{t} = \int_0^\infty t\,E(t)\,\mathrm{d}t. \tag{52}$$

The spread of the RTD is characterized by the standard deviation σ or the variance σ^2:

$$\sigma^2 = M_2 - M_1^2 = \int_0^\infty (t - \bar{t})^2 E(t)\,\mathrm{d}t, \tag{53}$$

where

$$M_2 = \int_0^\infty t^2 E(t)\,\mathrm{d}t$$

is the second moment around the origin.

Higher order moments allow calculation of quantities such as skewness and kurtosis (measures of the asymmetry and flattening) of the RTD function, but they are often difficult to estimate and not frequently used.

RTDs are often expressed in terms of dimensionless time $\theta = t/\bar{t}$, thus:

$$E(\theta) = \bar{t}\, E(\bar{t}). \tag{54}$$

The distribution $E(\theta)$ is also area normalized. Similarly the moments, i.e. MRT, and variance of the $E(\theta)$ curve are found from the following relations:

$$\bar{\theta} = \int_0^\infty \theta E(\theta) \mathrm{d}\theta, \tag{55}$$

$$\sigma^2(\theta) = \int_0^\infty \left(\theta - \bar{\theta}\right)^2 E(\theta) \mathrm{d}\theta. \tag{56}$$

If N reactors are connected in series then the MRT and variance of the cascade can be obtained from the following relations:

$$\bar{t}_{\mathrm{cas}} = \bar{t}_1 + \bar{t}_2 + \bar{t}_3 + \ldots + \bar{t}_N, \tag{57}$$

$$\sigma^2_{\mathrm{cas}} = \sigma^2_1 + \sigma^2_2 + \sigma^2_3 + \ldots + \sigma^2_N. \tag{58}$$

For a constant density fluid flowing in a 'closed–closed' system (meaning that back dispersion is not allowed at the inlet and outlet of the system) of volume V at flow rate Q, the MRT of the fluid (holding time) is theoretically defined as:

$$\bar{t} = V/Q. \tag{59}$$

For all normally operating systems, the experimentally measured MRT is the same as the holding time but may differ in the case of abnormal performance of the system.

3.6.3. Axial dispersed plug flow

Some attention is devoted here to the popular axial dispersed plug flow model, because it is extensively used in the peak decomposition techniques reviewed in the next section.

This flow is the superimposition of convection (bulk movement of the fluid in a plug-like fashion) and some amount of dispersion. In one dimension, and provided that dispersion can be expressed by a Fickian law, tracer concentration C is given by the following balance equation:

$$\frac{\partial C}{\partial t} + U\frac{\partial C}{\partial x} = D\frac{\partial^2 C}{\partial x^2}, \tag{60}$$

where U is the fluid velocity and D is the dispersion coefficient.

This equation is rigorously applicable to flows in long pipes (i.e. those with a very large length to diameter ratio) or in monodimensional columns filled with a porous medium. It is a useful approximation for quite a variety of monodimensional or quasi-monodimensional situations (e.g. river flow, underground water flow and flow in packed columns). For the non-dimensional case, two parameters appear: a characteristic time constant $\tau = L/U$, where L is the length of the system, and the non-dimensional Péclet number $\mathrm{Pe} = UL/D$, which represents the ratio of convective to dispersive effects. In other words, dispersion is predominant when Pe is low and negligible when it is large.

To be integrated, Eq. (60) has to be completed with initial conditions and boundary conditions. The initial condition is obviously $C = 0$ (zero concentration before tracer injection). There are many possibilities for the boundary conditions, depending on whether dispersion is allowed or not at the boundaries of the system. This point has given rise to much academic controversy and will not be discussed here. The reader is referred to Refs [11] and [31]. Besides, all available expressions become close whenever the Péclet number is large enough, which some authors consider as a necessary condition for the equation to hold (a value of 20 is mentioned by Schweich [32]).

A very popular analytical solution of Eq. (60) describes the tracer concentration field as a function of time and distance, when N moles of tracer are injected as a Dirac pulse at ($t = 0$, $x = 0$) and dispersion is allowed at both ends of the domain (so-called open–open boundary conditions):

$$C(t,x) = \frac{N}{\sqrt{4\pi Dt}}\exp\left(-\frac{(x-Ut)^2}{4Dt}\right). \tag{61}$$

The RTD at $x = L$ is easily deduced from this solution:

$$E(t) = \frac{1}{2}\left(\frac{\mathrm{Pe}}{\pi\tau t}\right)^{0.5} \exp\left(-\frac{\mathrm{Pe}(\tau - t)^2}{4\tau t}\right). \tag{62}$$

Another useful expression corresponds to the well known two measurements configuration: tracer concentration is monitored at two separate stations downstream from the injection. The following equation gives the impulse response function between these measurement stations (or in other words, the deconvolution of the signal from the second station by the signal from the first one):

$$E(t) = \frac{1}{2}\left(\frac{\mathrm{Pe}\tau}{\pi t^3}\right)^{0.5} \exp\left(-\frac{\mathrm{Pe}(\tau - t)^2}{4\tau t}\right). \tag{63}$$

Other variants of the axial dispersed plug flow model have no simple analytical form. Such is unfortunately the case with the so-called closed–closed model, where the measurements are made at the inlet and outlet piping of a column-like system, a very common configuration in practice. The differences are, however, immaterial at large to moderate Péclet numbers.

It has been seen that axial dispersed plug flow models have two parameters: τ and Pe. The former sets the timescale of $E(t)$. The effect of varying the latter is illustrated in Fig. 64 using Eq. (63). The curves become sharper and sharper when Pe is increased. They always have a single peak, and the peak height and tail length are correlated (the tail is short when the peak is sharp and vice versa).

Finally, the values of the MRT (first moment) and variance (second centred moment) are indicated as a function of τ and Pe, in the case of Eq. (63), in Table 6.

TABLE 6. FIRST AND SECOND MOMENTS OF AXIAL DISPERSED PLUG FLOW MODEL (Eq. (63))

First moment $\bar{t}$	Second moment σ^2
τ	$\frac{2\tau^2}{\mathrm{Pe}}$

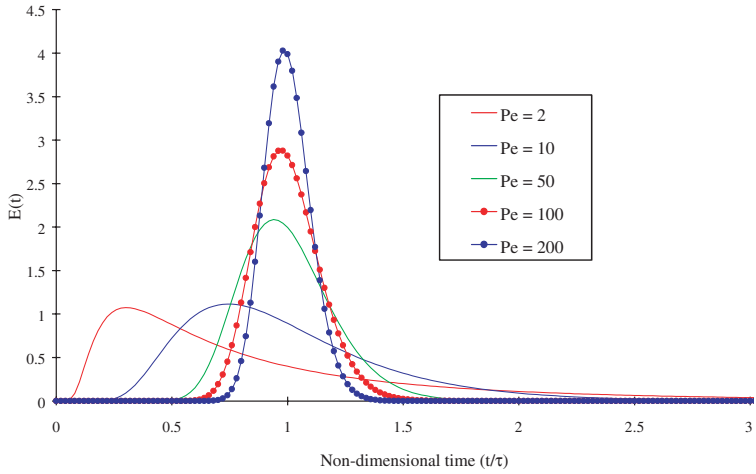

FIG. 64. Axial dispersed plug flow as a function of the Péclet number.

3.6.4. Decomposition into elementary flows

Data can be exploited further in an accurate and easy fashion, as far as they unambiguously represent a single fluid stream, the propagation of which is monitored from one detection point to another. More complicated is the case when collected data are the sum of different tracer contributions due to different fluid streams (e.g. because of leaks or because the tracer cloud is divided in different parts of the reactor, etc.) or to temporal interactions, for example recycling. In both cases, global tracer information is cumulated by the probe as a function of time, and the recorded data are the sum of different contributions. A necessary step is therefore to decompose the global response in order to isolate individual flows and, if needed, to identify their histories by making correlations between probe responses. This step can be performed through the use of appropriate systemic models. Construction and adjustment of these models is however difficult, and a simpler method (so-called peak decomposition) is proposed here, taking advantage of the availability of more and more sophisticated software, implemented on efficient personal computers.

Amongst a wide variety of cases, this section presents some typical examples of the method, namely:

— Bypass quantification;
— Recycling removal (FCC, catalyst tracing experiment);

— Multi-injection interpretation (FCC, gas phase tracing experiment);
— Behaviour of solid materials in the kiln of a chlorinated waste treatment plant.

3.6.4.1. Decomposition methodology

As far as decomposition is concerned, the shape of the individual contributions has to be estimated. Data recorded by a probe during a tracer test have an overall shape which is close to that of restitution curves obtained in chromatography. Both cases involve the flow of species through a system. In the field of chromatography, analysis of restitution curves has been investigated in particular, either from a chemical point of view with the determination of theoretical functions relevant to analytical solutions of chemical and physical mechanisms, or from a practical and optimization point of view, with the proposal of empirical functions [33]. In the latter case, parameters have no physical meaning, but such functions allow decomposition of complex spectra and the separation of overlapping peaks. When analysing tracer test response curves, if overlapping peaks, tortuous shapes and shoulders are apparent, and if the physical reasons for cumulating information are credible, advantage can be taken of the theoretical and practical chromatography background.

Chromatography peaks are generally characterized by their position, breadth and skewness (asymmetry). Band broadening arises from a wide array of phenomena, from axial diffusion and dispersion to extra column effects, mass transfer resistances and kinetic resistances. This clearly demonstrates the similarity between a chromatography peak and a tracer peak, when flow investigations are performed. Amongst a wide range of chromatography functions, two appear very useful for interpretation of tracer curves. Both are based upon the assumption of an impulse input into the column.

The exponentially modified Gaussian (EMG) function is the convolution of a Gaussian with an exponential:

$$h(t) = \frac{a_0}{2a_3} \exp\left(\frac{a_2^2}{2a_3^2} + \frac{a_1 - t}{a_3} \right) \left[\operatorname{erf}\left(\frac{t - a_1}{\sqrt{2}\, a_2} - \frac{a_2}{\sqrt{2}\, a_3} \right) + 1 \right], \tag{64}$$

where erf is the error function,

$$\operatorname{erf}(x) = \frac{2}{\sqrt{\pi}} \int_0^x \exp\left(-t^2\right) \mathrm{d}t \tag{65}$$

and the four independent parameters are: a_0 the Gaussian peak area, a_1 the Gaussian peak centre, a_2 the Gaussian peak width and a_3 the time constant of the exponential.

The appearance of this function is that of a distorted Gaussian, with an exponential tail on the right side. It has already been mentioned in the 'convolution' section (3.6.1 — see, e.g., Fig. 51). Its ability to fit a tracer peak is therefore obvious.

Axially dispersed plug flow can be written as:

$$y(t) = \frac{1}{2}\frac{U}{\sqrt{\pi Dt}}\exp\left(-\frac{(L-Ut)^2}{4Dt}\right), \tag{66}$$

which is a version of Eq. (62) expressed with U and D. Full details of this very classical function in the field of tracer experiments are given in Section 3.6.3.

A second class of very useful functions are the transition functions, which allow the transition from a state $h(t)$ to a state $g(t)$ to be depicted analytically over a short period of time. The parameters of such functions are the centre and width of the transition region. The most important practical use of transition functions is the analysis of a recycling component. Two functions may be applied to such adjustments:

(1) The sigmoidal function:

$$y(t) = \frac{a_0}{1+\exp\left(-\frac{t-a_1}{a_2}\right)}, \tag{67}$$

where a_0 is the amplitude, a_1 the centre of the transition region and a_2 its width.

(2) The cumulative function:

$$y(t) = \frac{a_0}{2}\left[1+\operatorname{erf}\left(\frac{t-a_1}{a_2}\right)\right] \tag{68}$$

with the same definitions for a_0, a_1 and a_2. In this case, the transition region is defined in terms of the error function.

A third class of functions would be analytical solutions of simple models, such as an exponential decay which applies to the modelling of perfect mixing.

Decomposition of a complex response, which implies least squares fitting of the set of previously mentioned functions to experimental data, can be made by software for curve fitting of non-linear equations. The examples presented in this section have been computed by the Peakfit software [26] on personal computers. This software accomplishes complex curve fitting using the Marquardt–Levenberg algorithm in a user friendly and interactive manner. It is of prime importance to control the optimization procedure in order to produce a realistic and physically meaningful decomposition.

3.6.4.2. Applications: Test cases

(a) Bypass quantification

Bypass quantification, which means estimating the proportion of the bypass flow versus the main flow, is a quite straightforward example of an application. Shoulders or overlapping peaks can be interpreted as the occurrence of leakage, as shown in Fig. 65: the restitution of one fraction of the tracer occurs more rapidly than that of the other fraction, which means that two different flows are traced. Since both are recorded by the same probe, with the same geometry, quantitative information can be derived from the ratio of the areas of the separated RTD curves. If the peaks are overlapping, identification of the individual contributions can be achieved by curve fitting. In the case presented in Fig. 65, decomposition of the tracer function is performed by the combination of two axially dispersed plug flow functions that allow the estimation of the proportion of leakage, time parameters, velocities and dispersion characteristics of both flows. In this case, the leakage appears very early in the reactor: the leakage peak is very close to a plug flow function (high Péclet number), the main flow being far more dispersive.

(b) Recycling removal

Figure 66 presents the response of the probe located in front of the riser outlet in an FCC unit (actually probe number 6 in Fig. 31), collected when performing a catalyst tracing experiment. Recycling interferes with the first tracer wave.

Quantitative temporal information about the first tracer wave and recycling can be obtained after decomposition. Recycling is fitted by a cumulative function which allows determination of the parameters such as the time of arrival, average time and time width of recycling at the measurement point. The first tracer wave cannot be fitted by a single function. The optimized combination of two EMG functions and a cumulative function gives a perfect

fit of the experimental curve. The first tracer passage can be interpreted as the combination of two different pieces of information: one about the exit flow of tracer from the fountain at the end of the riser and the second about the behaviour of the tracer in the portion of the disengager that is surveyed by the collimated probe. If this assumption is valid, as suggested by the time coherence of readings by the different probes, quantitative information can be derived from a moments analysis of the reconstructed individual peaks.

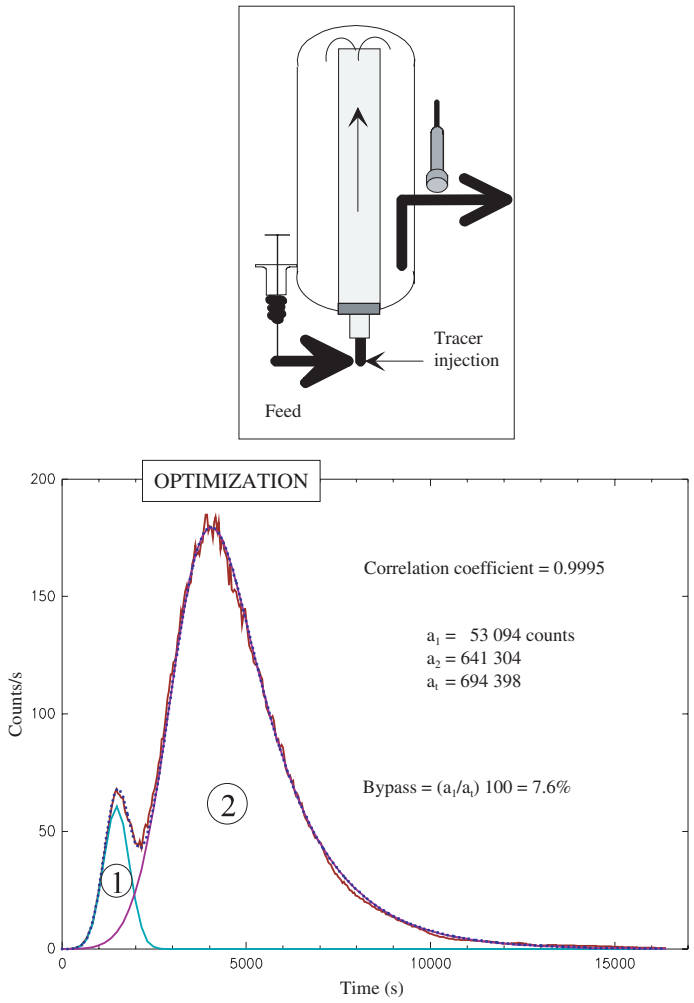

FIG. 65. RTD decomposition: bypass proportion identification.

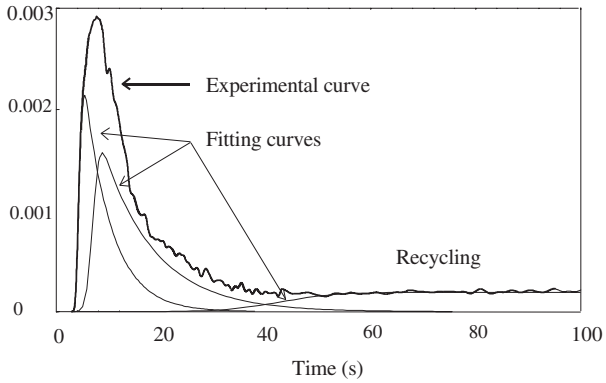

FIG. 66. Catalyst tracing experiment in an FCC unit. Decomposition of the response of the probe located in front of the riser outlet.

(c) Multi-injection experiment

The experiment described in this section is not, appropriately, a determination of flow parameters but rather the interpretation of a test which was designed to be simple but was revealed to be extremely complex.

The problem to be investigated was the behaviour of the gas phase in the standpipe of an FCC unit. Operational reports mentioned complex behaviour of the gas phase in terms of velocity and dispersion. A specific tracer test was designed in order to collect information about this part of the FCC unit. An adequate amount of tracer was injected as a Dirac impulse through an existing injection line at the top of the standpipe. A probe was positioned outside the reactor, at the medium level, for monitoring the behaviour of the gas phase in the standpipe and then in the regenerator (Fig. 67(a)). Thus, the signal from this probe was expected to appear as two waves. Figure 67(a) depicts the actual experimental results. The probe response is very complex: the signal rises without delay and appears as intense peaks leading to a plateau and a tail. The timescale of the response is abnormally long. The experiment was repeated and gave the same results, especially concerning the shape of the curve and the positions of the peaks (Fig. 67(a)).

The explanation lies in the particular nature of the injection line. This line is used for process operations. It is actually a distributor for steam feed at five different levels in the standpipe. The tracer was expected to go up a single line but was divided between all the lines. Detector recordings are thus due to all the flows from this multipoint injection system. An attempt to decompose the response into all possible contributions was successful, as illustrated in

Fig. 67(b). The first peaks are explained by the tracer passing through the injection lines, the other peaks by the passing of tracer waves originating from the different particular injection lines, in the standpipe and in the regenerator. The number of peaks, their shapes (plug flow with low dispersion in the standpipe and plug flow with high dispersion in the regenerator) and the order of their appearance were all found to be consistent with the detection capabilities of the collimated probe.

As an example, Fig. 67(c) depicts the contribution of injection through line C (the line which is approximately in front of the detector) and the three successive waves accounting for flows in the injection line, standpipe and regenerator. When dealing with injection through line D (Fig. 67(d)) for instance, the flow in the standpipe is not visible because the injection point is below the probe level, outside the detection solid angle.

This interpretation and decomposition was possible because the information collected by the probe was reliable, especially as far as the positions of the peaks and bumps are concerned. For this test case, this means high frequency data acquisition and efficient FFT filtering, without loss of information.

According to the shape of the curve, the solution to the number of underlying peaks is unique, but, due to the number of parameters to be optimized, the coherence of peak shapes and peak occurrences has to be carefully controlled by the operator during the curve fitting process.

(d) Behaviour of solid materials in the kiln of a chlorinated waste treatment plant

The RTD analysis of solid and gaseous phases in the rotary kiln of a chlorinated waste treatment plant was performed with two objectives:

(1) The residence time of the gaseous phase in the kiln has to be lower than 2 s in order to prevent formation of dioxin in the quenching tower of the plant. Radioactive tracers, in this case ^{79}Kr, are perfectly convenient to achieve the necessary quality of measurement (high sensitivity, high resolution due to high frequency recordings and on-line measurement).
(2) Knowledge of the RTD of the solid phase, which is important for energy consumption considerations. The materials are expected to move inside the kiln in a plug flow fashion, allowing step by step continuous destruction of chlorinated materials.

The tracer of the solid phase was ^{140}La, obtained by direct activation of lanthanum oxide powder. The walls of the kiln (a steel wall covered by an

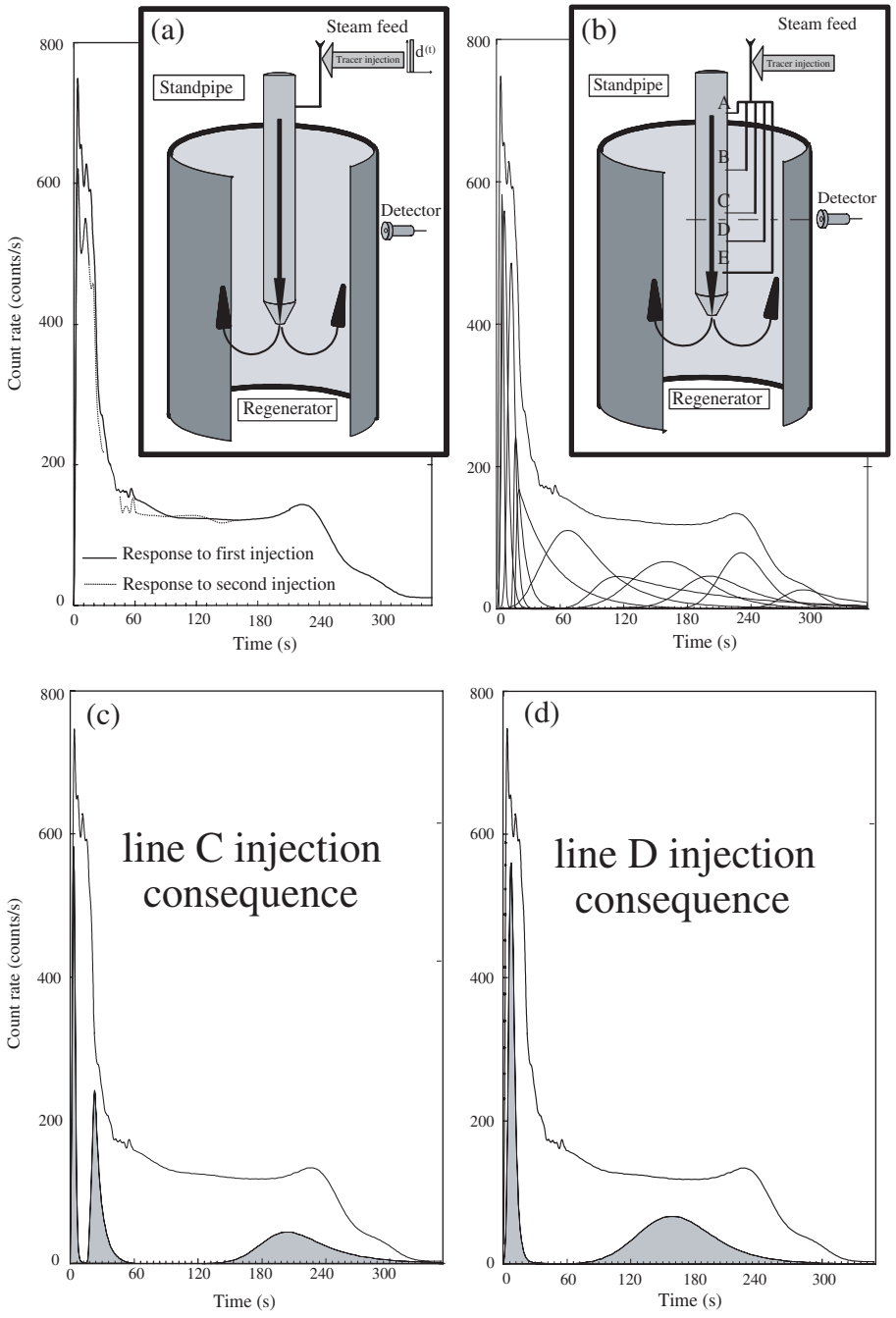

FIG. 67. Multi-injection tracer test experiment (gas phase tracing) — interpretation.

internal brick heat shield) dictate the use of a high energy tracer. The tracer, as a powder, is directly and instantaneously introduced into the feed. Detectors are located close to the kiln, first of all at a short distance from the feed inlet in order to survey the input into the kiln, at the exit and halfway along the kiln (Fig. 68). Typical results are shown in Fig. 69.

As expected, the input function can be considered as a Dirac pulse. The responses of the other detectors are characterized by peaks, overlapping peaks and shoulders. A global analysis can be performed. The first moments of the RTD functions can be easily extracted, leading to the information required: the average time for the materials to reach the middle of the kiln and the average time for the materials to reach the exit.

The good resolution of the peaks in each RTD function gave an opportunity to try to go further in the interpretation. Interpretation relies on

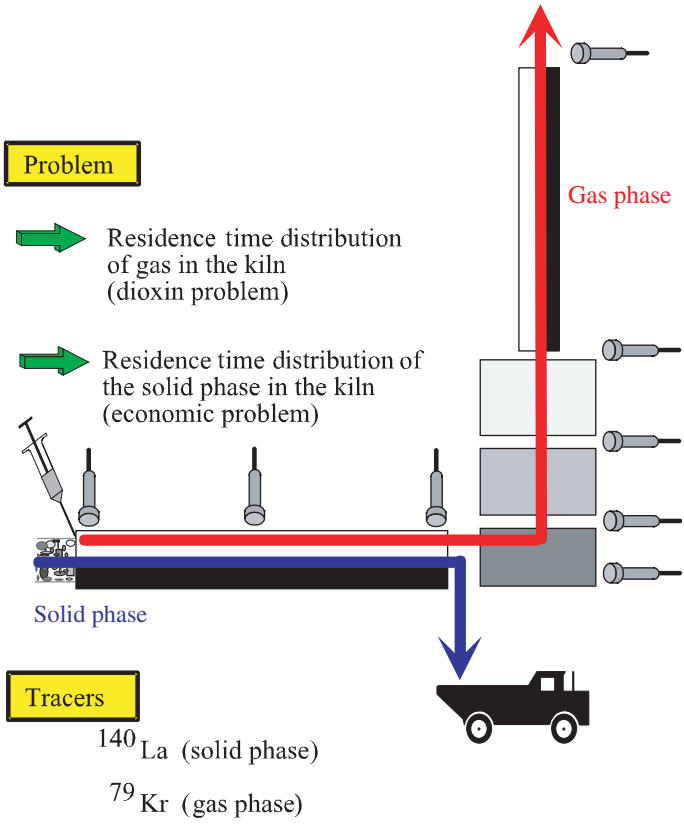

FIG. 68. Solid phase tracing in a chlorinated waste incinerator facility — design of the experiment.

the assumption that the tracer, as a powder, is irreversibly absorbed or fixed on the materials during the injection. The feed is composed of very heterogeneous objects: heavy and light ones, large and small ones, so the tracer tags different classes of population. RTD functions are decomposed into the minimum number of axially dispersed plug flow functions. Only seven elementary functions are necessary to fit the RTD functions perfectly. The first function represents the objects that progress fastest inside the kiln, probably light and

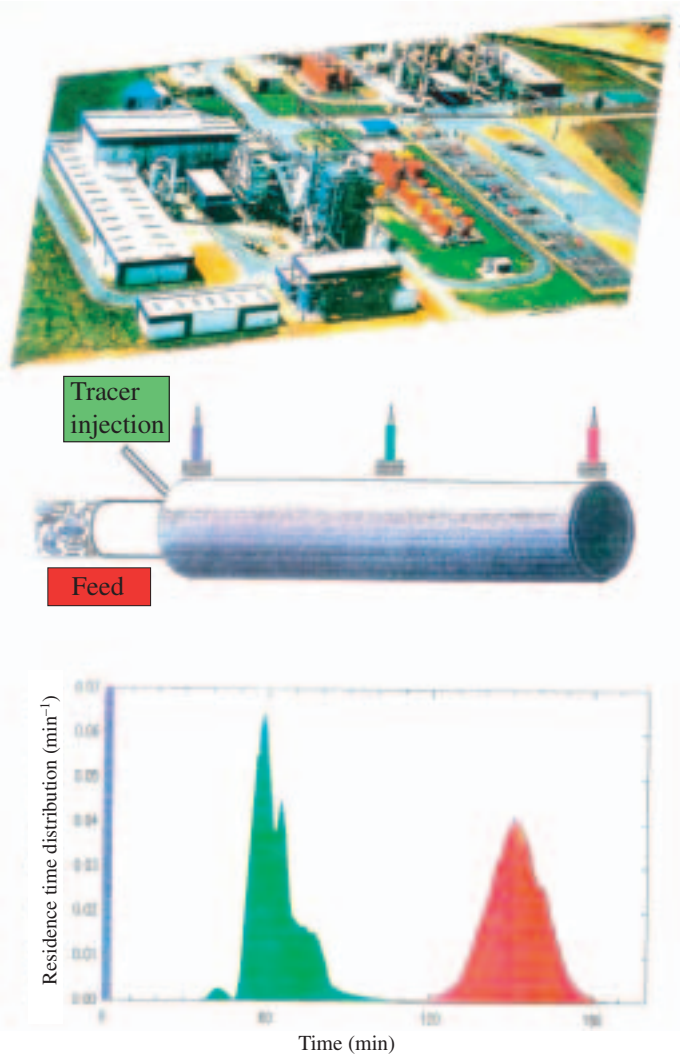

FIG. 69. Solid phase tracing in a chlorinated waste incinerator facility — results.

small ones. Correlations are made between each pair of peaks, leading to a specific overview of the behaviour of the seven different classes of population inside the kiln. The parameters, i.e. velocity and dispersion, are directly derived from the axial dispersed plug flow function parameters, as represented in Fig. 70 for the velocity distribution.

The conclusions reached are that:

(a) The velocity distribution is wider at the middle of the kiln, ranging from 3.5 to 6.5 m/h.
(b) All these velocities decrease and have a tendency to homogenize in the second part of the kiln.

This experiment was repeated: the RTD shapes were the same but with new classes of populations. The behaviour and velocity distributions were likewise the same. A few bricks were introduced at the inlet of the kiln. Restitution times were near the value for peak 7 in Fig. 70, leading to the conclusion that this peak is representative of large and heavy objects.

The mathematical decomposition of RTD functions was successful because of the large number of parameters (in this case 21, for seven peaks with three parameters: velocity, dispersion and area). The chances to obtain a good fit are obviously greatly enhanced by such a large number of parameters. This physical interpretation relies on the hypothesis that the tracer is fixed irreversibly on specific materials that it comes into contact with. This hypothesis is of course debatable. Nevertheless, this is a good example of the application of the method of peak decomposition.

These examples demonstrate the interest of response decomposition, in order to extract more quantitative and qualitative information from tracer test experimental curves, when signs of overlapping are obvious and can be attributed to physically significant phenomena. In such circumstances the interpretation of a tracer test, the aim of which is basically problem solving, may be improved. The test cases detailed in this section may seem to be quite complex and pushing the peak decomposition method to its limits. They show that decomposition of a tracer test curve cannot be an automatic routine operation. It relies very much on the operator, who has the ability to devise initial guesses and control the optimization process. It is the operator's responsibility to produce solutions with physical meanings and to analyse the validity of the method (i.e. the number of potential solutions, the most reliable solution and the limits to the interpretation).

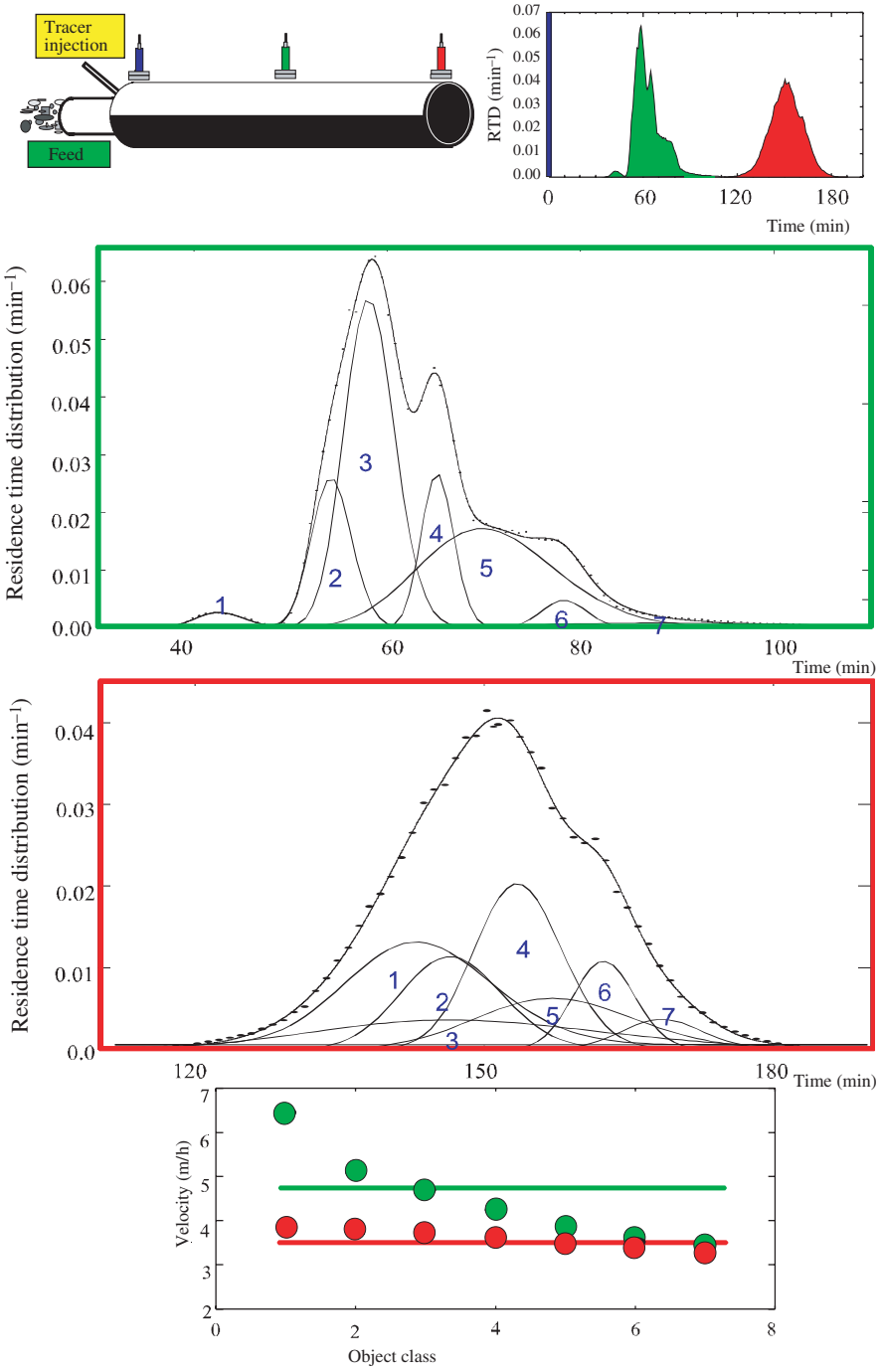

FIG. 70. Solid phase tracing in a chlorinated waste incinerator facility — interpretation by decomposition of RTD curves.

3.6.5. RTD system analysis

3.6.5.1. Methodology

From a well conducted tracer experiment it is expected to obtain, in the best case, the true RTD of the traced material in a system or in part of a system. Under less favourable circumstances, only an impulse response function between two points in the system can be obtained. This impulse response function does not possess the same conceptual power as a true RTD, but still contains valuable information. It has been seen in the previous section that one way to access this information is through decomposition into parallel elementary flows. This method is not always applicable as is, but it can be generalized to accommodate all shapes and types of RTDs or impulse response functions. In this approach, one tries to build a model consisting of an arrangement of basic flow elements so that the response of the model is identical, or as close as possible, to the signal from the tracer experiment in the system under study. This approach is sometimes known as system or systemic analysis. The following inputs are required:

(a) A set of elementary flow models that describe the basic phenomena of fluid flow,
(b) A set of rules to combine these elementary models,
(c) Some kind of optimization procedure that will make the model response fit the data from the tracer experiment.

The first two points are taken up here. The last point is a question of computer science and will not be dealt with. The software packages for RTD systemic analysis include Thyn's RTD software [16] and DTSPro [17].

It must be emphasized that, apart from these purely mathematical or numerical tools, some amount of intuition, experience and self-criticism is also required to make a sound systemic analysis of a tracer experiment.

3.6.5.2. Elementary models

Here a few elementary models that can be used as building blocks for a systemic model of a system are presented. For each model we indicate:

(1) The physical basis of the model.
(2) The parameters of the model and their meaning.
(3) A graph of its impulse response $E(t)$ (i.e. the response to a unit Dirac stimulus) and, whenever possible, the corresponding mathematical

expression. (We have chosen not to give the expression in the Laplace domain, which is quite useful for computational purposes but not very easy to manipulate.)

(4) An expression for the first moment (average residence time $\bar{t}$) and the centred second moment (variance σ^2) defined as:

$$\bar{t} = \int_0^\infty t\,E(t)\,\mathrm{d}t$$
$$\sigma^2 = \int_0^\infty (t-\bar{t})^2 E(t)\,\mathrm{d}t. \tag{69b}$$

Additional information, if required, can be found in Refs [10–12].

(a) Ideal models: Plug flow and perfect mixer

(1) In the plug flow model (Fig. 71) it is assumed that matter flows without any dispersion. In other words, this flow is purely convective. A Dirac injection is therefore transported without any deformation and shifted by a time lag τ, which is the only parameter of the model.

The mathematical expression for this model is:

$$E(t) = \delta(t-\tau), \tag{70}$$

where δ is the Dirac impulse function. The moments of this model are given in Table 7.

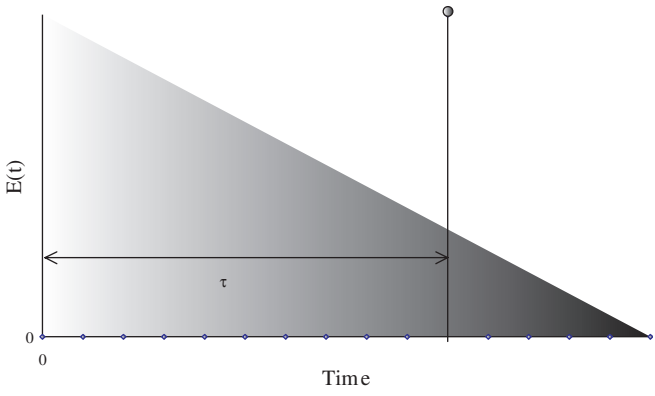

FIG. 71. Matter flow in the plug flow model.

TABLE 7. FIRST AND SECOND MOMENTS OF THE PLUG FLOW MODE

First moment $\bar{t}$	Second moment σ^2
τ	0

(2) In the case of a perfect mixer model (or perfect mixing cell model) (Fig. 72), tracer is assumed to be mixed instantaneously and uniformly throughout the volume of the system. This model has one parameter, the time constant τ which is equal to the ratio of system volume V and volumetric flow rate Q.

The mathematical expression for this model is:

$$E(t) = \frac{1}{\tau} \exp\left(-\frac{t}{\tau}\right) \tag{71}$$

and its moments are given in Table 8.

The plug flow and perfect mixer models can be seen as two limiting cases, where mixing is either non-existent or total.

(b) Dispersion models: Axial dispersed plug flow and perfect mixers in series

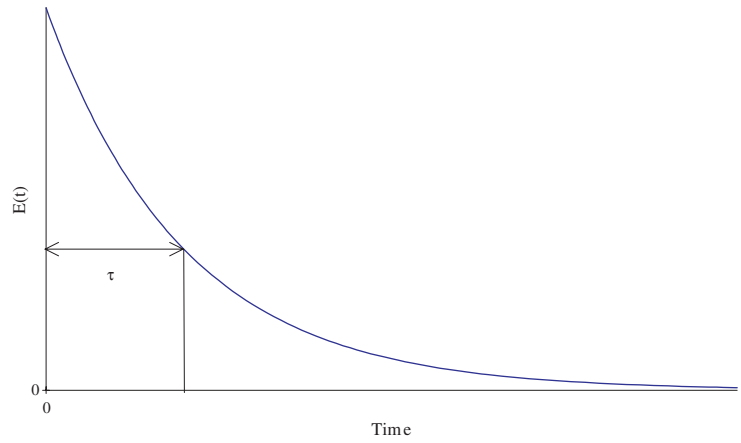

FIG. 72. Matter flow in the perfect mixer model.

TABLE 8. FIRST AND SECOND MOMENTS OF THE PERFECT MIXER MODEL

First moment $\bar{t}$	Second moment σ^2
τ	τ^2

Real flows often behave as intermediates between pure convection (plug flow) and pure mixing (perfect mixer). Among these flows, many can be seen as the superposition of a pure transport (convective) effect and a dispersive effect that blurs out the concentration gradients. It is often necessary to characterize these effects; convection is related with velocities and flow rates; dispersion has an adverse effect on heat and mass transfer which it is important to quantify. Two types of model can be used for this purpose:

(1) Axial dispersed plug flow (already described in Section 3.6.3),
(2) Perfect mixers in series — also called tanks in series or perfect mixing cells in series.

As indicated by its name, the model with perfect mixers in series is composed of perfect mixers connected in series (Fig. 73).

In Fig. 73, V is the total volume of the system and Q the flow rate. The number of mixers is traditionally termed J. Writing balance equations for tracer concentration in each mixer shows that the model parameters can be reduced to the time constant $\tau = V/Q$ and J. Some mathematical manipulation leads to:

$$E(t) = \left(\frac{J}{\tau}\right)^J \frac{t^{J-1} \exp\left(-Jt/\tau\right)}{(J-1)!}. \tag{72}$$

This expression behaves in much the same way as the one for the axial dispersed plug flow model, J playing the same role as Pe, as shown in Fig. 74 (which may be compared with Fig. 64).

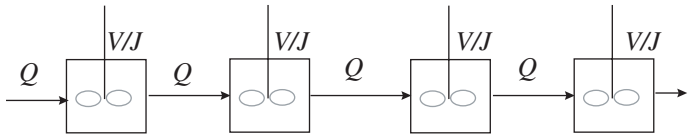

FIG. 73. Perfect mixers in series.

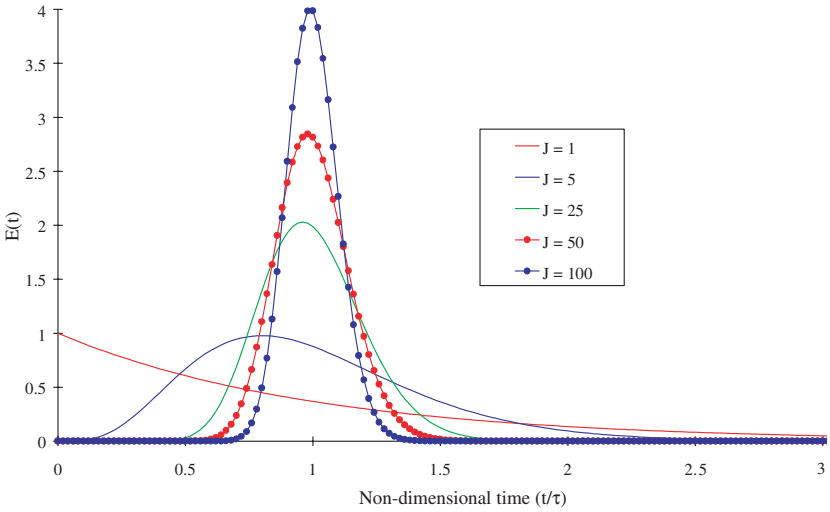

FIG. 74. Model with perfect mixers in series as a function of J, the number of perfect mixers.

As J becomes large, the impulse response becomes closer and closer to that of the axial dispersed flow model. Differences are insignificant beyond $J \approx 50$. The following equivalence relationship is often quoted for large values of J:

$$\mathrm{Pe} \approx 2(J-1). \tag{73}$$

Equation (72) has been established for integral values of J. It is possible to extend it to non-integral values (by the use of the Γ function instead of the factorial) so that J can be a continuous parameter just like the Péclet number. It may appear strange to have a non-integral number of mixers (what is the physical meaning of having, say, two and a half mixers?). Equation (72) can be seen as a purely ad hoc formulation for representing convection and dispersion phenomena. The moments of the model with perfect mixers in series are given in Table 9.

TABLE 9. FIRST AND SECOND MOMENTS OF THE PERFECT MIXERS IN SERIES MODEL

First moment $\bar{t}$	Second moment σ^2
τ	τ^2/J

One final question is the choice between the axial dispersed plug flow model and the mixer in series model, since both can be used to represent experimental curves with one peak and with a moderate tail. This question holds only for low to medium values of J or Pe. On the one hand, the axial dispersed plug flow model can be well suited to a continuous system, such as a pipe or a column. On the other hand, the physical relevance of this model can be suspect at low Péclet numbers. It is tempting to recommend, following the example of Villermaux [12], the model that is easiest to manipulate, i.e. the perfect mixers in series model. An exception might be the case when responses have to be computed at intermediate locations along the system, and not at the inlet and outlet only.

(c) Dispersion and exchange models

We have seen that dispersion models account only for moderate tailing in impulse response curves. Many experimental curves unfortunately do not fall within that category. This is especially the case for processes involving exchanges between a main flow and a stagnant fluid or a porous solid phase. Special models have been developed for that case, on the basis of either the continuous axial dispersed plug flow concept or the discrete perfect mixers in series model. Once again these two approaches can be shown to be equivalent. We shall therefore limit the present discussion to the discrete model with perfect mixers in series with exchange, which is simpler from a mathematical point of view.

The conceptual representation of this model is given in Fig. 75.

The main flow rate Q goes through a row of J perfect mixers of volume V_1 in series; each perfect mixer exchanges flow rate αQ with another mixer of

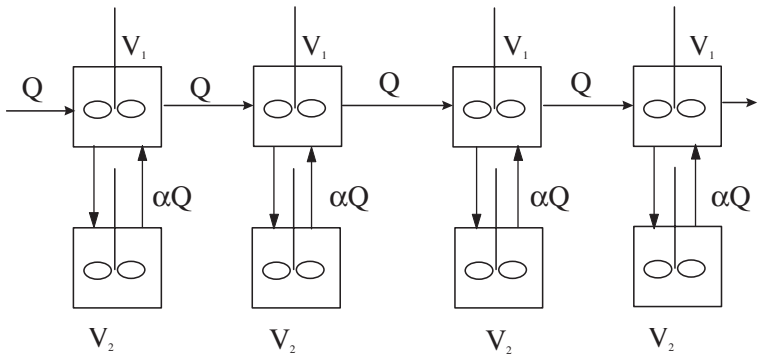

FIG. 75. Perfect mixers in series with exchange.

volume V_2. This model has four independent parameters that can be combined in many ways; one way is to consider the following parameters:

$$\tau = \frac{JV_1}{Q}, J, \; t_m = \frac{V_2}{\alpha Q} \text{ and } K = \frac{V_2}{V_1}.$$

Here τ and J are the parameters for the main flow; t_m is the time constant for the exchange between the main flow and the stagnant zones, or the inverse of a transfer coefficient between these two elements (the larger t_m, the smaller the exchange). K represents the relative importance of a stagnant zone with respect to the main flow. The effect of varying t_m and K is illustrated in Fig. 76.

The curves usually exhibit one peak. The sharpness of the peak is not coupled with the extent of tailing (as it was in the axial dispersed plug flow model), which makes this model quite versatile. This point is illustrated by the following example (shown in Fig. 77) from an experiment in a wastewater treatment plant, where fits have been attempted successively with the models with mixers in series and mixers in series with exchange.

It should, however, be noted that the model with mixers in series with exchange can have two, usually very unequal, peaks, as illustrated in Fig. 78 ($J = 500$, $t_m = 0.4$, $K = 1$).

There is no simple analytical expression for $E(t)$, although its equivalent in the Laplace domain is quite straightforward. The moments of this model are given in Table 10. This model is suitable for quite a number of processes (e.g. river flows, flows of chemically active substances in porous media and flows in trickle bed reactors or packed columns).

3.6.5.3. Rules for combining simple models

The models that have been reviewed are obviously not able to reproduce all possible tracer experiments (for instance, none is able to produce the

TABLE 10. FIRST AND SECOND MOMENTS OF THE MODEL WITH PERFECT MIXERS IN SERIES WITH EXCHANGE

First moment $\bar{t}$	Second moment σ^2
$\tau(1+K)$	$\frac{\tau^2(1+K)^2}{J} + 2K\tau t_m$

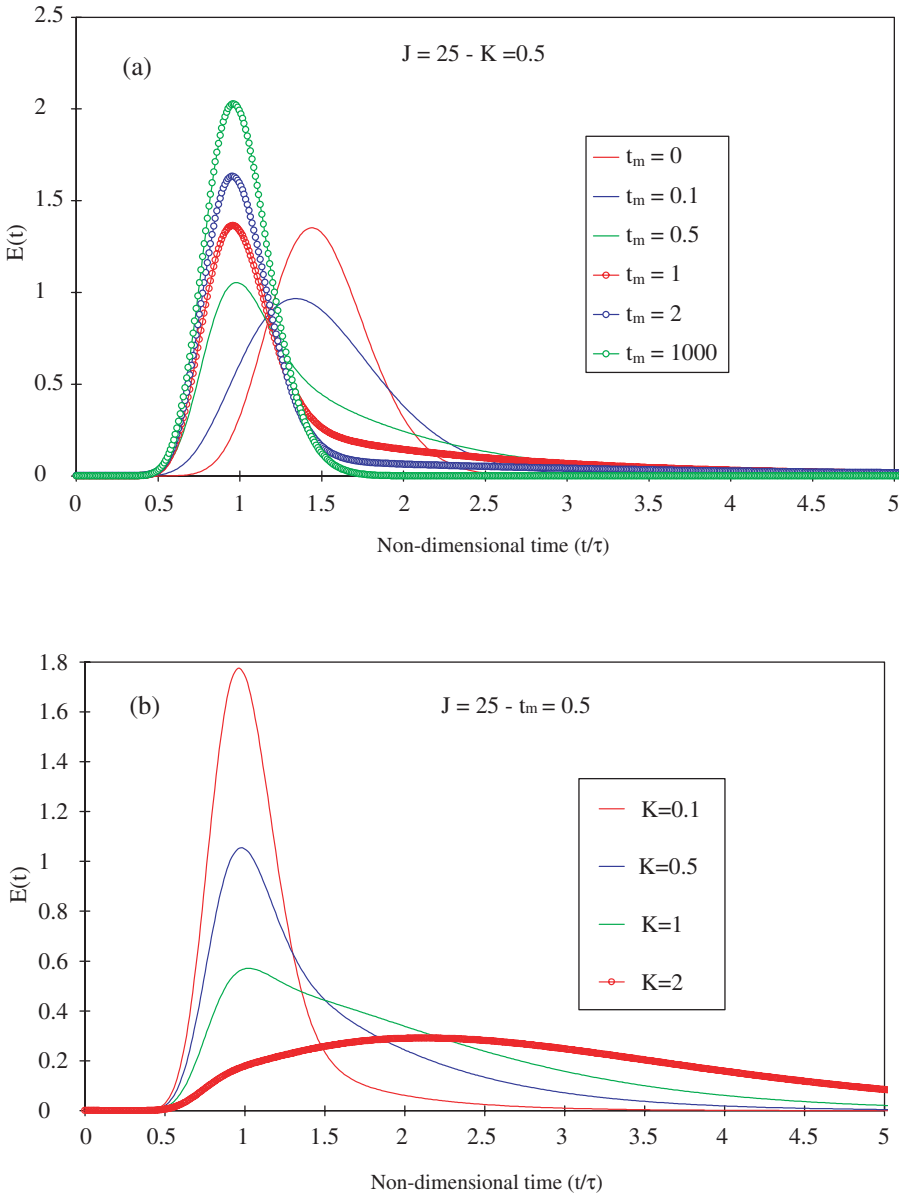

FIG. 76. Response of the model with perfect mixers in series with exchange to a variation in (a) t_m and (b) K.

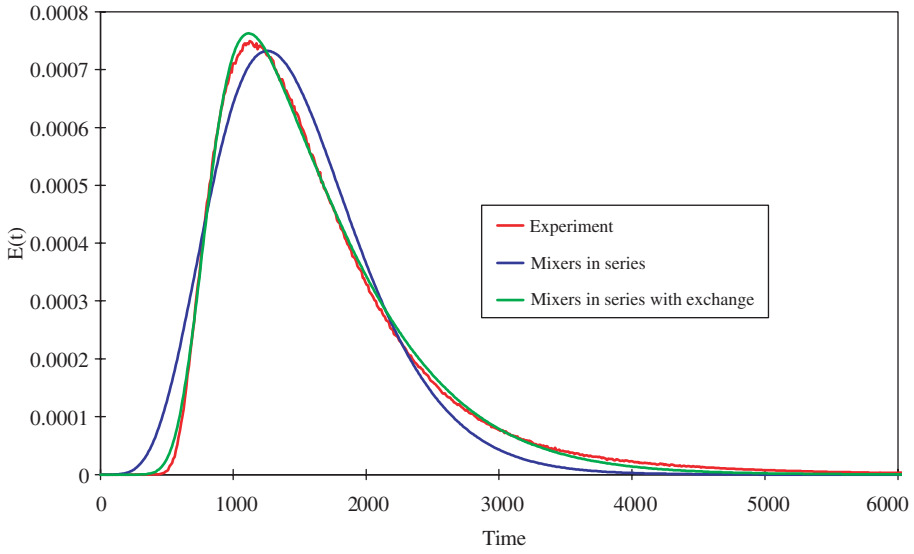

FIG. 77. Comparison of models with mixers in series and mixers in series with exchange.

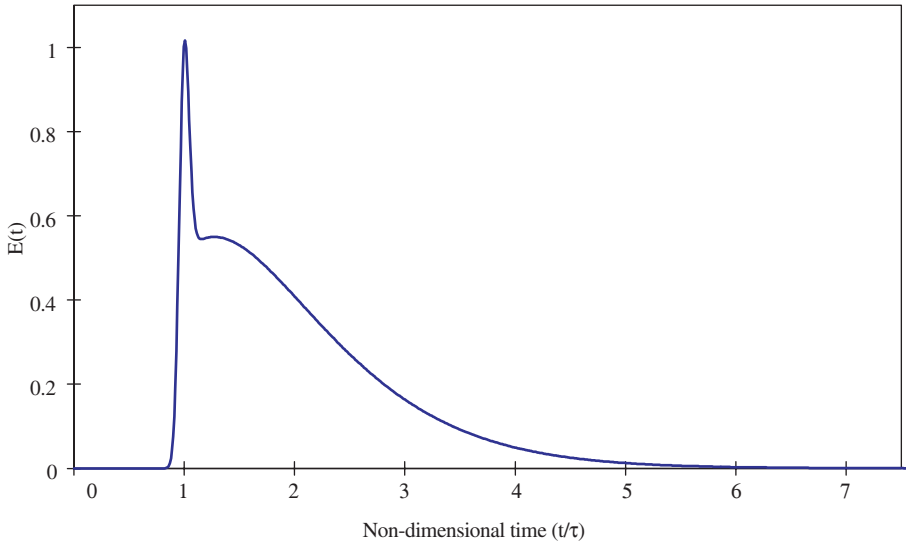

FIG. 78. Peak discrimination by a mixers in series with exchange model.

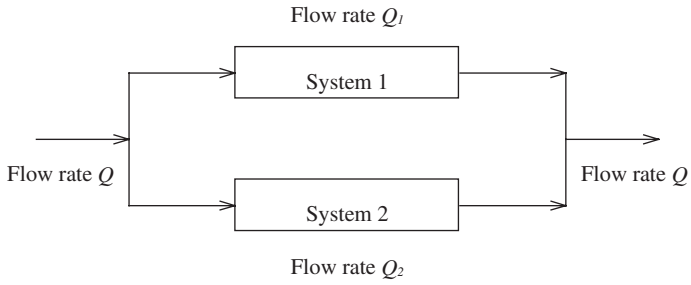

FIG. 79. Parallel models.

multiple peaks observed in systems with recycling). It is therefore necessary to have a set of rules for combining these models, in order to accommodate any shape of RTD or impulse response function.

Basically, systems can be associated in three ways: parallel, series and with recycling.

(a) Parallel models

The pattern of this type of model is shown in Fig. 79.

The system i has RTD $E_i(t)$, MRT $\bar{t}_i$ and variance σ_i^2. The rule for determining the RTD of the global system, $E(t)$, is as follows:

$$E(t) = \frac{Q_1}{Q} E_1(t) + \frac{Q_2}{Q} E_2(t). \tag{74}$$

The moments are given in Table 11.

TABLE 11. FIRST AND SECOND MOMENTS FOR PARALLEL MODELS

First moment $\bar{t}$	Second moment σ^2
$\frac{Q_1}{Q}\bar{t}_1 + \frac{Q_2}{Q}\bar{t}_2$	$\frac{Q_1}{Q}\sigma_1^2 + \frac{Q_2}{Q}\sigma_2^2 + \frac{Q_1 Q_2}{Q}\left(\bar{t}_1 - \bar{t}_2\right)^2$

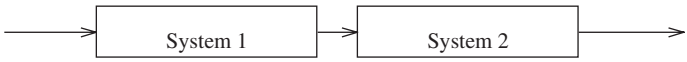

FIG. 80. Series models.

(b) Series models

The pattern of this type of model is described in Fig. 80.
The rule for series models is:

$$E(t) = E_1(t) * E_2(t), \tag{75}$$

where the asterisk denotes the convolution product (the ordinary product in the Laplace domain).

The moments for these models are given in Table 12.

(c) Models with recycling

The pattern of this type of model is shown in Fig. 81.
The rule for associating the RTDs is not simple in the time domain. We shall only mention that writing a tracer balance at node A yields:

$$E_1(t) * \left[\delta(t) + \alpha E_2(t) * E(t)\right] = (1+\alpha) E(t). \tag{76}$$

This equation can be solved for $E(t)$ in the Laplace domain only. Finally, the moments are expressed in Table 13.

TABLE 12. FIRST AND SECOND MOMENTS FOR SERIES MODELS

First moment $\bar{t}$	Second moment σ^2
$\bar{t}_1 + \bar{t}_2$	$\sigma_1^2 + \sigma_2^2$

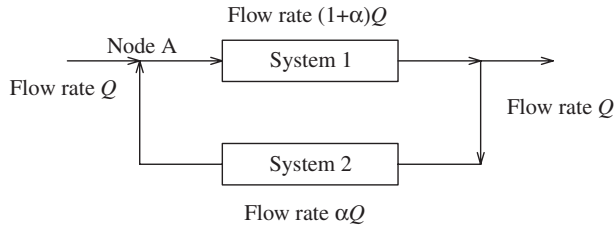

FIG. 81. Models with recycling.

3.6.6. RDT analysis and computational fluid dynamics modelling

At the present time two methods can be used for the study of complex systems: systemic analysis and CFD modelling. The advantages and disadvantages of each method are well known and are fairly complementary:

(a) Systemic analysis is simple and CFD is not.
(b) CFD is predictive and systemic analysis is not.
(c) CFD has also been shown to be prone to fail when hydrodynamics and physicochemical interactions are coupled.

Moreover, there is obviously some similarity between systemic models based on arrangements of perfect mixers and CFD models, and especially so in the case of finite volume models. It is therefore tempting to:

— Compare these approaches for specific cases, keeping in mind that this comparison will improve our understanding of the system under study;
— Try to 'unify' them into a single, rational approach that would benefit from the advantages of both.

These ideas are illustrated here through the example of a crystallization reactor. This reactor is fed countercurrently by two gaseous streams, a cold one

TABLE 13. FIRST AND SECOND MOMENTS FOR MODELS WITH RECYCLING

First moment $\bar{t}$	Second moment σ^2
$(1+\alpha)\bar{t}_1 + \alpha\bar{t}_2$	$(1+\alpha)\sigma_1^2 + \alpha\sigma_2^2 + \alpha(1+\alpha)(\bar{t}_1 + \bar{t}_2)^2$

and a hot one, the interaction of which creates solid particles. Tracer experiments were made on each stream, with a sufficient number of detectors to build a detailed systemic model that is represented on the left hand side of Fig. 82.

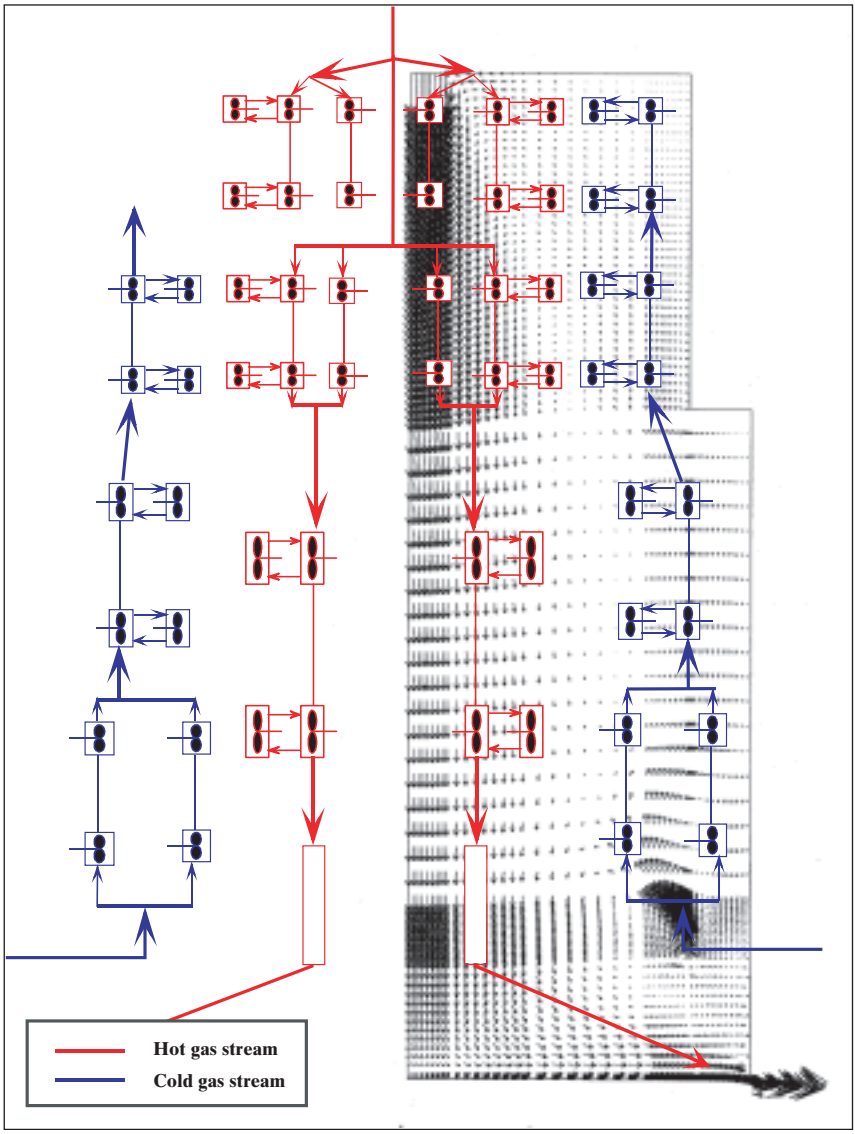

FIG. 82. Comparison of systemic and CFD models for a crystallization reactor (CFD computation performed with the CASTEM 2000 code).

A CFD calculation was also performed with a finite element code in two dimensions, because the reactor has an axial symmetry, with the k–ε model and standard wall functions (i.e. the same methods as in Section 3.3.1.2). A few minor developments were, however, required for this computation. Thermal effects and, especially, heat production by phase changes were taken into account, but not the specific behaviour of the solid phase; particles were assumed to be small enough to follow the bulk gas flow. On the right hand side of Fig. 82, the systemic model for hot and cold gas streams is superimposed on the computed mass velocity field. The qualitative agreement between these representations is quite remarkable. It may be interpreted in this way: the systemic approach detects and characterizes the main features of the flow (mixers, recirculations and so forth) while CFD enables them to be identified and located.

Another example, dealing with ventilation in an industrial facility, is presented in some detail as case study No. 2 (Section 4.2). These examples show that systemic and CFD models can be made to coincide. This means that CFD can be used to characterize (in terms of volumes, flow rates, locations, etc.) the flow patterns that have been identified by RTD experiments and systemic modelling. In this sense, CFD can be used in a quantitative way to complement the information obtained from the systemic approach. Another conclusion is that CFD may also be considered as a tool to analyse flows in a qualitative way and provide useful guidelines for the construction of detailed systemic models. In this way these approaches are more complementary than they are incompatible.

4. CASE STUDIES

4.1. CASE STUDY No. 1: DISPERSION IN A PACKED COLUMN

4.1.1. Introduction

Packed columns for gas–liquid contact have been extensively used for a long time [34] but increased attention has been paid in the last few years to the removal of volatile organic compounds from water [35], due to a new sensitivity to environmental pollution. New packings including random [36] and structured ones [37] have thus been developed. Among the numerous measuring techniques for characterizing these gas–liquid contacts [38, 39], the

radioactive tracer methodology appears to be particularly interesting [40–42]. The main reason is that non-radioactive techniques are generally unsuitable for providing reliable local measurements over a whole reactor without several intrusive data collection devices. Moreover, using this methodology either locally or globally should help in the derivation of more accurate and reliable models [43].

In the present work a column on the pilot scale has been used for determination of the hydrodynamic characteristics of a packing. This characterization includes the determination of velocities and dispersivities of both gaseous and liquid phases at different locations along the column.

4.1.2. Experimental design

The column is a 30 cm diameter glass column packed over 3.6 m as illustrated in Fig. 83. It works countercurrently and is filled with a Raschig Ralu flow 25 random packing made of polypropylene. The bed porosity was estimated by double weighing of a section of the column before and after saturation with water. The value was 95 ± 1%, which perfectly agrees with the data given by Raschig GmbH, Ludwigshafen; this value may evolve slightly with time due to a gradual settling of the packing. The water and air flow rates range from 0.5 to 2 and from 100 to 300 m^3/h, respectively.

4.1.2.1. Detection configuration

Several NaI 1.5 in. × 2 in. (38 mm × 51 mm) scintillation detectors were located at four different positions along the column from the bottom (gas distributor) to the top (liquid distributor). At each location two or four detectors were positioned at right angles in order to visualize any possible radial maldistribution of the concentrations of the labelled phase (Fig. 84). The collimators (shielding) are cylinders made of lead 32 mm thick and 120 mm high.

4.1.2.2. Selection of radiotracers

The gas phase (air) was marked with 74 MBq of the ^{41}Ar isotope and the liquid phase (water) with 370 MBq of the ^{82}Br isotope as ammonium bromide (NH_4Br). It can be shown that the quantity of radioactive argon injected in the air flow is sufficiently low not to change the total partial pressure of argon and

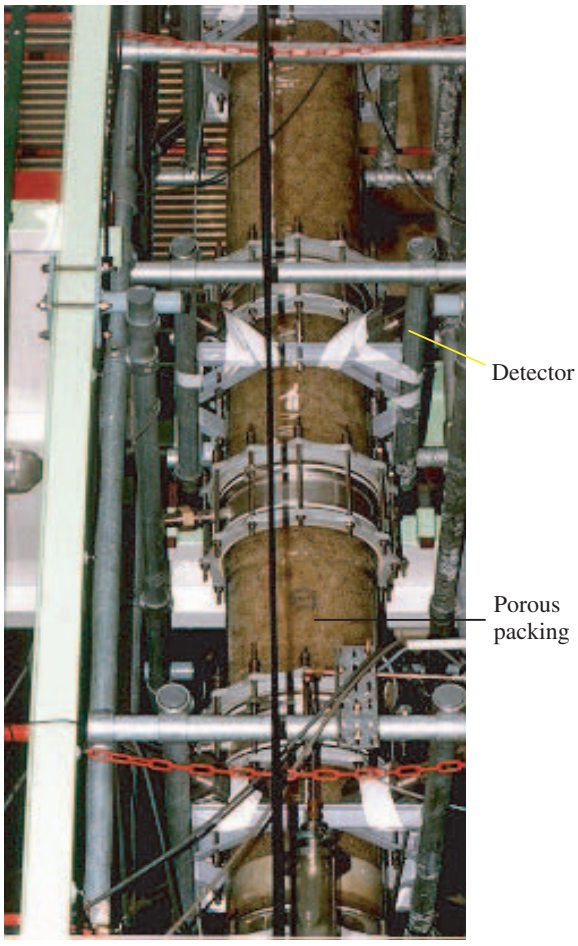

FIG. 83. A typical packed column.

thus the quantity initially dissolved in water. In the same way, the chemical form of bromine ensures that this tracer will remain integrally in the liquid phase.

The above activities have been chosen by simulating with the Monte Carlo code ECRIN the response of the NaI probes to a uniformly distributed source of tracer in the column. For such simulations, the porous medium has been simulated by water due to the fact that the linear attenuation coefficient of photon beams for both compounds are about the same. Figure 85 illustrates the simulated geometry.

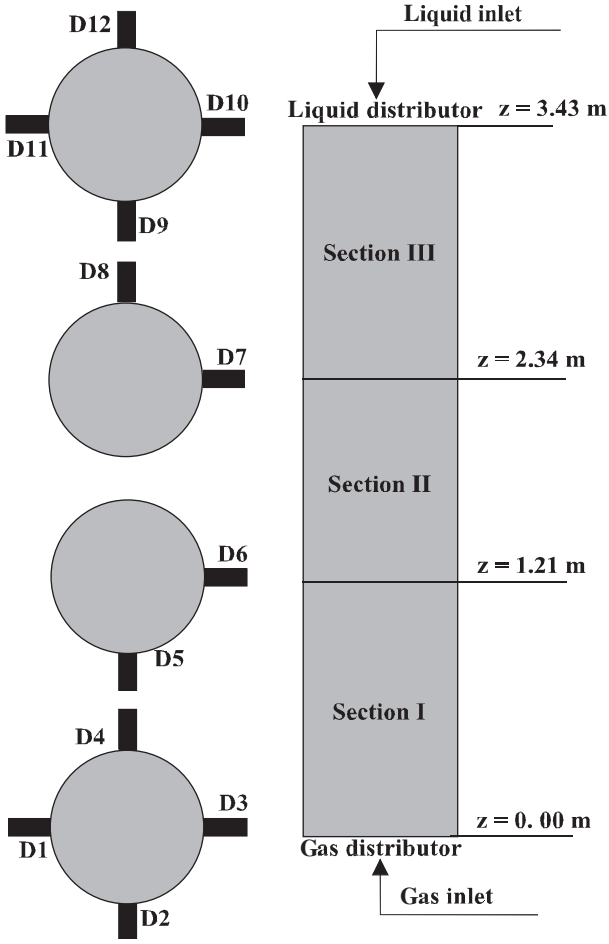

FIG. 84. Location of the detectors around the column.

For ^{82}Br, the simulated counting rate is 5.3×10^6 counts/s per 3.7×10^{10} Bq/m^3. Owing to the above mentioned assumption in the Monte Carlo simulation, the ^{82}Br volumetric activity is referred to the volume of the column, which leads to a counting rate equal to 2.2×10^7 counts/s per 3.7×10^{10} Bq. Therefore an activity of 370 MBq has to be sufficient for tracing the water flow while being adapted to local regulations concerning radioactivity handling. The axial spatial resolution of the measurement is illustrated in Fig. 86. This resolution is about ±20 cm, thus ensuring no intersection in the different volumes of detection along the axis of the column.

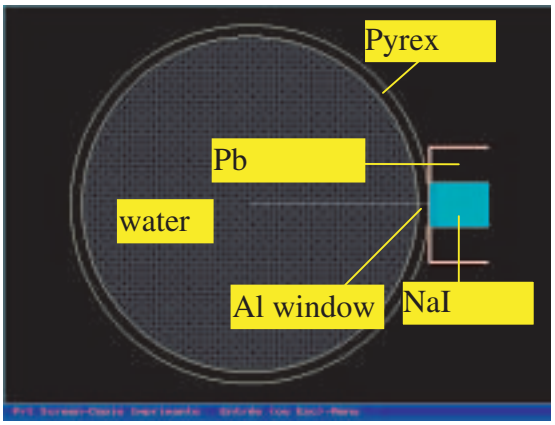

FIG. 85. Simulated geometry with the Monte Carlo code ECRN.

For ^{41}Ar, the simulated counting rate is 1.6×10^6 counts/s per 3.7×10^{10} Bq/m^3, which leads to 6.7×10^6 counts/s per 3.7×10^{10} Bq. In that case 74 MBq is a good compromise between a sufficiently large counting rate and the regulations concerning this isotope. The axial distribution of counting rates on both sides of a probe is about the same (±20 cm in width) as for ^{82}Br (Fig. 86).

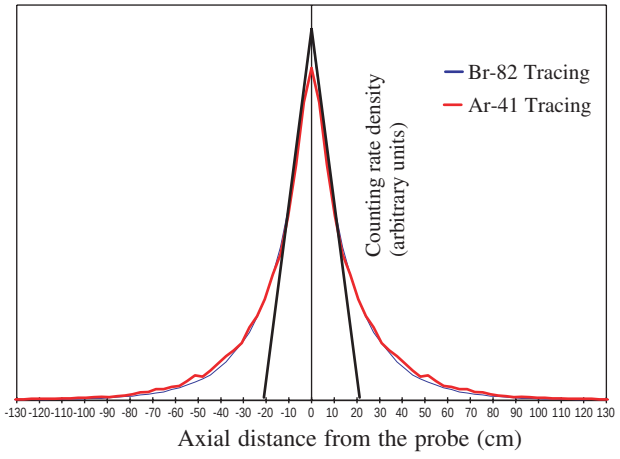

FIG. 86. Axial resolution, liquid and gas.

4.1.3. Data processing methodology

Owing to the fast phenomena occurring in the column, the sampling period has been reduced to 10 ms for the first 30 s of the experiments, with simultaneous data acquisition for all the detectors. The sampling period is 100 ms after the first 30 s.

4.1.3.1. Raw data treatment

Prior to be being quantitatively interpreted in terms of column dynamics, the raw signals have to be corrected for:

(a) Natural decay of the radioisotope ($T_{1/2}$ = 110 min for argon and $T_{1/2}$ = 36 h for bromine);
(b) Counting statistics, which follow the Poisson law;
(c) Background noise that can increase during the test due to the accumulation of radioactivity in the experimental device.

The whole treatment is performed by the PeakFit software [26]. Noise filtering is based either on the FFT algorithm if the points are equally spaced in time or on the Loess procedure in the case of irregular sampling periods ranging in the situation considered from 10 to 100 ms.

If necessary, prior to the baseline correction, data can be extrapolated using either an exponential e^{-at} (turbulent diffusive flow) or a power a/t^3 (laminar flow) decrease in order to make the signal return to the baseline at the end of the experiment.

The interpretations presented hereafter assume that the tracer is uniformly distributed over the inlet cross-section.

4.1.3.2. Total count analysis

The detection system was fine tuned to make sure that the responses of all the detectors were identical. It was therefore possible to compare their signals in terms of total counts (providing that there was not too much noise). Such a comparison can yield interesting information, as indicated below.

In a given cross-section, identity of total counts is a strong indication that the flow of the labelled phase is axisymmetrical. This is because the width of the detection volume of each detector was significantly narrower than the column diameter, due to a suitable arrangement of the collimators, so that there was minimal overlapping. Another reason is the attenuation of radiation by the medium inside the column, which follows the classical extinction law:

$$\frac{dI}{dx} = -\mu I, \tag{77}$$

where I is the intensity of the radiation and μ is the linear attenuation coefficient, which depends on the nature and the density of the medium.

In the case considered, the attenuation coefficients for water and polypropylene are both approximately equal to 7×10^{-2} cm^{-1} and the gas is practically transparent. Integrating this equation along the diameter of the column, d_c, gives the following relation:

$$N = \int_0^{d_c} I_0(x) \exp\left(-\int_0^x \left[\varepsilon_l(y) + \varepsilon_p(y) \right] \mu \, dy \right) dx, \tag{78}$$

where N is the actual count number, $I_0(x)$ is the intensity of radiation emitted at distance x from the detector, which is proportional to local activity and therefore to the local tracer concentration, and ε_l and ε_p refer to the liquid and packing volume fractions, respectively.

N can therefore be seen as a truly weighted average of the activity contained in the detection volume. If the liquid phase is uniformly distributed in the cross-section, the barycentre of this weighting function is about 10 cm away from the detector. In a given cross-section, identical total counts along different diameters or from opposite detectors are thus an indication that the flow of the labelled phase is axisymmetrical.

A few numerical simulations were made with Eq. (78) to estimate the effects of attenuation as a function of the distribution of the liquid phase in a cross-section of the column, provided that it remains axisymmetrical (e.g. uniform, concentrated in the centre of the column or concentrated near the walls). It was shown that attenuation was relatively insensitive to the latter, for ε_l ranging from 0 to 40%. This observation allows the distribution of the liquid phase to be considered homogeneous when analysing these data. Another important consequence is that differences in total counts at two levels can only be attributed to a variation in ε_l, which in turn mainly depends on the thickness of the liquid films. For example, Eq. (78) indicates that total counts should decrease by 35% when ε_l increases from 0 and 40%. This result is consistent with the observed variation of the count number along the column in the gas tracing experiments.

4.1.3.3. RTD analysis

Since the phases seem to be uniformly distributed in a cross-section, Eq. (78) shows that the total count is proportional to I_0. Thus, RTDs are simply obtained by area normalization of the signals.

The review by Shah et al. [38] lists a variety of methods for the exploitation of RTDs. We have used two of them. Firstly, the RTDs were analysed in terms of statistical moments. The differences in RTD first moments at levels i and j give the transit time t_{ij} and the interstitial velocity u_{ij} between the two points:

$$u_{ij} = t_{ij}/L_{ij}, \tag{79}$$

L_{ij} being the distance between i and j. Provided that some kind of model is assumed, the differences between the variances (centred second order moments) σ_i^2 and σ_j^2 should yield, at least theoretically, some information on the flow Péclet number Pe and the dispersivity. Assuming, for example, one dimensional dispersive plug flow in an infinite medium, Pe is given by:

$$\mathrm{Pe} = \frac{2t_{ij}^2}{\sigma_i^2 - \sigma_j^2}, \tag{80}$$

where

$$\mathrm{Pe} = u_{ij}L_{ij}/D$$

and D is the dispersion coefficient.

As will be shown later, this method did not prove very effective for the experiments discussed here.

Another method is to adjust the flow parameters of a model. Assuming once again one dimensional dispersive plug flow in an infinite porous medium, one obtains [44] the following RTD E_{ij} between two measurement points i and j:

$$E_{ij}(t) = \frac{L_{ij}}{\sqrt{4\pi Dt^3}} \exp\left(-\frac{\left(L_{ij} - ut\right)^2}{4Dt} \right). \tag{81}$$

The signals $S_i(t)$ and $S_j(t)$ recorded by detectors i and j are thus related by the convolution integral:

$$S_i(t) = \int_0^t E_{ij}(t-\tau) S_j(\tau)\,\mathrm{d}\tau. \tag{82}$$

The convolution integral was computed using a Fourier transform. The time steps were 10 and 100 ms for the gas and liquid tracer experiments, respectively. The parameters u and D were optimized by a modified Levenberg–

Marquardt algorithm to have the best least squares fit with the experimental signals.

There are two limitations to this method:

(1) It should, strictly speaking, be applied neither to the detectors near the entrance (because the flow is not yet fully developed) nor to those at the outlet of the column (because the porous medium is not infinite). This means that only the measurements from detectors 5, 6 and 7, 8 (Fig. 84) should be exploited. Considering, however, that the detection volume of the other detectors is still mostly in the packing and that an excellent fit could always be obtained (see, e.g., Figs 88 and 90), we chose to use the measurements from detectors 1–4 and 9–12 as well.

(2) It implies that both u and D are constant along the column; the same values should therefore be obtained from all detector pairs. This is unfortunately not the case, as will be shown later. An explanation might be that the model is indeed inadequate and that a more sophisticated one — for example, the model with axial dispersed plug flow with exchange proposed by Van Swaaij et al. [45] or the stochastic model developed by Briens et al. [46] — should be used. Considering once again that Eqs (81) and (82) could always be fitted very well with the experimental data, the choice made here is to assume 'slowly varying' u and D and to interpret the values of u_{ij} and D_{ij} obtained from detectors i and j as the average interstitial velocity and dispersion coefficient, respectively, in section i–j. The fact remains that the values obtained from the end sections (and especially the entrance section) should not be taken too literally but rather be seen as an indication of the trends in the variations of velocity and dispersivity.

4.1.4. Results and discussion

4.1.4.1. Gas tracing

The total net counts and operating conditions in a typical experiment are given in Table 14.

Table 14 shows that:

(a) Total counts are almost identical at each level (1–4, 5 and 6, 7 and 8, 9–12). This strongly suggests that the flow is always axisymmetrical. This observation allows us to consider the signals from all the detectors at a given cross-section as simultaneous measurements of the same quantity

TABLE 14. TOTAL COUNTS RECORDED BY EACH DETECTOR IN THE GAS TRACING EXPERIMENT CONSIDERED

(liquid flow rate, 2 m^3/h; gas flow rate, 200 m^3/h)

Detector No.	Surface (counts)
1	10 386
2	9 910
3	10 921
4	11 158
5	17 177
6	16 563
7	16 556
8	16 243
9	17 139
10	17 041
11	16 939
12	17 357

and therefore to use them to estimate the uncertainty on cross-section averaged quantities.

(b) On the other hand, total counts increase dramatically between the first (1–4) and second (5 and 6) measurement stations and then remain approximately constant. This is an indication that the equivalent thickness of absorbing material, i.e. solid + water, is much larger at the bottom of the column (with $\mu = 0.07$ cm^{-1}, this extra thickness can be very roughly evaluated as about 10 cm — a third of the column diameter). This may be interpreted either as an increase in ε_l at the bottom of the column or as a consequence of entrance effects due to the vicinity of the gas distributor.

RTD moment analysis proved disappointing. The values for u and D obtained by this method resulted in poor agreement with experimental data when used in Eqs (81) and (82), as shown in Fig. 87. More precisely, velocity appeared to be correct while the dispersion coefficient was clearly overestimated.

A similar observation has already been reported in Ref. [47]. The reason is that the second order moments are not reliable because of the excessive weight of count fluctuations at large times. This shows that moment analysis is only useful for estimating velocities and making initial guesses of D for the model optimization procedure. An interesting finding is nevertheless that the velocity is significantly higher in the first section than in the rest of the column (1 and 0.85 m/s, respectively, see Fig. 89). This observation is in good agreement with our interpretation of total count variations, since an increase in ε_1 obviously leads to a reduction of the gas flow sectional area.

Optimization of u and D in Eqs (81) and (82) allowed an excellent fit of the experimental data, as shown in Fig. 88. The values for the gas interstitial velocity and the dispersion coefficient are summarized in Fig. 89. They have been calculated for each consecutive section of the column (I, II and III in Fig. 84). The error bars in Fig. 89 are the standard deviations of the values obtained from each pair of detectors in the studied section.

As already shown by moment analysis, the velocity in section I was found to be significantly larger than in the following sections. This demonstrates once again the influence of end effects, possibly liquid film thickening near the gas distributor. As a consequence, the dispersive plug flow model is probably at fault in this region. On the other hand, the velocity was stable in sections II and III, which suggests that a developed flow regime was practically reached and that the model should be reliable in these sections.

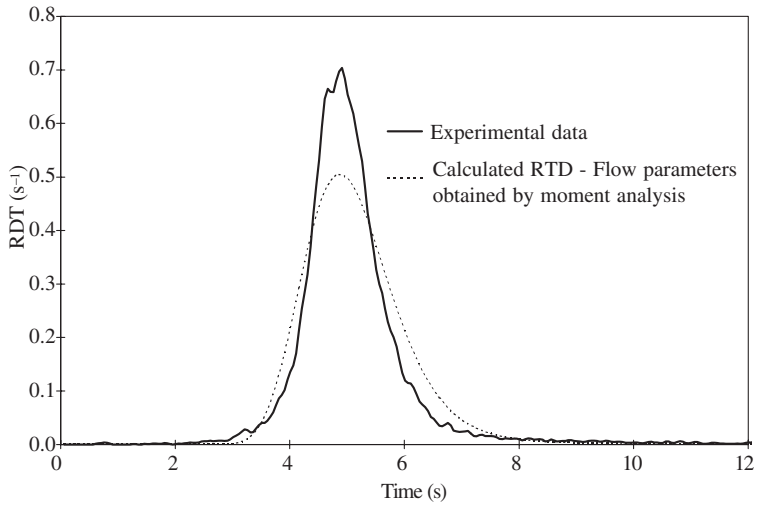

FIG. 87. Experimental and calculated gas RTDs with flow parameters calculated by moment analysis.

4.1.4.2. Liquid tracing

The operational conditions are identical to those of the previous gas experiment (Table 14). The raw signals contained much more noise than those in the gas experiments, which led to inconsistent observations when applying the total count analysis. Moreover, this noise induced a larger uncertainty in the estimation of the flow parameters.

Moment analysis did not perform better than for the gas flow and, once again, strongly overestimated the dispersion coefficient. This analysis, however, suggested that liquid velocity was about constant along the column.

An excellent fit could again be obtained by model optimization (Fig. 90). The axial liquid velocity was shown to be uniform along the column, as depicted in Fig. 91, where the velocity variations all lie within the error band. On the other hand, the liquid dispersion coefficient (also shown in Fig. 91) was found to increase continuously as the fluid moves down the column. The increase was especially significant in section I.

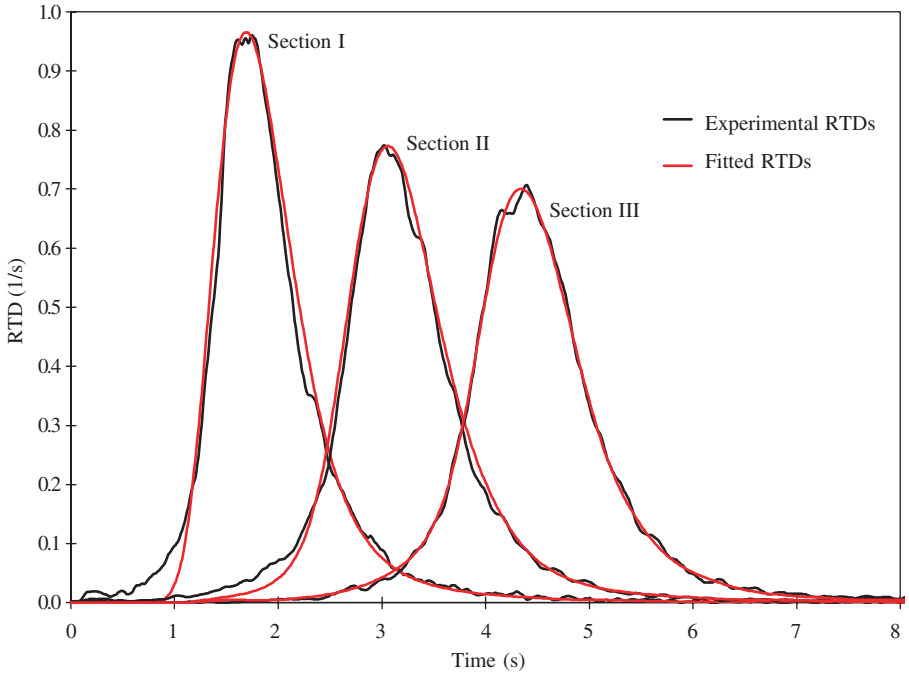

FIG. 88. Experimental and calculated gas RTDs with flow parameters obtained by optimization.

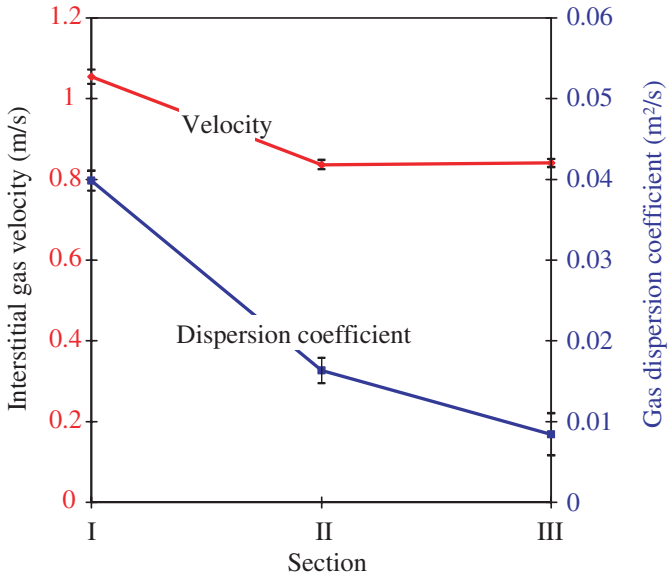

FIG. 89. Evolution of gas interstitial velocity and dispersion coefficient in the column.

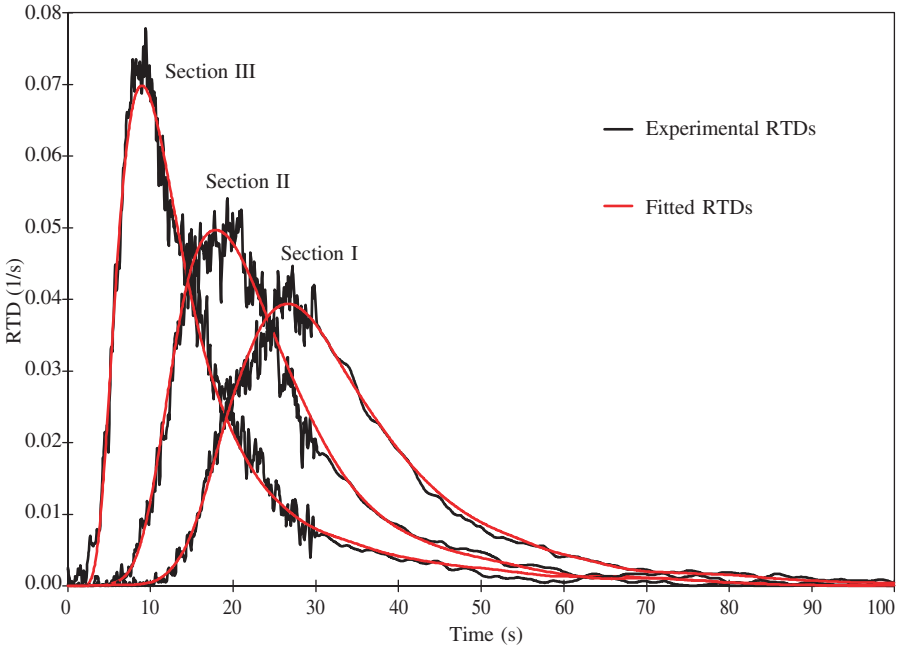

FIG. 90. Experimental and calculated liquid RTDs with flow parameters obtained by optimization.

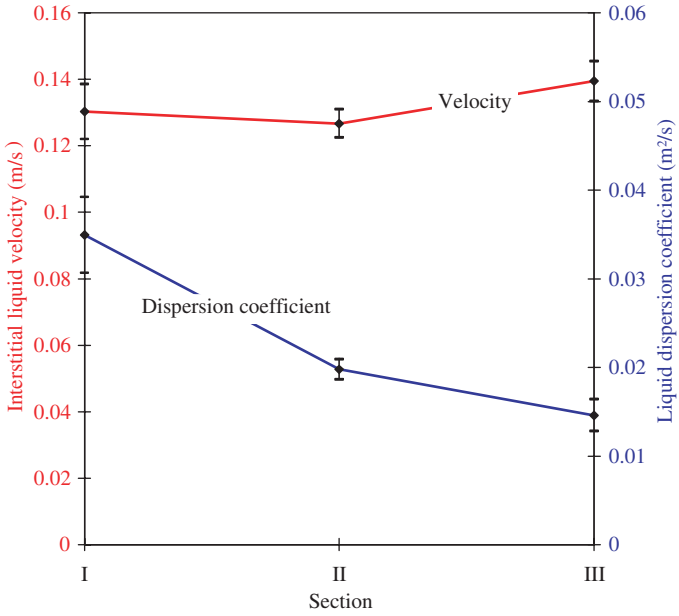

FIG. 91. Evolution of liquid interstitial velocity and dispersion coefficient in the column.

Axial dispersion may in fact result for two reasons: the truly diffusive character of the flow (due to molecular or turbulent diffusion) or the existence of a velocity profile in the radial direction (i.e. a convective effect). Both phenomena are lumped into a single apparent dispersion coefficient by the axial dispersed plug flow model. It is in theory possible to determine which phenomenon is predominant: RTD variance should be proportional to axial distance in the case of purely diffusive effects and to the square of distance in the case of convective effects.

Since direct calculation of second order moments is not reliable, the variances can be reasonably estimated from the optimized axial dispersed plug flow curves. Figure 92 shows a typical plot of the second moment as a function of distance from the uppermost detectors (9–12). The resulting points seem to be correctly fitted by a parabola, but no definite trend can be given. Probably both convective and diffusive effects occur. This evolution also sheds some doubt on the soundness of a global input–output approach based on the dispersive plug flow model.

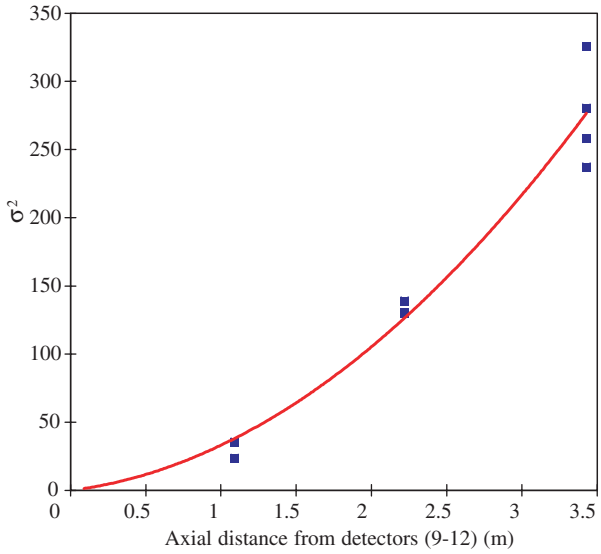

FIG. 92. Evolution of variance as a function of axial distance.

4.1.4.3. Influence of flow rate

All the flow parameters considered in this section are relative to the middle section of the column (section II), to avoid any interference from end effects. Both the liquid and gas interstitial velocities have been determined as the corresponding mean values obtained from all the detectors in this section.

The influence of the gas and liquid flow rates on the interstitial gas velocity u_g is shown in Fig. 93. It appears that this velocity depends solely on the gas flow rate whatever the liquid superficial velocity u_l in the range from 2×10^{-3} to 8×10^{-3} m/s (i.e. flow rate between 0.5 and 2 m^3/h). The variation of the gas velocity can then be expressed using a linear relationship, from which one can deduce that the gas hold-up ε_g, defined as:

$$\varepsilon_g = \frac{Q_g}{Su_g} \tag{83}$$

is practically constant and equal to about 83% in the studied range of flow rates.

On the other hand, the interstitial liquid velocity is an increasing function of the gas flow rate but also depends on the liquid flow rate as shown in Table 15.

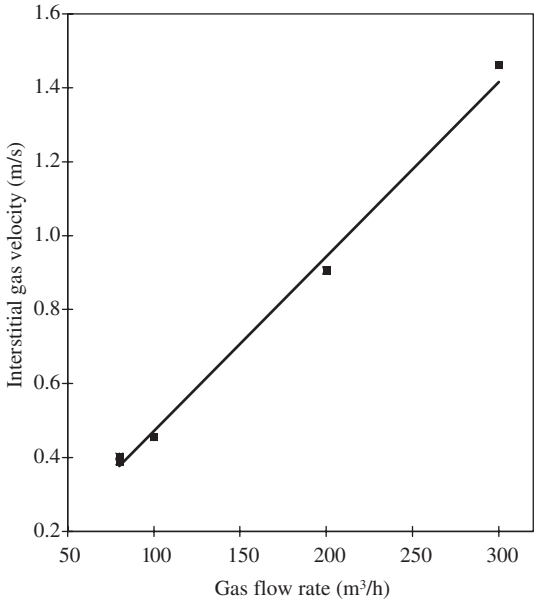

FIG. 93. Evolution of the interstitial gas velocity as a function of the gas flow rate.

Nevertheless the resulting variations of the liquid hold-up (defined in the same way as the gas hold-up) are quite low. The mean value is about 5% and the standard deviation is 1% in the range of gas and liquid flow rates studied. The sum of the gas and liquid hold-ups is then about 88%, i.e. the total material balance (gas + liquid + packing) is approximately 93 instead of 100%. We consider this result as satisfactory, keeping in mind that the standard deviations

TABLE 15. EVOLUTION OF INTERSTITIAL LIQUID VELOCITY AS A FUNCTION OF GAS AND LIQUID FLOW RATES

Gas flow rate (m^3/h)	Liquid flow rate (m^3/h)	Interstitial liquid velocity (m/s)
200	1	0.096
200	2	0.134
300	2	0.156
300	3	0.197
100	1	0.105
100	2	0.129

on ε_g and ε_l are 4 and 1%, respectively, and that the relative uncertainty of Q_g is 1.5% and that of Q_l ranges from 0.5 to 2%.

4.1.4.4. Comparison with existing correlations

The literature gives numerous correlations for the dispersive properties of packed columns. In these correlations the particle Péclet number for phase *n* is defined by:

$$\mathrm{Pe}_n^* = \frac{d_p u_n}{D_n}, \tag{84}$$

where d_p denotes the equivalent particle diameter, expressed as a function of the Reynolds number:

$$\mathrm{Re}_n = \frac{u_n d_p}{\nu_n}. \tag{85}$$

These correlations appear to be remarkably heterogeneous: the parameters taken into account differ widely and so does the variation with a given parameter (e.g. Pe_l^* increases with liquid Reynolds number in some correlations and decreases in others). Subject to the above mentioned limitations of the diffusive model, it has been shown that the axial mixing seems to increase as the liquid moves down the column, even if it has not been possible to determine the origin of this phenomenon. This evolution could then be responsible for the considerable discrepancies between the liquid and gas Péclet numbers found in the literature.

We have compared our results with these expressions which have mostly been established for values of Re_g (~100) and Re_l (~100) smaller than the ones considered here (Re_g ~ 1000; Re_l ~ 300), for bed porosities of less than 73%, for generally small scale reactors and naturally for other packings than our own. It is worth noting that, despite these differences, the orders of magnitude given by these correlations are generally in good agreement with the experimental values, as shown in Figs 94 and 95.

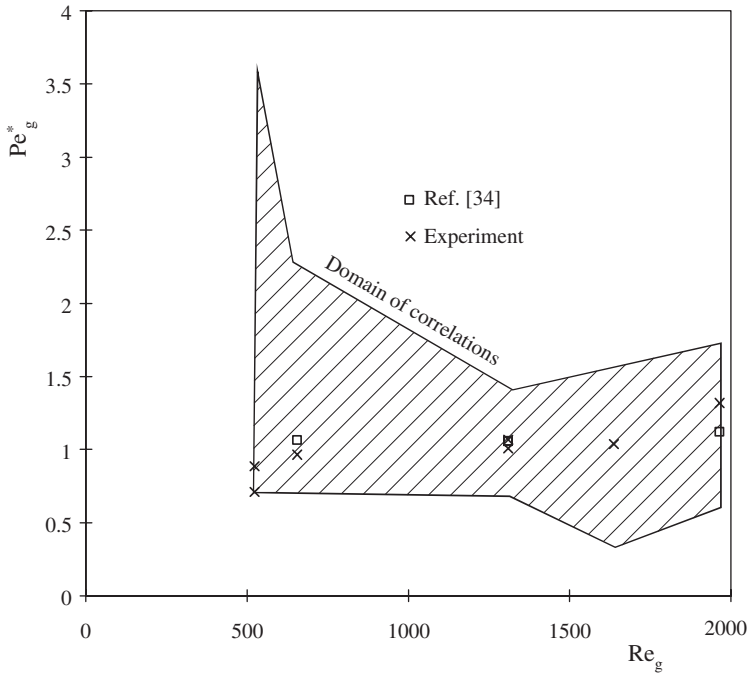

FIG. 94. Comparison of experimental and calculated values [34] of the gas Péclet number.

4.2. CASE STUDY No. 2: ROOM VENTILATION

4.2.1. Introduction

In order to help prevent hazards in industrial premises, the design of a proper air distribution system is essential. Such a design requires not only the measurement of the air change rate, but also a sufficiently detailed description of the air flow pattern. To achieve these goals, several tools are available, including:

(a) Gaseous tracers: When properly carried out and interpreted, a tracer pulse experiment can yield detailed information on the circulation of air inside the room; a particularly interesting, though little used, category of tracers are radioisotopes [48].
(b) RTD analysis and systemic, or zonal, models: This approach was first developed for chemical engineering [49] but seems to have gained in

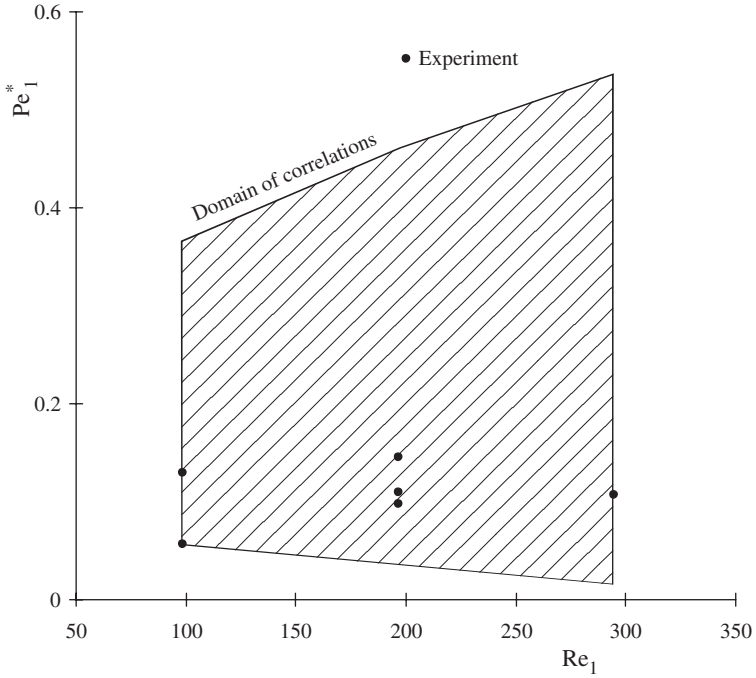

FIG. 95. Comparison of experimental and calculated values [34] of the liquid Péclet number.

popularity in the ventilation community [50–52]. Zonal models are simple and cost effective, but they should be handled with some care.

(c) CFD: Although this has received a lot of attention in the past, numerical predictions of flows in complex three dimensional enclosures are not yet reliable enough [53]. CFD is nevertheless valuable for identifying the main features of flow patterns.

The aim of this example is to emphasize the potential of the systemic approach in so far as it is supported by sufficiently detailed tracer gas measurements. Confidence in the physical relevance of the systemic model can be enhanced by CFD calculations. An application of this approach is presented for the study of room ventilation in industrial facilities.

4.2.2. Experimental design

The room under study is not very large ($5 \times 4.5 \times 3.2\ m^3$, i.e. $72\ m^3$ including internals) and separated into two unequal parts by a wall (Fig. 96). It

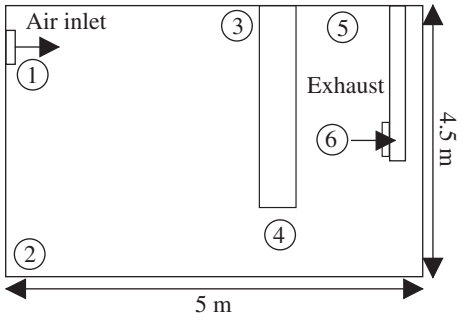

FIG. 96. Room layout for case study No. 2.

is ventilated by means of an air inlet and an exhaust duct. The air flow rate is 670 m^3/h, which corresponds to a nominal air change rate of 9.3 h^{-1}. The aim of this tracer experiment was basically to measure the air change rate in the room. It was also hoped that this would give some insight into the flow pattern.

The tracer gas was ^{133}Xe, obtained by irradiation of natural xenon in a nuclear reactor. This gas is a gamma emitter (half-life, 5.27 days; main gamma energy, 81 keV). Tracer activity was limited to 1850 MBq for each test, which allowed good measurement accuracy and limited exposure to radiation.

The gamma detectors were scintillation probes, composed of a 2 in. × 1.5 in. (5.12 cm × 3.81 cm) NaI(Tl) scintillator, a photomultiplier and a voltage divider. They were calibrated prior to the experiment. Their response decreases very sharply with distance. Table 16 shows the relative intensity of the signal (i.e. the signal at distance *d* divided by the signal at distance zero) due to a ^{133}Xe point source, as a function of distance.

The signal from a detector can therefore be seen as a measurement of the volume averaged activity in a sphere of about 40 cm in diameter.

The tracer was injected as a pulse into the bulk of the air inlet flow. This provided a Dirac function as the input signal and also ensured good mixing of

TABLE 16. RELATIVE VARIATION OF SIGNAL INTENSITY WITH DISTANCE

Distance to detector (cm)	Relative signal intensity (%)
0	100
20	0.5
40	0.1
100	0.02

the tracer. Detection was performed at six points in the room (1–6 in Fig. 96), including the inlet (point 1) and the exhaust opening (point 6).

The signals of the respective probes were continuously and simultaneously monitored (as counts per second) by a microcomputer with an acquisition frequency ranging from 0.2 to 100 Hz. This acquisition system can accommodate as many as twelve probes. The raw signal was corrected for radioactive decay of the tracer. After subtracting the baseline, the signal was smoothed and normalized to area. This procedure, performed by the Peakfit software package [26], led to the local RTDs of the tracer in the room [44].

This test was part of a series of experiments in a large industrial facility. Reproducibility was checked in another room, very similar in size and arrangement to this one. The reproducibility was found to be quite satisfactory.

Figure 97 shows typical RTDs (detectors 3 and 6). The signals from detectors 2–4 exhibit two to three peaks, which suggests there is a certain amount of recirculation inside the room. After about 100 s, the RTDs all decrease in a quasi-exponential fashion.

This experiment is a good illustration of the advantages of radioactive tracers. The timescale of the first peaks is very short (about 1 s) but it was nevertheless possible to monitor them at several locations simultaneously. No chemical tracer system offers both of these features.

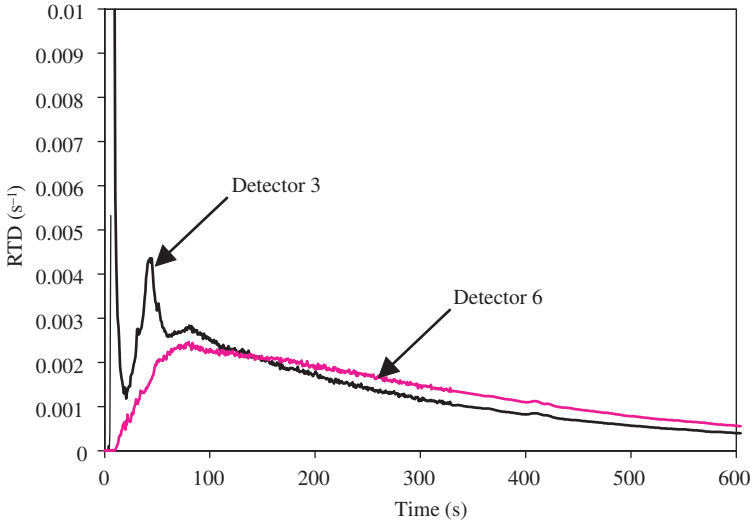

FIG. 97. Experimental RTD curves for case study No. 2.

4.2.3. RTD analysis and CFD modelling

The RTDs show that the air flow successively reaches points 3, 4, 2, 6 (exhaust) and 5. By examining the layout of the room, it is possible to infer that:

(a) The blow opening creates an air jet which flows across the room and strikes the opposite wall.
(b) The jet is then redirected as, more or less, a radial wall jet that reaches point 3 very quickly.
(c) This wall jet later reaches the space between the two parts of the room (point 4).
(d) At the same time, it creates a recirculation loop in the first part of the room. Point 2 is included in this loop.
(e) It then flows into the other part of the room and reaches the exhaust.

This (speculative) flow pattern is shown in Fig. 98. We have tried to support it by CFD simulations. The idea was not to have very precise predictions, but simply to highlight the main features of the flow structure.

Simulations were made with the finite volume code TRIO-VF version 8.7 [54], with a very coarse cubic grid (0.2 m in size). The turbulence model was the classical high Reynolds k–ε. First, the flow field was computed, then the RTDs were calculated by solving the convection–diffusion equation. The resulting concentrations were averaged over eight mesh cells, to account for the detection volume of our probes.

The results did not compare badly with the measurements: the period between the peaks was correctly predicted and so was the exponential tail of the RTDs. On the other hand, the height and number of peaks were grossly

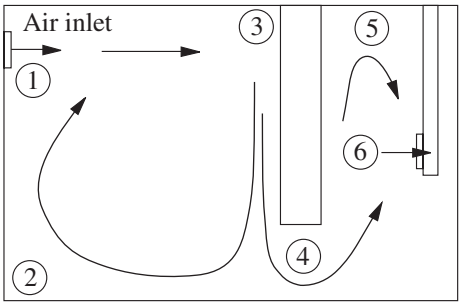

FIG. 98. Postulated flow pattern.

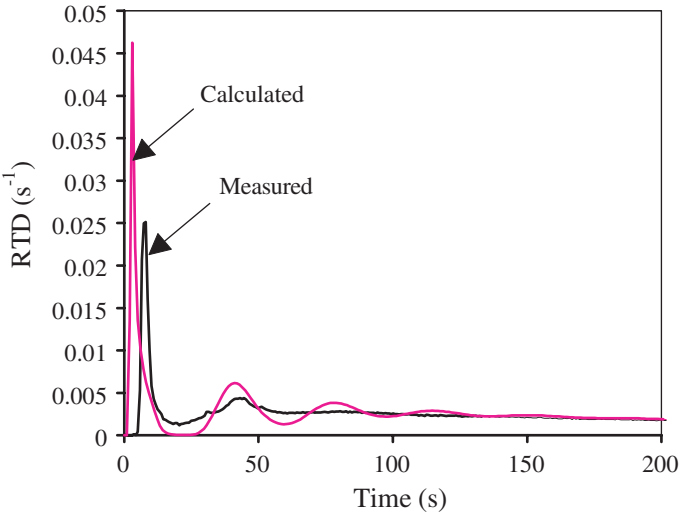

FIG. 99. Experimental and calculated (CFD) RTD curves for detector 3.

overestimated (Fig. 99 shows a typical result for detector 3). Such a behaviour is quite typical in simulations of RTDs in ventilated rooms with TRIO-VF [55]. It appears that diffusion is underestimated in the calculations — a paradoxical finding in finite volume computations with coarse grids! Alternatively, the k–ε model may be inadequate.

An excellent agreement was achieved for detectors 5 and 6 (Fig. 100 shows the results for detector 6, i.e. the exhaust opening). This CFD simulation is considered to be reasonably successful and we are confident that it reproduces, at least in a qualitative way, the main features of the flow pattern.

Figures 101 and 102 illustrate the transport of a tracer puff emitted in the air inlet, as calculated by the code, 5 and 50 s, respectively, after injection of the tracer. The simulation is therefore being used as a rather sophisticated smoke visualization test — the advantage being that the entire concentration field is known as a function of time. The structures of the calculated flow are comfortingly consistent with the flow pattern that was inferred from the shape of the RTDs (cf. Fig. 98).

4.2.4. Zonal modelling

The circulation pattern in Fig. 103 was then translated into a zonal model composed of plug flow elements and perfectly stirred tanks. The response of this model was calculated by means of the DTS software developed by

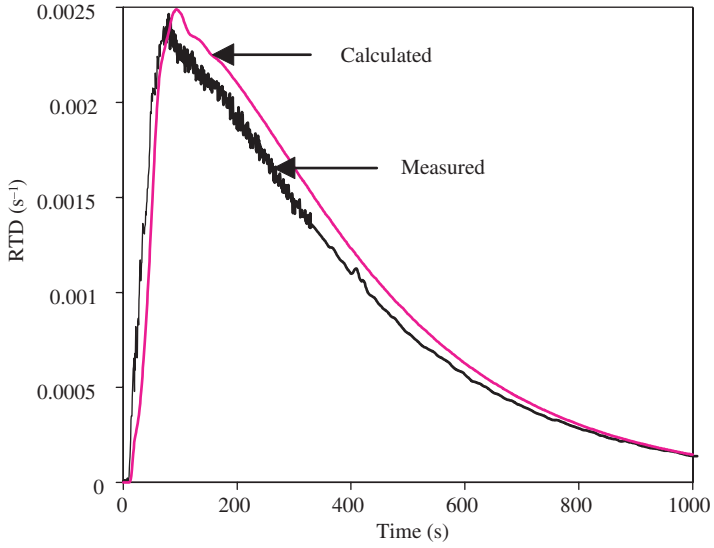

FIG. 100. Experimental and calculated (CFD) RTD curves for detector 6.

PROGEPI [56]. A trial and error process then allowed its structure to be optimized while trying to keep it as simple as possible. Model parameters were then determined by a built-in optimization procedure. The (fairly ambitious) aim was to have the best possible fit between calculated and experimental RTDs at all the measurement points — not at the outlet only. To our knowledge, this approach, based on a detailed set of experimental results, is a

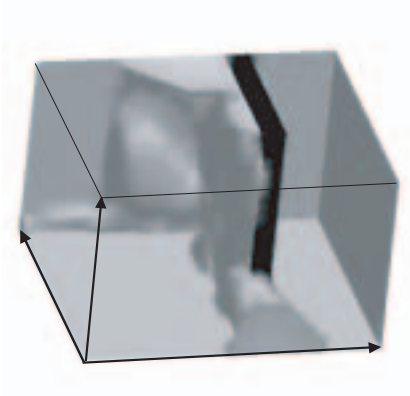

FIG. 101. Concentration field in the room 5 s after tracer injection (the internal wall is in black).

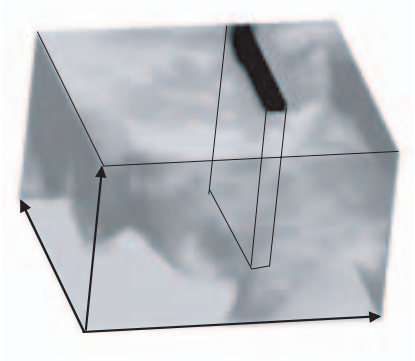

FIG. 102. Concentration field in the room 50 s after tracer injection.

significant advance from the classical inlet–outlet analysis and, when successful, should greatly enhance confidence in zonal modelling.

Figure 103 shows the final flow model, where the recirculation loop is clearly identified; the location of the detectors is also indicated. This model is still quite close to the circulation pattern described above and we believe it retains some physical significance.

Agreement with the experimental RTDs ranged from fair (detectors 3 and 4) to excellent (detectors 5 and 6), which is proof of the relevance of this zonal model. It should, however, be noted that the calculated RTD for detector 2 was too noisy to be exploited (this is a known problem with the DTS software; the response at nodes near the injection point may be incorrect).

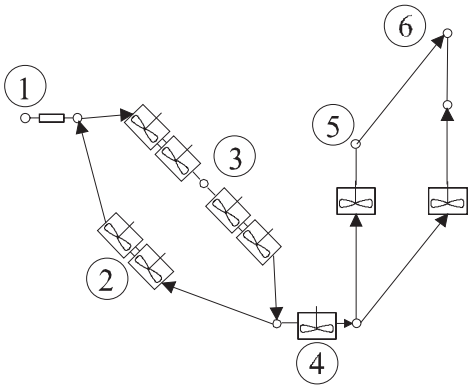

FIG. 103. Structure of the zonal model.

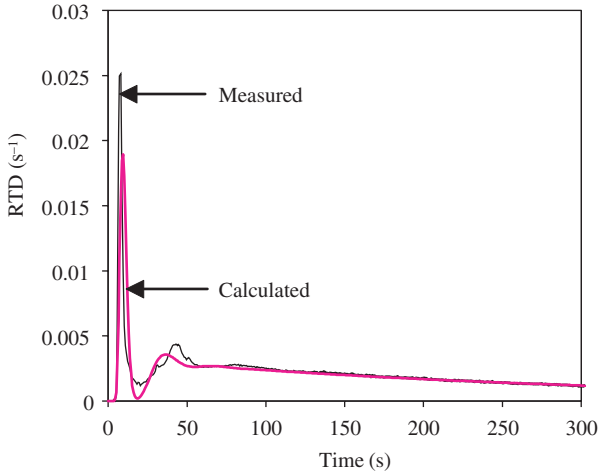

FIG. 104. Experimental and calculated (DTS) RTD curves for detector 3.

Figures 104 and 105 illustrate this comparison for detectors 3 and 6 (comparison with Figs 99 and 100 indicates that the zonal model is, not surprisingly, more successful than the CFD calculation).

Model parameters give an estimate of flow rates and volumes in the different branches:

(a) Recirculation is very strong (the flow in branch 2 is about nine times larger than the inlet flow rate); the volume of branch 2 is estimated at about 38 m^3.
(b) By comparison, the volume of direct branch 3 is only about 15 m^3.
(c) The cumulated volume of branches 4, 5 and 6 is around 13 m^3; this is quite consistent with the dimensions of the part of the room beyond the internal wall.

4.2.5. Conclusions

The tracer gas technique has been used to qualify the ventilation system of a room in an industrial facility. The choice of a radioactive tracer allowed simultaneous measurements to be made at several points in the room with very good time resolution, which proved quite beneficial. Analysis of the experimental RTD curves suggested the structure of the flow model. The results of a (rather crude) CFD calculation were consistent with that structure, which was then translated into an arrangement of plug flow elements and stirred tanks.

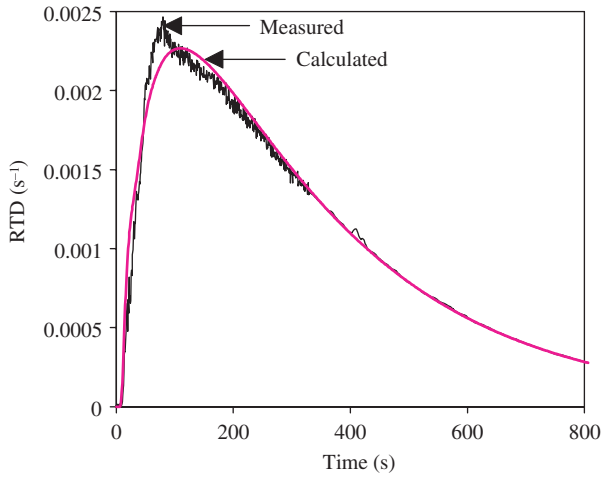

FIG. 105. Experimental and calculated (DTS) RTD curves for detector 6.

With some parameter identification, this zonal model of the room reproduced quite satisfactorily the experimental RTDs, both at the exhaust and inside the room. This illustrates that it is possible to build a simple but reliable systemic model of the ventilation system.

On the other hand, the model benefited from several factors: apart from the presence of an internal wall, the room geometry was not very complicated, the ventilation system was quite rudimentary, only one air flow rate was investigated, and luck may have played some part in the success of this CFD simulation. This approach should therefore be tested in more complex situations (e.g. internal obstacles, multiple inlets or exhausts and diffusers); a crucial test would also be the ability of the zonal model to emulate the RTDs with different ventilation flow rates.

4.3. CASE STUDY No. 3: POLLUTED STREAM WASTE TREATMENT PLANT EFFICIENCY USING RADIOTRACER TECHNIQUES

4.3.1. Introduction

Sewage is one of the major pollutants in urban areas so it is essential to treat it. The process of sewage treatment may be considered as an industrial process where sewage constitutes the raw material and the treated water and sludge are the final products. Thus it is natural that tracer techniques, which are well established methods in process dynamics studies in industry, may also be

applied to investigate sewage treatment process dynamics. Radiotracer experiments were carried out to investigate the RTD of various units of a wastewater treatment plant at Islamabad, Pakistan.

The sewage treatment plant was built in two phases. The capacity of each phase is 10 ML/d. The Leh stream passes nearby this plant. The sewage flows to the plant in an underground concrete pipeline. Figure 106 shows the layout of the plant, which is based on a conventional activated sludge system. The main plant constituents are the pulverizer, pumping station, primary clarifiers, aeration tanks, secondary clarifiers, digester and drying beds. This system employs a primary clarifier before the aeration tank in order to remove the easily settling solids from the influent water.

The solids are removed for further treatment in the digester unit and ultimate disposal as fertilizer. The effluent from the primary clarifier, having less organic matter, imposes a smaller load on the aeration section than that of raw sewage, thus making smaller aeration tanks possible and having lower requirements for oxygen. The organic matter remaining in the primary effluent is consumed by active masses of microbes (activated sludge). The processes occurring in the aeration tanks are the adsorption of particulates and assimilation of the carbonaceous organic matter both for energy supply and for new cell production. The activated sludge (mixed liquor) is settled in the secondary clarifier. Excess activated sludge is transferred to a primary clarifier, which is the only point of removal of solids from the sewage water. Finally, the overflow of the secondary clarifier is disposed of in the Leh stream.

4.3.2. Experimental design

As a first step, the experiments to be conducted were designed and the amount of radioactive tracer was calculated as per requirement. The selection of radioactive tracer was made considering the conditions of the experiment as well as the radiological safety of the workers and the general public. The radioactive tracer selected was ^{82}Br in the form of KBr. The tracer was prepared at the nuclear reactor and transported to the experimental site in a suitable transport container observing necessary safety/radiation protection aspects. Radiation detectors were placed at suitable points in the wastewater treatment plant, and the data acquisition system was set up at a central point to acquire data from all the detectors. The background radiation was measured over a suitable interval of time before injecting the tracer. A radioactive injection in the form of a Dirac pulse was made at the inlet points using a special injection system. The tracer was detected at the inlet and outlet of the systems with a NaI detector with a crystal 2 in. x 2 in. (5.12 cm × 5.12 cm) in area.

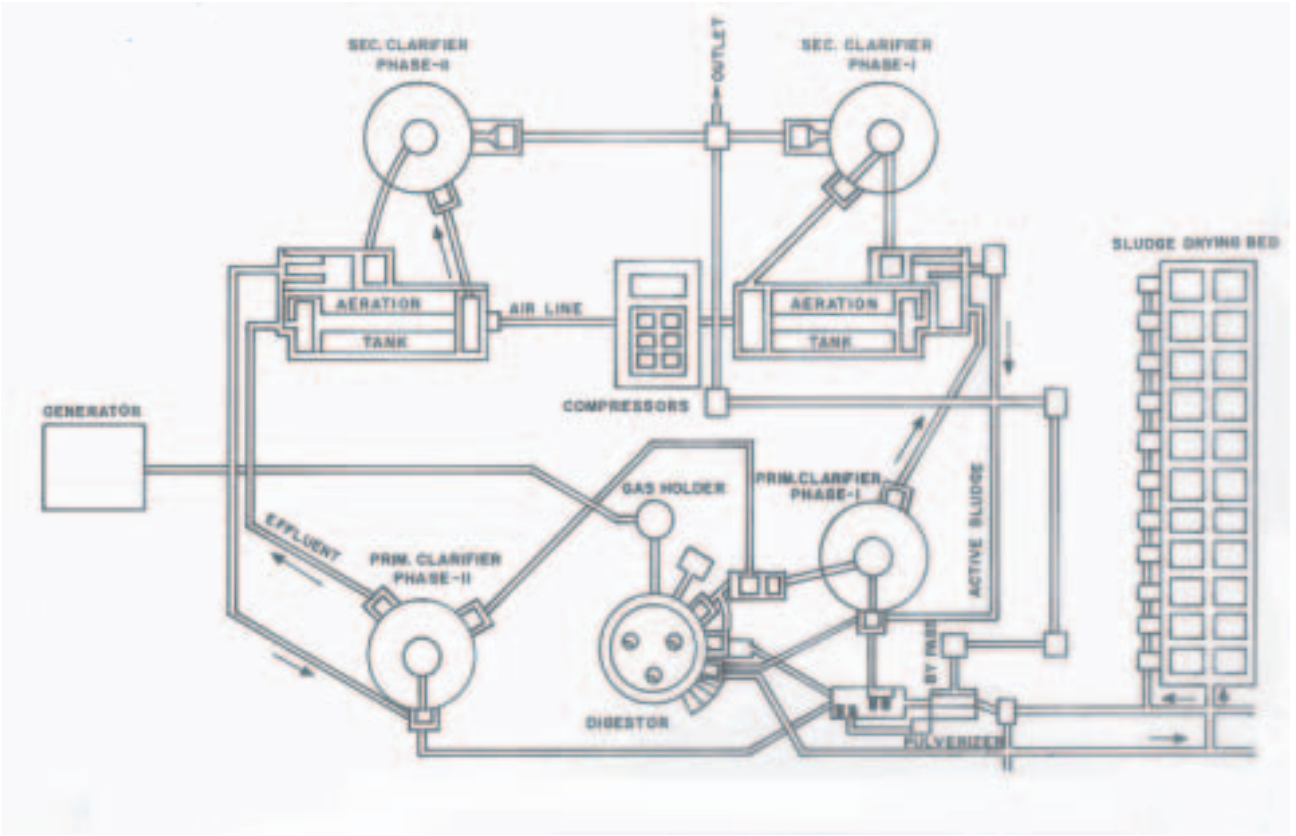

FIG. 106. Layout of the wastewater treatment plant at Islamabad.

4.3.3. Preliminary treatment of experimental data

The preliminary treatment of the experimentally obtained data involves the following steps that were performed using the DTS PRO 4.2 software before the analysis of the data:

(1) Background correction,
(2) Radioactive decay correction,
(3) Extrapolation of the experimentally obtained curve (where necessary),
(4) Normalization of the experimental curve.

The tracer concentration curve was normalized by dividing each data point by the area under the curve to obtain the normalized RTD function:

$$E(t) = \frac{C(t)}{\int_0^\infty C(t)\mathrm{d}t}. \tag{86}$$

Since the tracer distribution is measured in discrete time intervals, the above equation can be written as:

$$E(t) = \frac{C(t)}{\sum_0^\infty C(t)\Delta t}. \tag{87}$$

The area under the normalized RTD function $E(t)$ is equal to unity, thus:

$$\int_0^\infty E(t)\mathrm{d}t = 1. \tag{88}$$

4.3.4. Calculation of dead volume

If the entire volume of the operating system is utilized for flow then the system has no dead volume. However, if some regions of the systems have residence times 5–10 times greater than the holding time of the rest of the fluid then these regions can be considered as dead for all practical purposes. If the experimentally measured MRT is less than the theoretical MRT then the system has a dead volume. The amount of dead volume present in the system can be estimated by:

$$\mathrm{DV}(\%) = \left(1 - \frac{\mathrm{MRT}_{\mathrm{exp}}}{\mathrm{MRT}_{\mathrm{th}}}\right)100. \tag{89}$$

If the experimental MRT is greater than the theoretical MRT then there may be an error in the flow rate measurement or the volume measurement, or the tracer may not be suitable for the system under investigation.

4.3.5. Modelling of tracer data

RTD models have been applied to industrial process investigations successfully where fluids and solids are involved. Mathematical simulations and the construction of computational models are found to be useful. Radioactive tracers are valuable tools enabling investigation of the physical phenomena and making possible the identification and optimization of industrial processes. Physical and mathematical descriptions of the flow and mixing characteristics of fluids or solids in systems are called flow models. The flow models give macroscopic lumped sum descriptions which are sufficient for the majority of engineering process calculations [57, 58].

In general, the selection of flow models and the determination of parameters from tracer studies is based on analyses of the impulse response functions $E(t)$, which are the RTDs obtained from tracer inputs to a system in the form of Dirac delta functions (instantaneous injection).

The software package that simulates dynamic models derived from RTD experiments developed by PROGEPI/SYSMATEC [17] was used for modelling of the experimental data obtained from different units of a wastewater treatment plant. This software package can model complicated flow patterns by properly interconnecting elementary units such as the perfect mixing cell, plug flow reactor and perfect mixing cell with exchange to a stagnant zone, and the model parameters can be chosen so as to fit an experimental outlet response. The composition of the test models can be made directly on-screen as a graphic network by assembling and interconnecting the elementary units. The response to any entry function can be obtained at any node and at the outlet of the network.

4.3.6. Investigation of the different units of the wastewater treatment plant

4.3.6.1. Primary clarifier (phase I)

The design of a circular centre feed primary clarifier with a scraper sludge removal system is shown in Fig. 107. The total volume of the primary clarifier is 1387 m^3 and the volumetric flow rate is 4.83 m^3/min, which gives the theoretical MRT as 287 min. Bromine-82 radioactive tracer was injected into the inlet of the primary clarifier (phase I). The tracer data were processed and the experi-

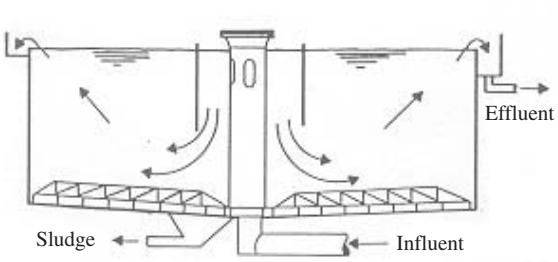

FIG. 107. Design of a circular centre feed primary clarifier.

mental MRT of the primary clarifier was estimated as 164 min. This means that the system has a dead volume of 42.7%.

The tracer data were modelled using RTD software (DTS PRO 4.2) to understand the fluid dynamics inside the system. Various models with different parameters were tried. A model that fits well with the experimental curve is shown in Fig. 108. In this model, node No. 1 is the inlet and tracer input, node No. 7 is the outlet while V_1, V_3 and V_5 are perfect mixing cells, and V_2 and V_4 are plug flow reactors. From the inlet node the flow passes through a small perfect mixing cell and reaches the centre of the clarifier. From node No. 2 to node No. 4, the flow is through a perfect mixing cell connected to a plug flow reactor. Then there is a recycle flow between node No. 2 and node No. 4 (with a recycle ratio of 0.87) through a perfect mixing cell connected with a plug flow reactor. Node No. 7 is the outlet visualization node.

The experimental and model output responses of the primary clarifier are shown in Fig. 109, which shows first a large peak, then a drop and finally a very small peak. The MRT of the model curve was calculated from the first order

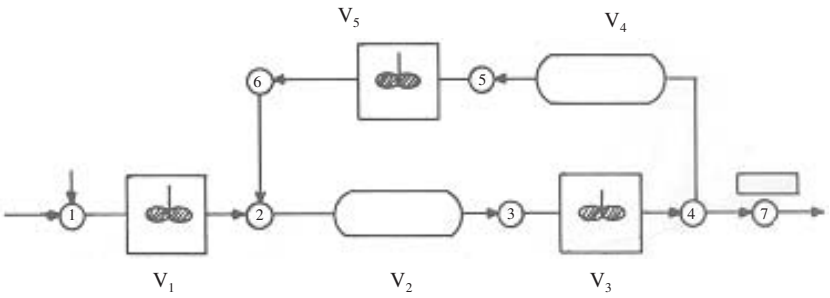

FIG. 108. Model of a primary clarifier (V_1 = 96.2 m^3, V_2 = 285.78 m^3, V_3 = 201.8 m^3, V_4 = 76.3 m^3, V_5 = 199 m^3).

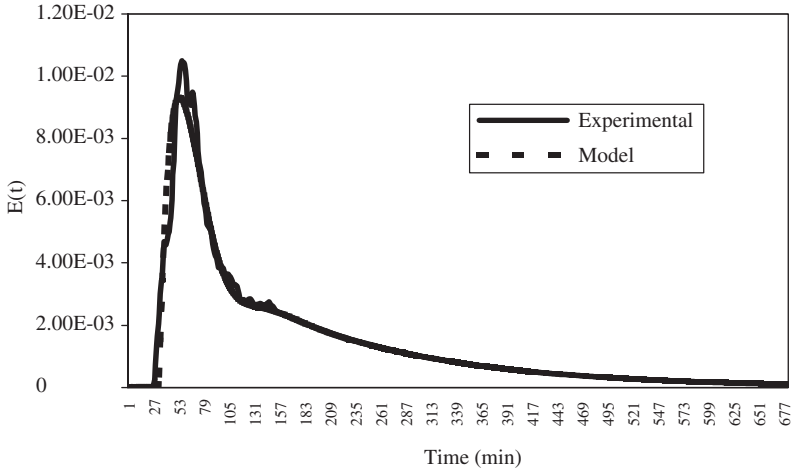

FIG. 109. RTD of the primary clarifier.

moment of the model curve and was found to be 165.7 min, i.e. very close to the experimental value of the MRT.

4.3.6.2. Aeration tank (phase I)

In the wastewater treatment plant under investigation, the output of the primary clarifier was fed to the aeration tanks, where compressed air is blown to increase the dissolved oxygen content of the wastewater. The wastewater flows through various activation tanks within the aeration tank. In these activation tanks complex biological reactions take place, resulting in the removal of dissolved organic compounds from the solution, which is the result of the actions of microorganisms in the activated sludge. The degree of conversion depends first of all on the residence times, on the initial concentration of sludge and concentration of pollutants, and on the activity of the microorganisms of the mixed culture [59]. A radiotracer experiment was conducted to investigate the RTD of wastewater in the aeration tank. A plan view of the aeration tank is shown in Fig. 110. The volume of unit No. 1 of the aeration tank is 567.5 m^3 and the volumetric flow rate during the experiment was 2.08 m^3/min. This gives a theoretical MRT of 272.4 min. Bromine-82 radioactive tracer was injected into the inlet of the aeration tank. The experimental MRT of the unit was estimated as 272 min with a very small dead volume (0.19%).

The DTS Pro. 4.20 software was used to understand the hydrodynamics inside the aeration tank. The model used for the aeration tank (unit No. 1) is

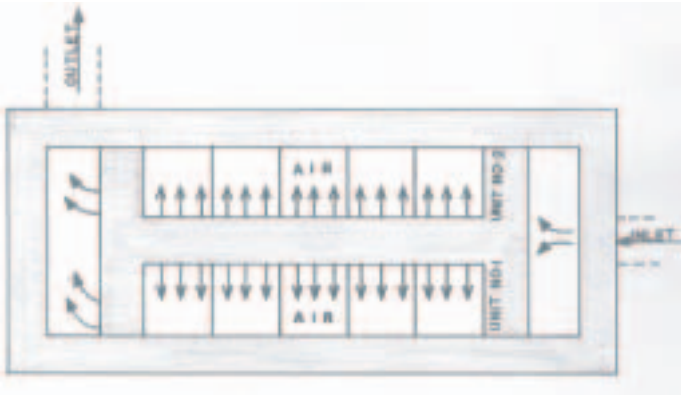

FIG. 110. Design of the aeration tank (plan view).

shown in Fig. 111. The model consists of five perfect mixers in series with back-mixing and connection with a plug flow reactor at the beginning. After the injection point, the incoming wastewater passes through a narrow duct before it enters the series of tanks through small holes. For this reason, a plug flow reactor is used between node No. 1 and node No. 2. The back-mixing ratio of the tanks connected in series was found to be 8.8.

The experimental and model output responses of the aeration tank (unit I) are shown in Fig. 112. The MRT of the model curve is 268.7 min, which is almost the same as the experimental MRT. The dead volume from the model was calculated to be only 1%, and is thus very small. The results of this experiment show that the aeration tank does achieve the designed residence time and does work efficiently.

4.3.6.3. Secondary clarifier (phase I)

Clarifier hydrodynamics play an important role when combined with the biological factors in the performance of the whole system [60]. In wastewater treatment plants, the output of the aeration tanks is fed to the secondary

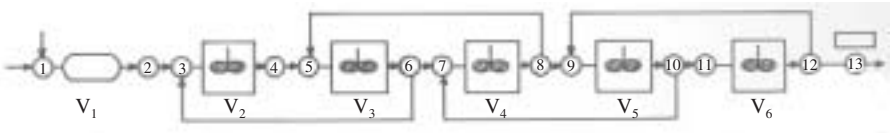

FIG. 111. Model of the aeration tank (V_1 = 80 m^3, V_2 = 101 m^3, V_3 = 100 m^3, V_4 = 100 m^3, V_5 = 97.71 m^3, V_6 = 106.65 m^3).

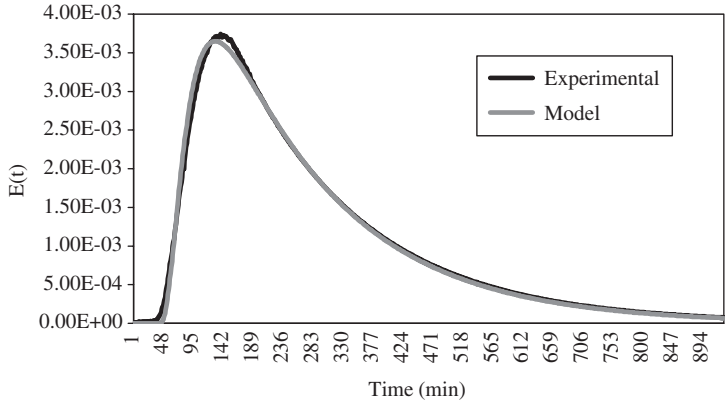

FIG. 112. RTD of the aeration tank.

clarifiers which further remove the sediments from the incoming wastewater. The purpose of this investigation was to determine the RTD of sewage water in the secondary clarifier, which is necessary to evaluate the efficiency of the unit. The design of the secondary clarifier is the same as that of the primary clarifier, i.e. a circular centre feed with a scraper sludge removal system as shown in Fig. 107. The total volume of the secondary clarifier is almost double that of the primary clarifier (2790 m^3), and the volumetric flow rate during the experiment was 4.2 m^3/min giving a theoretical MRT of 669.6 min. Bromine-82 radioactive tracer was injected into the inlet of the secondary clarifier. The experimental MRT of the secondary clarifier was estimated as 284.7 min. The dead volume was determined to be 57.4%. This shows that the working efficiency of the unit is very poor because more than half of the system volume is not taking part in the process.

The DTS PRO 4.2 software was used to understand the fluid dynamics of the secondary clarifier. The model used here was the same as for the primary clarifier (Fig. 108). Fitting of the model gave the following values: V_1 = 29 m^3, V_2 = 230.18 m^3, V_3 = 374 m^3, V_4 = 314.06 m^3, V_5 = 315 m^3.

The experimental and model output responses of the secondary clarifier are shown in Fig. 113. It shows a large peak, then a sudden drop, followed by another smaller peak. The MRT of the model curve is calculated from the first order moment of the model curve, which gives 260.17 min, i.e. a value close to the experimental value of the MRT.

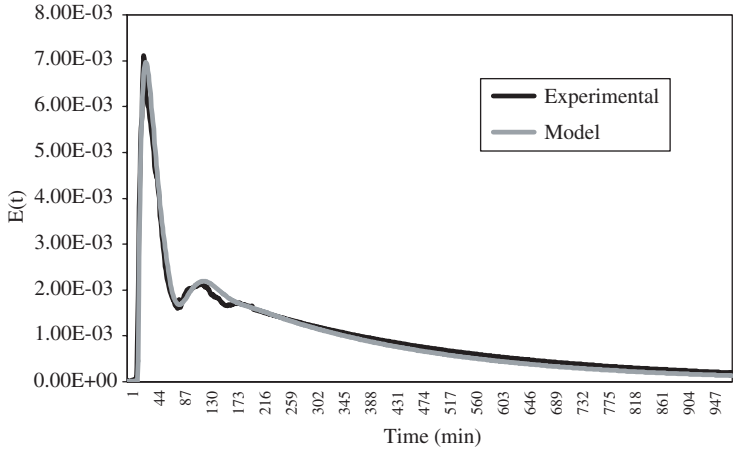

FIG. 113. RTD of the secondary clarifier.

4.3.7. Summary

The radioactive tracer ^{82}Br in the form of potassium bromide (KBr) was used to investigate the different units of a wastewater treatment plant. The activities of ^{82}Br injected into the primary clarifier, aeration tank and secondary clarifier were 1295, 1110 and 1480 MBq, respectively. The tracer was detected at different points with NaI detectors. The on-line data acquisition was performed using ratemeters interfaced with the computer. The theoretical MRT of the primary clarifier was 287 min, while its experimental MRT was found to be 164 min. Therefore, a dead volume of 42.8% was estimated in the primary clarifier. The theoretical MRT of the aeration tank was 272.4 min while its experimental MRT was found to be 272 min. Therefore, an almost negligible amount of dead volume was estimated in the aeration tank. This is due to the vigorous mixing process inside the aeration tank. The theoretical MRT of the secondary clarifier was 669.6 min while its experimental MRT was found to be 284.7 min. Therefore, a dead volume of 57.4% was estimated in the secondary clarifier. The DTS PRO 4.2 software was used for the preliminary treatment of the experimental data and the modelling of these systems. The MRTs obtained from the models proposed for the systems under investigation were found to be very close to the experimental MRTs. All these results are summarized in Table 17.

TABLE 17. SUMMARY OF THE RESULTS OF A TRACER EXPERIMENT IN A WASTEWATER TREATMENT PLANT

System under investigation	Volume (m^3)	Flow rate (m^3/min)	Theoretical MRT (min)	Experimental MRT (min)	Model MRT (min)	Dead volume (%)
Primary clarifier	1387	4.83	287	164	166	42.7
Aeration tank (unit I)	567.5	2.08	272.4	272	269	0.2
Secondary clarifier	2790	4.2	669.6	284.7	260.2	57.4

5. PERSPECTIVES — INDUSTRIAL PROCESS TOMOGRAPHY

Flow pattern visualization is the new trend in radiotracer methodology. Work in progress is reported in two aspects of industrial process tomography: detection chain modelling and tracer flow imaging in two dimensions.

5.1. DETECTION CHAIN MODELLING

Considerable space has been devoted in this report to the methods for tracer data interpretation and modelling. In our opinion, available software and methods now allow correct treatment of these points when dealing with mainly one dimensional flows, such as flow of one or more phases in a pipe, in a packed column with a low diameter to length ratio or some such object. The situation is not so favourable when velocity profiles or flow patterns can be suspected to have an impact on the measurement. Suppose, for example, that a detector is located near a recirculating flow pattern, caused for instance by flow enlargement as illustrated in Fig. 114.

If the detection volume is small enough, the readings from the detector will characterize flow velocity in the reverse part of the recirculation and will be easy enough to interpret. This is what happened in case study No. 2, where the estimated reach of the detector (about 40 cm) was obviously much smaller than the length scale of the recirculations (roughly the size of the room in

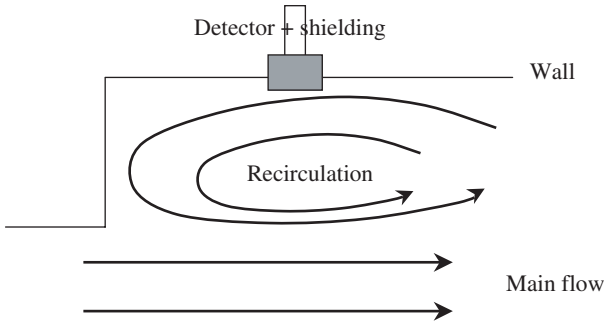

FIG. 114. Recirculating flow near a detector.

which the experiment was performed). On the contrary, if the detection volume reaches the direct part of the recirculation, or even the main flow, its signal will be an intricate combination of contributions from each part of the flow. Another example, involving the existence of a velocity profile, was presented in Section 3.1.

Separating out these contributions will require some knowledge of:

(a) The flow pattern; CFD may again be useful here, but as it is mentioned in the introduction this point will not be developed further here.
(b) What the detector really 'sees'; this is where some amount of modelling of the detection chain may be required.

It should be noted that, even in the simple one dimensional case, knowledge may be desirable since the detection chain may in some cases induce some blurring of the true tracer signal. This problem is, however, not a common one and simple ways do exist to correct it whenever necessary [61].

The vast majority of the applications presented in this report involve gamma emitting tracers. Gamma photons undergo multiple random interactions (with the fluid itself, the walls, the screens, the collimator, etc.) until they reach the detection probe, usually composed of a crystal scintillator and a photomultiplier. The importance of these interactions is a function of the energy of the emitted photons and of the nature (density and chemical composition) of the fluid and the materials. The link between the tracer concentration and the detector signals is therefore not a direct one, the problem lying mainly in the correct representation of these interactions.

A relatively simple solution for the problem is the Monte Carlo method [62]. The basic principle is to choose randomly the initial position, energy, direction and free path of a photon. Its new position is then calculated. If the photon has not left the system, it is going to interact with the surrounding matter. For tracer applications, the major types of interaction to be considered are the photoelectric effect, Rayleigh effect, Compton effect and pair creation. The probability of these processes is calculated as a function of the energy of the incident photon. The type of interaction is chosen randomly and the procedure is repeated until the photon either leaves the system or is absorbed by any material in the simulated system (to be quite precise, another photon may be generated at this stage and has to be followed until it is lost or absorbed). When a sufficiently large number of photons have been treated in this way, it is possible to build statistics in terms of detected photon energies and numbers which in turn can be translated into count numbers, i.e. the very quantity that is measured in a gamma tracer experiment. Thus, the Monte Carlo procedure mimics the very functioning of the measurement chain. Even if the basic principle is straightforward, its numerical implementation is more complicated, and appropriate algorithms have to be used to make the calculation more efficient [18].

As with all computer codes, validation is an imperative. As an example, a few results obtained with the INSPECT computer code are presented here, validated against some experimental data. The basic configuration is a point gamma source placed at different locations in a plexiglas tube fitted with a detector (Fig. 115). Several aspects have been investigated: the nature of the source (^{137}Cs and ^{60}Co), the nature of the fluid (air and water) and the collimator geometry. The results shown in Fig. 115 are fairly satisfactory. It should be noted that no parameter adjustment was necessary.

Once this confidence building step has been completed, attention should be turned to more complex and realistic situations (moving and/or distributed sources). The final aim should be the coupling of the detector model with a CFD code and its validation against adequate experiments. The resulting tool would be of great value for both the design and the interpretation of experiments involving radioactivity. At the design stage, it would allow various tracers, detector arrangements and experimental procedures to be tested numerically, so to speak, to find the optimum configuration. At the stage of interpretation it would give access to purely hydrodynamic signals by deconvolution of the detector response from the raw signals.

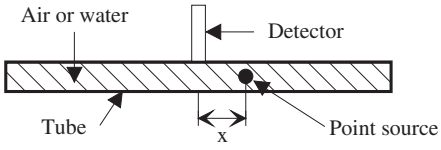

(a) Experimental set-up

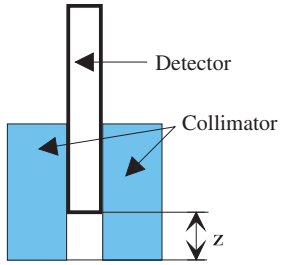

(b) Detector and collimator geometry

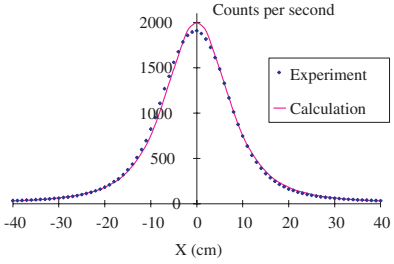

(c) ^{137}Cs in air, z = 0

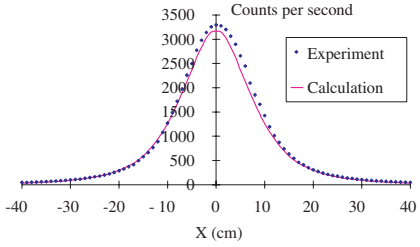

(d) ^{60}Co in water, z = 0

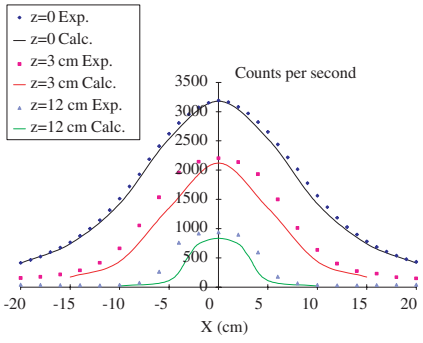

(e) ^{60}Co in air, as a function of z

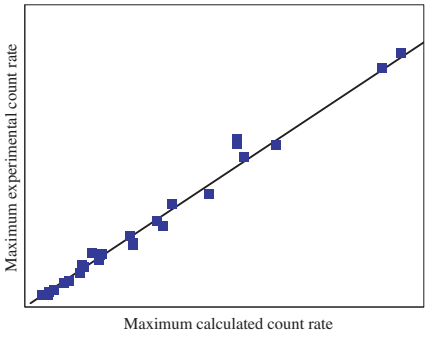

(f) Comparison of experimental and calculated maximum count rates

FIG. 115. Detector modelling: comparison with experiments.

5.2. TRACER FLOW IMAGING

A classical gamma radioisotope tracer experiment involves nuclear detectors the measurements of which are essentially volume averaged, with very good time resolution. Since the detectors are reasonably cheap and small, it is often possible to use several adequately collimated probes simultaneously so as to have some spatial resolution as well. This extra information may prove valuable. For instance, it was possible to show good axial symmetry but considerable end effects by locating several probes at different levels along a countercurrent gas–liquid packed column [63]. Measuring two dimensional concentration profiles as a function of time would nevertheless represent great progress. For instance, it would allow not only hypotheses as to the origin of the end effects in the column to be checked but also maldistributions flow in industrial devices to be located. Among the various techniques, the single photon emission computed tomography method shows some promise. Two dimensional imaging with a gamma ray camera is also an attractive method at the laboratory scale. Results concerning both methods are presented hereafter and illustrate the attraction of two dimensional imaging when gamma emitters are used.

5.2.1. Single photon emission computed tomography (SPECT)

The device presented here has been developed to visualize gamma emitting radiotracers flowing inside a system with a relatively small number of detectors [64]. From the theoretical point of view, it includes a method for the estimation of the photon transport matrix associated with the acquisition system. This method relies on a model of the count number profiles obtained from point sources distributed in the volume under scrutiny. A Monte Carlo simulation, very similar to the one that was mentioned above for detector response modelling, allows those photons that have been diffused in matter and those that have been directly collected to be discriminated. The influence of the tracer energy, a key parameter, is taken into account. The reconstruction algorithm uses a maximum likelihood method, optimization being made by the statistical estimation–maximization (EM) algorithm. To summarize, this procedure is able to compute the most likely tracer distribution in the measurement volume, i.e. a flat almost two dimensional cylinder, for a given output from a particular arrangement of detectors. It should be noted that this result is quantitative, i.e. the final results are numerical values of the concentration.

An experimental set-up was built to test the feasibility of this method. The set-up is composed of 36 detectors distributed around a cylindrical test

section (diameter, 24 cm; height, 2 cm). A transverse water flow was generated in the test section, which in some cases was also filled with a porous medium. A tracer, a radioactive solution of ^{99m}Tc containing some dye, was injected into the water inlet. The reconstructed image of the concentration distribution could be compared with video images of the dye concentration. Figure 116 illustrates one such comparison in a non-porous medium. Both qualitative and quantitative analyses of the results demonstrate that visualization of the fluid circulation in a system is indeed feasible with a limited number of detectors.

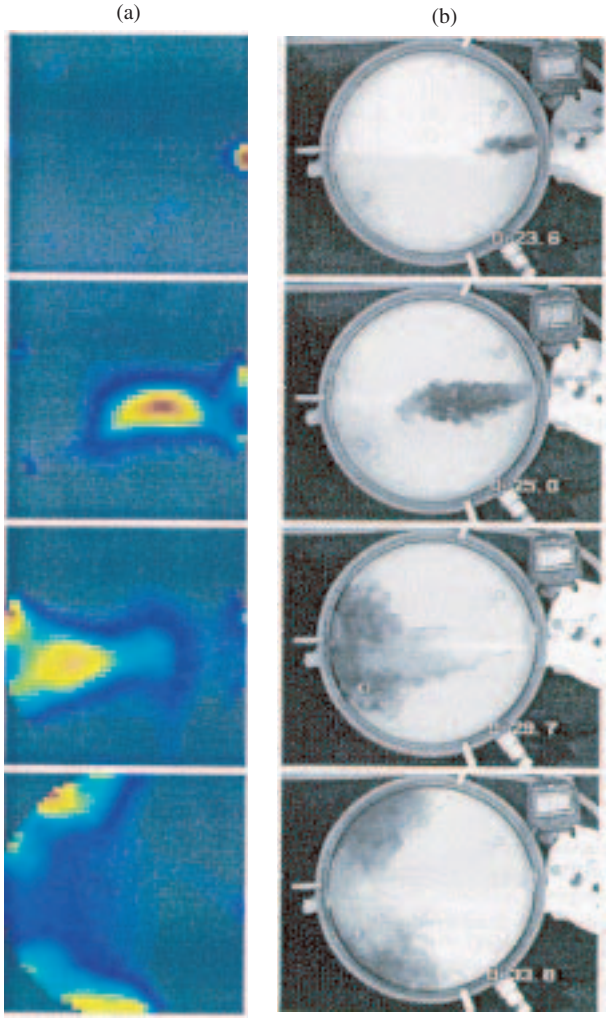

FIG. 116. Images of flow in a flat cylinder: (a) SPECT image, (b) video image.

This system has now been applied to the packed column mentioned above [65]. One of the aims was to obtain a fundamental insight into the detailed flow structures and mechanisms. Interesting results have been found regarding the dispersive characteristics of flow in various regions of the column. The other aim was to prove the ability of the technique to detect flow maldistribution (gas or liquid), from simple to complex situations.

5.2.2. Gamma ray cameras

Gamma ray cameras provide another way to study non-uniform tracer concentration fields. A gamma ray camera is composed mainly of a very large crystal scintillator fitted with a multiple hole collimator. Signals from a large number of photomultipliers are then processed to give a two dimensional image of the distribution of the photons detected inside the crystal. One problem is that this image bears no simple relationship with the tracer concentration. If the Compton interaction can be neglected, i.e. if the tracer energy is small enough, the image can be seen as an attenuation weighted average of the concentration profiles in the direction perpendicular to the collimator. This means that a large computing effort is required to make gamma ray camera images quantitative.

A gamma camera was used here to try to estimate local gas hold-up as a function of impeller velocity in a model Mahoney–Robinson reactor [22]. The reactor is about 20 cm in height. Experiments were made with a low energy (81 keV) gaseous tracer, ^{133}Xe. Figure 117 shows two side views, with the impeller at rest (Fig. 117(a)) and at nominal velocity (Fig. 117(b)). The feature at the top of these figures is the image of the gaseous ceiling. Gas entrainment into the liquid phase is clearly visible; an excess of gas can even be seen inside the catalyst basket, in the middle of the reactor.

Owing to the low tracer energy, it is a reasonable expectation that more quantitative information will be obtained from this experiment given some modelling effort.

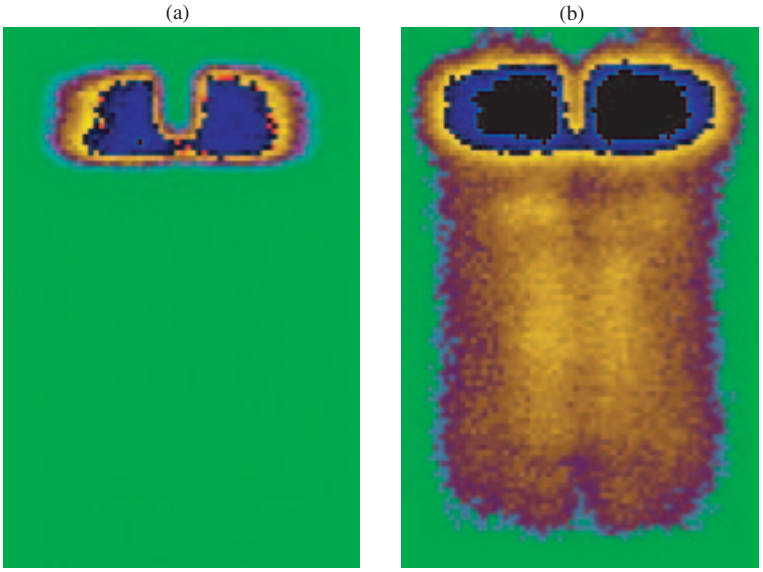

FIG. 117. Two gamma camera images of a reactor: (a) impeller at rest, (b) impeller at nominal velocity.

6. TRACERS IN OILFIELDS AND GEOTHERMAL RESERVOIRS

The tracing fluid flows in oilfields and geothermal reservoirs have both similarities and differences. The similarities are obviously:

(a) Both deal with fluid flows in (mainly saturated) porous media of natural minerals under extreme temperature and pressure conditions.
(b) Both need passive tracers for the fluids involved and the corresponding methods for tracer preparation, injection, sampling and analysis.

Among the differences are the following:

(1) Temperatures are, in general, considerably higher in geothermal reservoirs. Thus, the stability of tracers at high temperatures is particularly important.

(2) Pressures are generally higher in most oil reservoirs (although there is a considerable span in pressures between various reservoir types), thus affecting the behaviour of some gas tracers differently from that in geothermal reservoirs.
(3) Geothermal reservoirs deal with the relatively simple two phase flow of liquid and gaseous water. Flows in oil reservoirs are either three phase, composed of oil (including condensate), liquid water and natural gas, or four phase, including also water vapour in fields where thermal recovery is used. These characteristics place different constraints on the tracers, leading to the conclusion that certain tracers may be used in geothermal reservoirs but not in oil reservoirs and vice versa.

The similarities suggest that these subjects should be included together in the same section of this report. The differences suggest that they should be treated individually in two separate sections. The latter course is followed here, with oilfields being treated in Section 6.1 and geothermal reservoirs in Section 6.2.

6.1. RADIOTRACER TECHNOLOGY AS APPLIED TO INTERWELL COMMUNICATION IN OILFIELDS

6.1.1. Introduction

6.1.1.1. Oil recovery

Natural production mechanisms, or primary production, contribute to the extraction from reservoirs of about 25% of the original oil in oilfields. This means that 75% of the existing oil remains in the pores and fissures of the oil bearing rocks.

The production flow rate depends on the differential pressure between the permeable layer and the bottom of the well, the average permeability, the layer thickness and the oil viscosity. The main natural production mechanisms are the expansion of oil, water and gas and in certain cases the water influx from aquifers connected with the reservoir.

When primary oil production decreases in a field because of reduction in the original pressure, water is usually injected to increase the oil production again. Water injected into special wells (injection wells) forces the oil remaining in certain layers to emerge from other wells (production wells) surrounding the injector. This technique, commonly called secondary recovery, contributes to the extraction of up to 50% of the original oil in oilfields.

Although this technique was first used in old reservoirs in which oil production had decreased, it is today a common practice to begin the exploitation of new wells with fluid injection as a way to optimize oil recovery. For this reason, the term secondary recovery is being replaced by the more general term water flooding.

The efficiency of the water flooding process is highly dependent on the rock and fluid characteristics. In general it will be less efficient if heterogeneities are present in the reservoir, such as permeability barriers or high permeability channels that impede a good oil displacement by the injected water.

6.1.1.2. Tracers in interwell studies

Tagging the injection water with a suitable nuclide and measuring the samples taken from production wells makes it possible to obtain the response curves (concentration of activity versus time), which represent the dynamic flow behaviour of the pattern (injector plus producers) under study.

Most of the information found by analysis of the response curves cannot be obtained by means of any other technique. Detailed analysis of the response curves obtained from interwell studies allows:

— Detection of high permeability channels, barriers and fractures;
— Detection of communications between layers;
— Evaluation of the fraction of the injection water reaching each production well;
— Determination of RTDs;
— Indication of different stratifications in the same layer;
— Determination of preferential flow directions in the reservoir.

All this information can be used to make operational water flooding decisions in order to increase oil production.

Interwell tracer tests provide quantitative information on the fluid dynamics in a reservoir. Now dynamic information from a reservoir may in addition be obtained by three other methods: logging of production rates (profiles) of reservoir fluids, pressure testing and time lapse seismic examinations (four dimensional seismics). However, these methods and the tracer testing are complimentary and cannot directly replace each other.

6.1.1.3. Tracer behaviour in field application

The fluid flow in most reservoirs is anisotropic. The reservoir structures are usually layered and frequently contain significant heterogeneities leading to directional variations in the extent of flow (Fig. 118).

Hence, the effective fluid movement can be difficult to predict. Here is where tracer technology plays an important role, assuming that the movement of the tracer reflects the movement of the injected fluid. Obviously, it is most important to ensure that the properties of the tracer meet this requirement as closely as possible: there should be a minimum amount of undesired loss or delay. Reservoir physical and geochemical conditions define the constraints. As a result, tracers found to work properly in one reservoir may not work satisfactorily in another.

Tracers have been used to measure fluid flow in reservoirs for several decades. Some of the earliest reports are found in Refs [66–69]. A summary of the earlier use (before 1990) from the perspective of tracer behaviour is provided in Ref. [70]. There are some successes and some reports of experiments which have largely failed. The reason for failures is mainly insufficient knowledge of the tracer behaviour under changing reservoir conditions.

Knowledge of tracer behaviour is gained through dedicated laboratory investigations through the above mentioned oilfield experience, groundwater

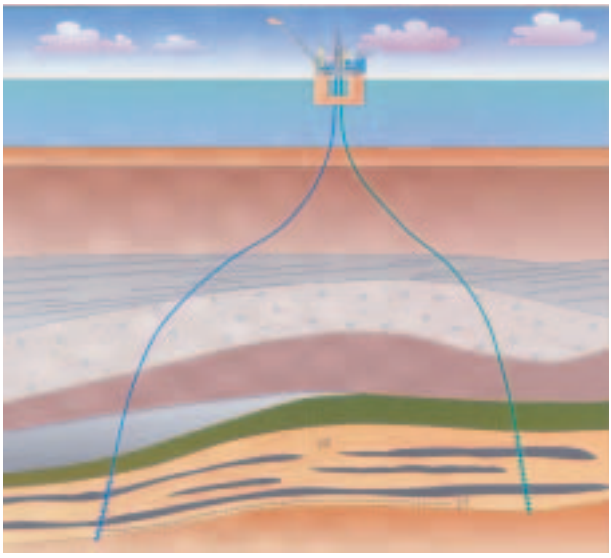

FIG. 118. Tracer pulse movement between wells in a layered reservoir.

movement investigations, atmospheric tracing experiments and also, to a significant degree, through the work carried out on migration of radioactive species in the soil for the purpose of evaluating radioactive waste repository sites.

Although the sum of knowledge from these areas is substantial, the information acquired is not always consistent. The results from one area of investigation cannot readily be transferred to new fields because of both scaling problems and changing experimental conditions. During the last 10–15 years there have been substantial programmes on tracer technology development. This has resulted in advances in basic knowledge and technology.

The present state of knowledge on specific radiotracer capabilities and limitations for interwell oil reservoir applications is summarized briefly here.

6.1.2. Methodology

6.1.2.1. Interwell tracer test step by step

A field radiotracer investigation consists, in brief, of the following main steps:

(a) Design of a tracer strategy together with reservoir engineers who work in the field;
(b) Selection of applicable tracers;
(c) Application to the relevant authorities based on a safety report;
(d) Tracer mixture preparation, calibration and quality assurance;
(e) Selection and design of tracer injection and sampling procedures;
(f) Tracer transportation to the injection site;
(g) Implementation of radiation safety procedures at the injection site;
(h) Tracer injection;
(i) Radioactive contamination survey;
(j) Injection equipment decontamination and handling of radioactive waste;
(k) Tracer sampling and sample transportation to the analytical laboratory;
(l) Tracer analysis;
(m) Data evaluation and simulation;
(n) Reporting of results.

Most of these steps will be discussed further in the following sections.

6.1.2.2. Required amount of tracer

The best estimate of the amount of tracer required for an interwell study involves the use of a mathematical model for a computer simulation of the pattern behaviour on the basis of the reservoir parameters. The amount of tracer (mass or activity) needed for a specific experiment is then calculated from the theoretical response and the detection limit.

As a general rule, tracer groups do not have this kind of software, and if they have, they need to make a number of assumptions about the pattern characteristics for the model to work properly. This information is not always available for tracer specialists, especially when account is taken of the fact that the objective of a tracer experiment is precisely to have better knowledge about the pattern behaviour.

Consequently some simple assumptions need to be made in order to have an idea about the amount of tracer to be injected when a complex mathematical model is not available.

Lacking better information, it can be assumed that the mean tracer concentration in the output of the production well is the ratio of the total amount of tracer to the pore volume involved in the experiment. The latter may be calculated using a radial approximation of the pattern geometry:

$$V_p = \pi x^2 h \phi S_w, \tag{90}$$

where

h is the thickness of the tagged layer (m),
x is the distance between the injection well and the production well (m),
ϕ is the porosity of the tagged layer (non-dimensional) and
S_w is the degree of water saturation (non-dimensional).

The expected output mean concentration is established from the detection limit, L_d, which in the case of a radiotracer depends on the background and measurement time. The activity, A_0, to be injected to obtain a mean concentration equal to ten times the detection limit is:

$$A_0 = 10 L_d V_p. \tag{91}$$

The required activity calculated using Eq. (91) only represents an approximation, but it is good enough as a reference value. The experience gained after having carried out a number of operations in different reservoirs is a valuable

tool at the moment the estimated values are modified in order to determine the real amount of tracer to use.

6.1.3. Selection and optimization of radioactive tracer

6.1.3.1. Tracer categories

There are, in principle, two tracer categories:

(1) *Passive or conservative (also called, less precisely, ideal) tracers:* Such a tracer is required to follow passively the fluid phase or phase fraction into which it is injected without any chemical or physical behaviour different from that of the traced component itself. In addition, the tracer must not perturb the behaviour of the traced phase in any way, neither must the fluid phase nor its components perturb the tracer behaviour.
(2) *Active (also called, less precisely, non-ideal or reacting) tracers:* The tracer takes an active part in the process in qualitatively predictable ways, and is used to measure a property of the system into which it is injected. The degree to which an active role is taken is a quantitative measure of the property to be determined.

In petroleum reservoirs, passive tracers are used for all the tasks mentioned in Section 6.1.1.2.

Active tracers may be:

(a) Phase partitioning (the potential to measure the remaining oil saturation);
(b) Sorbing to rock reversibly or irreversibly (the potential to measure the ion exchange capacity of formation rock);
(c) Hydrolyzing (for instance, for measurement of water saturation);
(d) Thermally degrading (to measure reservoir temperature away from wells);
(e) Microbially degrading (to measure microbial activity).

6.1.3.2. Tracer types

It is found to be practical to divide the available interwell reservoir tracers into three types based on their different means of production, treatment and analysis:

(a) Stable isotope ratios,

(b) Non-radioactive chemical species,
(c) Radioactive atoms or molecules.

Zemel [72] argues that radioactive and non-radioactive chemical tracers are not necessarily different kinds of tracers: "Radioactive tracers are only radioactively tagged chemical tracers." He might as well have included tracer type (a) above in this argument by saying that isotopic ratio tracers are only chemical tracers labelled with a different stable isotope ratio. It is correct that the flooding properties and survivability in reservoirs are determined by the chemical properties of the tracer compound. It is not, however, generally valid that "the same materials without a radioactive tag are also useful tracers". This all depends on the degree of their natural occurrence in reservoir fluids and on their detectability by non-radiochemical methods.

We will exclusively concentrate here on passive radioactive tracers for water and include near-ideal (not passive!) tracers for tracing of natural gas.

6.1.3.3. Generic practical quality requirements for interwell tracers

For unambiguous single phase tracing of water or gas phases in secondary or tertiary recovery production schemes, the following practical tracer selection criteria apply to passive tracers for injected water:

(a) Insignificant degradation during injection and under reservoir and production conditions (i.e. high thermal, chemical, physical and microbiological stability);
(b) Insignificant phase partitioning and sorption to rock;
(c) Insignificant natural occurrence in involved fluids (low background);
(d) Detectability in very low concentrations in reservoir fluid samples;
(e) Toxicity and radiotoxicity at an acceptable level;
(f) Non-problematic logistics and handling;
(g) Sufficient commercial availability;
(h) Acceptable cost.

6.1.3.4. Tracer qualification — laboratory experiments

(a) Thermal and chemical stability

The thermal stability of tracers is tested in batch experiments where aliquots are heat sealed in individual glass cylinders and exposed to different temperatures for different time periods. Tritiated water, HTO, is always added

in a known amount to act as a standard reference tracer. The experiments may be carried out under aerobic or anaerobic conditions.

Samples are analysed with respect to the remaining original tracer concentration as a function of time at the different temperatures. The analysis is carried out by liquid scintillation counting (LSC) or gamma spectrometry if the radionuclide permits.

If $R(T)_0$ is the volume specific count rate (in counts·s^{-1}·mL^{-1}) of the tracer in the original vials before the start of the experiment ($t = 0$) at temperature T, and $R(T)_t$ is the volume specific count rate of the tracer after time t, the survived fraction F is found from the simple expression:

$$F\,(\%) = R(T)_t \times 100/R(T)_0. \tag{92}$$

An example of an F plot is given in Fig. 119.

(b) Microbial stability

Microbial stability is demonstrated in the tests described above by a substantial degree of degradation at temperatures below 70°C while the tracer survivability may be better at higher temperatures. An example of this is the formate ion $H^{14}COO^-$, which seems to be degraded to $^{14}CO_2$.

It is also possible to add certain specific bacterial cultures to the vials to check the effect. The experiments may be somewhat difficult to control.

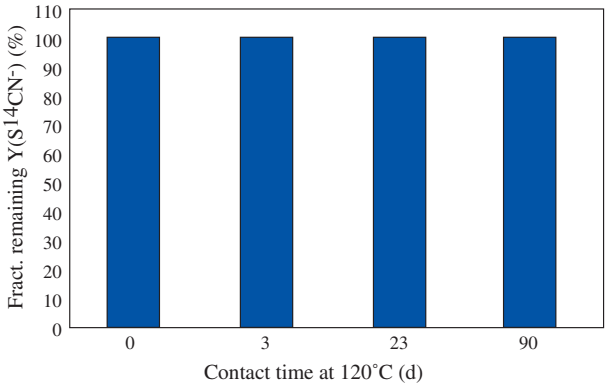

FIG. 119. Thermal stability of $S^{14}C\ N^-$ in sea water at 120°C expressed by the fractional remaining activity F calculated from Eq. (92).

(c) Sorption characteristics

Tracer candidates that pass the tests above are subject to static batch sorption experiments. Crushed reservoir or reservoir-like rock is added to the same type of vials as used above. Convenient test materials are Clashack sandstone and chalk representing the main reservoir rock types, and kaolinite representing clays.

The survivability yield F is calculated from Eq. (92). One example of a static sorption curve is given in Fig. 120.

(d) Phase partitioning

Experiments should be carried out to examine the potential for tracer distribution between the water and the oil phase. Two different methods are:

(1) Static batch experiments, where phase mixing and separation takes place in a mixing apparatus where samples can be extracted from each phase for analysis of tracer concentration.
(2) The dynamic or chromatographic method, where a small tracer pulse is forced through a porous medium with known oil saturation at a moderate linear flow rate (25–50 cm/d), together with the standard reference non-partitioning tracer HTO. The difference in tracer transportation times is a measure of the degree of partitioning.

The first method will give the true equilibrium partition coefficient, while the second might give a more realistic 'effective' partition coefficient because it

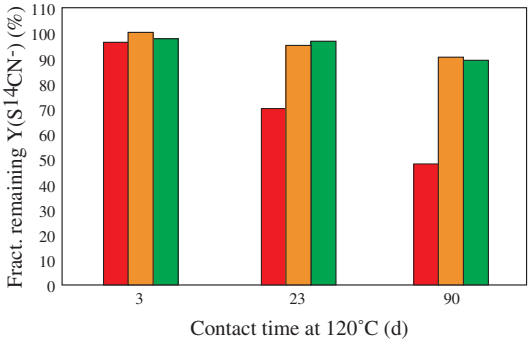

FIG. 120. Stability of $S^{14}C\ N^-$ in contact with sandstone (red bar), carbonate (orange bar) and clay (green bar) substrates at 120°C as a function of contact time. The fractional remaining activity is found from Eq. (92).

includes kinetic effects such as diffusion rates and the rates of exchange between phases (across liquid boundaries). The best situation occurs when the results from both experiments match.

The degree of partitioning is expressed by the partition coefficient:

$$K = C(\mathrm{tr})_o/C(\mathrm{tr})_w. \tag{93}$$

This quantity is directly derived in method (1) above by counting of water and oil samples. Since C is proportional to the disintegration rate, we have $C(\mathrm{tr})_o = R_o/\varepsilon_o$ and $C(\mathrm{tr})_w = R_w/\varepsilon_w$, where ε is the counting efficiency and R is the count rate in the oil (o) and water (w) phases. Thus,

$$K = R_o\varepsilon_w/R_w\varepsilon_o. \tag{94}$$

In dynamic experiments the practical partition coefficient K' is derived on the basis of the recorded tracer production curve (or chromatogram). This curve is established by sampling the fluid effluent from the chromatographic column and counting by LSC and/or gamma spectroscopy. K' can be calculated from Eq. (95):

$$K' = (V_{tr} - V_w)\,[(1 - S_o)/V_w]\,S_o, \tag{95}$$

where

V_{tr} is the retention volume of the tracer candidate, i.e. the volume from the start of injection to the peak maximum of the tracer production curve (which may be found by curve fitting),

V_w is the retention volume of the water represented by the non-partitioning standard reference water tracer HTO and

S_o is the oil saturation or fraction of volume which is occupied by oil.

$K \approx 0$ for passive water tracers. Compounds with $K > 0$ are of interest for the measurement of the remaining oil saturation (see below).

Figure 121 shows an example of a simple piece of batch experimental laboratory equipment used mainly for water/oil partitioning experiments. Gas tracers require more elaborate experimental equipment.

Figure 122 gives an example of results from a batch partitioning experiment. The results show that there is no detectable partitioning of $S^{14}CN^-$ to the oil phase as expected. Of most importance is examination of the partitioning of water tracers with an organic basis.

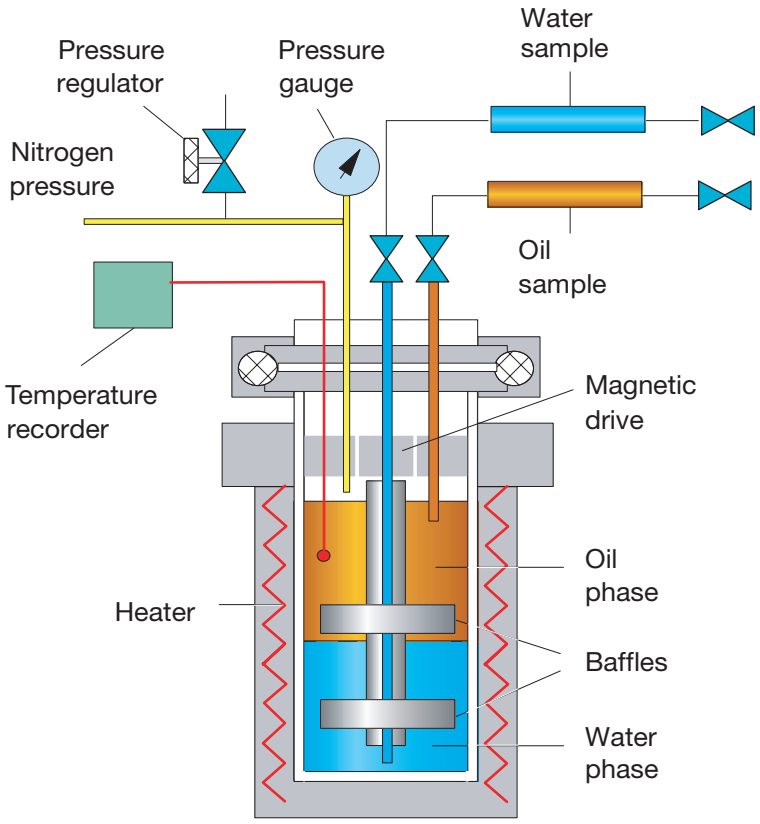

FIG. 121. Mixing chamber with external magnetic drive for measuring oil/water partition coefficients of water tracers at elevated temperatures. Each phase may be sampled separately under the various experimental conditions.

(e) Dynamic flooding properties

Tracers that pass all the batch tests advance to the dynamic tests, where their flooding properties are examined in core flooding experiments.

Different types of equipment are available. It is common to use cores of consolidated reservoir rock or reservoir-like rock (i.e. sandstones such as Clashack, Berea, Bentheimer and Felzer, and carbonate materials such as chalk and limestone). Core dimensions normally range from $d \times l = 3.8 \times 7.6$ cm^2 (1.5 $\times$ 3 in.^{2}) to $d \times l = 5.1 \times 51.2$ cm^2 (2 $\times$ 20 in.^{2}). Other equipment is based on the use of crushed rock material filled into a chromatographic column of varying dimensions.

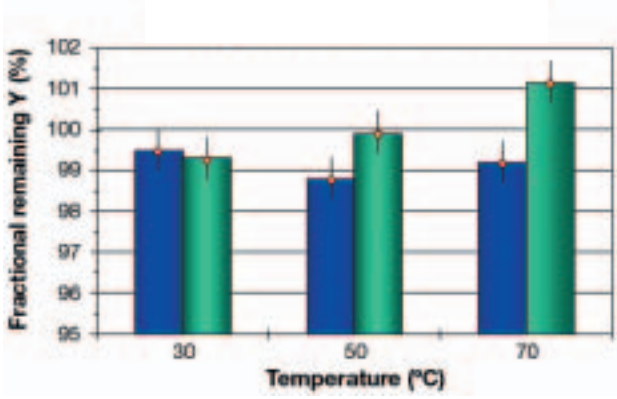

FIG. 122. Fractional remaining activity ($S^{14}CN^-$ + HTO) in the water (seawater) phase after shaking with stock tank oil as a function of contact temperature. The blue and green bars represent two parallel experiments.

Figure 123 illustrates a flow rig based on a 200 cm long chromatographic column with 11 mm internal diameter. Experiments are normally conducted with a typical reservoir linear fluid rate of 25 cm/d.

The most frequently used testing method utilizes pulse injection into the core. The tracer candidate is always co-injected with a standard reference tracer. For water this is normally tritiated water, HTO, and for gas it is most often tritiated methane, CH_3T.

The production profiles of the tracer candidate and the standard reference tracer may be directly compared. Examples of such profiles are given in Section 6.1.3.5.

6.1.3.5. Radiolabelled water tracers

In order to qualify a water tracer on the basis of dynamic behaviour as passive (very good) or nearly passive (good), the type of function expected of the tracer has to be defined closely. If the aim is to measure fluid communication exclusively, a nearly passive tracer may be as good as a true passive tracer.

(a) Non-charged tracer species

A passive water tracer is one that mimics all the movements that water molecules make in the traced water volume and all their interactions. The

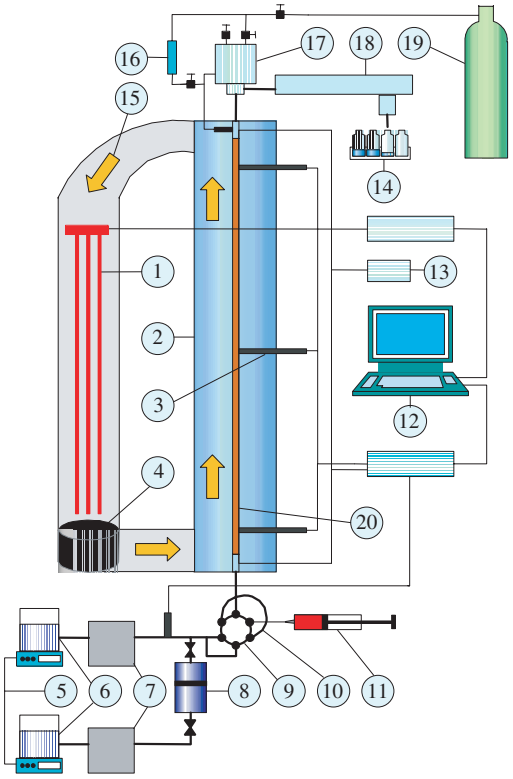

1. *Electric heating elements*
2. *Thermally insulated column housing*
3. *Thermo elements*
4. *Air circulation pump*
5. *Balance*
6. *Column elution liquid*
7. *High pressure pump*
8. *Piston cylinder*
9. *Six port valve*
10. *Constant initial tracer mixture volume*
11. *Syringe for filling of tracer volume*
12. *Computer for logging*
13. *Differential pressure gauge*
14. *Collected liquid samples*
15. *Circulating hot air*
16. *Pressure equalizer*
17. *Back-pressure regulator*
18. *Sample changer*
19. *Nitrogen reservoir for dome pressure*
20. *Chromatographic column with crushed reservoir material*

FIG. 123. Flow rig for dynamic tracer testing of water tracers.

radioactive compound that best fulfils this requirement is radioactive water, HTO. Movements can, for instance, be the free movement in and out of dead-end pores that is insensitive to the Coulombic forces set up by negatively charged rock surfaces. Interactions can be exchanged with connate water in the rock pores or with crystal water molecules. Thus, HTO sometimes seems to lag behind the injection water breakthrough as measured, for instance, by the salt balance (ionic logging), or the HTO production profile may be somewhat more skewed. This has in the literature been wrongly interpreted as HTO being unstable at reservoir conditions, and that it may be subject to isotope exchange reactions of tritium with hydrogen in neighbouring hydrogen containing compounds, some of which are stationary.

Other non-charged tracers are methanol, CH_2TOH, and the other light alcohols. These will behave qualitatively in a similar way to HTO in the diffusive and convective parts but their interactions differ.

(b) Anionic tracers

Of electrically charged tracers, anions represent the more applicable ones. In laboratory experiments, however, clear evidence is seen of ion exclusion, i.e. negatively charged species tend to be repelled from the negatively charged rock surfaces. As a result, these tracers tend to flow in the middle of the fluid conducting pores. They will not easily enter dead-end pores or pass through narrow pore throats. This results in a smaller available pore volume for anions than for non-charged species. The production profile differs in reproducible ways from that of HTO.

Anionic tracers are represented here by $S^{14}CN^-$. A typical production profile, using the flow rig in Fig. 123, is given in Fig. 124. This profile is compared with the production profile of the simultaneously injected HTO. The difference in shape is more easily revealed when subtracting the normalized HTO profile from the normalized $S^{14}CN^-$ profile. The result is given in Fig. 125. It is evident from the curve that the breakthrough of HTO is in front of $S^{14}CN^-$ and that the tail of the HTO profile is more pronounced. This profile difference

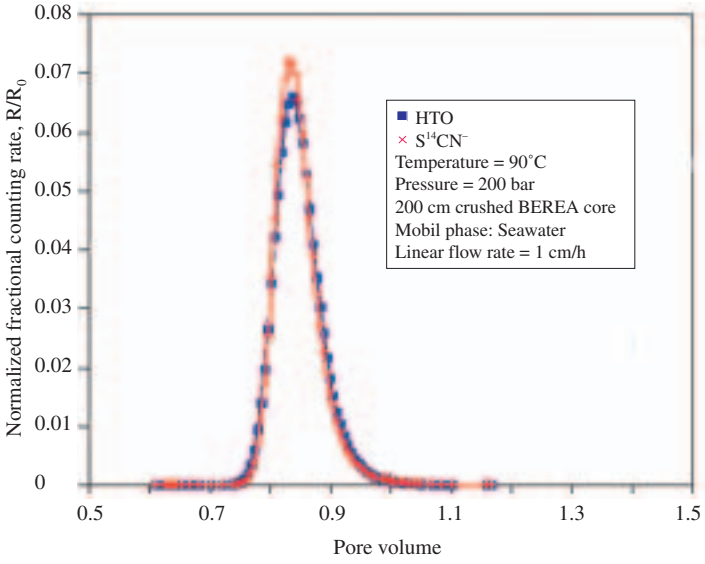

FIG. 124. Normalized production curves of HTO and $S^{14}CN^-$ from flooding experiments on sandstone with the flow rig illustrated in Fig. 123. The experimental parameters are given in the inset.

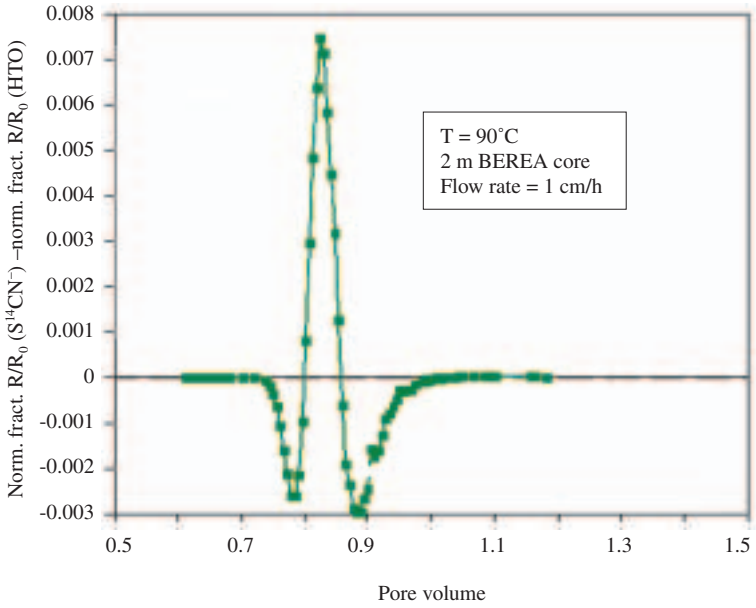

FIG. 125. Difference between the normalized tracer dispersion curves of HTO and $S^{14}CN^-$ from Fig. 123.

is qualitatively reproduced for all nearly passive anionic water tracers. However, if the linear flow rate is increased, for instance by a factor of 10 (i.e. up to 200 cm/d), the first down-dip in the normalized difference curve disappears, and the breakthrough of the anionic tracer comes in front of that of the reference tracer HTO.

On the basis of such curves, retention factors may be derived from Eq. (96) based on production profiles found by such experiments,

$$1 + \beta = V_T/V_S, \tag{96}$$

where β is the retention factor, V_T is the retention volume for the tracer candidate and V_S is the retention volume for the standard reference tracer.

The retention volume may be represented by the peak maximum value or the mass middle point (the first moment, μ_1) for non-symmetric profiles. These values are best found by fitting the profile with an analytical function consisting of polynomials.

For monovalent anions, the retention factors are in the range of 0 to –0.03, i.e. such tracers pass faster through the reservoir rock than the water itself (represented by HTO).

Some anionic tracers may show complex behaviour. Radioactive iodine ($^{125}I^-$ and $^{131}I^-$) breaks through before water but has a substantially longer tail than HTO. Both reversible sorption and ion exclusion seem to play a role here.

(c) Cationic tracers

These are in general not applicable. However, experiments have qualified $^{22}Na^+$ as an applicable water tracer in saline (higher than seawater salinity) waters. In such waters the non-radioactive $^{23}Na^+$ ions will operate as a molecular carrier for the tracer molecule. The retention factor has been measured in the range of $\beta \approx 0.07$ at reservoir conditions in carbonate rock (chalk) [72]. Accordingly, the tracer is somewhat delayed by sorption and ion exchange to reservoir rock, but in a reversible manner.

In the literature there is also a report on the successful use of $^{134}Cs^+$ and $^{137}Cs^+$ in a carbonate reservoir [73]. This tracer cannot, however, be generally used. It will adsorb strongly (and irreversibly under ordinary reservoir conditions) on clay containing rocks. There is also reported use of other cationic species such as $^{60}Co^{3+}$ and other cobalt isotopes, but these compounds have been lost.

Applicable radioactive water tracers are listed in Table 18.

6.1.3.6. Radiolabelled gas tracers

Injection gases may roughly be divided into three types — natural gas (lean gas), composed mainly of CH_4, and its lighter homologues N_2 and CO_2. These gases behave differently in reservoirs. Their behaviour is mainly determined by their different temperature and pressure critical values and by their different solubilities in the oil and water phases under reservoir conditions.

A further complexity to this picture is added by the fact that even the individual components in the natural gas behave differently. This is the reason why it can hardly be claimed that there exists an ideal gas tracer for injected gas in general. Only for pure CO_2 injection may radioactive $^{14}CO_2$ serve as an ideal tracer with respect to molecular behaviour. For references to field use of gas tracers see Ref. [71].

In comparison with water tracers, gas tracers are laboratory tested in a somewhat different way:

(a) Stability tests include examination of isotope exchange and radiolysis for the organic gases;
(b) Phase partitioning;

TABLE 18. OVERVIEW OF THE MOST COMMON RADIOLABELLED WATER TRACERS IN OIL RESERVOIR EXAMINATIONS

Water tracer compound/ion	Half-life	Main radiation characteristics	Comments
HTO	12.32 a	β^- (18 keV)	Generally applicable
CH_2TOH[a]	12.32 a	β^- (18 keV)	Caution at temperatures >100°C (partition into gas phase)
CH_3CHTOH[b]	12.32 a	β^- (18 keV)	Caution at temperatures >100°C (partition into gas phase), some biodegradation below 70–80°C
$CH_3CTOHCH_3$	12.32 a	β^- (18 keV)	Reasonably general application
$CH_3CH_2CH_2CHTOH$	12.32 a	β^- (18 keV)	Reasonably general application, some partition into oil
$S^{14}CN^-$	5730 a	β^- (156 keV)	For $T < 90$–100°C, long term experiments
$^{35}SCN^-$	87 d	β^- (167 keV)	For $T < 90$–100°C, medium term experiments
$^{36}Cl^-$	3×10^5 a	β^- (709 keV)	High temperature reservoirs, long term, EMS analysis
$^{125}I^-$	60 d	γ (35.5 keV), e^-	Reducing chemical conditions, medium term
$^{131}I^-$	8 d	β^- (606 keV), γ (364.5 keV)	Reducing chemical conditions, short term (fracture detection)
$^{56}Co(CN)_6^{3-}$	77.7 d	β^+ (1459 keV), γ (846.8 keV, 1238.29 keV)	Use with caution at $T < 90$°C, medium term
$^{57}Co(CN)_6^{3-}$	271.8 d	γ (122.1 keV, 136.5 keV)	Use with caution at $T < 90$°C, medium to long term
$^{58}Co(CN)_6^{3-}$	70.9 d	β^+ (470 keV), γ (810.8 keV)	Use with caution at $T < 90$°C, medium term
$^{60}Co(CN)_6^{3-}$	5.27 a	β^- (317.9 keV), γ (1173.2 keV, 1332.4 keV)	Use with caution at $T < 90$°C, long term
$Co(^{14}CN)(CN)_5^{3-}$	5730 a	β^- (156 keV)	Use with caution at $T < 90$°C, long term

[a] The alcohol tracers may also be labelled with ^{14}C.
[b] The position of tritium in the alcohol compounds heavier than methanol may vary.

TABLE 18. OVERVIEW OF THE MOST COMMON RADIOLABELLED WATER TRACERS IN OIL RESERVOIR EXAMINATIONS (cont.)

Water tracer compound/ion	Half-life	Main radiation characteristics	Comments
$^{35}SO_4^{2-}$	87 d	β^- (167 keV)	Caution, not generally applicable, avoid alkaline earth containing waters
$^{22}Na^+$	2.6 a	β^+ (545 keV), γ (1274.5 keV)	High temperature tracer in saline reservoirs, long term, slightly reversible sorption
$^{134}Cs^+$	2.065 a	β^- (658 keV), γ (604.7 keV, 795.8 keV)	Caution, not generally applicable, sorption on clays
$^{137}Cs^+$	30.2 a	β^- (512 keV), γ (661.6 keV)	Caution, not generally applicable, sorption on clays

(c) Dynamic properties are tested, for instance, in slim tube arrangements (as in Fig. 127).

(a) Isotopic exchange

Isotopic exchange is of practical interest only for gas tracers labelled with tritium or ^{14}C. Little is published about gas tracer stability against isotopic exchange with surrounding media containing hydrogen or carbon. Some basic experiments are being carried out in a few laboratories in developed countries. The calibrated amounts of tritiated methane and ethane were mixed with distilled water and decane at 90°C, and ^{14}C labelled methane and ethane were mixed with decane in different sealed ampoules for different time periods up to six months. After the pre-selected heating periods, the water and decane phases were purified by boiling under reflux to remove dissolved radiolabelled gases. Subsequently, the liquids were analysed by liquid scintillation. The results are illustrated in Fig. 126. Fractional exchange is calculated from the formula:

$$F_E = R_l V_s \times 100/(\varepsilon V_T D_g), \quad (97)$$

where

R_l is the net counting rate of T or ^{14}C in a known fraction of water or decane,
V_s is the volume of the liquid aliquot extracted for counting (in mL),
ε is the counting efficiency of T or ^{14}C in water or decane mixed samples,

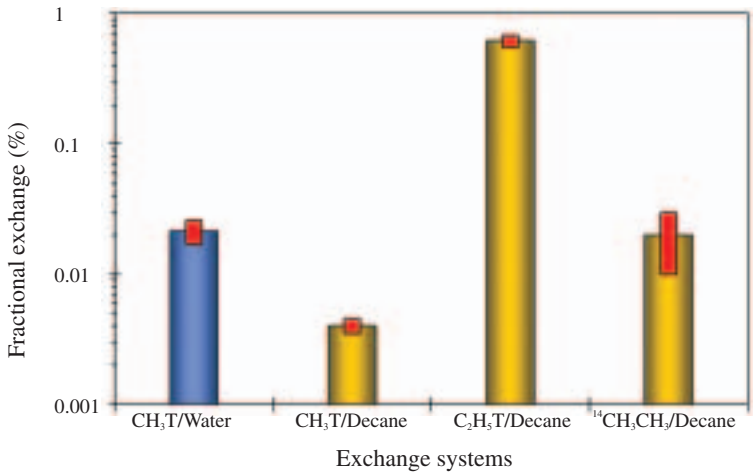

FIG. 126. Isotopic exchange of T and ^{14}C between radiolabelled gas (methane and ethane) and liquids containing hydrogen and carbon. Errors (σ) are indicated by red bars.

V_T is total liquid (water or decane) volume in the sealed reaction vials (in mL), and

D_g is the total disintegration rate of T or ^{14}C in the gas in each reaction vial.

The highest degree of exchange is seen for tritiated ethane in contact with decane after six months, in which case the fractional exchange is found to be $F_E = 0.62 \pm 0.07\%$. This is still a small value, and isotopic exchange is not considered a problem for methane or ethane in field operations. Heavier hydrocarbons have not yet been tested.

(b) Gas/oil partitioning

Gas/oil partitioning experiments should be conducted with equipment suited for simulating reservoir conditions. Practical partition coefficients may be obtained using the slim tube illustrated in Fig. 127. Oil saturation on the column is independently measured. If the total pore volume PV_T can also be derived independently, the partition coefficient for the tracer gas can be calculated by a modified Eq. (95):

$$K_{tr} = (V_{tr} - PV_g)[(1 - S_o)/S_o]PV_g, \quad (98)$$

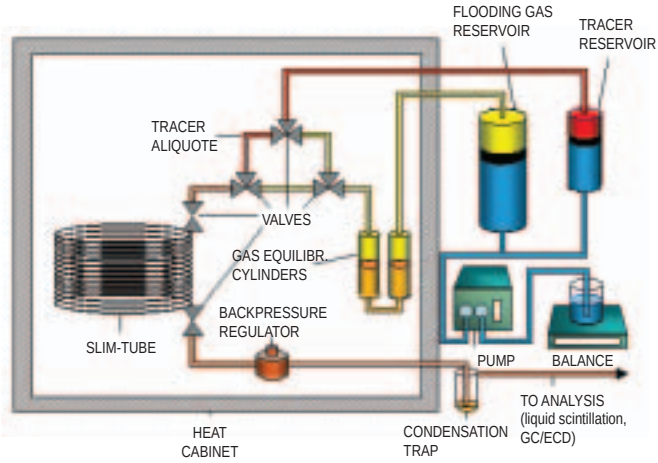

FIG. 127. Flow rig based on a slim tube for examination of gas tracers under simulated reservoir conditions. The slim tube may be filled with crushed rock material and prepared to residual water and/or oil saturation.(GC stands for gas chromatography and ECD for electron capture detector.)

where PV_g is the total free pore volume available for non-partitioning gas (= $PV_T - S_o$) and S_o is the residual oil saturation or fraction of total pore volume that is occupied with stagnant oil.

If the free gas pore volume is not known, it is necessary to use two tracers simultaneously. Oil saturation is measured by independent methods. If only one oil saturation value is used, the K value has to be known for one of the tracers. Then the K value for the second tracer, K_{tr2}, can be derived from Eq. (95):

$$K_{tr2} = [(1 - S_o)(V_{tr2} - V_{tr1}) + S_o V_{tr2} K_{tr1}]/(S_o V_{tr1}), \quad (99)$$

where

V_{tr1} is the retention volume of tracer 1,
V_{tr2} is the retention volume of tracer 2, and
K_{tr1} is the partition coefficient of tracer 1 (which must be a known quantity if the experiments are to run with one single value of S_o; if another experiment can be conducted in the same equipment with a different S_o value, then an equation (Eq. (99) can be obtained where K_{tr1} and K_{tr2} are the only unknowns).

The partition coefficient is a function of oil type, pressure and temperature.

(c) Flooding properties

The slim tube arrangement shown in Fig. 127 is used to examine the relative dynamic behaviour of gas tracer candidates. The slim tube is 6–12 m long and in the simplest experiments is filled with sand of silicate rock. The experiments are conducted at simulated reservoir temperature and pressure.

Normally, before the porous medium is prepared to either residual water or oil saturation, or both, experiments are conducted on the dry rock material to reveal any tracer delay due to reversible sorption on the mineral surfaces. Figure 128 gives an example of CH_3T and $^{14}CH_3CH_3$ used simultaneously in a slim tube with a dry silicate rock filling. The figure shows a slightly broader distribution for ethane compared with that for methane, but the centroids coincide within the experimental errors.

Figure 129(a) illustrates how methane and ethane are separated (chromatographically) in a slim tube with 30% residual oil due to different partitioning into the stagnant oil phase. The experiment is conducted at 50°C temperature and 150 bar pressure. Note the change in both absolute and relative peak positions when the pressure is increased to 250 bar (Fig. 129(b)). The methane

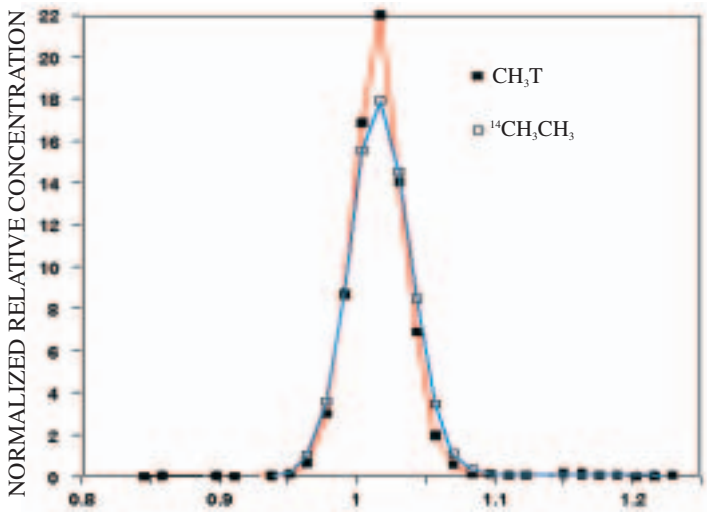

FIG. 128. Dispersion curves of radiolabelled methane and ethane injected simultaneously from slim tube experiments on dry silica rock at simulated reservoir conditions.

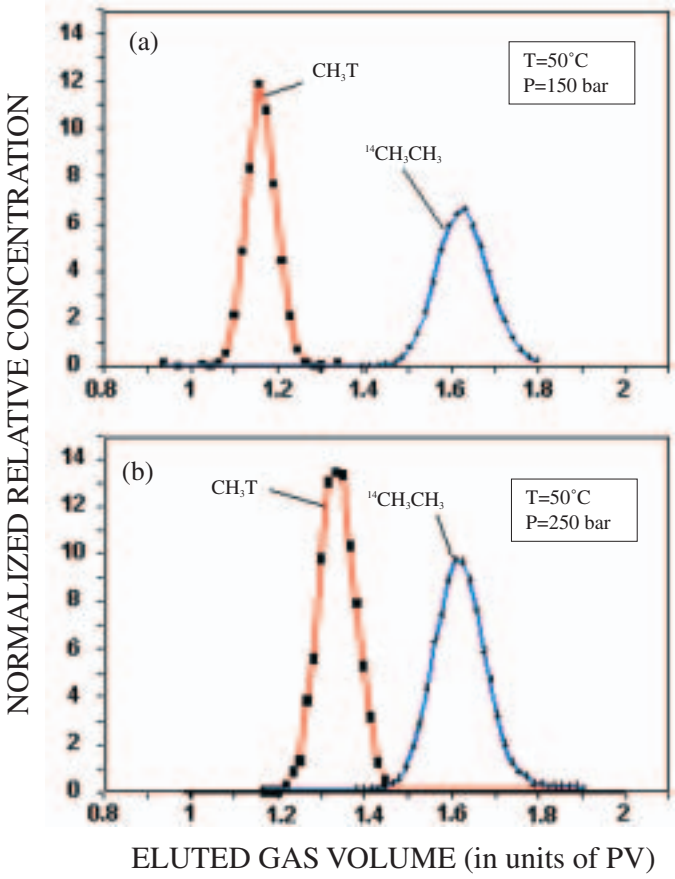

FIG. 129. Slim tube experiment with radiolabelled methane and ethane, where the slim tube is prepared to 30% residual oil saturation. Experiment (a) is conducted at 150 bar pressure and experiment (b) at 250 bar pressure.

peak increases. The ethane peak moves only slightly to the left and the distribution half-width decreases slightly, while the methane peak moves to the right and the half-width of the distribution increases slightly, i.e. the partition coefficient *K* value stays essentially constant with a slight decreasing tendency.

At higher pressures, the two peaks continue to approach each other, methane moving to the right and ethane to the left, but there is no full overlap at normal reservoir conditions.

Heavier homologues follow the ethane trend, but the *K* values are higher and decrease more rapidly.

Experiments have been carried out with several radiolabelled gas tracers. One of the non-organic tracers is ^{85}Kr. Krypton is a noble gas and is virtually inert against chemical reactions at reservoir conditions. Its flooding properties fall between that of methane and ethane.

Applicable gas tracers are listed in Table 19.

6.1.3.7. Quality assurance of tracer mixtures

(a) Water tracers

For tracers composed of single ions such as $^{125}I^-$ and $^{22}Na^+$, tests are simpler than for tracer compounds based on molecular complexes. This is exemplified here with the tracer compound cobalt hexacyanide, $Co(CN)_6^{3-}$. This molecule may be labelled with ^{56}Co, ^{57}Co, ^{58}Co, ^{60}Co or ^{14}C and it may be used as the unlabelled complex. The latter requires a sensitive analytical method such as thermal neutron activation analysis for cobalt. One single molecular carrier may then give rise to six different tracers. The total complex constant of this molecule (β_6) is reported to be very high (10^{38}–10^{64}) [71, 74]. The conclusion may be drawn, incorrectly, that the $(CN)_6$ ligand molecule is very stable and that it will exist in this molecular form more or less regardless of the chemical environment. This argument has led to extensive and somewhat uncritical field use of radiolabelled versions of these molecules. In many cases, good results have been obtained, while in others the tracer has never been found. Heavy radioactive contamination in the injection equipment and on steel parts of the injection area has also been reported. An unreported contamination incident in the North Sea led to a ban on the use of these tracer compounds until a better knowledge of handling and interactions had been gained. This incident and other reported failures initiated a thorough investigation of radiolabelled $Co(CN)_6^{3-}$ [76]. A few results of this study follow.

Cobalt-60 labelled hexacyanide was purchased from one of the largest commercial producers of radiochemicals as a ready-to-inject solution. One of the quality control methods was the electrophoresis technique. Batches purchased at different times showed different results indicating a radiochemically impure product. A new synthesis has been tested with a procedure provided by the commercial company. The results from this experiment are shown in Fig. 130. The electrochromatogram shows a relatively broad distribution with two distinct peaks. This indicates that the ^{60}Co label exists in, at least, two different anionic forms. These forms are not identified. They may have different stabilities and chemical behaviour. The compound was then synthesized by a modified method. This procedure gave chromatograms like that shown in Fig. 131.

TABLE 19. OVERVIEW OF THE MOST COMMON RADIOLABELLED GAS TRACERS IN OIL RESERVOIR EXAMINATIONS

Gas tracer compound	Half-life	Main radiation characteristics	Comments
CH_3T[a]	12.32 a	β^- (18 keV)	First choice radioactive gas tracer, long term experiments, high temperature reservoirs
CH_2TCH_3 [a]	12.32 a	β^- (18 keV)	Applicable gas tracer, long term experiments, slight isotope exchange of the T label to H containing media
CH_3CHTCH_3 [a]	12.32 a	β^- (18 keV)	Reasonable gas tracer, long term experiments, unknown T exchange, larger partitioning into oil
$CH_3CHTCH_2CH_3$ [a]	12.32 a	β^- (18 keV)	Can be used if necessary, long term, unknown T exchange, high partitioning into oil
^{85}Kr	10.76 a	β^- (687 keV)	Long history in reservoir examinations, chemically inert, high temperatures, long term experiments, dynamic behaviour close to that of methane at reservoir conditions
$^{14}CO_2$	5730 a	β^- (156 keV)	Applicable tracer for injection gas, ideal for CO_2 injection, long term experiments, high temperatures
^{133}Xe	5.25 d	β^- (346 keV), γ (81 keV)	Chemically inert, high temperatures, dynamic reservoir movement rate in-between methane and ethane, usable for detection of high permeability streaks and 'super' conducting flow channels, detectable until 25 d after injection
^{127}Xe	36.4 d	γ (202.9 keV, 172.1 keV, 375.0 keV)	Dynamic behaviour as for ^{133}Xe, applications as for ^{133}Xe, but may be detected until 180 d after injection

[a] These molecules may also be labelled by ^{14}C.

Cobalt hexacyanide from the commercial company was then the subject of thermal stability and sorption investigations. A fast sorption to corroded

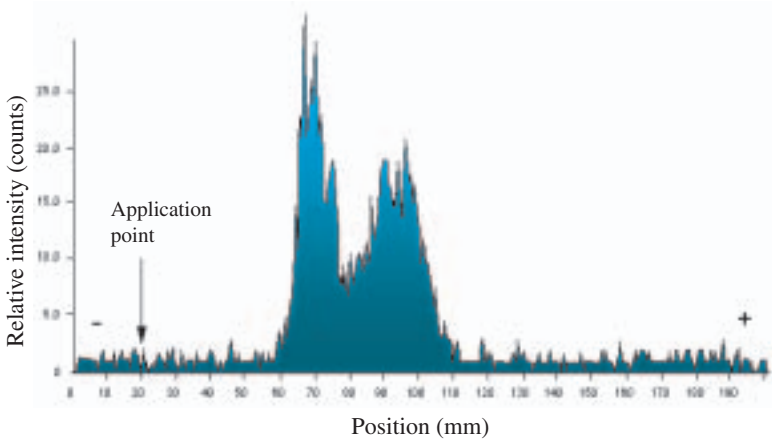

FIG. 130. Electrophoresis chromatogram of $^{60}Co(CN)_6^{3-}$ synthesized according to the procedure provided by Amersham International plc.

steels was found already at ambient temperatures, but the sorption became even more pronounced at elevated temperatures. Liquid solutions after heating to 120°C for 24 h were again investigated by the electrophoresis technique. The results are shown in Figs 132 and 133. A substantial fraction is uncharged and does not move away from the application point. On the positive potential side

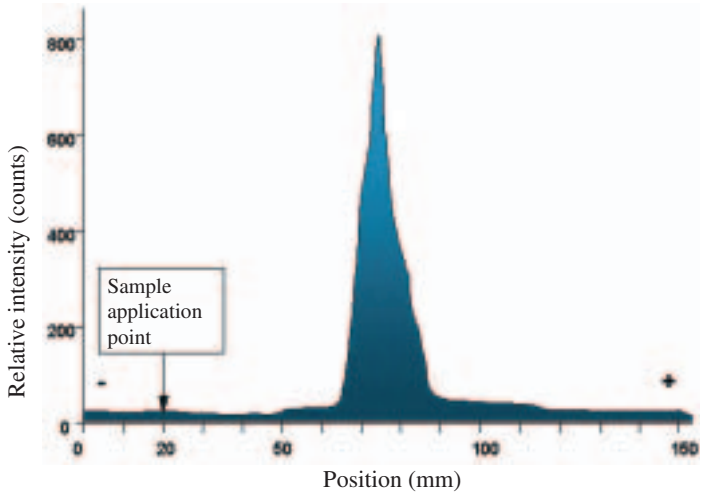

FIG. 131. Electrophoresis chromatogram of $^{60}Co(CN)_6^{3-}$ synthesized according to a revised procedure. This product has, in addition, been exposed deliberately to 10^5 rad of ^{60}Co gamma radiation in a gamma irradiation facility.

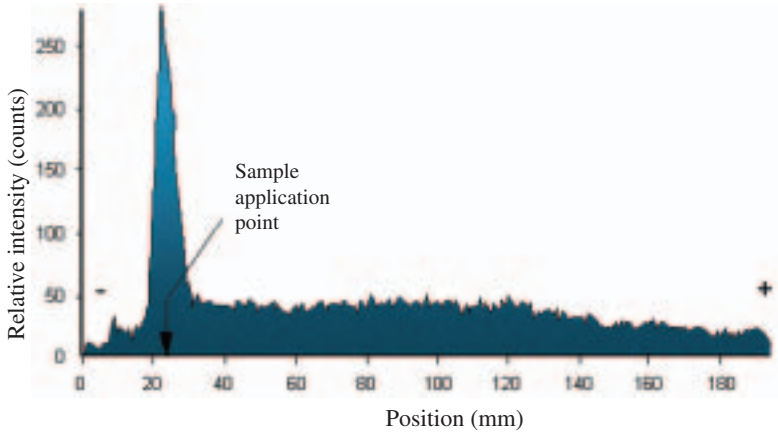

FIG. 132. Electrophoresis spectrum of ^{60}Co containing components in a seawater solution of commercial $^{60}Co(CN)_6^{3-}$ on the anionic side after a state heating period of 24 h at a temperature of 120°C. The sample was a blank (no substrate)

is a relatively low and broad, nearly constant distribution, indicating different ^{60}Co labelled anionic forms. On the negative potential side is also a substantial and broad distribution, indicating various positively charged complexes. Accordingly, heating leads to breakdown of the hexacyanide complex into a range of different complexes with varying masses and uncharges. It may be

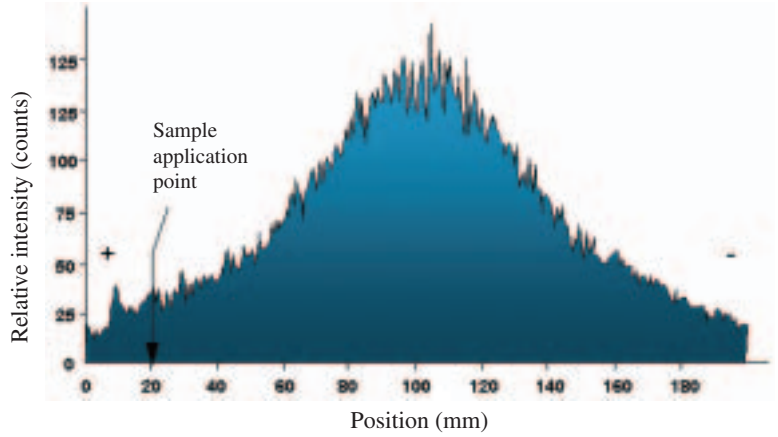

FIG. 133. Electrophoresis spectrum of ^{60}Co containing components in a static seawater solution of commercial $^{60}Co(CN)_6^{3-}$ on the cationic side after heating for 24 h at 120°C. The sample was a blank (no substrate).

suggested that CN ligands can be exchanged to some degree with Cl^-, OH^- or even H_2O to saturate the co-ordination number of 6. This leads to complexes with different charges and different chemical properties. The experimental investigations [76] showed that the quality control on the radiochemical purity is very important: pure $Co(CN)_6^{3-}$ should be ensured at the start of any field application. One should not use this tracer compound at reservoir temperatures of more than 90°C.

(b) Gas tracers

Quality assurance of radioactive gas tracer mixtures is needed for two purposes:

(1) Tracer concentration. When tracers are purchased from a commercial supplier, it is imperative to check that the total activity corresponds to the design activity for the injection. This is done by extracting a small aliquot for calibration before injection.
(2) Radiochemical purity. Especially for tritiated and ^{14}C labelled organic gases, it is important to ensure that the radiochemical purity is acceptable. This is done by gas chromatography with a flow scintillation detector.

6.1.4. Injection

There are in practice two different injection methods:

(a) Continuous injection, where a constant concentration of tracer is injected over prolonged times (months and years).
(b) Pulsed injection, where a certain quantity of tracer (in Bequerels) is injected over a short period (seconds, minutes, hours).

6.1.4.1. Continuous injection

This method has been applied mainly for injected water. It is useful especially where unsaturated water-wet rock may absorb short tracer pulses by imbibing water from the injected water front edge. Ideally, the method requires continuous logging of the water injection rate and corresponding adjustment of the tracer dosage rate in order to maintain a constant concentration of tracer in the injected fluid. A simpler arrangement can be implemented if a constant water injection rate can be assured. An example of a tracer injection arrangement is given in Fig. 134. Typically, the tracer used is HTO and the

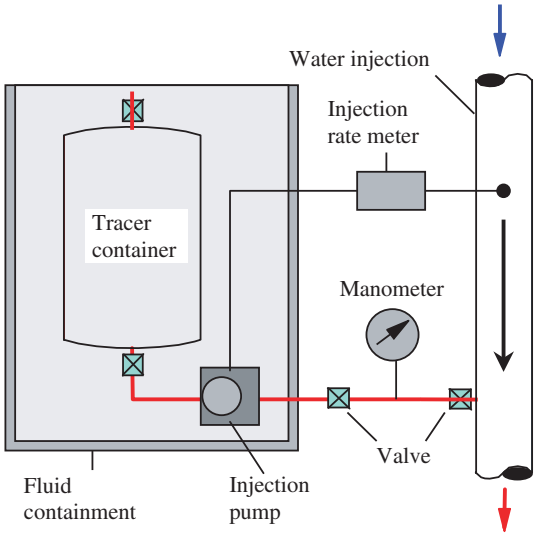

FIG. 134. Tracer injection arrangement for a continuously constant concentration injection of beta radioactive water tracers.

concentration in the tracer container is 370 MBq/L. The tracer concentration in the injected water, and the corresponding rate of tracer dosage, depends on the detection limit in the analytical laboratory and on the expected fraction of traced injected water in the produced water. The design should have a tracer concentration at the top of the production curve (at equilibrium) corresponding to some 100–1000 Bq/L in the produced water.

An example of a field experiment with continuous injection of water tracer (HTO) and a subsequent tracer pulse injection ($^{125}I^{-}$) is found in Ref. [76]. Such operations may be laborious and cumbersome, especially for off-shore operations. They require access to tracer engineers on a continuous basis. In addition, long term storage and operation of radioactive solutions give rise to some scepticism among petroleum rig personnel. This method should be used only if there are clear advantages over the pulsed injection method.

6.1.4.2. Pulsed injection

There are two main procedures for tracer pulsed injection:

(1) Integral (topside) injection at the well head, where the tracer enters all available perforated zones and is injected into the reservoir according to the injectivity in the various zones.

(2) Downhole injection, where different tracers may be injected into different isolated zones.

(1) Topside injection

This is the simplest, cheapest and most frequently used injection method. The practical implementation procedure depends on the tracer to be injected, i.e. the procedure is simplest for beta emitters and somewhat more cumbersome for strong high energy gamma emitters. The techniques range from mechanical crushing of tracer containing glass vials in the injection stream to controlled pump operated injection.

Here, we describe a well proven technique for water tracer injection and one for gas tracer injection. The tracer mixture is prepared in 100 mL flowthrough high pressure steel cylinders fitted with high pressure valves at both ends (total liquid volume ≈70 mL). For beta tracers, a small amount of a short lived gamma emitter (often $^{131}I^-$) is added for monitoring purposes.

Figure 135 illustrates a typical piece of small sized injection equipment. The equipment is coupled as a bypass to the main injection line at two positions across a throttle valve to set up a pressure difference between the two positions. The tracer container is connected to the equipment as shown. There are possibilities for pump operation of preparative fluids (inlet for chemicals) before tracer injection. The tracer is injected by bypassed injection water driven by the pressure difference, and without any use of pumps. The injection efficiency is monitored by external gamma detectors. The typical injection time is less than 10 s for more than 99% of the tracer. However, rinsing continues for 60 min to clean out any traces of remaining activity from the injection apparatus.

For some tracers it is advantageous to apply an extra non-radioactive molecular carrier in the injection phase (for instance, for $^{125}I^-$ and radiolabelled $Co(CN)_6^{3-}$). These tracers are injected using the same injection apparatus but now connected only to the main flow line at the outlet connection point. The injection is performed by pump operation where injection water containing carrier and other tracer preserving chemicals is pumped from an injection water reservoir.

Gas tracer injection may be implemented by a somewhat modified version of the same equipment in pump operation. Gas tracer cylinders are sometimes larger than 100 mL, and have to be mounted vertically with the inlet of the displacing liquid in the bottom. The displacing liquid may be methanol.

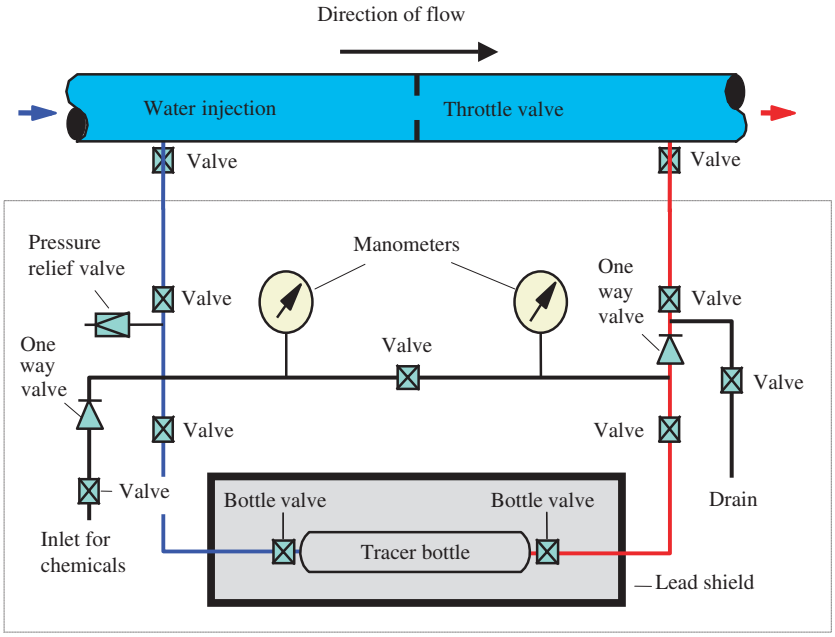

FIG. 135. Small sized injection apparatus for topside pulsed injection. Both beta and gamma tracers may be used. For high energy gamma emitters, heavy shielding is applied around the tracer bottle. It operates as a bypass to the main injection stream but may also be operated through the 'inlet for chemicals' valve with the help of a high pressure pump.

(2) Downhole injection

Downhole injection offers several advantages over topside injection:

(a) Removal of the danger for contamination of topside equipment. This may be especially important for radiolabelled $Co(CN)_6^{3-}$ and possibly other traces which may react chemically in the injection tubing.
(b) For stratified reservoirs, each zone may be uniquely labelled with a special tracer. This gives the possibility to examine the vertical permeability in reservoirs and to detect any extensive sealing.
(c) For horizontal wells, which cover an extensive lateral reservoir section, zone injection is absolutely desirable for optimal information.

Downhole injection is not yet in general use although field tests have been successfully carried out [73]. A few attempts have been made to construct

tools for general application, one of which is described in Ref. [77]. They are mainly constructed for vertical and inclined wells, and can be lowered into the well by a wireline with a possibility for signal transfer. The tools are remotely operated from a topside personal computer. They are based on the principle of a moving arm sealing onto the perforated section of the well through which the tracer solution is pumped at low speed at a somewhat reduced ordinary water injection rate. Such tools are not yet in operation due to high cost of operation.

In recent times it has become technically possible to position downhole injection tools in horizontal wells by means of a well tractor. Combined with inflatable packers on the same line, sections may be isolated for specific tracer injection. Such injection equipment is composed of general and readily available components. Downhole injection is now therefore technically possible with zone injection, but the first large scale field experiment has still to be performed.

6.1.5. Radiation detection and measurement

6.1.5.1. Sampling

(a) Water tracers

Sampling operation is generally carried out by oil company personnel. It is not a complex task, especially when working with tritium, due to the very low concentrations usually present in the production water.

Ideally, one sample per day should be taken but only some can be sent to the analytical laboratory. When the tracer is detected in any sample the previous ones can be measured in order to rebuild the response curve for detection of tracer breakthrough. Nevertheless, in the case of having performed several simultaneous injections, it is difficult to manage the number of samples involved and for that reason it is convenient to elaborate a less ambitious sampling plan. However, it is always advisable to measure only some of the collected samples and return to previous samples when tracer appears.

The sampling plan should include a relatively high sampling rate during the first days after injection and a somewhat more time spaced sampling as time passes. The sampling rate should increase when breakthrough is detected, in order to monitor more precisely that part of the tracer production curve where most abrupt changes take place. After having passed the maximum of the production profile, two samples a month should be enough and just one sample per month afterwards. The objective of a good sampling plan is to have enough information to obtain a good response curve with a minimum number of samples to be taken.

The reason for a high sampling frequency immediately after injection is the possibility of some canalization that makes the injected water flow very quickly to the production well. In such a case the tracer longitudinal dispersion will be very small and the response curve will be short with a sharp rise edge and high amplitude. All the information will be concentrated in a short time and many samples will be needed to recover it. (If channelling is expected, it is advisable to run a pre-test with a short lived radionuclide such as $^{131}I^{-}$).

The volume of the samples depends on the tracer and the measurement technique selected. In general, the samples are stored in plastic bottles labelled with the sampling date and the well number to which they belong. This information has to be written using permanent ink.

It is important to remember that a background sample should be taken from each production well before the injection.

(b) Gas tracers

Constant sampling conditions: If constant sampling conditions with respect to temperature and pressure can be assured over the lifetime of the project, it suffices to collect one (or a few) integrated samples (oil and gas together) to establish the gas/oil partition coefficient under separator conditions. All subsequent samples may be pure gas phase samples. This enables calculation of the returned total amount of tracer. These samples have to be collected on pressure resistant sample cylinders. A flowthrough stainless steel cylinder of 500 mL volume constitutes a normal sized sample container.

Varying sample conditions: If constant sampling conditions cannot be assured, integrated samples will have to be taken throughout the experiment. Alternatively, one may log the sampling conditions for each sample (temperature and pressure) and generate the partition coefficient from tables prepared in the laboratory for changing experimental conditions.

The sampling procedure should be clearly written down in order to ensure that sampling is carried out by the same procedure throughout the experiment by different personnel.

For partitioning tracers, integrated samples will have to be taken.

6.1.5.2. Measurement techniques

Measuring techniques depend on the tracers' radiation characteristics (beta, gamma or stable chemical ones), but all of them include some sample treatment prior to the measurement itself.

When counting a radioactive sample it is well known that the instrument reading is a measure of the sample activity plus the background activity. The latter

must be subtracted in order to evaluate the actual net sample activity. The background activity is usually taken to be the activity measured by using the sample taken before the injection (blank sample). If, however, the tracer does not appear immediately (there are no canalizations), more representative information on the background activity is obtained by measuring several of the samples and averaging the results, taking into account that the more samples, the lower the background variation coefficient. The variation coefficient is the ratio between the standard deviation and the mean value.

At this point it is convenient to remember that radioactive decay is an inherently random phenomenon that follows, strictly speaking, the binomial distribution. Nevertheless, the Poisson distribution is an excellent approach that takes into account some of the radioactive decay characteristics (the random event disintegration is repeated many times and the individual probability for an atom to disintegrate is very low).

The Poisson distribution depends on just one parameter, generally symbolized by the Greek letter σ, and the distribution mean value and variance are both equal to σ. This property is very useful in radioactive measurements. Once the count rate has been determined, its numerical value can be used as the expected average value and its square root as the standard deviation.

Furthermore, in the case that the number of events approaches infinity the binomial distribution and the Poisson distribution converge towards another statistical distribution called the normal or Gaussian distribution, which is continuous and symmetric around its mean value. In a normal distribution the probability for the random variable to take values close to the mean value is very high, while the distribution approaches zero asymptotically for large values located in the positive and negative tails.

As a rule of thumb it is usual to require that all random variable values fall in a 2.5 standard deviation interval around the mean value. In such a case a confidence level of 98.76% (99% in practice) for the measurement is established. This means that there is a 1.24% probability that the true mean value is outside the range given by the measured mean value and ±2.5 standard deviations.

Consequently, two measurements may be said to belong to different populations when their measured mean values differ by at least five standard deviations. This criterion is also applied to determine whether a sample is active or not, i.e. whether a sample has some radioactivity of its own when its count rate is five standard deviations greater that the background.

In general, the following condition is established to calculate the lower detection limit (minimum detectable concentration), L_D, on the basis of the instrument background:

$$R_N > 2\sigma_{R_B}.$$

This means that the sample count rate should be at least double its own standard deviation in order to be distiguished from the background. The standard deviation is given by the following expression:

$$\sigma_{R_N} = \sqrt{\frac{R_G + R_B}{t_c}}, \tag{100}$$

where

σ_{R_N} is the standard deviation for the net count rate R_N (counts/s),
R_G is the gross count rate (counts/s),
t_c is the counting time (s), and
R_B is background count rate (counts/s).

After some operations and approximations the following expression is obtained for L_D:

$$L_D = \frac{2.8}{\varepsilon V}\sqrt{\frac{R_B}{t_c}}, \tag{101}$$

where

L_D is the lower detection limit (or minimum detectable activity concentration) in Bq/L,
ε is detection efficiency (counts per disintegration), and
V is sample volume.

As a consequence of statistical dispersion, some pre-processing of experimental data is usually needed in addition to background subtraction in order to filter noise and smooth the response curves.

Finally, a radioactive decay correction is needed. Although in the case of tritium its half-life is long enough to avoid this kind of correction when the sampling periods last only a few months, in a general situation an interwell study implies more than a year of sampling and tritium decays at a rate of 0.45% per month.

(a) Beta radioactive tracers

The most common beta radioactive tracers for interwell studies are labelled with tritium (^{3}H), ^{14}Cr or ^{35}S. All of them are usually measured by means of the liquid scintillation counting technique.

A small volume of a liquid sample is mixed with a special solution known as a scintillation cocktail, commonly in a 20 mL light transparent (glass, polypropylene or Teflon) vial. Beta particles cause emission of light when passing through and slowing down in the scintillation cocktail. These light pulses are registered by photomultiplier tubes (PMTs) suitable for that particular photon wavelength. The light output in a pulse (light intensity) is proportional to the energy of the beta particle. This process is called scintillation, and since it occurs in liquid media, it is known as liquid scintillation.

The vial is placed inside an instrument, an LSC, which has normally two PMTs operated in co-incidence to reduce background. The LSC analyses the pulses from the PMTs and provides information about the energy of the beta particles and the rate of beta emission (activity) in the sample.

Pulses are sent to an analog-to-digital converter (ADC), where they are digitized and stored in an address memory according to their amplitudes that are proportional to their beta energies (energy spectrum measured by a multichannel analyser).

In order to further reduce the background arising from natural radiation, a lead shield usually surrounds the PMTs and the vial while the sample is in the measuring position. Modern low background detection equipment also has a so-called active shield. In most cases it consists of a liquid scintillation detector surrounding the PMTs and the counting sample. This shield detector is operated in anticoincidence with the PMTs, i.e. so that any event which is registered both in the two PMTs and in the shield (cosmic rays or environmental radiation) detector simultaneously is rejected. In the case of simple non-spectrometric detection equipment (single channel analyser), the contribution of the background to the sample count rate can be further reduced by setting a counting window only over the interesting energy portion of the energy distribution. This is achieved by selecting narrow upper and lower limits. In the case of tritium, for instance, the upper gate should be set at 19 keV.

Various processes may perturb the beta spectrum obtained in a liquid scintillation process. Here, only the most important will be mentioned briefly:

(1) *Chemiluminescence*: When different chemicals are mixed in the sample vial together with the scintillation cocktail, chemical processes may start which have relatively slow kinetics and which result in emission of low

energy photons. These photons may contribute to the very low energy end of the beta spectrum. Chemiluminescence may be reduced or completely removed by gently heating the vial to 50–60°C for some minutes to speed up the chemical process before counting.

(2) *Phospholuminescence*: When a sample vial with the scintillation cocktail is exposed to white light (day light or lamp light), the light energy may be temporarily stored and slowly given off during sample counting (phosphorescence). In addition, this light will contribute to the far low energy end of the beta spectrum. Therefore, counting samples should always be stored in the dark a few hours before counting starts.

(3) *Colour quenching*: Coloured sample liquid may absorb some of the light emitted by the scintillator. Yellowish or brown colours are the heaviest colour quenchers. Hence, one should try to remove such colours during the sample preparation process and before counting.

(4) *Chemical quenching*: Some components in the sample may disturb the energy transfer process that takes place in the scintillation cocktail which eventually results in light emission. Such chemicals absorb the energy and release it in the form of heat. Organic compounds containing oxygen, and in particular chlorine, are instances of heavy chemical quenchers.

(5) *Physical quenching*: Solid particles or non-transparent emulsions in the sample may prevent light from being detected by the PMTs.

All these forms of quenching result in a shift of the energy spectrum towards lower channel numbers because the number of photons detected by the PMTs per beta decay is reduced. Figure 136 shows the principle of the effect of quenching.

Quenching may change from one sample to another. Evaluation of the quenching effect is necessary in order to calculate the counting efficiency.

In conclusion, liquid scintillation counting requires careful sample preparation. Most often, chemical separations are involved. When these procedures are optimized, very low detection limits may be obtained ranging from 2 Bq/L for HTO to less than 0.02 Bq/L for $S^{14}CN$ [78].

(b) Gamma tracers

Gamma tracers are commonly measured using either solid scintillation detectors or semiconductor detectors.

Solid scintillation detectors: These are of different types, but the most generally applicable is the detector based on a single crystal of sodium iodide doped with traces of thallium, the so-called NaI(Tl) detector. The crystal is

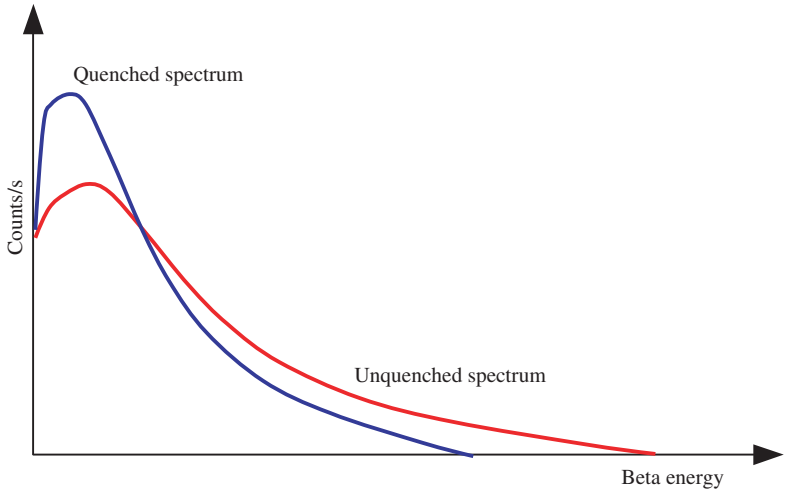

FIG. 136. Sketch of the principle of the effect of quenching on a liquid scintillation beta spectrum.

optically coupled to a PMT. Interaction of a gamma photon with the scintillation crystal results in emission of light, which is detected by the PMT. The light output is proportional to the gamma energy. The electronic system associated with the PMT analyses the pulses according to pulse amplitude (energy) and stores the results in an MCA. Thus, energy and intensity are recorded, and the result is the gamma energy spectrum of the radiation source.

The NaI(Tl) detector has a high intrinsic efficiency but a limited energy resolution. The scintillation crystals are provided in different sizes. The efficiency for high gamma energies increases with detector volume. Common counting equipment has cylindrical crystal sizes of 5.08×5.08 cm^2 (2 in. × 2 in.) to 12.7×12.7 cm^2 (5 in. × 5 in.) (height × diameter). The larger the crystal, the higher the price. The detectors can be made quite rugged, and they are therefore suitable in field instrumentation.

Semiconductor detectors: At present, these are mainly based on high purity germanium crystals, so-called HPGE detectors, where a semiconductor junction is created by suitable elemental dopants on the crystal surface. A gamma ray interacting with the detector will result in an excitation of electrons from the valence band to the conduction band in the crystal, and a small electric pulse is created in a high voltage field. The pulse height is proportional to the gamma energy. The pulses are sorted and stored in an MCA.

The intrinsic efficiency of semiconductor detectors has, for many years, been lower than that of NaI(Tl) detectors. At present it is, however, possible to

purchase detectors with efficiencies of more than 100% relative to that of a 7.62 × 7.62 cm^2 (3 × 3 $in.^2$) NaI(Tl)detector, but prices are very high. The main advantage with an HPGE detector is, however, its excellent energy resolution. This property may be indispensable for analysis of complex radiation sources. HPGE detectors need cooling to liquid N_2 temperature during operation, and are not as generally applicable as field instrumentation.

In general, gamma tracer detection requires little sample preparation except for the extreme low energy emitters (i.e. ^{125}I).

There are several ways to reduce the minimum concentration detectable:

(1) Increase the detector intrinsic efficiency:
This is a matter of cost.
(2) Increase the counting sample volume (constant activity concentration in the sample leads to higher total activity in the sample):
There is a practical limit to the sample size.
(3) Optimize the counting geometry by shaping the counting sample:
For a given radionuclide, a selected detection set-up and a certain sample volume, there is an optimum shape of the sample volumes. For practical reasons these are most often cylindrical-like shapes.
(4) Enrich the tracer by reducing the sample volume (increased total activity for a better sample counting geometry):
This requires sample treatment either by liquid evaporation or by chemical separation. Sample treatment time and cost increase.
(5) Reduce the background level (Eq. (100)) by effective detector shielding:
This is most often done by passive shielding with lead walls (5–10 cm thickness) around the detector and sample.

A typical counting set-up for a NaI(Tl) detector and a liquid sample in a Marinelli beaker is shown in Fig. 137.

With NaI(Tl) detector based analytical equipment, detection limits of less than 0.2 Bq/L can be obtained using Marinelli beakers and reasonable counting times for common radionuclides such as ^{22}Na [79], ^{60}Co and ^{125}I.

For HPGE detectors, the corresponding detection limits are less than 0.1 Bq/L.

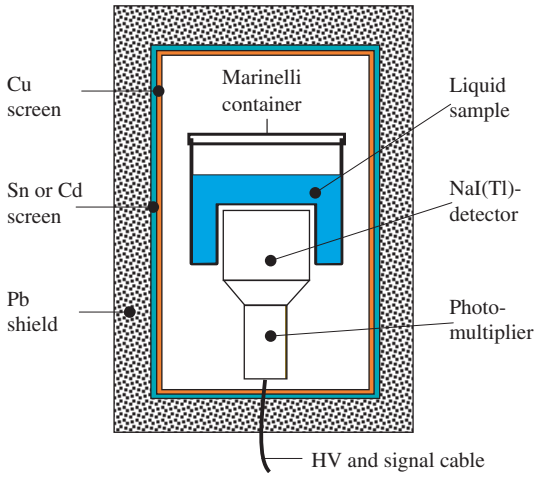

FIG. 137. Common set-up for the counting of gamma active liquid samples: 1000 mL Marinelli sample container, 7.62 × 7.62 cm^2 (3 × 3 in.^{2}) NaI(Tl) detector, Pb shield (5–10 cm), an Sn (or Cd) screen to filter away Pb X rays generated by the sample activity in the Pb shield, and a Cu filter screen to filter away Sn (or Cd) X rays generated by the Pb X rays in the Sn (or Cd) screen.

6.1.6. Data analysis and modelling

6.1.6.1. Response curves

A good sampling programme and measurement of these samples with adequate detectors (high efficiency, low background and low statistical error) are the way to obtain good response curves, which are the bases for further interpretation.

(a) Time response

The time response is the graphic representation of the concentration of activity (after background subtraction and decay correction) as a function of time. Pre-processing of the experimental data can also be used in order to smooth the response.

From this curve the cumulative response (recovered activity versus time) is derived by a simple numerical integration. The application of complex integration methods is not justified because of statistical dispersion in the original data and variations in the pattern parameters.

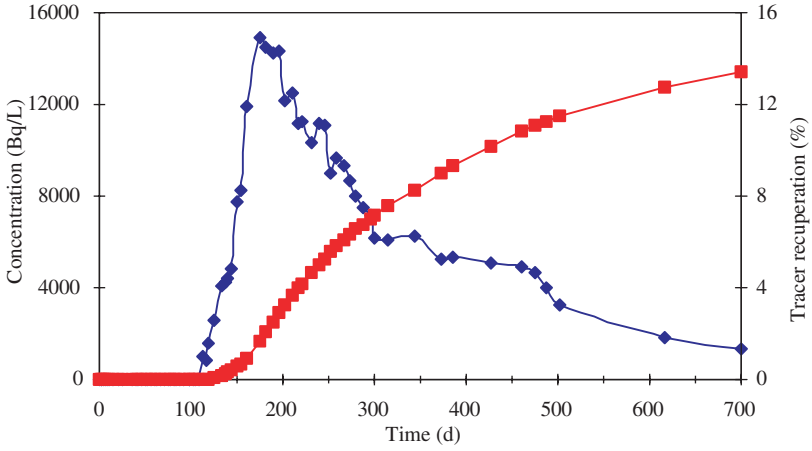

FIG. 138. Instantaneous (diamonds, left hand scale) and cumulative (squares, right hand scale) tracer response profiles in a production well.

The example illustrated in Fig. 138 shows real field data and both instantaneous and cumulative response curves to an HTO injection.

Concerning the cumulative response, the following expression gives the activity recovered up to an instant t_i:

$$A(t_i) = \int_0^{t_i} A(t)q(t)\mathrm{d}t, \tag{102}$$

where

$A(t_i)$ is the total tracer recovery (Bq) up to time t_i,
$q(t)$ is the production water flow rate (m^3/d) as a function of time,
$A(t)$ is the activity concentration (Bq/m^3) in the samples collected as a function of time, and
t_i is the elapsed time (days after injection).

Normalized concentrations (fractions of the total activity (in Bq) injected) are calculated from Eq. (112). For a chemical tracer the chemical concentration $C(t)$ in kg/m^3 replaces the activity concentration $A(t)$ in Eqs (102) or (112).

Information about the production flow rate is usually available from the oil company concerned.

Among the information obtained from the time response, the tracer breakthrough is the first to be obtained. It is the time in which the tracer concentration exceeds the detection limit.

The mean residence time ($\bar{t}$) is another important parameter. Its definition is identical to the one used in process studies, i.e. the ratio between the volume V_T involved in this process and the flow rate Q that feeds it:

$$\bar{t} = \frac{V_T}{Q}. \tag{103}$$

From the experimental data $\bar{t}$ is defined by:

$$\bar{t} = \frac{\int_0^\infty tA(t)\mathrm{d}t}{\int_0^\infty A(t)\mathrm{d}t}. \tag{104}$$

The final time is the time at which the response falls under the detection limit. However, in oilfield experiments it is very common to stop the sampling before this point. Thus, the final time is evaluated from the extrapolated response curve. For extrapolation purposes the exponential function gives the best fit of the tail of the experimental curve.

Knowing the distance between injection and production wells, it is easy to calculate the maximum, mean and minimum water velocities from the breakthrough, MRT and final time, respectively.

Tracer recovery in each well is determined from the extrapolation of the cumulative response for times approaching infinity on the basis of the exponential approximation for the concentration curve. The fraction of injected tracer recovered in each well in the pattern equals the fraction of the injected water that arrives at this well (F from Eq. (112)).

The total tracer recovered in all the wells belonging to a given pattern should be identical to the amount of tracer injected, in order to have a perfect mass balance. However, the tracer recovery is seldom higher than 80% and it can be as low as 30% for HTO, which is supposed to be an ideal tracer for water. There are three reasons for this: firstly, the tracer molecules continue moving towards second line wells and not all of them emerge for the wells immediately surrounding the injector; secondly, the injected water pushes the oil to production wells and replaces it in the rock pores (imbibition to immobile water); finally, a fraction of the tracer mainly in the tail of the response curve suffers a dilution that makes the concentration fall under the detection limit. Sampling second line wells is a good idea for improving the mass balance and obtaining additional information about the pattern under study.

(b) Volumetric response

When tracers are used to analyse industrial processes it is common to express the tracer concentration in the system output in terms of elapsed time, and then to calculate the mean residence time, variance and other parameters related to the time response.

Although the time response is generally used in interwell studies it has some problems that reduce its usefulness. In effect, alterations in the pattern such as variations in the injection rate, very common in any oilfield, result in a biased response curve. To avoid this inconvenience, a good alternative is to express the tracer concentration as a function of the cumulatively injected or produced water volume, which is rate independent. Nevertheless, time representation is often preferred because in many cases the volumetric data are not available.

Figure 139 shows time and volumetric responses for the same well. It is obvious that they are nearly identical, since the cumulative volume was calculated from the injection flow rate, which in this case was rather stable.

The volumetric response in a production well when an instantaneous tracer injection has been performed is a measure of the pore volume swept by the injected water. The tracer breakthrough is sometimes used as an indicator of the swept pore volume, but the mean of the distribution is a better locator because it represents the average volume swept by the injected water and takes into account the shortest as well as the longest paths followed by the tracer:

$$\overline{V_T} = \frac{\int_0^\infty VA(V)\mathrm{d}V}{\int_0^\infty A(V)\mathrm{d}V}. \tag{105}$$

For chemical tracers, activity concentrations $A(V)$ are exchanged with chemical concentrations $C(V)$.

The swept volume between an injection well A and a given production well B which is due to the fluid injected in A is equal to the average volume swept, taken from Eq. (105), multiplied by the fraction of the injected water that reaches this production well, calculated using Eq. (112).

6.1.6.2. Interpretation

Interpretation of the response curves is the final objective of an interwell study. A good analysis of the information given by the tracers allows the oil

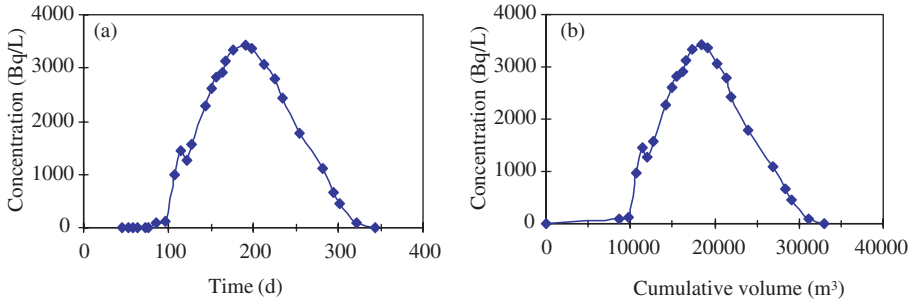

FIG. 139. Time (a) and volumetric (b) tracer response profiles.

engineers to better understand the behaviour of the reservoir by knowing some of its parameters and, from these data, to increase oil production.

Analysis of the response curves can be carried out on different complexity levels. In this report the interpretations made have been divided into three levels.

The simplest level is a qualitative one. By examining the curves, the following pattern characteristics can be derived: injection water arrival time (breakthrough); high permeability channels, barriers and fractures between two wells; communications between different layers; stratification in the same layer; preferential flow directions in the reservoir. This interpretation level is completed by means of some simple calculations from the numerical response, first of all the determination of the MRT. Furthermore, the cumulative response can be obtained by integration of the concentration versus time curve supposing the production flow rate is known. From this new curve, the fraction of injected water reaching each producer is easily calculated. A common spreadsheet is the best way to make all these calculations.

The second level involves the use of basic mathematical models to fit simple response curves by means of theoretical expressions and to decompose complex responses into several simpler functions. In this way partial residence times as well as other parameters can be determined for each function. Mathematical models also allow the evaluation of some important parameters such as permeability and make it possible to predict the behaviour of unknown patterns [80–82].

At the third level it is possible to make use of complex mathematical models such as numerical simulators in order to achieve a deeper analysis. Such tracer simulators may be coupled to full field reservoir simulators where the current reservoir model is used as an input (to geology, stratification, etc.). This

is especially useful when the well pattern is complex, the reservoir heavily faulted or the production strategy complex.

Reservoir simulators with a tracer option are powerful tools for determining the parameters of the systems under study, and for planning infill well drilling and future tracer examinations. Well known reservoir simulators such as ECLIPSE and VIP both have relatively simple tracer options which may be used for passive water tracers, while it is probably the simulators from the Computer Modelling Group (CMG) in Calgary, represented by STARS, which have the most advanced tracer simulator included [83]. This simulator can also be used for reversibly sorbing and phase partitioning tracers.

6.1.6.3. Simplified permeability evaluation

Permeability is a property of a porous material and a measure of its capacity for transmitting a fluid. Permeability is largely dependent on the size and shape of the pores in the substance and, in granular materials such as sedimentary rocks, on the size, shape and packing arrangement of the grains.

In general, permeability is evaluated in the laboratory by analysing samples taken from the oilfield, but the results obtained by this technique are subject to considerable uncertainty. Firstly, the core samples are small and limited to sectors around the wells. There is always a question about the representativeness of the sample for the reservoir. On the contrary, the use of interwell tracers allows average values of the permeability in the swept volume between wells to be derived.

On the basis of Darcy's law and making many simplifications, the following simple formula for permeability evaluation has been developed:

$$k = \frac{\phi S_w \mu}{\bar{t}\,\Delta P}\left(d^2 - r^2\right)\ln\left(\frac{d}{r}\right), \tag{106}$$

where

K is permeability,
ϕ is porosity,
S_w is water saturation,
μ is viscosity,
r is the radius of the production well,
d is the distance from injection well to production well,
ΔP is the differential pressure between wells, and
$\bar{t}$ is mean residence time.

Although this expression presupposes a number of simplifications, it constitutes an acceptable approach from the experimental point of view. Its main use is in the derivation of comparative values related to the permeabilities of different layers in the same pattern or of several stratifications in a unique layer.

6.1.7. Case studies

6.1.7.1. Case 1

Figure 140 shows a pattern belonging to a reservoir sited in southern Argentina with characteristics given in Table 20, where an interwell study by means of radiotracers was performed some years ago [85].

Since HTO was the selected tracer, the liquid scintillation technique was used for measurement. The detection limit was calculated using the parameters given in Table 21. Because of operative limitations in the measurement laboratory, samples were not distilled before counting and, in addition, a short counting time was used. For that reason the detection limit was much higher than usual.

From the detection limit the mean output concentration was fixed as ten times this value (295 Bq/L), which leads to an activity of 167 GBq (4.5 Ci). In fact, 10 Ci of HTO were injected into a K-22 pattern well using the bypass device shown in Fig. 141.

Figure 142 shows an example of tracer concentration and cumulative response curves for well K-329, whose output was followed for a full year and

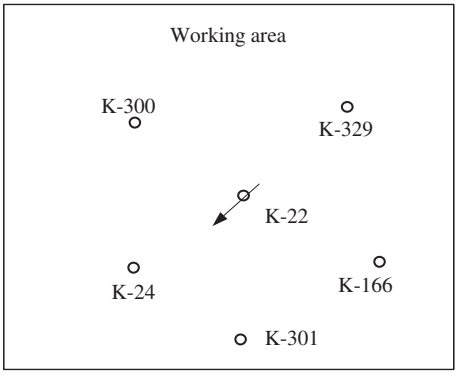

FIG. 140. Pattern for case study No. 1.

TABLE 20. RESERVOIR PARAMETER VALUES FOR K-22 PATTERN WELLS

Parameter	Value
Maximum injector–producer distance	284 m
Mean layer porosity	0.32
Water saturation	0.5
Mean layer thickness	14 m
Volume	567 590 m^3

belongs to the K-22 pattern. The information in Table 22 has been extracted from a quick analysis of the graphs in Fig. 142.

The distance between wells K-22 and K-329 is 251 m, and the minimum, medium and maximum water velocities were 0.78, 1.3 and 2.9 m/d, respectively.

Permeability was also evaluated using the simplified expression introduced above (Eq. (106)). A value of 282 mD (milliDarcy) was obtained, which looked reasonable to reservoir engineers.

Making use of specialized software designed in Argentina for the basic processing of the response curves arising from interwell studies, an approach by means of a radial dispersion model was made. An MRT of 210 d and a dispersivity factor of 0.04 were used. Figure 143 shows the result.

TABLE 21. DETECTION SET-UP PARAMETERS FOR HTO ANALYSIS OF SAMPLES FROM A K-22 PATTERN WELL

Parameter	Value
Background	20 counts/min
Efficiency	0.28 (counts/dis)
Counting time	10 min
Volume of sample	8 mL
Detection limit	29.5 Bq/L

FIG. 141. Tritium injection using the bypass technique.

Using this theoretical approach the basic parameters were calculated again. Table 23 provides a comparison between the two sets of data.

The volumetric response for well K-329 is shown in Fig. 144 in terms of the cumulative injected volume. In this case the information in Table 24 is extracted from a quick analysis of the graph.

The swept volume value in Table 24 is the pore volume swept from the injector to the production well (K-329) and equals the mean volume multiplied by the recuperation factor (0.092 or 9.2%).

From the same pattern, well K-301 is another good example because the sampling was interrupted before the output concentration reached the background level as can be appreciated from Fig. 145. The distribution tail was

TABLE 22. INFORMATION DERIVED FROM THE TRACER RESPONSE CURVE FOR WELL K-329

Parameter	Value
Breakthrough	86 d
Mean residence time	193 d
Final time	321 d
Tracer recovery	9.2%

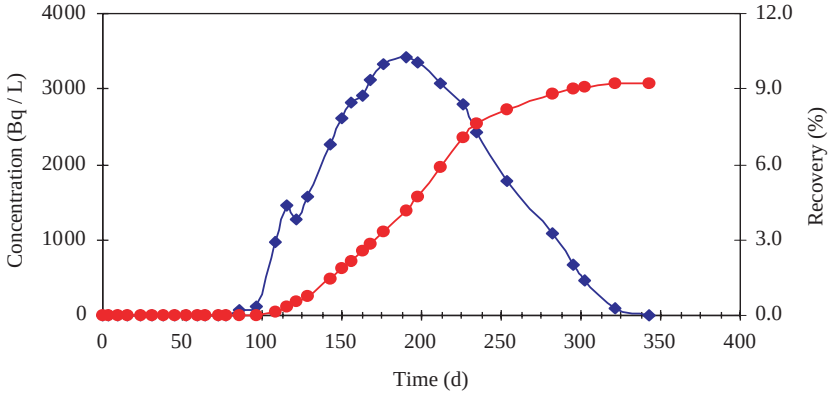

FIG. 142. Instantaneous (diamonds, left hand scale) and cumulative (circles, right hand scale) response curves for well K-329.

extrapolated on the basis of the points surrounded by the ellipse in Fig. 145, arriving at the result shown in Fig. 146.

The following exponential function was used for extrapolation purposes [82]:

$$A(t) = 932 \exp\left[-0.0083\,(t - 542)\right]. \tag{107}$$

From the complete curve (the experimental data plus the extrapolated tail) a better evaluation of the basic parameters is obtained. A comparison is presented in Table 25.

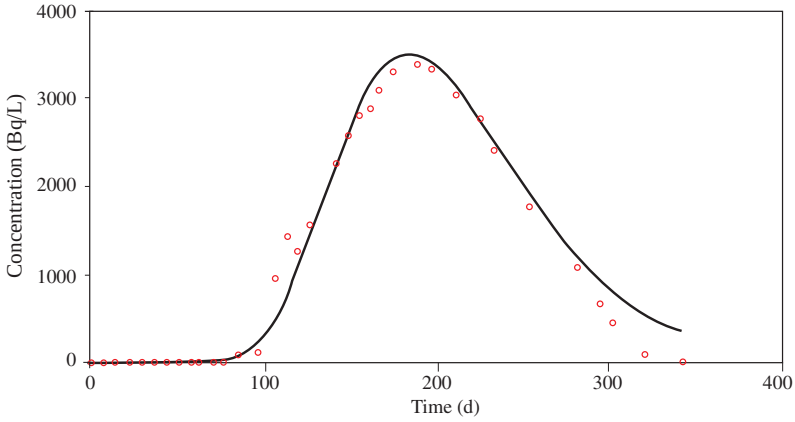

FIG. 143. Radial dispersion model approach for well K-329.

TABLE 23. COMPARISON BETWEEN EXPERIMENTAL AND THEORETICALLY DERIVED TRACER RESPONSE CURVE PARAMETERS FOR WELL K-329

Parameter	Experiment	Model
Breakthrough (d)	86	75
Mean residence time (d)	193	210
Final time (d)	312	410
Tracer recovery (%)	9.2	9.1

The tracer distribution for the wells belonging to the K-22 pattern is shown in Fig. 147. The total tracer recuperation was 62.8%.

6.1.7.2. Case 2

Figure 148 shows the pattern belonging to another reservoir also sited in southern Argentina. Figure 148 shows not only first line wells but also second line ones from which some samples were taken. In this case 555 GBq of tritium as tritiated water was injected into one of the layers using the bypass technique and selected injection.

What is really interesting about this pattern is the fast response into one of the wells (PC-1276), where tracer arrived the day following the injection.

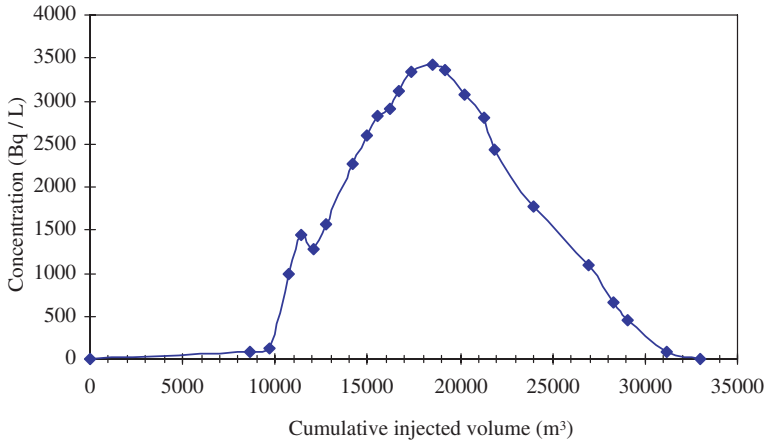

FIG. 144. Volumetric response curve for well K-329.

TABLE 24. RESERVOIR INFORMATION EXTRACTED FROM THE TRACER RESPONSE CURVE FOR WELL K-329

Parameter	Value
Breakthrough	86 d
Mean volume	19 073 m^3
Swept volume	1775 m^3

This implies very strong channelling. Hence, the water injection towards this well is useless. As a consequence of this tracer experience, the layer under study was closed in well PC-1276. Figure 149 shows the tracer response curve as a function of time for this well.

In first line wells only 30% of the injected tracer was recovered, mainly through well PC-1276 (17.2%). Less than 5% was measured in the other wells.

6.1.7.3. Case 3

Tritiated water was used as a tracer to evaluate the behaviour of water injected into an oilfield sited in the Santa Cruz province, Argentina. From 1993 to 1997 nineteen injections were performed in different patterns, and more than 5700 samples coming from 126 production wells were analysed up to the beginning of 1999. The oilfield under study, Piedra Clavada, is very heterogeneous with respect to its environmental characteristics, as well as to the variety of the oil produced.

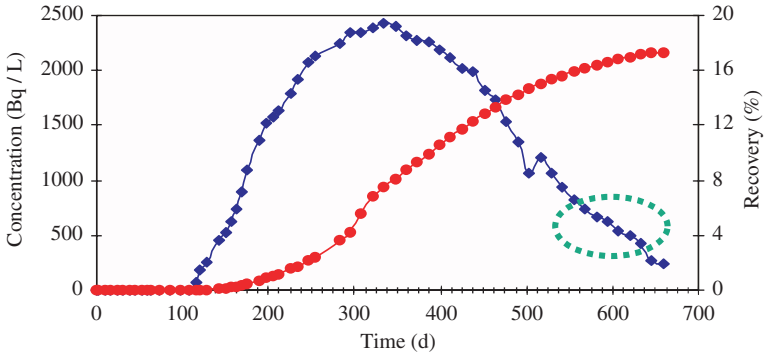

FIG. 145. Instantaneous and cumulative response curves (diamonds, tracer concentration; ovals, tracer recuperation) for well K-301.

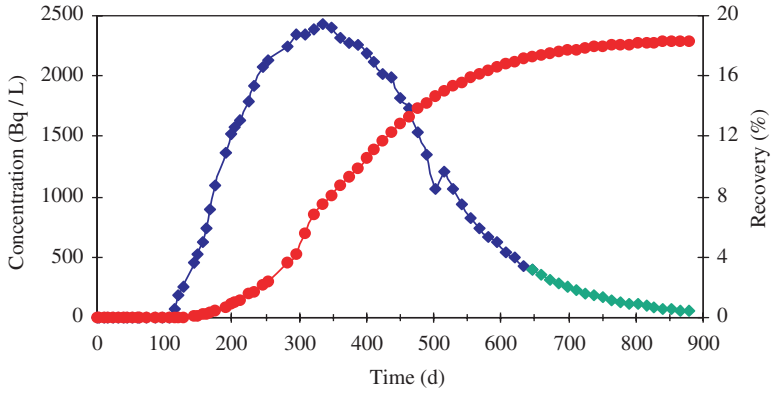

FIG. 146. Concentration curve (blue diamonds) with extrapolated tail (green diamonds) for well K-301.

The idea in this case study is not to introduce experimental techniques or calculation procedures, but to expose the results and conclusions obtained from a large scale investigation.

The following results were obtained from the radiotracer response curves [85]:

(a) *Canalization (anisotropy)*: Channelled flow is predominant in most of the patterns (86%) in one preferential direction.
(b) *Water recovery*: The amount of water recovered in each pattern is almost 55% on average with a maximum of 69% and a minimum of 10%.

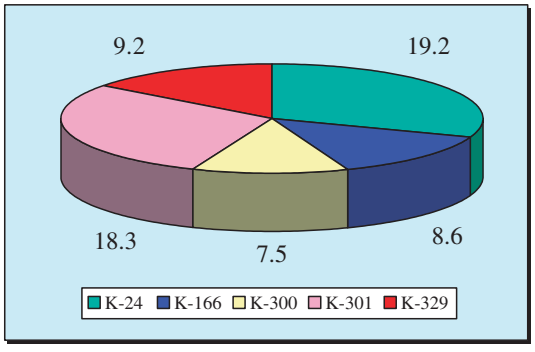

FIG. 147. Tracer distribution for the wells belonging to the K-22 pattern.

TABLE 25. COMPARISON OF DATA FOR WELL K-301

Parameter	Experimental data	Experimental data + extrapolated tail
Breakthrough (d)	115	115
Mean residence time (d)	363	380
Final time (d)	659	880
Tracer recovery (%)	17.3	18.3

(c) *Breakthrough*: The values of the arrival times were spread throughout a very large range, from one day to two years. In general the average was 90 days for channelled patterns and 157 days for other ways.

(d) *Fault characterization*: Four faults were characterized as not impermeable and another fault was confirmed as impermeable. This information was useful to improve the use of numerical simulators in this area.

(e) *Injection optimization*: After information was derived from radiotracer experiments, some changes in the injection regime were made in order to improve oil production. Several strongly canalized layers were closed, and in many cases the injection flow rate was modified. Furthermore, the results obtained helped reservoir engineers make predictions related to waiting times in tertiary recovery operations in which chemical products are injected or in thermal processes such as hot water injection.

(f) *Numerical simulation*: Response curves were used to calibrate numerical simulators. In this way more accurate calculations were carried out to evaluate porosity and permeability in some patterns.

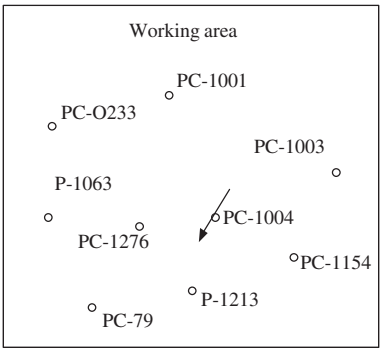

FIG. 148. Pattern for case study No. 2.

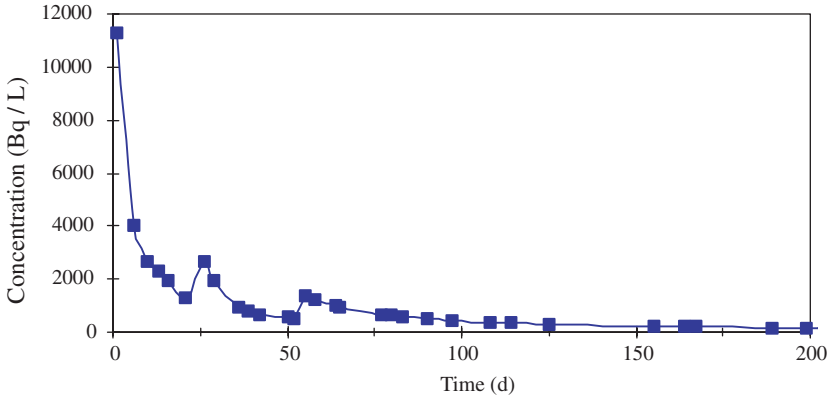

FIG. 149. Tracer dispersion curve with rapid breakthrough: example of strong canalization (well PC-1276).

The following conclusions drawn were:

(1) Interwell tracers made it possible to better understand the characteristics and properties of the Piedra Clavada oilfield.
(2) The predominant flow was confirmed to be canalized, especially in directions parallel to the main geological faults.
(3) Most of the faults in the oilfield are partially permeable but there are also some impermeable faults.
(4) About 80% of the injected water moves along a preferential direction.

Around 50% of the tracer was not recovered. This non-recovered volume is a measure of the efficiency with which the injected water sweeps the fluids and increases the system pressure.

6.2. RADIOACTIVE TRACER TECHNIQUES IN GEOTHERMAL RESERVOIRS

6.2.1. Introduction

In this part of the report, an overview is presented of the state of the art of the procedures in the application of radiotracers in geothermal reservoir management. Owing to the similarity of geothermal tracing to that for oilfields, most of the principles and procedures described in the previous sections are applicable to geothermal tracing, especially as far as the preparation of tracers

and laboratory measurements are concerned. This section will therefore focus on those issues and procedures specific to geothermal application such as field techniques and data interpretation, explained with the use of examples of actual geothermal reservoir tracer tests. A general background and a brief history of the use of radiotracers in geothermal reservoir management are also presented [85, 86].

6.2.1.1. Geothermal reservoir management

Geothermal energy is a renewable, environmentally friendly energy source based on the internal heat of the earth. It is associated with volcanic activity, hot crust at the depth of tectonically active areas or permeable sedimentary layers at great depth. Geothermal energy is now utilized in more than 50 countries, with electricity production in about 20 countries. The largest single geothermal electricity producer is the USA (2228 MW(e) installed capacity in 2000). The Philippines is the second largest producer (1909 MW(e)) and the country for which geothermal power represents the largest percentage of its energy supply (21.5%). Other countries with significant amounts (greater than 100 MW(e)) are Costa Rica, El Salvador, Iceland, Indonesia, Italy (the first country to exploit geothermal energy for electricity production), Japan, Mexico and New Zealand [87, 88]. Direct geothermal heat use is most significant in China, Japan, Iceland and the USA, with energy production of 10 500, 7500, 5600 and 5600 GW(th)·h annually, respectively, in the year 2000.

The energy production potential, or capacity, of geothermal systems is highly variable. It is primarily determined by the pressure decline caused by mass extraction, and also by the heat content. Pressure declines continuously with time in systems that are closed or have limited recharge. The production potential of geothermal systems is, therefore, often limited by a lack of water rather than a lack of heat. Geothermal resource management involves controlling energy extraction from geothermal systems underground so as to maximize the resulting benefits, without overexploiting the resource.

When geothermal systems are overexploited, production from the systems has to be reduced, often drastically, resulting in an insufficient steam supply to power plants or in loss of wells. Overexploitation mostly occurs for two reasons. Firstly, because of inadequate monitoring and data collection, the understanding of such systems is poor and reliable modelling is also not possible; therefore, the systems have unpredicatable responses to long term production. Secondly, overexploitation occurs when many users utilize the same resource/system without common management or control.

6.2.1.2. Applications of tracer tests in geothermal reservoir management

The main purpose of tracer testing in geothermal reservoir management is to predict possible cooling of production wells due to long term injection of colder fluid and/or due to invasion of natural groundwater.

In a geothermal field the primary resource is water, both as liquid and as steam. A direct measure of its behaviour is thus of obvious importance to field management. Water tracing is the only technique that gives a direct indication of underground flow patterns and velocities.

Information gained from tracer testing includes:

(a) Diagnostics of the properties of the reservoir, including evidence of direct connections between the tracer injection point (either within or outside the field) and the monitoring wells in the field;
(b) Measurement of the direction, speed and MRTs of water movement;
(c) Determination of the extent to which groundwater downflows intrude into production wells;
(d) Identification of breakthrough or injected water into a field and, when this is detected, quantification of the amount;
(e) Information needed for calibration or verification of the physical models applied to the geothermal reservoir.

All of this information will aid in the understanding of the nature of a geothermal system, but the measurements, which bear upon injection and groundwater intrusion or cooling potential, have the greatest impact on field management.

(a) Providing evidence of interwell connections

Injection of a tracer into one well and then monitoring of the tracer returns in several wells surrounding it will result in identification of preferential flow directions and of interconnections between individual wells. Mapping of the results on the well field scale will provide a picture of the flow paths, which is useful in planning the location of injection wells.

(b) Identification of injection returns

Injection is an essential part of any modern, sustainable, environmentally friendly geothermal application and an important part of the management of geothermal resources. It started out as a method of wastewater disposal for environmental reasons. In geothermal fields a large amount of wastewater

remains after extraction of steam for electricity production. This water is too cool for further steam extraction but typically contains high concentrations of chloride and silica as well as lower concentrations of many other elements. The common strategy for disposal of this wastewater is injection into formations that are not directly linked to the production field.

Recently, injection has also been used to counteract pressure drawdown, i.e. as artificial water recharge, and to extract more of the thermal energy in reservoir rocks [86]. Injection will increase the production potential considerably in most cases, as has been learned from both experience and theoretical studies.

After the tracer has been injected, the production wells in the field are monitored for the presence of the tracer. It is often true that a null result from a test, i.e. no detection of the tracer at all, is the best result since this is direct evidence for a lack of connection between the reinjection well and the production field. Where tracer is found in the production zone, the tracer results can be used to measure how much of the injected water returns to the field and aid in decision making concerning the use of the injection well. The results can also be used to predict the effects on the fluid chemistry, for example the chloride levels, for correlation with geochemical measurements.

(c) Detection of groundwater intrusion into the production field

Groundwater intrusion can occur when a well tapping a production zone passes through a permeable groundwater aquifer. The pressure exerted by production of high temperature fluid usually prevents intrusion of the groundwater, but breaks in production, such as for maintenance, can result in groundwater intrusion, which quenches the well. Not only is production from that well lost but cool water also enters the field with potential adverse effects. In the case of groundwater intrusion studies, tracer is injected into the well where the downflow occurs. Subsequent detection of tracer in production wells can help in decisions pertaining to remedial work by giving information on the impact of the intrusion upon production of the individual wells, primarily by measuring how much of the output of the well derives from the groundwater. At the same time such studies will provide evidence for direct links between different parts of the field and estimates of the time lag between groundwater intrusion and cooling of the field.

6.2.1.3. Radiotracers in geothermal reservoir management

As discussed in previous sections, radiotracers have many advantages over chemical tracers. In geothermal applications, the capacity for sustaining

high temperature and high detection sensitivity are, among others, the main factors that have made radiotracers the tool of preference and in some cases the only possibility for tracer testing in geothermal reservoir management.

The first example of geothermal field water tracing was reported by Einarsson et al. [86] with the use of tritiated water, HTO, as a tracer in 1971 at Ahuachapan in El Salvador. In this water dominated field a tracer return of 10% was observed in one well. Gulati et al. [87] reported another case in the use of HTO. At The Geysers in California, a vapour dominated field, a return of 18% of injected tracer was measured from the steam discharge in 1975. The anionic tracer $^{131}I^-$ was first used in New Zealand (1990) in single well experiments which showed that tracer flowed from wells in the then unexploited geothermal field at Ohaaki on a timeframe of hours and was thus suitable for well-to-well experiments. At Wairakei this tracer was used to help delineate the intrusion of cold water into the production field. Tracer methods then also began to be used to study water movement within fields. They gained a prominent role in investigations into the possibility of injection of wastewater, particularly after the introduction of the longer lived iodine isotope ^{125}I. These investigations yielded much of the information that was used in the design of the injection system eventually constructed at Ohaaki.

6.2.2. Methods and procedures

In the following, the basics of tracer testing will be reviewed, including tracer test design and execution, the basics of the theory of solute transport in hydrological systems, tracer test interpretation and cooling predictions. Finally, field examples are given.

6.2.2.1. Tracer test design

When designing a tracer test the following aspects must be considered carefully: (1) which tracer to select, (2) the amount of tracer to inject, and (3) the sampling plan to follow (sampling points and frequency). These aspects will now be discussed.

The tracer selected needs to meet the following criteria:

(a) It should not already be present in the reservoir (or, if present, it should have a constant concentration much lower than the expected tracer concentration).
(b) It should not react with or be absorbed by the reservoir rocks.
(c) It should be easy (fast/inexpensive) to analyse.

The radiotracers most commonly used in geothermal applications are ^{125}I, ^{131}I and HTO.

6.2.2.2. Tracer selection

The mass flows of water in a geothermal field are very high. Hundreds of tonnes per hour from a well are common. Thus the dilution of the added tracer is high, so that tracers that can be detected with high sensitivity instruments are necessary. In addition the temperatures encountered are very high (often in excess of 200ºC), so good thermal and chemical stabilities are necessary. Most geothermal tracing has thus been done with chemically simple tracers, namely water itself (HTO) and iodide ions ($^{131}I^-$ and $^{125}I^-$).

The background levels of radiotracers may be expected to be negligible; they are detectable at extremely low concentrations. The procedure for measuring the radioactive tracer concentrations in the samples collected is, on the other hand, more complicated and time consuming than the procedure for measuring the concentration of most other kinds of tracers.

When selecting a suitable radioactive tracer, their different half-lives must be taken into account. Figure 150 shows a comparison between the decay rates of ^{131}I and ^{125}I, which have half-lives of 8.5 and 60 days, respectively. The initial activity of the two tracers is based on the initial activity commonly used in tracer tests, 74×10^9 Bq for ^{131}I and 18.5×10^9 Bq for ^{125}I. The figure shows that after about a month the activity of ^{125}I is still of the order of 13×10^9 Bq, while the activity of ^{131}I is only of the order of 5.6×10^9 Bq. After two months the activity of ^{125}I will be about 9.3×10^9 Bq, while the activity of ^{131}I will only be about 5.6×10^9 Bq, rendering it almost undetectable when dilution factors are

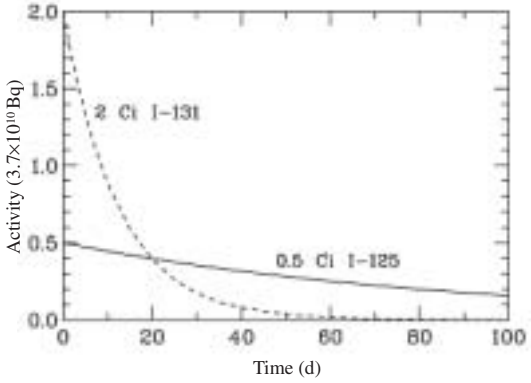

FIG. 150. Comparison of the decay of samples of ^{131}I and ^{125}I.

high. Therefore, ^{131}I is only suitable for tracer tests expected to last less than, or of the order of, a month or so. Iodine-125, which is considerably more expensive, will have to be selected for tests that will last for more than 1–2 months.

Care must be taken to choose a tracer appropriate for the task, particularly with regard to its behaviour in a two phase system. For example, iodide ions function as a liquid water tracer but do not enter the vapour phase. Tritiated water functions as either a liquid or a vapour phase tracer and in a two phase system will distribute itself between the liquid water and steam according to the relative amounts of the two phases on the local scale. A noble gas such as xenon (or an inert chemical tracer such as SF_6), on the other hand, is sufficiently soluble to dissolve in water but, in a two phase region, will be concentrated in the gas phase.

Tritiated water is an obvious tracer choice and has been used in a limited number of cases. However, in New Zealand, for example, its application as an environmental tracer has precluded its use. If it is used to study short or medium term effects, then, because of its long half-life (12.3 a), care should be taken that backgrounds have not been affected by previous injections.

Iodide ions have been used extensively in New Zealand. Initially work was carried out with $^{131}I^-$, which was readily available and economic, could be transported by air in significant quantities (important when no local production facilities are available) and could be readily detected in the field by means of its gamma radiation, using equipment developed for general tracing work. Amounts up to 185 GBq (transportable by air in a type A package) were routinely used. At a later stage, when the need arose for a longer lived tracer, the use of $^{125}I^-$ was introduced. This required the development of a laboratory extraction method, as ^{125}I cannot be readily detected in the field. The resulting technique was based on liquid scintillation counting of iodide extracted from 2 L water samples. Amounts up to 18.5 GBq were used.

Geothermal water (in the fields in New Zealand at least) is moderately saline (about 2000 ppm), slightly alkaline, and reducing (e.g. it contains H_2S). This will prevent oxidation of iodide ions to volatile iodine. It is free of organic debris which may absorb iodide ions. It contains typically about 0.1 ppm of iodide ions to act as a carrier (and fields in many other countries have higher concentrations). Under such conditions, unlike in some cases of groundwater tracing, iodide can be expected to perform well as a water tracer.

Other potential tracers have serious drawbacks. Reference to Table 18 indicates that most tracers are unstable at high temperature, while ^{82}Br has a short half-life (36 h) and emits radiation of significantly higher energy than ^{131}I, limiting the amount that can be transported. More than 20 different liquid water tracers, including HTO and cobalt complexes, have been studied under laboratory conditions by Vetter and Zinnow [89]. A group of nine of these did

not require the presence of a carrier to elute completely in these tests. Of a small group selected for full testing, iodide had the best elution characteristics, followed by tritium and then hexacyanocobaltate ions. No adsorption of iodide was found under the conditions considered to be most favourable for adsorption. Furthermore, the adsorption tests in Ref. [89] were carried out at comparatively low temperatures and the adsorption processes have a negative temperature coefficient. Thus independent confirmation of the suitability of iodide as a tracer exists.

Gas tracing has been carried out with ^{3}H and with ^{133}Xe. An obvious choice for longer term studies is ^{85}Kr and various other species as shown in Table 19 (provided they withstand the high temperatures of geothermal fields). A major drawback with the noble gas tracers is the requirement to separate them from high concentrations of the noble gas ^{222}Rn, which occurs in geothermal fields. This adds considerably to the difficulty of using these tracers, especially considering the availability of chemical tracers such as SF_6.

If samples can be stored and conserved for 40 days before analysis, separation may not, however, be required, because more than 99.9% of the ^{222}Rn has died away.

After a suitable tracer has been selected the mass of tracer to inject needs to be determined. This is always difficult to determine beforehand, and depends on several factors:

(a) Detection limit,
(b) Tracer background (if any),
(c) Injection rate q,
(d) Production rate Q and the number of wells involved,
(e) Distances involved,
(f) Return rate anticipated (slow/fast).

The required mass may be estimated very roughly through mass balance calculations, wherein injection and production rates are taken into account as well as an expected recovery time span. This time span depends on the distances involved, and on how directly the wells involved are connected. In this respect the activity of radioactive tracers is proportional to their mass. In general, tracer tests should be designed such that tracer concentrations reach at least 5–10 times the detection limit. The mass to inject may also be estimated through theoretical calculations, for example using the software TRCURV included in the ICEBOX software package. It is based on a flow channel model, which will be discussed later. In most of the geothermal fields, the radioactive tracers ^{125}I and ^{131}I are normally injected with an initial activity of 0.5 and 2 Ci, respectively.

6.2.2.3. Tracer test execution

Tracer test execution can involve from one well pair to several injection and production wells. In the latter case several tracers must be used, however. The geothermal reservoir involved should preferably be in a semi-stable pressure state prior to testing. This is to prevent major transients in the flow pattern of the reservoir, which would make the data analysis more difficult. In most cases a fixed mass M of tracer is injected instantaneously, i.e. in as short a time as possible, into the injection well(s) in question. Sometimes a fixed concentration is injected for a given period. Samples for tracer analysis are most often collected from flowing/discharging wells, while downhole samples may need to be collected from wells which are not discharging.

6.2.2.4. Injection methods

Tracer injections have been performed by a variety of methods. Some of them, like those described in the previous section, also qualify for the description 'home-made'.

(a) Surface injection

The tracer, in the vial in which it has been transported from the supplier, is placed in a device which can be used to crush it while a flow of water is passed directly into the well. This is usually done by placing it in a ball valve modified with a bar across its exit end to hold the vial in place. This procedure minimizes the external radiation hazard as the ball valve can be well shielded with lead. The periods when the tracer is unshielded (during transfer into the ball valve and when being flushed away from the valve after crushing) can be kept short.

A disadvantage of this procedure is that, if the injection is into a closed down well, there is no control over where the tracer enters the underground formations other than the well casing construction. In the case of reinjection experiments, where this technique is most commonly used, this is not a problem as the aim is to trace the fate of the reinjected water and this will be achieved as long as the tracer mixes in the well. If a reinjection experiment is in progress (i.e. water is being pumped down the well) it is convenient to break the tracer vial in a bypass from the main flow and then briefly divert the main flow through the bypass. Such a system is shown in Fig. 151. In other situations a supply of water and a pump must be provided in order to inject from the surface. Sufficient water should be provided to flush the well several times above the expected entry point into the aquifer. Gas tracers have been injected by an equivalent technique using a supply of nitrogen from a bank of cylinders.

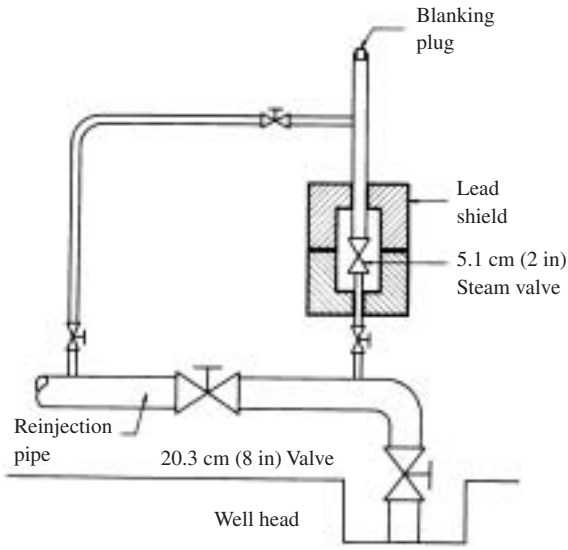

FIG. 151. Radioactive tracer injection system.

In some cases negative pressure exists at the well head. This occurs in reinjection systems when the hydrostatic pressure exerted by the water column flowing down the well is greater than the pressure at depth. This can simplify the injection process if a breaker is used, since it is not necessary to insert the tracer into a system running at high pressures and temperatures. A relatively simple device consisting of a steel tube up to several metres long can be suspended from the top of the well, the vial dropped to the bottom of the tube and then broken by the resulting blow on a steel rod inserted in the tube. Alternatively, negative pressure can be used to suck tracer from its transport vial directly into the flow.

(b) Downhole injection

A Kleyn water sampler [90] was modified to be used to break a vial of tracer and disperse the tracer in the surrounding fluid rather than use it to collect a sample. The bottom half of the tool was replaced with a much smaller unit, which allowed the base of a 10 mL glass vial to be penetrated by the plunger, which was normally used to break the neck of a much larger container. A disadvantage of this method is that the vials used to transport tracers such as iodide ions are too strong to be broken and the tracer must be transferred into a specially made vial. This procedure can potentially involve high radiation

doses to the person performing the transfer and carries a risk of spillage of the highly concentrated tracer. An advantage is that the technique allows injection of tracer at a specified depth in the injection well.

An alternative downhole method is to insert a capillary tube from a breaking device into the well to the required depth and then to pump water through the breaker with a suitable pump. Again this allows tracer to be injected from the surface to a specific depth. Such systems are not simple to set up, however, and have been used only when already available in the well for sampling purposes.

Gas tracer injections have been performed at depth using both these techniques. For example, ^{133}Xe tracer has been injected at depth by breaking its transport vial in a modified Kleyn sampler. The particular vial used is more fragile than that used for iodide tracers and it was possible to avoid the step of transferring tracer to another container, simplifying the procedure.

6.2.2.5. Sampling

Iodide ion tracers, i.e. $^{125}I^-$ or $^{131}I^-$, are soluble in liquid water. Thus, sampling is done from liquid water, whether at atmospheric pressure as from a weir box or at higher pressure from a pipeline to a flash plant. Atmospheric pressure sampling is a simple process carried out with a ladle or bucket. Higher pressure sampling is done with additional equipment such as a portable Weber separator. It should be borne in mind that, due to loss of water as steam, the sampling process will modify the tracer concentration from that in the well head and allowance must be made for this, as appropriate.

If non-producing wells are to be sampled, devices such as the Kleyn sampler may be used to collect samples from depth. Alternatively, wells may be temporarily discharged or bled slowly for the duration of the test, as appropriate.

Gas tracers are collected from the steam phase using the standard method for sampling non-condensable gases. In this technique steam is condensed into a cooled evacuated flask containing NaOH solution. Since most of the material in a gas sample is steam, this condensation reduces the volume by a large amount. The predominant non-steam gas components CO_2 and H_2S are absorbed in the NaOH solution (together with H_2S), leaving only non-condensable gases in the vapour phase. The collection flask is weighed before and after to measure the amount of steam collected.

HTO tracer can be collected by any of these methods but thought must be given to sampling methods when two phases are present.

The sampling frequency is case specific. It should in general be quite high initially (a few samples per day), but may be reduced as a test progresses (a few

samples per week). A sampling programme comparable to the one suggested below may quite often be applicable:

Week 1:	two samples per well per day,
Week 2:	one sample per well per day,
Weeks 3–8:	three samples per well per week,
Following weeks:	one sample per well per week.

This programme is aimed at detecting any rapid tracer returns during the first few days after injection of the tracer. After the first week a sharp tracer return is not expected because of greater dispersion. Therefore, the sampling frequency may be reduced. Figure 152 shows this schematically. It may also be mentioned here that as a general rule it is better to collect too many samples than too few. This is because the outcome of a tracer test is never known beforehand. Not all samples need to be analysed, in fact. The sampling frequency is also often affected by technical restrictions such as available workforce, the number of wells being sampled and measurement techniques. However, again a general tendency towards lower sampling frequency, as time progresses, should apply.

Methods of analysing and interpreting tracer test data are discussed in the following, but some aspects may be observed directly. These include:

(a) Tracer breakthrough time (or rather the time of first detection), which depends on the maximum fluid velocity;
(b) Time of concentration maximum, which reflects the average fluid velocity;

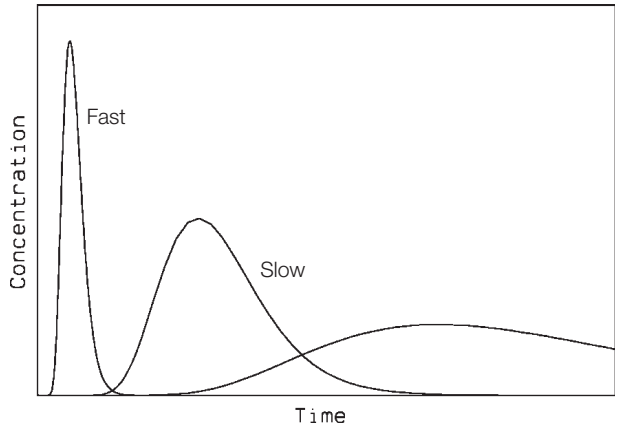

FIG. 152. Typical fast and slow tracer return profiles.

(c) Width of the tracer pulse, which reflects the flow path dispersion;
(d) Tracer recovery (mass or percentage) as a function of time.

6.2.2.6. Tracer detection in the field

For detection of tracer in the field (i.e. ^{131}I) a system has been designed to maximize detection efficiency. This is shown in Fig. 153. It consists of a 200 L drum in which a waterproof sodium iodide scintillation detector was suspended and through which water from the well being sampled was passed continuously. The 200 L drum was surrounded by a 5000 L tank fed by a continuous flow from a local cold water supply. The outer tank served to both cool the input from the well and reduce the background count rates. At most wells the water to be measured is available at 100°C and atmospheric pressure from a well head separator. This was piped through a pre-cooler fed by the overflow from the main cooling tank. If only higher pressure water was available, it was first passed through a mini-separator to reduce the pressure to atmospheric. The sample water was then piped in a copper coil through the cooling tank and into the central drum containing the detector. This system reduced the water temperature to below 40°C, thus enabling the detectors to be operated safely. The tanks were usually covered with a waterproof sheet after it was discovered that naturally occurring radioisotopes (radon decay products) were flushed into the system during rainfall, especially after a long dry spell.

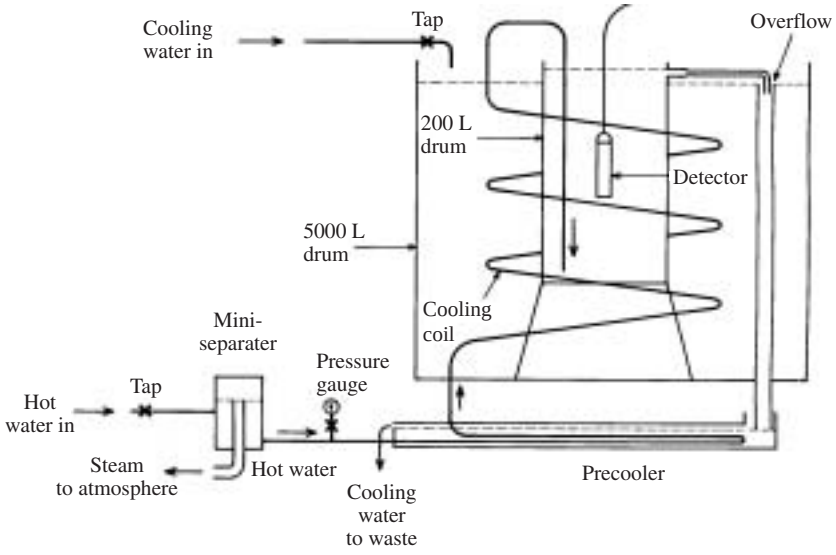

FIG. 153. Radioactive tracer sampling system.

This system gave a detector response of about 0.5 Bq in a concentration of 1 Bq·L^{-1} with a background of about 5 Bq. Typically counts occurring over periods of more than two hours were accumulated, and theoretically this could result in a limit of detection of 0.1 Bq·L^{-1} at 95% confidence level. In practice such a limit was not attained because of environmental effects, primarily the radon washout mentioned above and temperature variations. As detailed by Barry [91], careful work was carried out to reduce the background variation and this resulted in a limit of detection which is difficult to define exactly but which would be better than 0.5 Bq·L^{-1}. The continuous detection of tracer response was a significant factor in reducing the limit of detection as isolated excursions could be readily identified. Counting samples in the laboratory could achieve a lower limit (see discussion and Fig. 137 in Section 6.1.5.2 (b)) but without the advantage of multiple systems and continuous detection.

The detectors used consisted of rugged waterproof NaI(Tl) scintillation counters developed for field and industrial uses. These were powered by portable battery operated ratemeters which converted input pulses from the detector above a preset threshold to a logic pulse output.

Ratemeter power was supplied from a remote point up to two kilometres away via a light two core cable which, with the appropriate line drivers, was able to carry the digital signals back to the remote point for recording by either or both of analog chart recorders and digital data loggers. The same remote point was used to run detectors at up to twelve well heads simultaneously. This use of central sites has made supply of mains power relatively easy. Continuously charged batteries could be used to provide a buffer against data loss due to power failure. If mains power was not available the system could be run by battery power alone.

6.2.2.7. Tracer detection in the laboratory

(a) Iodide tracers

An initial version of the scheme involved oxidation of iodide to iodine followed by extraction into toluene before reduction back to iodide and subsequent counting. The current version of the iodide extraction technique is based on formation of a silver iodide precipitate followed by liquid scintillation counting (see Section 6.1.5.2 (1)) [92]. This version is as follows:

(1) The samples (nominal volume: 2 L) are delivered in plastic bottles and are weighed to determine their exact volumes. A known amount of inactive iodide (usually 5 mg) is added to act as carrier as well as to ensure that the final precipitate is of sufficient mass (about 10 mg) to be reliably

filtered and weighed. The samples are then filtered if inspection reveals any debris or cloudiness, and NaOH is added to make the samples slightly alkaline (pH about 9).

(2) The iodide is then oxidized to iodate with $KMnO_4$ and allowed to stand for about 20 min. At the same time any sulphide present (which would form Ag_2S precipitate in competition with AgI) is oxidized to sulphate. A longer time might be used if organic matter is present (say, if surface features are sampled) or if there is a high sulphide concentration.

(3) The iodate (including the carrier) is then reduced back to iodide by adding an acid mixture (HNO_3 and HF) followed by Na_2SO_3 solution. The HF is included to inhibit formation of silica, which would clog filters and add spurious weight to the final precipitate. Sulphate is unaffected by this step, thus effectively removing sulphide interference. After standing, the solution is filtered to remove any traces of silica which might have formed.

(4) An excess of $AgNO_3$ solution is added soon after the filtration to form a precipitate of AgI. Because AgI is much less soluble than AgCl, it is precipitated preferentially despite the approximately thousand-fold excess of chloride ions. However, small amounts of AgCl (and AgBr) are formed. After standing in the dark the precipitate is filtered through cellulose acetate paper under vacuum (the filter papers are pre-dried and left to equilibrate at room temperature before weighing to a precision of ±0.1 mg). The AgCl and AgBr are then removed by washing with ammonia. The precipitate, now pure AgI, is then passed quickly through a further oxidation–reduction cycle for purification purposes before being dried and weighed.

(5) The precipitate is then dissolved in the liquid scintillation cocktail. This is done by inserting the rolled filter paper into the cocktail vial, adding about 20 mg of acidified thiourea to complex the AgI, and then immersing the vial in an ultrasonic bath to disperse the AgI into the cocktail. The paper is translucent and should be left in the vial. Small vials (around 5 mL) are preferable as the background is reduced without sacrificing counting efficiency. The precipitates are dried and weighed. A suitable cocktail must be found by experimentation as commercially available cocktails are made with other purposes in mind.

(6) The analytical yield is calculated by dividing the mass of iodide in the AgI precipitate by the amount of iodide added plus that known from prior analysis to be in the sample, typically 0.1–0.2 $mg \cdot L^{-1}$.

The method has been applied to both iodine isotopes despite being developed for use with ^{125}I. In fact, it works somewhat better for ^{131}I since this isotope may

be counted more efficiently than ^{125}I (close to 100% efficiency compared with 75%).

(b) Tritium

Analysis is a simple matter of boiling thoroughly to drive off any dissolved gases (in particular H_2S), followed by distillation to collect clean water and then counting by liquid scintillation. The sample size is only about 10 mL, as this is all that can be mixed with the cocktail using any of the many cocktails available for tritium (HTO) counting. Higher sensitivity may be achieved, when required, at significant expense by enriching the tritium by a factor of approximately 80 by the method used for environmental tritium analysis [20].

(c) Gas tracers

Tritium as tritiated water is treated as described above. Xenon tracer is mixed in geothermal fluid samples with both other non-condensable gases and radioactive radon, which occurs in large excess. Separation of xenon from the non-condensable gases is achieved by trapping it on charcoal at dry ice/alcohol temperature. The xenon and radon are then separated on a size basis by passing them twice through a molecular sieve column at room temperature, followed by trapping on silica at liquid nitrogen temperature [91]. The silica is then quickly transferred to a vial containing a liquid scintillation cocktail for subsequent counting.

6.2.2.8. Relative sensitivities

Counting of the iodine isotopes and tritium can be compared using Outteridge's [93] counting figure of merit $R_G^{1/2} - R_B^{1/2}$, where R_G and R_B are the gross and background count rates, respectively, for each method. This criterion essentially compares the statistical accuracy obtained with the same counting time. These values are given in Table 26 for an activity concentration of 0.1 $Bq \cdot L^{-1}$. At this concentration (which is actually below the limit of detection for the ^{131}I field method) the net count rates for the two iodine isotopes in the extraction method are about half the background rate.

As can be seen, the extraction figures of merit for the iodine isotopes are higher than that for the field method. This is mainly due to the much lower background. The comparative advantage increases for lower tracer concentrations. It should be remembered, however, that the field method uses continuous sampling in which counting times are in total much greater than

TABLE 26. FIGURES OF MERIT FOR TRACER ANALYSES
(calculated using counts/min)

	^{131}I	^{125}I	^{3}H
Field method	0.086	—	—
Extraction method	1.07	1.00	0.003

those for the extraction methods and for which up to twelve wells can be monitored simultaneously. This tends to offset some of the advantage of the extraction method especially at higher tracer concentrations. On the other hand, the field method is subject to additional variations such as temperature effects and washout of radon daughter products by rain. As noted previously, experience has suggested that such effects tend to be greater than the purely statistical effects allowed for in the calculation of the figures of merit. Additionally, in practice the sampling technique is much less expensive in human resources than the field measurements and it is easier to make measurements on a larger number of wells. Considerations such as these, together with the greater sensitivity, eventually resulted in replacement of the ^{131}I field measurements by the extraction method.

It should also be noted that the sensitivity of the tritium detectors is much less than that of the iodine isotope detectors, primarily because of the small sample size (10 mL as against 2 L). This can be partially offset by the greater quantities of tritium which are available relatively cheaply and by the fact that tritium decays much more slowly.

6.2.2.9. Counting conditions

The spectra of ^{125}I and ^{131}I in the liquid scintillation counting cocktail currently in use in New Zealand are shown in Figs 154 and 155, together with the background spectrum. The main counting windows were chosen to enclose virtually the entire isotope spectrum in both cases; these are shown in the figures. An error analysis, also using the figure of merit $R_G^{1/2} - R_B^{1/2}$, indicated that narrower intervals were statistically preferable at low count rates, basically because they included a lower proportion of the background spectrum. These are labelled as the optimum window in the figures. As can be seen, this required siting of one or the other of the window extremes in a high count rate region of the spectrum. Because it was felt that this could make the measured count rate overly susceptible to gain shifts, the optimum window was not made the main counting window.

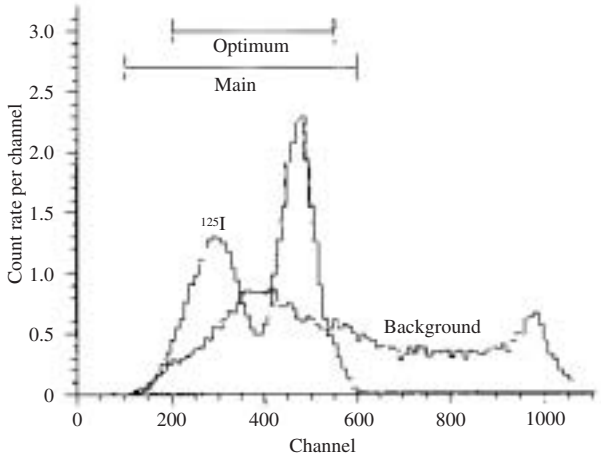

FIG. 154. Liquid scintillation spectrum of ^{125}I.

6.2.2.10. Calculation of concentrations and errors

Calculation of tracer concentrations is straightforward for the field method once calibrated by counting a standard solution in a large tank. In the case of the extraction method for iodide tracers it is complicated by quenching

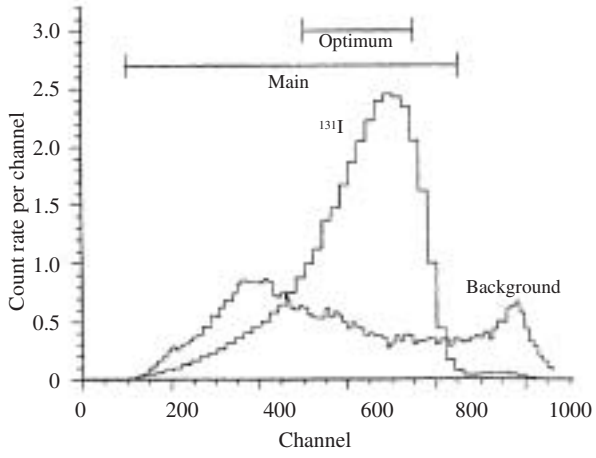

FIG. 155. Liquid scintillation spectrum of ^{131}I.

in the liquid scintillation counting and by the possibility of repeat counting. The AgI precipitates naturally vary slightly in colour and mass, causing quench variations (see discussion in Section 6.1.5.2 (a)). The raw count rate recorded by the LSC must be corrected for this phenomenon and for decay of the tracer. In the case of decay, different factors must be applied for repeat counts, which are often made when counter time is available. To avoid possible deterioration of the cocktails it is wise to limit such repeat counts to no later than ten days after preparation of the sample. For tritium, greater sample uniformity is possible and repeat counts do not need application of different decay factors.

The necessary procedures may be illustrated by reference to those that have been developed for counting with a Beckman LS2800 LSC. This instrument measures quench by a quantity known as the *H* number. Like most counters, the LS2800 has a built-in system of quench correction, which is used for counting the tracers, but even application of this leaves some residual variation of background and efficiencies with *H* number. These are shown in Figs 156 and 157. Equivalent data should be generated as appropriate for the type of counter. Tracer concentrations are derived from the count rate measurements as follows.

Let R_{GH} be the gross count rate (in counts/min) measured in a count of duration t_c minutes at a measured quench of *H* starting at a time t_d after a reference time (conveniently, either the injection time or the time at which the tracer quantity is defined by the manufacturer). The activity (or disintegration rate in dis/min) D_t in a sample is then given by $D_t = (R_{GH} - R_{BH})/\varepsilon_H$, where ε_H and R_{BH} are the efficiency and background at quench level *H*. The activity D_0

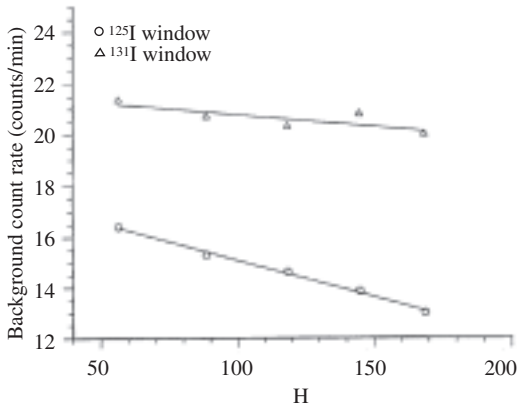

FIG. 156. Variations of background for ^{125}I and ^{131}I with a Beckman LS2800 LSC.

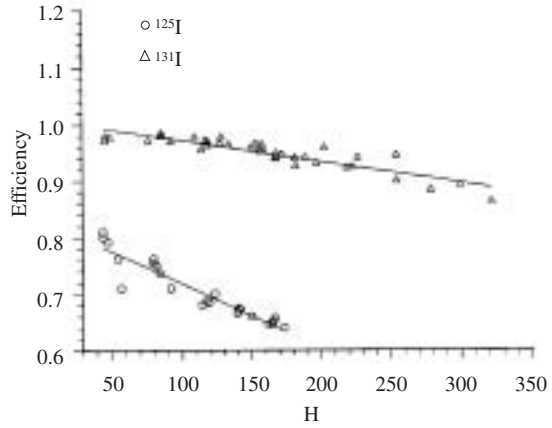

FIG. 157. Variations of efficiency for ^{125}I and ^{131}I with a Beckman LS2800 LSC.

(in dis/min) at the reference time is then given by $D_0 = D_t f$, where f, the decay factor, is given by $f = \exp(\ln 2t_d/t_{1/2})$, $t_{1/2}$ being the radionuclide half-life.

The activity concentration A_0 in the sample (in dis/(min·mL)) corrected back to time $t_d = 0$ is then given by $A_0 = D_0/(YV)$, where Y is the chemical yield (fraction in the range 0–1) of the extraction process and V is the sample volume (in millilitres). For purposes of comparison between different tests and tracers it is best to use the normalized activity concentration $A_N = A_0/A_{I0}$ $(=A_t/A_{It})$, where A_{I0} is the activity injected at $t_d = 0$. A_N has the dimension $(\text{volume})^{-1}$.

As noted above, counts are often repeated. The calculated normalized concentrations for one sample are then averaged with weighting directly proportional to the counting times and inversely to the decay factors, i.e.

$$A_{N0} = \frac{1}{YVA_0} \sum_{i=1}^{n} [(R_{GH_i} - R_{BH_i})/\varepsilon_{H_i}]t_{c_i} \Big/ \sum_{i=1}^{n} (t_{c_i}/f_i) \tag{108}$$

if the number of counts is n.

The standard deviation is used for estimating errors. According to the standard propagation of error theory [94], the standard deviation σ_y of a quantity y is given by

$$\sigma_y^2 = \sum_{i=1}^{n} \left(\frac{\partial y}{\partial x_i} \right)^2 \sigma_{x_i}^2, \tag{109}$$

where y is a function of the n independent variables x_i.

Application of this equation is straightforward but tedious. Using standard statistical expressions for the radioactivity counting errors the result is:

$$\sigma^2_{A_{N0}} = \left[\left(\frac{\sigma_Y}{Y}\right)^2 + \left(\frac{\sigma_{A_0}}{A_0}\right)^2\right] A^2_{N0} + \frac{\sum_{i=1}^{n} \frac{t_i^2}{\varepsilon^2_{H_i}} \left[\frac{R_{GH_i}}{t_{c_i}} + \sigma^2_{R_{BH_i}} + \left(\frac{R_{GH_i} - R_{BH_i}}{\varepsilon_{H_i}}\right)^2 \sigma^2_{\varepsilon_{H_i}}\right]}{\left(YVA_0 \sum_{i=1}^{n} \frac{t_{c_i}}{f_i}\right)^2}. \tag{110}$$

This quantity can be referred to as the total error. However, it should be noted that one of the identified contributors to it is systematic, namely the error in A_0, since only one value is used for each test. Furthermore, the errors in R_{BH} and ε_H are effectively systematic, since it transpires that there is only a second order variation in these quantities due to errors in the determination of H. Therefore the errors in these three quantities do not add to the scatter of results within an individual test. Thus we may also refer to the random error, i.e. that due to errors in the chemical yield Y and to the counting statistics. The expression for this quantity is the following, a simplified version of the expression for the total error:

$$\sigma^2_{A_{N0}} = \left(\frac{\sigma_Y}{Y}\right) A^2_{N0} + \frac{\sum_{i=1}^{n} \frac{f_i^2 t_{c_i} R_{GH_i}}{\varepsilon^2_{H_i}}}{\left(YVA_0 \sum_{i=1}^{n} t_{c_i}\right)^2}. \tag{111}$$

A question that arises frequently is whether or not a tracer response has been observed, i.e. a particular measurement is above background. In answering this question it is only necessary to compute the net count rate $R_{NH} = R_{GH} - R_{BH}$. This net count rate can then be regarded as being above background at the 95% confidence level if $R_{NH} > 2R_{BH}$. It should be emphasized that in practice in a geothermal tracing test a sequence of consistently positive values from a succession of samples is needed to confirm the presence of a tracer response, particularly when the response is small and difficult to distinguish from the background.

All these calculations are implemented in spreadsheet form for ease of calculation. Calculations based on typical data show that for both random and total errors the influence of the counting statistics only becomes dominant at net count rates less than background.

6.2.2.11. Data analysis

Of particular interest are tracer recovery in a well (particularly in reinjection studies, where it is used to calculate the extent of contamination of the well fluid by reinjected water) and predictions of contamination.

The expression for the total fractional tracer recovery in a well is:

$$F(t_\infty) = \int_0^\infty A_{N0}(t) q(t) \mathrm{d}t, \tag{112}$$

where $q(t)$ is the instantaneous value of the volumetric flow of liquid water in the sampling well and A_{N0} is the normalized activity concentration as defined above.

Multiplying the reinjection flow rate by $F(t_\infty)$ gives the flow of water in the sampling well derived from the reinjection. This in turn enables calculation of the concentrations of components of the reinjection fluid (e.g. chloride) due to the reinjection. In the case of groundwater intrusions the fraction of the intrusion which enters a particular well can be measured, but there must be an estimate of the intrusion flow rate available to calculate how much of the water produced from the sampling well is groundwater.

In practice, integration is carried out numerically from the available figures for both normalized activity concentration and well discharge. Details of the calculation should be given in individual cases, particularly when, as is often the case, extrapolation is used to predict the final part of the curve. It should be noted that integration is carried out over the entire extent of the pulse. This calculation gives the recovery applying to the conditions in the field at the time of measurement, conditions which ideally would be steady state.

Concentrations are measured from time to time in non-producing wells, either by downhole sampling or by slow bleeding of the well. The concept of tracer recovery has no relevance in this case. However, it is possible to use results from an instantaneous tracer injection to calculate the effect in the responding well of a continuous reinjection of water, for example to predict concentrations of contaminants from the reinjection (including the reinjected water itself). It is assumed that the water reinjection has been proceeding for a time at least equivalent to the duration of the instantaneous injection response.

Let the volumetric reinjection flow rate be Q_0 and the concentration of a component of the reinjection water p_0. Provided the component behaves ideally with respect to the water flow (like a passive water tracer), the concentration p of the component in the responding well is given by:

$$p = p_0 Q_0 \int_0^\infty A_{N0} \mathrm{d}t. \tag{113}$$

Again, details of the integration should be given for individual cases.

6.2.3. Safety issues

Handling of any radioactive tracer in injection quantities presents potential radiological hazards, so that all tracer handling procedures must be approved by the competent authority in the country concerned.

The maximum risk occurs at the injection site where external exposure is at its maximum. This is particularly acute for ^{131}I, which emits medium energy gamma radiation. The effects of this are limited by tracer injection techniques which emphasize minimal and speedy handling, avoiding transfers from one container to another and carrying out the injection within the well head pipework. Essentially no external radiation is emitted by tritium and very little by ^{125}I, so external exposure is a minor issue for these two tracers. With all tracers, procedures must, of course, minimize the possibility of spillages.

Once the tracer has been injected, care should be taken to avoid contamination of the local environment. This may occur by intrusion of the tracer into natural outflows such as hot springs, and consideration should be given to measurement of radiation levels in such features. In addition some contamination can occur if wastewater is not injected but simply disposed of into a local water body. In this regard it should be realized that high contamination levels are unlikely. To take the most extreme case, reducing 185 GBq of ^{131}I to the concentration at which it is exempt [92] from regulation (100 Bq·g^{-1}) requires dilution into 1850 t of water. This represents less than a day's discharge for many wells. Experience has shown that tracer responses, when they occur, do so with durations at least equal to the time taken for the response to arrive, so it is only in the case of very short term responses that exempt levels can be exceeded. If a natural feature is affected in such a short time by flow from the injected well, this would be known from other studies. Furthermore, even if such contamination did occur it would have to be at a very much higher level to pose any significant risk to human health. The effects of ingesting the large

quantities of geothermal fluid which would be required to deliver a significant dose would be much more harmful.

6.2.4. Tracer test analysis and interpretation

6.2.4.1. Introduction

Comprehensive interpretation of geothermal tracer test data and consequent modelling for management purposes (production well cooling predictions) have been rather limited even though tracer tests have been used extensively. Their interpretation has mostly been qualitative rather than quantitative. This section presents a review of methods that may be used for this purpose. These methods are equally applicable to radioactive and other chemical tracers. The review is focused on software related to tracer test analysis, and injection simulation, which is included in the ICEBOX software package that has proven to be very effective (United Nations University Geothermal Training Programme, 1994). These programs are based on simple models which are able to simulate the relevant data quite accurately. Utilization of detailed and complex numerical models (such as TOUGH2 models) is seldom warranted, at least for a first stage analysis.

Interpretation of the tracer test data aims at quantifying the danger of cooling of production wells during long term injection, as already mentioned. Numerous models have been developed, or adopted from groundwater and nuclear waste storage studies, for interpreting tracer test data and consequently for predicting thermal breakthrough and temperature decline during long term injection [95–99]. It must be pointed out, however, that while tracer tests provide information on the volume of flow and flow paths connecting injection and production wells, thermal decline is determined by the surface area involved in the heat transfer from reservoir rock to the flow paths, which most often are fractures. With some additional information and/or assumptions, this information can be used to predict the cooling of production wells during long term (years to decades) injection.

The theoretical basis of tracer interpretation models is the theory of solute transport in porous/permeable media, which incorporates transport by advection, mechanical dispersion and molecular diffusion. This will be reviewed very briefly in this section. A method of tracer test analysis/interpretation which is conveniently based on the assumption of specific flow channels connecting injection and production wells will consequently be presented. The ICEBOX software package includes several programs that may be used for tracer test analysis [100]. In particular, the focus will be on TRINV, which is an interactive program for inversion of tracer test data, and TRCOOL, a program

used to predict cooling of production wells during long term injection. A few other programs can be of use in tracer work (DATE2SEC, TRMASS and TRCURV). The use of these programs will be discussed in Section 6.2.4.3.

6.2.4.2. Theory of solute transport

The theory of solute transport in porous and fractured hydrological systems underground is discussed in various publications and textbooks, but the reader is referred in particular to Bear et al. [101] and Javandel et al. [102]. The term solute indicates a chemical substance dissolved in fluid. The following are the principal modes of transport:

(1) By *advection and convection*, i.e. through movement of the fluid involved;
(2) By *mechanical dispersion*, which is reflected in variations in actual fluid particle velocities;
(3) By *molecular diffusion*, which causes the solute to diffuse from regions with high concentration to regions with lower concentration.

If the transport were only through constant velocity fluid movement, tracer test analysis and interpretation would be simple. But because of the other modes of transport — in particular, mechanical dispersion — its analysis and interpretation is much more involved. Figure 158 illustrates the main causes of mechanical dispersion, which are:

(a) The effect of pore/fracture walls,
(b) The effect of pore/fracture width,
(c) The effect of flow path tortuosity.

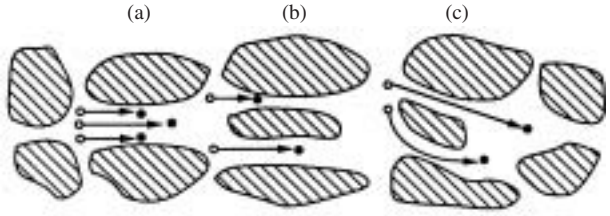

FIG. 158. Schematic diagram illustrating the causes of mechanical dispersion: (a) the effect of pore/fracture walls, (b) the effect of pore/fracture width and (c) the effect of flow path tortuosity.

The basic equations describing the solute flow are the following:

$$F_x = F_{x,\text{adv}} + F_{x,\text{disp}}. \tag{114}$$

where F_x denotes the mass flow rate of the solute (kg·m^{-2}· s^{-1}) in the x direction, and

$$F_{x,\text{adv}} = u_x \phi C \tag{115}$$

$$F_{x,\text{disp}} = \phi D_x \partial C/\partial x. \tag{116}$$

Equation (116) is the so-called Fick's law. In addition, u_x denotes the fluid particle velocity (m/s), ϕ the material porosity (dimensionless), C the solute concentration (kg/m^3) and D_x the so-called dispersion coefficient (m^2/s):

$$D_x = \alpha_x u_x + D^*, \tag{117}$$

where α_x is the dispersivity of the material (m) and D^* is the coefficient of molecular diffusion (m^2/s).

Comparable equations apply for the y and z directions.

The differential equation for solute transport is derived by combining the above flow equations and the conservation of mass of the solute involved. For a homogeneous, isotropic and saturated medium the differential equation is:

$$\frac{\partial}{\partial x}\left(D_x \frac{\partial C}{\partial x}\right) + \frac{\partial}{\partial y}\left(D_y \frac{\partial C}{\partial y}\right) + \frac{\partial}{\partial z}\left(D_z \frac{\partial C}{\partial z}\right)$$

$$- \frac{\partial}{\partial x}\left(u_x C\right) - \frac{\partial}{\partial y}\left(u_y C\right) - \frac{\partial}{\partial z}\left(u_z C\right) = \frac{\partial C}{\partial t}. \tag{118}$$

By combining this equation with appropriate boundary and initial conditions for the material domain being studied, a model is fully defined. Theoretically a mathematical solution should exist for any such problem, but in practice the solutions are often very complicated [102]. Such complicated problems may, of course, be solved numerically with the aid of powerful computers. Some simpler analytical solutions are possible after highly simplifying assumptions have been made concerning, for example, the geometry and the dispersion. One such model and the associated solution form the basis of the method for tracer test analysis/interpretation presented in the following.

Another example of an analytical solution to Eq. (118) is available for a model of a homogeneous, infinite, confined hydrological reservoir with constant reservoir thickness b and two dimensional radial flow. This solution is normally not suitable for analysing tracer test data, but can be of use in injection studies. Fluid with solute concentration C_0 is injected at a rate Q (m^3/s) from time $t = 0$ through an injection well at the centre of the reservoir, while the initial concentration C is zero. By neglecting molecular diffusion the following approximate solution may be obtained:

$$\frac{C}{C_0} \approx \frac{1}{2}\,\mathrm{erfc}\left[\left(\frac{r_D^{1/2}}{2} - t_D\right)\left(\frac{4}{3}r_D^3\right)^{-1/2}\right] \tag{119}$$

with $r_D = r/\alpha_L$, where r is the radial distance from the injection well, α_L is the longitudinal (radial) dispersivity, $t_D = Qt/\left(2\pi b\phi\alpha_L^2\right)$ and erfc is the complimentary error function.

6.2.4.3. Tracer test interpretation on basis of a one dimensional flow channel model

Before radioactive tracer test data are interpreted, some steps must be taken to correct and prepare the return data collected. These are:

(a) Correct the data for radioactive decay by the following equation:

$$C_{corr} = C_{meas}\exp(0.693t/t_{1/2}), \tag{120}$$

where

C is the measured activity of the tracer (Bq),
t is the time since the tracer was at full initial activity, and
$t_{1/2}$ is the half-life of the radioactive nuclide being used as tracer.

The half-lives of ^{131}I and ^{125}I are 8.04 and 60.1 days, respectively.

(b) Also correct by multiplying by

1/(sample volume)(measurement efficiency),

which results in concentration and activity values in units of Bq/L and Bq/m^3, respectively.

(c) It should be noted that, following these steps, radioactive tracer data are fully comparable to mass, and one may simply interchange kg and Bq. The return data are then compared with the initial activity (0.5–2 Ci, 1 Ci $= 37 \times 10^9$ Bq), just as conventional tracer test data are compared with the mass of tracer injected (kg).

When analysing tracer test data, it should be kept in mind that some of the tracers recovered through the production wells are injected back into the reservoir. If this amount is significant it will interfere with data interpretation and must be corrected for. This is seldom the case; however, Bjornsson et al. [103] have presented a method for making such a correction. The program TRCORRC in the ICEBOX package may be used for this purpose. In addition, the program TRCORRQ may be used to correct for small variations in production and/or injection rates.

The first step in analysing tracer test data involves estimating the mass (activity) of tracer recovered throughout a test. This is done on the basis of the following equation:

$$m_i(t) = \int_0^t C_i(t) Q_i(t) \mathrm{d}t, \tag{121}$$

where

$m_i(t)$ indicates the cumulative mass recovered in production well number i (kg), as a function of time,
C_i indicates the tracer concentration in well i (kg/L or kg/kg), and
Q_i is the production rate of well i (L/s or kg/s, respectively).

The program TRMASS in the ICEBOX package may be used for this purpose. An example of such mass recovery calculations is presented in Fig. 159.

A simple one dimensional flow channel tracer transport model has turned out to be quite successful in simulating return data from tracer tests in geothermal systems [104]. This model assumes that the flow between injection and production wells may be approximated by one dimensional flows in flow channels, as shown in Fig. 160. These flow channels may in fact be parts of near vertical fracture zones or parts of horizontal interbeds or layers. These channels may be envisioned as being delineated by the boundaries of these structures, on the one hand, and flow field streamlines, on the other. In other cases these channels may consist of larger volumes involved in the flow between wells. In

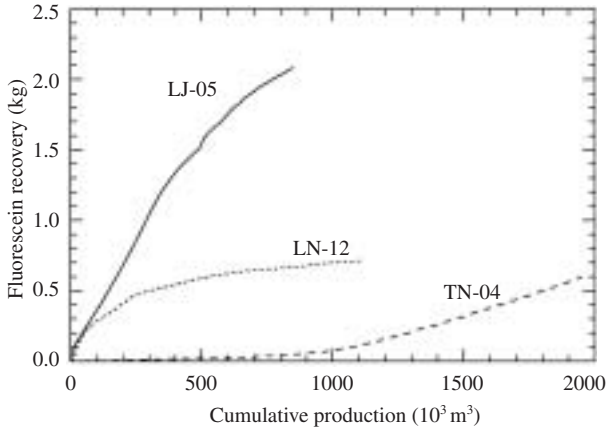

FIG. 159. Example of the results of tracer mass recovery calculations from the Laugaland geothermal field in northern Iceland, a tracer test during which 10 kg of sodium fluorescein were injected. The cumulative tracer recovery is shown in three production wells as a function of cumulative production from each well during a two year period from late 1997 through most of 1999.

some cases more than one channel may be assumed to connect an injection and a production well — for example, connecting different feed zones in the wells involved.

In the case of one dimensional flow, Eq. (118) simplifies to:

$$D\frac{\partial^2 C}{\partial x^2} = u\frac{\partial C}{\partial x} + \frac{\partial C}{\partial t}, \tag{122}$$

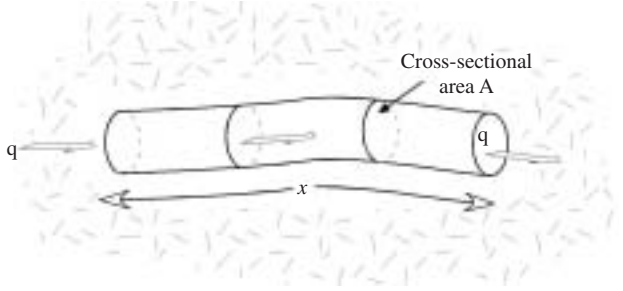

FIG. 160. Schematic diagram of a flow channel with one dimensional flow connecting an injection well and a production well.

where

D is the dispersion coefficient (m^2/s),
C is the tracer concentration in the flow channel (kg/m^3),
x is the distance along the flow channel (m),
u is the average fluid velocity in the channel (m/s) given by $u = q/\rho A\phi$, with q the injection rate (kg/s),
ρ is the water density (kg/m^3),
A is the average cross-sectional area of the flow channel (m^2), and
ϕ is the flow channel porosity.

Molecular diffusion may be neglected such that $D = \alpha_L u$ with α_L the longitudinal dispersivity of the channel (m). Assuming instantaneous injection of a mass M (kg) of tracer at time $t = 0$ the solution is given by:

$$c(t) = \frac{uM}{Q}\frac{1}{2\sqrt{\pi Dt}}\exp\left[-(x-ut)^2/4Dt\right]. \qquad (123)$$

Here $c(t)$ is actually the tracer concentration in the production well fluid, Q the production rate (kg/s) and x the distance between the wells involved. Conservation of the tracer according to $c \times Q = C \times q$ has been assumed. This equation is the basis for the method of tracer test analysis and interpretation presented here, which involves simulating tracer return data with Eq. (123). Such a simulation yields information on the flow channel cross-sectional area, actually on $A\phi$ and the dispersivity α_L as well as the mass of tracer recovered through the channel. This mass should of course be equal to, or less than, the mass of tracer injected. In the case of two flow channels or more, the analysis yields estimates of these parameters for each channel. It should be pointed out that through the estimate for $A\phi$ the flow channel pore space volume, $Ax\phi$, has in fact been estimated.

The tracer interpretation software TRINV, included in the ICEBOX software package, is used for this simulation or interpretation. It is an interactive DOS mode program which automatically simulates the data through inversion. The user defines a model with one or more flow channels and makes a first guess for the model parameters. TRINV, consequently, uses non-linear least squares fitting to simulate the data and obtain the model properties, i.e. the flow channel volumes $Ax\phi$ and dispersivity α_L. The software may also be used to plot the results. Section 6.2.6 presents some examples of the utilization of TRINV, from geothermal fields in El Salvador and Iceland.

6.2.4.4. Discussion

It should be noted that the method of analysis presented above should not be regarded as yielding unique solutions, even though it often results in solutions that are considered to be the most likely ones. Numerous other models have been developed to simulate the transport of contaminants in groundwater systems, and in relation to underground disposal or storage of nuclear waste. Many of these models are in fact applicable in the interpretation of tracer tests in geothermal systems. It is often possible to simulate a given data set by more than one model; therefore, a specific model may not be uniquely validated. The transport of dissolved solids through fractured rocks and the analysis of tracer tests conducted in fractured geothermal systems, for example, are discussed in several publications [105–109].

In addition to the distance between wells and the volume of flow paths, mechanical dispersion is the only factor assumed to control the tracer return curves in the interpretation presented above. Retardation of the tracers by diffusion into the rock matrix is neglected [110]. Through this effect, the chemical used as a tracer diffuses into the rock matrix when the tracer concentration in the flow path is high. As the concentration in the flow path decreases, the concentration gradient eventually reverses, causing diffusion from the rock matrix back into the fracture. This will, of course, affect the shapes of the tracer return curves obtained. In particular, it may cause the flow — through the channels discussed above — to be underestimated. Robinson and Tester [107], on the one hand, postulate that matrix diffusion should be negligible in fractured rock. Grisak and Pickens [108], on the other hand, point out that it may be significant when the fracture apertures are small, flow velocities are low and rock porosity is high.

6.2.5. Cooling predictions

6.2.5.1. Model presentation

The ultimate goal of tracer testing is to predict thermal breakthrough and temperature decline during long term injection, as already stated. These changes are dependent on the properties of the flow channel, but they are not uniquely determined by the flow path volume. This cooling mainly depends on the surface area and the porosity of the flow channel. Therefore, some additional information on the flow path properties and geometry is needed, preferably based on geological or geophysical information. Predictions may also be calculated for different assumptions as discussed below.

The model presented in Fig. 161 is used to calculate the temperature changes along the flow channel and hence the production well cooling predictions. It simulates a flow channel along a fracture zone, an interbed or a permeable layer. In the model, b indicates either the width of the fracture zone or the thickness of the interbed or layer, whereas h indicates the height of the flow channel inside the fracture zone or its width along the interbed or layer. The flow channel cross-sectional area is then given by $A = hb$. To estimate h and b on the basis of the main outcome of the tracer test interpretation, $A\phi$, an assumption must be made about the average flow path porosity, which is often known approximately, and the ratio between h and b.

The theoretical response of this model is derived through a formulation in which a coupling is considered between the heat advected along the flow channel and the heat conducted from the reservoir rock to the fluid in the channel. Solutions to similar problems have been presented by Carslaw and Jaeger [110] and by Bodvarsson [111]. The analytical solution for the temperature of the production well fluid is:

$$T(t) = T_0 - \frac{q}{Q}\left(T_0 - T_\mathrm{i}\right)\left[1 - \mathrm{erf}\left(\frac{kxh}{c_\mathrm{w} q\sqrt{\kappa\left(t - x/\beta\right)}}\right)\right], \tag{124}$$

with $T(t)$ the production fluid temperature, T_0 the undisturbed reservoir temperature, T_i the injection temperature, q and Q the rates of injection and production, respectively, erf the error function, k the thermal conductivity of

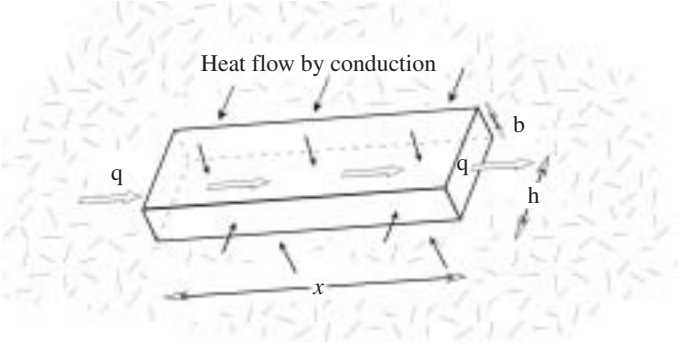

FIG. 161. Model of a flow channel along a fracture zone, a horizontal interbed or a permeable layer. The model is used to calculate the heating of injected water flowing along the channel and the eventual cooling of a production well connected to the channel.

the reservoir rock, κ its thermal diffusivity, x the distance between injection and production wells, and

$$\beta = \frac{qc_w}{\langle \rho c \rangle_f hb} \tag{125}$$

with

$$\langle \rho c \rangle_f = \rho_w c_w \phi + \rho_r c_r (1-\phi) \tag{126}$$

the volumetric heat capacity of the material in the flow channel. Here ρ and c are density and heat capacity, respectively, with the indices w and r standing for water and rock.

The TRCOOL program can be used for these calculations or predictions. It calculates the temperature at time points given by the user on the basis of information on the flow channel dimensions and the properties provided. When more than one flow channel is used to interpret the data, the cooling due to each channel must be calculated separately and then the various contributions added up. Examples of predictions calculated by TRCOOL, on the basis of tracer test interpretation, are presented in Section 6.2.6.

To deal with the uncertainty in calculating cooling predictions on the basis of tracer test data alone, the predictions may be calculated for different assumptions about the flow channel dimensions and properties. It is recommended that this be at least done for two extremes: firstly a high porosity, small surface area, pipe-like flow channel that can be looked upon as the most pessimistic scenario, resulting in rapid cooling predictions; secondly a lower porosity, large surface area flow channel, such as a thin fracture zone or thin horizontal layer, which can be looked upon as the most optimistic scenario, resulting in slow cooling predictions. Practical examples of such different cooling model calculations are presented in Section 6.2.6.

6.2.5.2. Discussion

A simple and efficient method of tracer test analysis and interpretation has been presented which is based on the assumption of specific flow channels connecting injection and production wells in geothermal systems. It has been used successfully in a number of geothermal fields worldwide. Computer software, named TRINV, which is based on this method, uses an automatic inversion technique to simulate tracer return data. It is part of the ICEBOX software package [100]. The results of the interpretation are consequently used for predicting thermal breakthrough and temperature decline during long term injection in geothermal systems.

It is important to keep in mind, however, that while tracer tests provide information on the volume of flow paths connecting injection and production wells, thermal decline is determined by the surface area involved in heat transfer from reservoir rock to the flow paths, which most often are fractures. To deal with the resulting uncertainty, geological information must be taken into account and predictions may be calculated for different assumptions about the flow channel dimensions and properties. It is recommended that this be at least done for two extreme cases, one resulting in conservative predictions and the other in optimistic predictions.

To summarize, the main steps in tracer test interpretation using the ICEBOX software package are the following:

(1) Write raw data into data file (ASCII): date, time, concentration;
(2) Subtract background;
(3) Correct for radioactive decay, sample volume and measurement efficiency;
(4) Correct for injection of tracer, if needed (TRCORRC);
(5) Change date and time to seconds (DATE2SEC);
(6) Calculate tracer recovery (TRMASS);
(7) Interpret data with TRINV and obtain information on flow channel volume $Ax\phi$ and dispersivity α_L;
(8) Predict production well cooling (TRCOOL).

It is also important to keep in mind that the results of the method of analysis presented here should not be considered unique solutions. Other models should be considered in many cases, for example models incorporating retention mechanisms such as matrix diffusion. The highly complex flow mechanism within the bedrock in many areas requires more detailed analysis and interpretation than is possible through the methods presented here.

6.2.6. Case studies

6.2.6.1. Groundwater intrusion studies

Well WK107 at Wairakei in New Zealand was permanently quenched by groundwater intrusion. Before the well was repaired, the fate of the inflow was studied by injecting $^{131}I^-$ tracer below the inflow using the modified Kleyn sampler and monitoring the tracer levels at adjacent wells. Within hours a high concentration of tracer was observed in production wells WK24 and WK48, proving that cool water was contaminating the field. Over the following days

much lower concentrations were observed at other wells in the same general area. These results are shown in Figs 162 and 163.

The data are smoothed using procedures described in Ref. [91]. This study and later tracer injections in two other wells with downflows showed that the groundwater inflows were predominantly along faults, as shown in Fig. 164. The results suggested that cool dense inflowing water sank to the base of the field, where the Waiora and Wairakei faults cross at a depth of about 1100 m. The intruding water was then first produced at WK48 and WK24, which intercept the Waiora and Wairakei faults, respectively, at about 750 m and later, after considerable further dilution, at the remaining wells which are drilled to about 600 m depths.

More recently, contamination by groundwater has been studied at Mahanagdong in the Philippines [112]. A tracer (15.6 GBq of ^{125}I as $^{125}I^-$) was injected into well MG-4DA, following which sixteen wells were monitored for nine months. Major responses occurred in MG-29D (11% return) and MG-27D (13%), while tracer was also measured in MG-28D, MG-30D, MG-31D and MG-26D. Since an estimate of the groundwater inflow was available, it was possible to calculate that approximately 8% of the flow from MG-29D was from that source.

Plots of the major returns are shown in Fig. 165. The liquid scintillation counter used for this study was not equipped with quench correction and this,

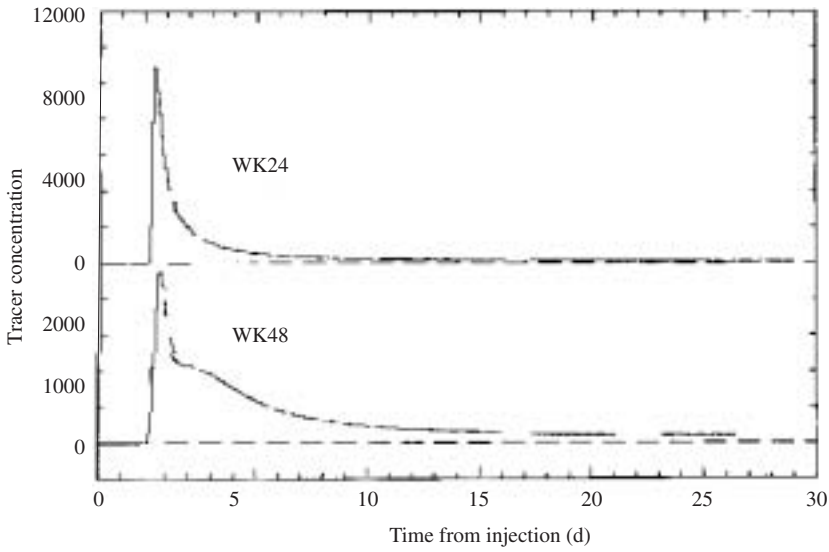

FIG. 162. Response curves for wells WK24 and WK48 at Wairakei.

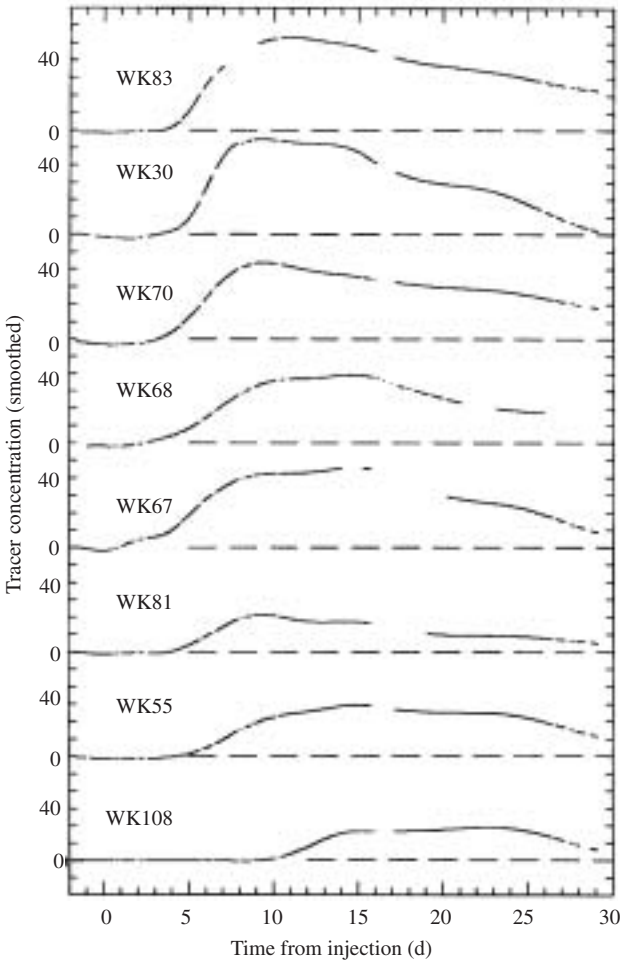

FIG. 163. Low response curves at various wells after injection into well WK107.

together with some instrumental difficulties, accounts for some of the variation from smooth curves, in particular the negative measured activities. The latter occurred in several wells towards the end of the test and may also be due to changing background levels being amplified by the decay correction.

The geology of the injection well and four of the wells in which tracer was detected is shown in Fig. 166. The results were consistent with movement of tracer along the Mamban fault to its intersection with the North Mamban fault and subsequently along the North Mamban fault and then the Ewex fault.

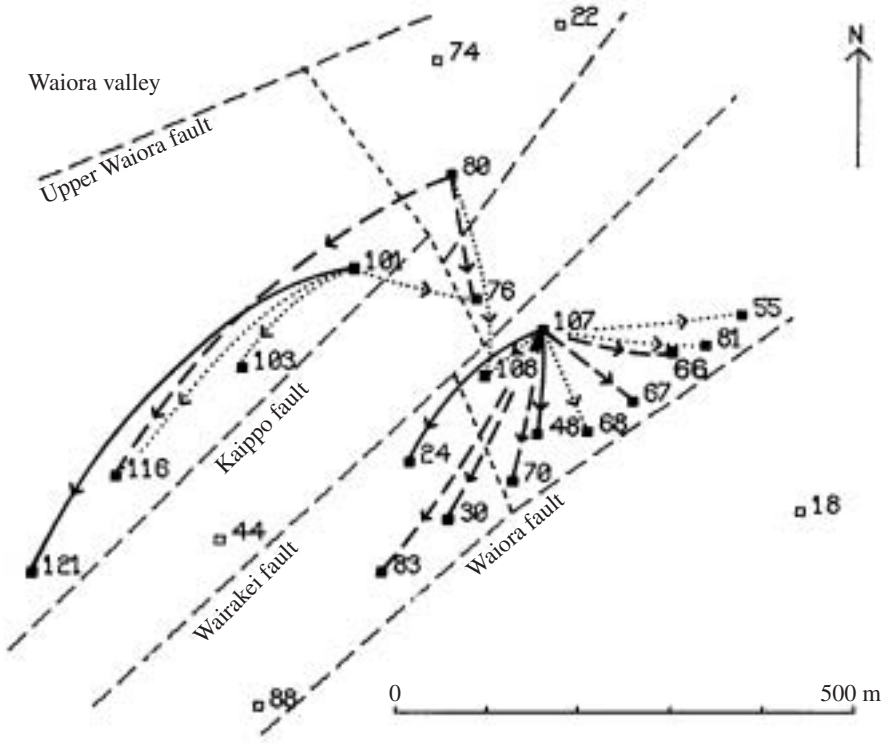

FIG. 164. Map of Waiora valley faults.

6.2.6.2. Injection studies

An injection of $^{125}I^-$ (15 GBq) was made into well PGM-22 of the Miravalles geothermal field in Costa Rica. A low concentration tracer response (Fig. 167) was observed in well PGM-42 starting after 15 days, and extending for 67 days when the test was terminated due to a power station shutdown. No other wells showed any response. The peak of the decay corrected concentration occurred at about 50 days after injection. Approximately 0.2% of the tracer had been recovered at that stage, leading to the conclusion that the connection between the two wells was weak.

At the Berlin field in El Salvador a tracer (73 GBq of $^{131}I^-$) was injected into well TR-12A, one of four reinjection wells located in the production zone. The four wells showed tracer returns totalling 14.2% of the injected tracer. The activities measured in TR-4C (the well with the greatest response) are shown in Fig. 168 and the normalized concentrations calculated from those data are

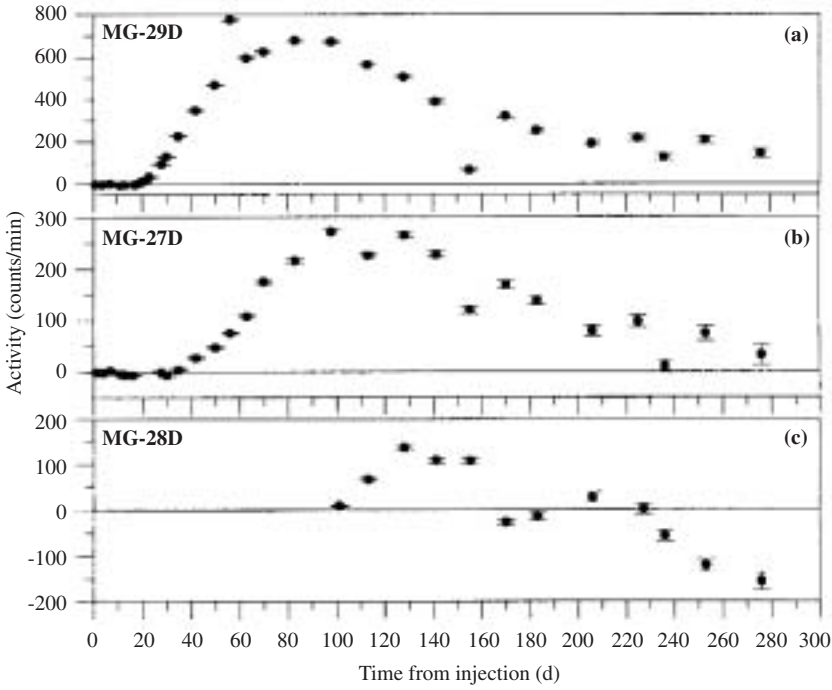

FIG. 165. Tracer return curves for various wells at Mahangdong.

shown in Fig. 169. The data from TR-4C were used as input to tracer modelling programs to estimate field parameters such as fracture cross-section and dispersivity, and to predict negligible cooling of the well for at least two years.

An injection test [87] involving the use of a gas phase tracer was one of the early applications of geothermal tracing. The Geysers field in California is a vapour phase field in which condensed steam is reinjected. Tritiated water (740 GBq) was injected with the condensate into well SB-1 and nearby production wells. The first response was measured after seven days. Monitoring continued for a period of over two years, at which point the tracer concentrations had dropped to below the detection limit in all the wells monitored. Tracer was observed in 20 wells and the total amount returned was 18%. This achieved two of the test objectives, of determining if any of the injected water vaporized and of quantifying the amount which reached the production wells. A third objective of determining regional flow patterns was partly achieved.

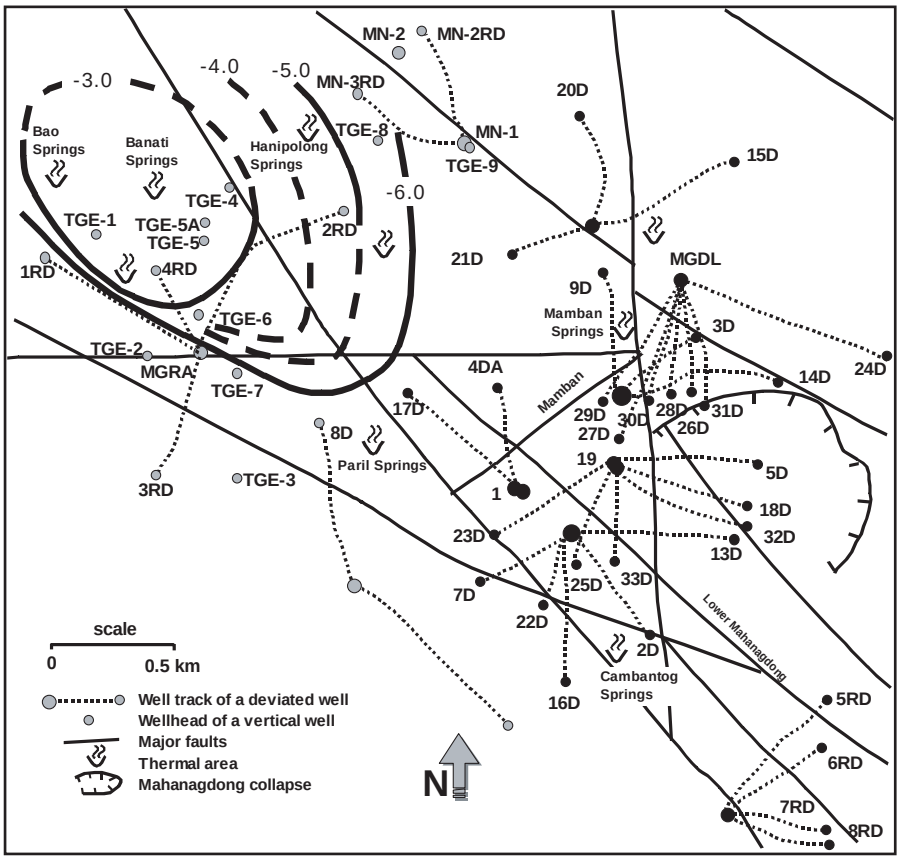

FIG. 166. Simplified plan view of Mahanagdong geothermal field, Philippines. Isolines are $\delta^{18}O$ values of geothermal fields (unit: ‰ VSMOW where VSMOW stands for Vienna standard mean ocean water).

6.2.6.3. Interwell connections

Some tracer tests have thrown light on the question of the origin of water in the production field. For example, one of the early $^{125}I^{-}$ tests at Wairakei involved an injection into WK218, a non-producing well to the south of the main field. Tracer was pumped in from the surface through equipment of the type shown in Fig. 151. As illustrated in Fig. 170, tracer returns were followed over a long period during which it is estimated that more than 50% of the tracer was recovered. Initially tracer was found in wells near the north end of the main production area (such as WK55, WK66 and WK67) and only several days

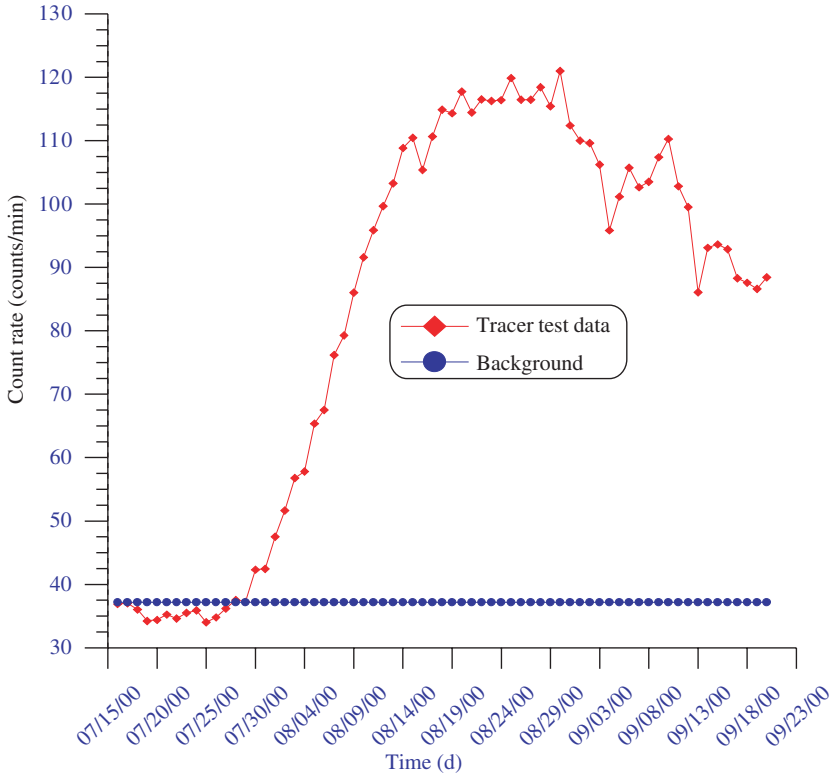

FIG. 167. Response at well PGM-42, Miravalles geothermal field, Costa Rica, to tracer injection in well PGM-22.

later was it detected in wells further south (such as WK88) nearer the injection well. This was interpreted as flow along the Waiora fault into the field in the region near WK55, followed by subsequent mixing in the local production area.

6.2.6.4. Cooling predictions for geothermal injection

Geothermal injection started in Ahuachapan (El Salvador) in 1969, The Geysers (California) in 1970 and Larderello (Italy) in 1974. It is now an integral part of the operation of at least 40 geothermal fields in 17 countries. Without injection the mass extraction, and hence electricity production, would only be a small part of what it is now in many of these fields.

The water injected into geothermal reservoirs includes wastewater and condenser water from power plants, return water from direct use (space heating, etc.), groundwater and surface water or even sewage water. Some

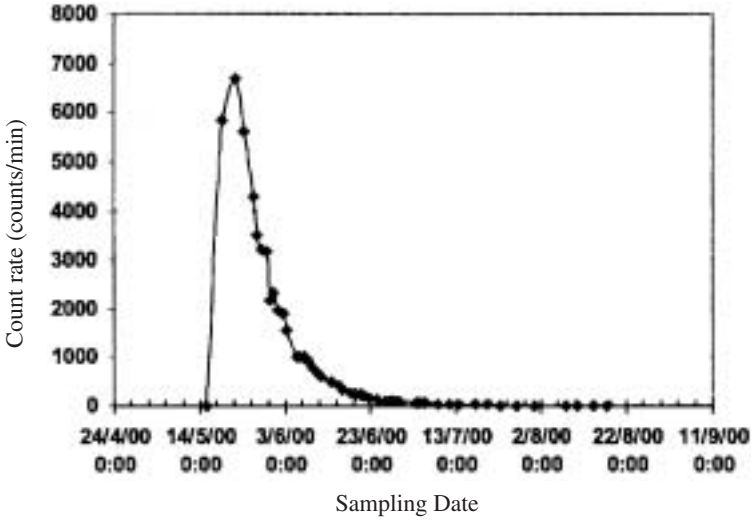

FIG. 168. Tracer production curve from well TR-4C, Berlin geothermal field, El Salvador. Injection date, 16/5/2000; percentage recovery, 9.44; Q = 2.83 kg/s; T_{res} = 285°C; WHP = 10.98 bar; arrival time, 1 day; T_{inj} = 180°C; Q_{inj} = 30 kg/s; ^{131}I activity, 1.96 Ci.

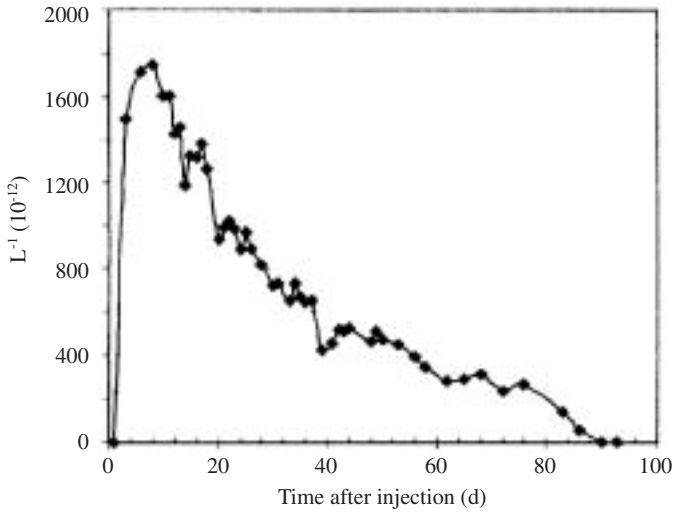

FIG. 169. Tracer return curve (9.44% recovery), Berlin geothermal field, El Salvador.

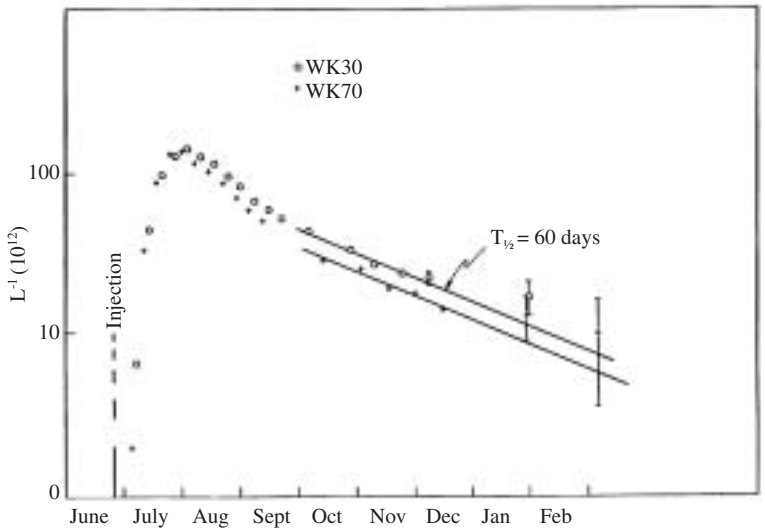

FIG. 170. Tracer return at Wairakei well WK201.

operational problems are associated with injection, such as an increase in investment and operation costs, cooling of production wells and scaling in surface equipment and injection wells [102]. Injection into sandstone reservoirs has, furthermore, turned out to be problematic.

The possible cooling of production wells, or thermal breakthrough, has discouraged the use of injection in some geothermal operations, although actual thermal breakthroughs caused by cold water injection have been observed in relatively few geothermal fields. In cases where the spacing between injection and production wells is small, and direct flow paths between the two wells exist, the fear of thermal breakthrough has been justified. Actual cooling, attributable to injection, has been observed in Ahuachapan (El Salvador), Palinpinon (Philippines) and Svartsengi (Iceland) [103]. The temperature of well AH-5 in Ahuachapan declined by about 30ºC due to an injection well located only 150 m away, while the temperature of well SG-6 in Svartsengi declined by about 8ºC during four years of injection. The temperature decline of well PN-26 in Palinpinon was reviewed by Malate and O'Sullivan [113], where the thermal breakthrough occurred about 18 months after injection started. Subsequently, the temperature declined rapidly, dropping by about 50ºC in four years.

Cooling due to injection is minimized by locating injection wells far away from production wells, while the benefit from injection is maximized by locating injection wells close to production wells. A proper balance between

these two conflicting requirements must be found. Therefore careful testing and research are essential parts of injection planning. Tracer testing, which is used to study flow paths and quantify fluid flow in hydrological systems, is probably the most important tool for this purpose.

Two case histories involving tracer test interpretation along the lines outlined above and consequent cooling predictions are presented below as field examples. These are from the Ahuachapan high temperature geothermal field in El Salvador and the Laugaland low temperature field in northern Iceland. The former example involved utilization of a radioactive tracer, while sodium fluorescein was utilized in the latter. It should be emphasized that the interpretation methods are independent of the tracer used, as already mentioned. In the case of Ahuachapan, emphasis was placed on evaluating the uncertainty in cooling prediction arising from the fact that the interpretation of tracer tests only yields information on flow path volumes. The data analysis was more elaborate in the Laugaland case since the data were much more detailed. In the Laugaland case the increase in energy production enabled through long term injection was, furthermore, estimated. This is important for management purposes and provides the basis for analysis of the economics of future injection at Laugaland. The Laugaland case has been described in detail by Axelsson et al. [114, 115].

(a) The tracer test at Ahuachapan, El Salvador

The Ahuachapan geothermal field in El Salvador has been utilized for electricity production for more than three decades [116]. Ahuachapan was the first geothermal field where injection was attempted, as mentioned above, yet injection was discontinued in the field in the early 1980s. Injection inside the geothermal field is now being reconsidered to counteract a substantial pressure drawdown and increase the production potential of the field. Therefore, an injection and tracer test was conducted in the field in September and October 2001. The test involved injection of about 100 kg/s of separated water from nearby production well separators into well AH-33A.

For the associated tracer test the radioactive tracer ^{131}I was injected into the well on 27 September 2001. The initial activity of the tracer was 6.5×10^{10} Bq. The recovery of the tracer was monitored in several nearby wells for a few weeks. Some recovery (~2% in two weeks) was noted in a few wells, namely wells AH-4bis, AH-19 and AH-22. These wells are all along the so-called Buenavista Fault, which is believed to play a major role in the hydrology of the Ahuachapan system. No recovery was noted in any other wells, except for a minor recovery in well AH-20.

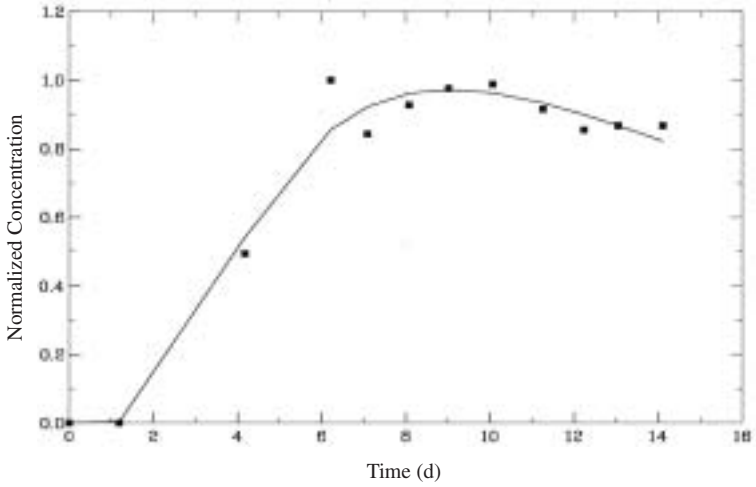

FIG. 171. Observed (boxes) and simulated (solid line) tracer recovery from well AH-4bis at Ahuachapan, El Salvador.

The data for the first two weeks from wells AH-4bis, AH-19 and AH-22 are presented in Figs 171–173, respectively. After two weeks the activity of ^{131}I had decreased to about 25% of the initial activity. The data were prepared and corrected as described above, and consequently simulated through using the tracer interpretation software TRINV. The simulated recovery is also

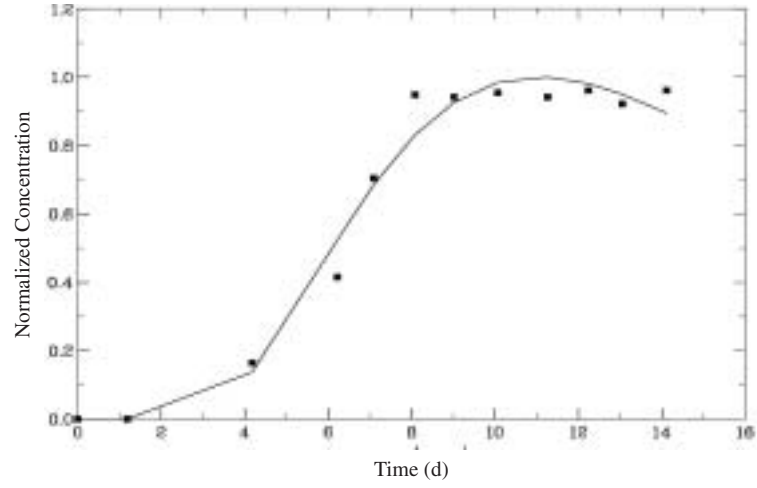

FIG. 172. Observed (boxes) and simulated (solid line) tracer recovery from well AH-19 at Ahuachapan, El Salvador.

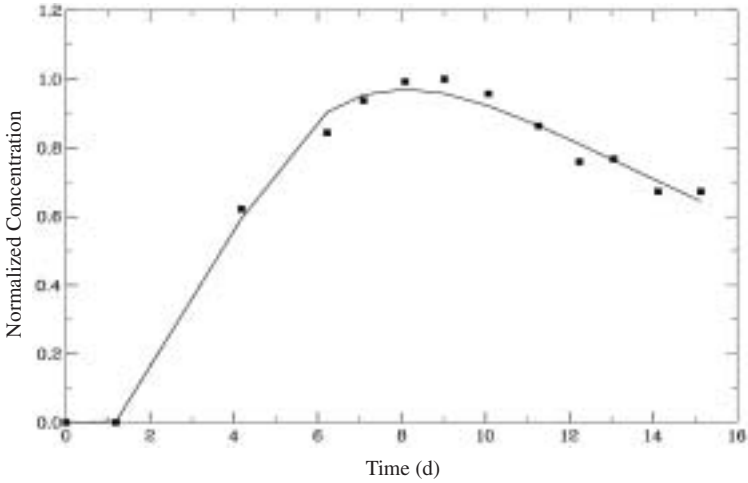

FIG. 173. Observed (boxes) and simulated (solid line) tracer recovery from well AH-22 at Ahuachapan, El Salvador.

presented in Figs 174–176. It should be noted that relatively few samples were collected. The initial sampling frequency, in particular, was not sufficiently high. Two samples per day during the first few days would have been more adequate. Therefore, the data analysis and interpretation presented here can be considered to be neither very accurate nor very detailed.

The principal results of the interpretation, along with basic information on the wells involved, are presented in Table 27. Only one flow channel was required for the simulation for each well pair; more detailed analysis was not warranted by the data. The main results are the flow channel volume (actually pore space volume as discussed previously) and flow ratio. The dispersivity values also appear reasonable. Small volumes and dispersivities indicate that well AH-33A is rather directly connected to wells AH-4bis, AH-19 and AH-22. Flow velocities are rather high, up to 60 m/d. However, a small fraction of the injected water is recovered through each of these wells, and thus the predicted temperature declines are not very great. Well AH-19 appears to be not as directly connected as the other two wells (perhaps it is further away from the Buenavista Fault).

The results in Table 27 were subsequently used to calculate cooling predictions for the three production wells. The cooling of the production wells is not uniquely determined by the flow path volume, it also depends on the surface area and porosity of the flow channels involved, as discussed before. A large flow channel surface area leads to slow cooling and vice versa. To study

TABLE 27. MODEL PARAMETERS USED TO SIMULATE ^{131}I RECOVERY FROM PRODUCTION WELLS AH-4BIS, AH-19 AND AH-22 FOR INJECTION INTO WELL AH-33A
(injection rate 100 kg/s)

Well	Distance[a], x (m)	Water flow rate (kg/s)	Steam flow rate (kg/s)	Flow channel volume[b], $xA\phi$ (m^3)	Dispersivity, α_L (m)	Flow ratio[c] (%)
AH-4bis	800	64	31	6300	240	4.9
AH-19	300	40	7	5300	40	4.0
AH-22	600	20	7	4200	150	3.9

[a] Included in this table is information on distances between wells and water/steam flow rates.
[b] The flow channel volume is the pore space volume (volume × porosity) in the flow channel.
[c] The flow ratio is the fraction of injected water recovered through each well.

the uncertainty arising because of this, cooling predictions for wells AH-4bis, AH-19 and AH-22, during long term injection, were calculated for three different assumptions/models. The TRCOOL software was used for this purpose. The following models were considered:

(a) A high porosity, small surface area, pipe-like flow channel. This can be looked upon as the most pessimistic case, resulting in predictions of rapid cooling.
(b) A low porosity, large volume flow channel. This model simulates dispersion throughout a large volume or fracture network.
(c) A high porosity, large surface area flow channel, such as a thin fracture zone or thin horizontal layer. This is the most optimistic case, resulting in predictions of slow cooling.

Detailed information on the models is presented below, where x indicates the distance between wells, b the width or thickness of the flow channel, H its height or extent, and ϕ its porosity:

Case (a): AH-4bis, x = 800 m, b = 3.1 m, H = 12.5 m, ϕ = 20%;
AH-19, x = 300 m, b = 4.7 m, H = 18.8 m, ϕ = 20%;
AH-22, x = 600 m, b = 3.0 m, H = 11.8 m, ϕ = 20%.
Case (b): AH-4bis, x = 800 m, b = 14.0 m, H = 56 m, ϕ = 1%;

AH-19, x = 300 m, b = 21.0 m, H = 84 m, ϕ = 1%;
AH-22, x = 600 m, b = 13.2 m, H = 53 m, ϕ = 1%.

Case (c): AH-4bis, x = 800 m, b = 0.3 m, H = 130 m, ϕ = 20%;
AH-19, x = 300 m, b = 0.5 m, H = 176 m, ϕ = 20%;
AH-22, x = 600 m, b = 0.3 m, H = 117 m, ϕ = 20%.

The results of the cooling predictions are presented in Figs 174–176.

The most pessimistic prediction model is considered very unlikely on geological grounds, but the results show that some cooling is predicted for wells AH-4bis, AH-19 and AH-22 as a result of long term injection into AH-33A. The greatest cooling is predicted for well AH-22, of 4–10°C, over ten years. This will cause some decline in the steam flow rate for the well (roughly estimated to be in the range 10–25%). However, injection inside the Ahuachapan production field will be beneficial because of pressure recovery, but it must be adequately planned and managed.

(b) The tracer test at Laugaland, northern Iceland

The Laugaland geothermal field has been utilized for space heating in the town of Akureyri in central northern Iceland since the late 1970s. The field is characterized by a principal fracture zone surrounded by low permeability rocks, limited recharge and great pressure drawdown. Therefore, injection has

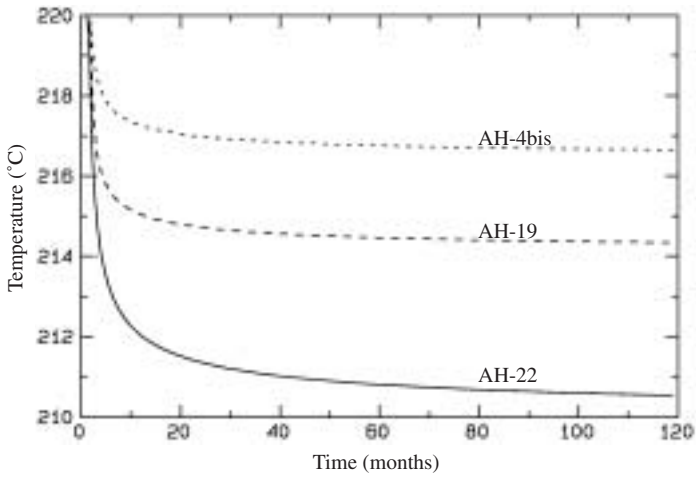

FIG. 174. Cooling predictions calculated for wells AH-4bis, AH-19 and AH-22 at Ahuachapan, during injection into well AH-33A, for a small surface area flow channel, the most pessimistic scenario.

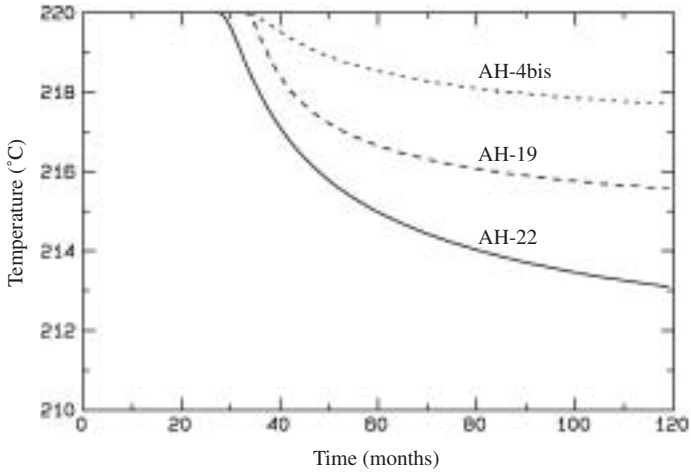

FIG. 175. Cooling predictions calculated for wells AH-4bis, AH-19 and AH-22 at Ahuachapan, during injection into well AH-33A, for a large volume flow channel scenario.

been considered a possible method of increasing the production potential of the field for a long time. Injection at Laugaland was initiated in September 1997 and has been continuous since then. The first two years were devoted to

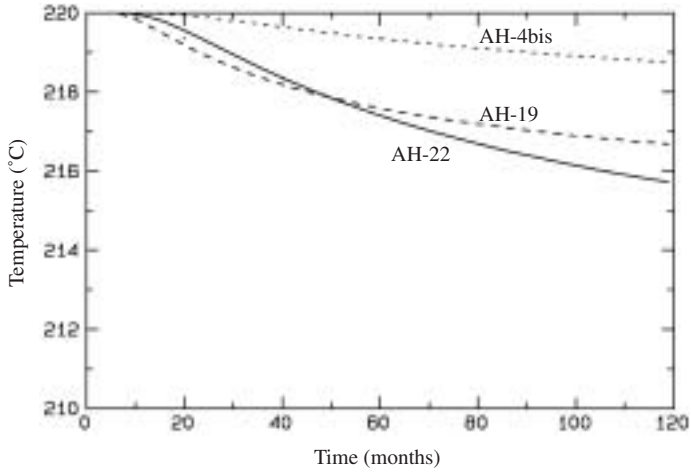

FIG. 176. Cooling predictions calculated for wells AH-4bis, AH-19 and AH-22 at Ahuachapan, during injection into well AH-33A, for a large surface area flow channel, the most optimistic scenario.

quite intensive research into the feasibility of long term injection. This included extensive tracer testing. A total of more than 1400 tracer samples were collected and analysed from production wells at Laugaland and in nearby areas, in conjunction with the tracer tests.

Three tracer tests were carried out between wells at Laugaland during the two year research period. The purpose of these tests was to study the connections between injection and production wells in order to enable predictions of the possible decline in production temperature due to long term injection. The tests were conducted under different conditions, i.e. for different injection rates and for different wells in use, both injection and production wells. Two tracers were used, sodium fluorescein and potassium iodide. Here, the results of the first fluorescein test will be reviewed.

The tracer return data collected at Laugaland indicate that the injected water travels throughout the bedrock in the area by two modes:

(1) Firstly through direct, small volume flow paths, such as channels along fractures or interbeds. These flow channels may even be looked upon as pipes containing porous material.
(2) Secondly by dispersion and mixing throughout a large part of the volume of the geothermal reservoir.

The Laugaland tracer test analysis was aimed at determining the volumes involved in mode (a) transport, while mode (b) transport was not expected to pose any danger of premature thermal breakthrough. As an example, Fig. 177 shows tracer test data for the well pair LJ-08 and LN-12 from September to November 1997, simulated by the software TRINV. Three separate flow channels were used in the simulation, which are assumed to connect the different feed zones of the injection and production wells. The properties of the channels are presented in Table 28.

The results in Table 28 indicate that only about 6% of the injected water travels through these channels from the injection well to the production well. Most of the injected water, therefore, appears to disperse and diffuse throughout the reservoir volume (transport mode (b)). The volumes of the channels also appear to be quite small. If one assumes an average porosity of 7% [107], the sum of the volumes of the three channels equals only 20 000 m^3. The results in Table 28 are the principal results of the analysis of the Laugaland tracer test data and form the basis for the cooling predictions presented later.

The observed fluorescein recovery in well TN-4 in the Ytri-Tjarnir field, which is a separate geothermal field located about 2 km north of Laugaland, was also analysed on the basis of the flow channel model (Fig. 178). Only a

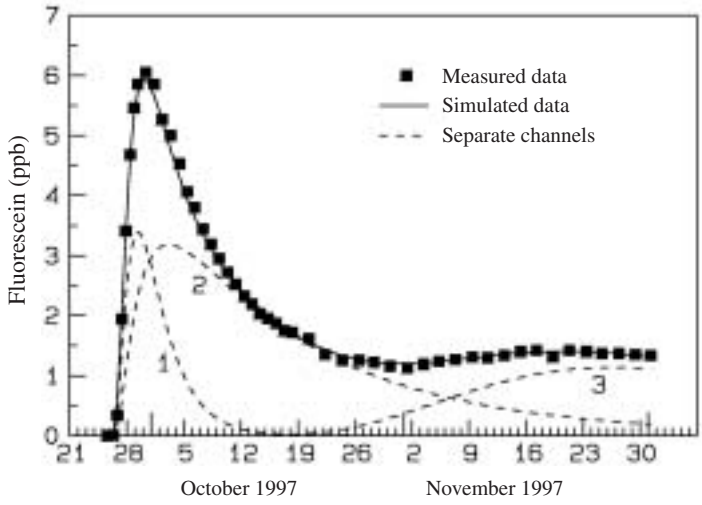

FIG. 177. Observed and simulated fluorescein recovery in well LN-12 at Laugaland during the first tracer test, involving injection into well LJ-08 and production from well LN-12.

single flow channel was required. The fluorescein background, which appears to be of the order of 50 ng/L, was subtracted from the data prior to the analysis. This background may be the remnants of an older tracer test. The results of the analysis yield a mean flow velocity of $u = 3.5 \times 10^{-5}$ m/s, which equals about

TABLE 28. MODEL PARAMETERS USED TO SIMULATE FLUORESCEIN RECOVERY FOR THE WELL PAIR LJ-08 AND LN-12 AT LAUGALAND

Channel length, x (m)	u (m/s)	$A\phi$ (m^2)	α_L (m)	M_i/M (kg/kg)
300	7.3×10^4	0.098	61	0.0087
500	4.8×10^4	0.53	264	0.0304
1000	1.7×10^4	1.08	62	0.0229
Total				0.0620

Note: The parameter u denotes the mean flow velocity, A the cross-sectional area, ϕ the porosity and α_L the longitudinal dispersivity of the flow channel. The variable M_i denotes the calculated mass recovery of tracer through the corresponding channel i, until infinite time, while M denotes the total mass of tracer injected.

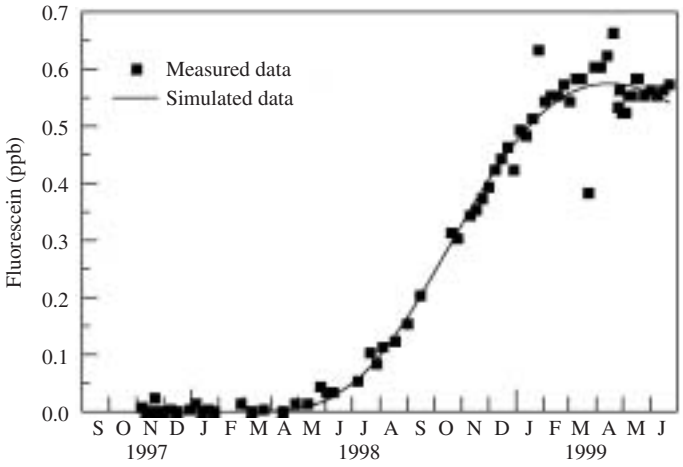

FIG. 178. Observed and simulated fluorescein recovery in well TN-04 at Ytri-Tjarnir, 1.8 km north of Laugaland.

90 m/month, a flow channel cross-sectional area of A = 360 m^2 (assuming a porosity of ϕ = 7%) and a dispersivity of α_L = 97 m. In addition the calculated relative mass recovery of the fluorescein through this flow channel, until infinite time, M_i/M, equals 7.2%.

This is quite an interesting result. Firstly, because it confirms a direct connection between Laugaland and Ytri-Tjarnir, which previously had been ruled out. Secondly, because it provides some quantitative information on this connection. The connection appears to be direct because of relatively low dispersivity (compared with the 1800 m distance between the fields) and small flow channel volume. On the one hand, if the flow channel is assumed to be along an interbed or a fracture zone of a few metres thickness, then its average width, or height, is of the order of 100 m. On the other hand, if the flow channel is more like a pipe, then its diameter would be of the order of only 20 m.

The purpose of the tracer tests at Laugaland was to try to quantify the danger of premature thermal breakthrough and rapid cooling of production wells at Laugaland during injection. The results of the interpretation of the tracer return data were, therefore, used to predict the temperature decline of the production wells, during long term injection into well LJ-08, for a few different injection scenarios. These are cases of 10, 15 and 20 L/s average yearly injections. Some short term variations in injection rate are, of course, expected but are discounted in the calculations. According to the estimated long term benefit from injection, these cases should result in increases in the potential production from the field of about 7, 10 and 13 L/s, respectively. Only cooling

by transport mode (a) is considered at this stage, and the software used in calculating the predictions is TRCOOL. These calculations are based on the same flow channel model as the tracer test analysis and the results in Table 28.

The cooling of the water travelling through the flow channels, or more correctly the heating of this water, depends on the surface area of the channels rather than their volume, as already discussed. Therefore, some assumptions must be made about the geometry of the channels. Here, the geometry that results in the most conservative predictions was selected, i.e. the geometry with the smallest surface area for a given flow path volume. This is the case where the width and height of the flow channel are equal. Figure 179 presents the results of the calculations for well LN-12, assuming an average production of 40 L/s for the well.

These predictions indicate that the temperature of the water pumped from well LN-12 will decline between 1 and 2ºC in 30 years, depending on the rate of injection. It is likely that an average injection rate of 15 L/s can be maintained, which will cause a temperature decline of only 1.5ºC for well LN-12.

Since the cooling predictions indicated that some cooling would take place already during the first two years of injection, the possibility arose to compare predicted and observed cooling directly. Unfortunately, some measurement discrepancies and other variations mask possible minor changes

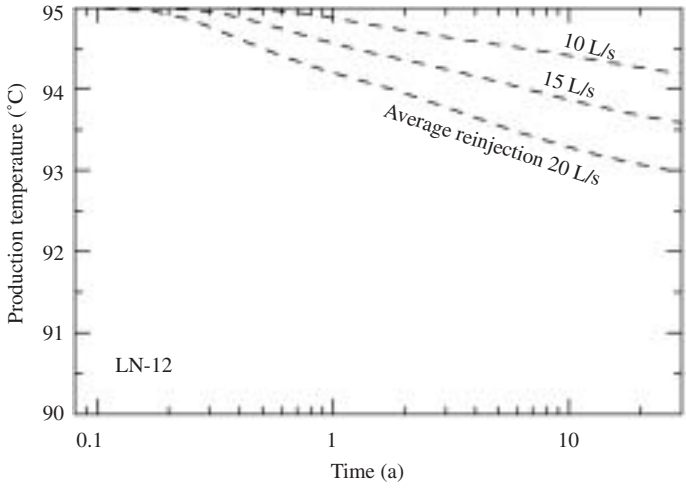

FIG. 179. Estimated decline in the temperature of well LN-12 for three cases of average long term injection into well LJ-08, due to flow through the three channels simulated in Fig. 177.

in the temperature of the production wells at Laugaland due to the injection. However, it can be stated that two years of injection at Laugaland did not cause a temperature decline greater than about 0.5°C. This is, in fact, less than the predicted temperature decline for well LN-12 presented in Fig. 179 (0.7°C in two years).

To estimate the increase in energy production enabled through long term injection into well LJ-08, the possible increase in mass extraction estimated and the predicted temperature changes are simply combined. The final result is presented in Fig. 180, which shows the estimated cumulative additional energy production for well LN-12 during the whole 30 year period being considered. It is considered likely that an average long term injection rate of about 15 L/s can be maintained at Laugaland. The maximum rate will be 21 L/s during the wintertime, when the return water supply is sufficient. During the summertime, the injection rate may, however, decrease to 10 L/s. Therefore, the above results indicate that future injection will enable an increase in energy production amounting to roughly 2 GW(th)·h/month or 24 GW(th)·h/a. This may be compared with the average yearly energy production from Laugaland during the last ten years, which has amounted to about 100 GW(th)·h/a. For this injection/production scenario the cumulative energy production, during the 30 year period considered, could reach more than 700 GW(th)·h. These results provide the basis for an analysis of the economics of future water injection at Laugaland.

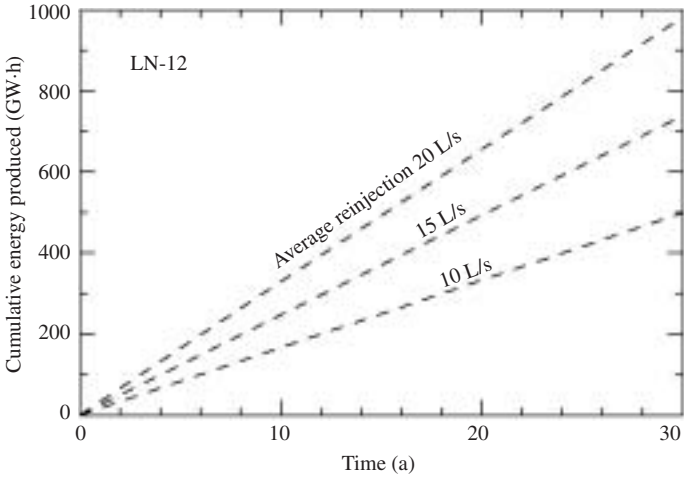

FIG. 180. Estimated cumulative increase in energy production for 30 years of injection into well LJ-08 calculated for three cases of average injection and assuming production from well LN-12.

REFERENCES

[1] FOOD AND AGRICULTURE ORGANIZATION OF THE UNITED NATIONS, INTERNATIONAL ATOMIC ENERGY AGENCY, INTERNATIONAL LABOUR ORGANISATION, OECD NUCLEAR ENERGY AGENCY, PAN AMERICAN HEALTH ORGANIZATION, WORLD HEALTH ORGANIZATION, International Basic Safety Standards for Protection against Ionizing Radiation and for the Safety of Radiation Sources, Safety Series No. 115, IAEA, Vienna (1996).

[2] INTERNATIONAL ATOMIC ENERGY AGENCY, Radiation Protection and the Safety of Radiation Sources, Safety Series No. 120, IAEA, Vienna (1996).

[3] INTERNATIONAL ATOMIC ENERGY AGENCY, Occupational Radiation Protection, Safety Standards Series No. RS-G-1.1, IAEA, Vienna (1999).

[4] INTERNATIONAL ATOMIC ENERGY AGENCY, Training in Radiation Protection and the Safe Use of Radiation Sources, Safety Reports Series No. 20, IAEA, Vienna (2001).

[5] INTERNATIONAL ATOMIC ENERGY AGENCY, Legal and Governmental Infrastructure for Nuclear, Radiation, Radioactive Waste and Transport Safety, Safety Standards Series No. GS-R-1, IAEA, Vienna (2000).

[6] INTERNATIONAL ATOMIC ENERGY AGENCY, Safety Assessment Plans for Authorization and Inspection of Radiation Sources, IAEA-TECDOC-1113, Vienna (1999).

[7] INTERNATIONAL ATOMIC ENERGY AGENCY, Regulations for the Safe Transport of Radioactive Material, Safety Standards Series No. TS-R-1 (ST-1, Rev.), IAEA, Vienna (2000).

[8] INTERNATIONAL ATOMIC ENERGY AGENCY, Preparedness and Response for a Nuclear or Radiological Emergency, Safety Standards Series No. GS-R-2, IAEA, Vienna (2002).

[9] INTERNATIONAL ATOMIC ENERGY AGENCY, Method for the Development of Emergency Response Preparedness for Nuclear and Radiological Accidents, IAEA-TECDOC-953, Vienna (1997).

[10] INTERNATIONAL ATOMIC ENERGY AGENCY, Guidebook on Radioisotope Tracers in Industry, Technical Reports Series No. 316, IAEA, Vienna (1990).

[11] LEVENSPIEL, O., Chemical Reaction Engineering, Wiley, New York (1972).

[12] VILLERMAUX, J., Génie de la réaction chimique, Tec. et Doc. Lavoisier, Paris (1993).

[13] CHARLTON, J.S., Radioisotope Techniques for Problem Solving in Industrial Process Plants, Leonard Hill (1986).

[14] KNOLL, G.F., Radiation Detection and Measurement, 2nd edn, Wiley, New York (1989).

[15] THYN, J., et al., Analysis and Diagnostics of Industrial Processes by Radiotracers and Radioisotope Sealed Sources, Vydavatelstvi CVUT, Prague (2000).

[16] THYN, J., Residence Time Distribution Software Analysis User's Manual, Computer Manual Series No. 11, IAEA, Vienna (1996).

[17] PROGEPI/SYSMATEC, Software DTSPro, V.4.2, Instruction Manual, PROGEPI/SYSTEMAC, Nancy (2000).
[18] TOLA, F., Logiciels d'aide à la conception et à l'interprétation de mesures basées sur la détection d'un rayonnement β, γ ou X, Rep. DAMRI/SAR/S/96-123/T41, Commisariat à l'energie atomique, Grenoble (1996).
[19] DANCKWERTS, P.V., Continuous flow systems, Chem. Eng. Sci. **2** (1953) 1.
[20] ASSOCIATION FRANÇAISE DE NORMALISATION, Mesure de débit de l'eau dans les conduites fermées — Méthodes par traceurs, Rep. ENF X10-131, AFNOR, Paris (1983).
[21] BIRD, R.B., STEWART, W.E., LIGHTFOOT, E.N., Transport Phenomena, Wiley, New York (1960).
[22] BLET, V., BERNE, P., TOLA, F., VITART, X., CHAUSSY, C., Recent developments in radioactive tracer methodology, Appl. Radiat. Isot. **51** (1999) 615.
[23] MAGNAUD, J.P., Discrétisation des équations de Navier–Stokes par une méthode d'éléments finis, Institut national des sciences et techniques nucléaires, Grenoble (1996).
[24] BLET, V., BERNE, P., LEGOUPIL, S., VITART, X., Radioactive tracing as aid for diagnosing chemical reactors, Oil Gas Sci. Technol. **55** 2 (2000) 171.
[25] TAYLOR, G.I., The dispersion of matter in turbulent flow through a pipe, Philos. R. Soc. Lond. A **223** (1954) 446.
[26] AISN SOFTWARE Inc., Peakfit, Peak Separation and Analysis Software, AISN, Framingham, MA (1995).
[27] WOLFRAM, S., Mathematica, A System for Doing Mathematics by Computer, Addison-Wesley, Reading, MA (1991).
[28] THE MATHWORKS, MATLAB, The Language of Technical Computing, The Mathworks, Natick, MA (2000).
[29] GROCOTT, S.C., McGUINESS, L., "Residence time distribution in Bayer process vessels — Development of a suitable liquor tracer", Light Metals 1990, Canadian Inst. of Mining, Metallurgy and Petroleum, Montreal (1990) 95.
[30] PRESS, W.H., TEUKOLSKY, S.A., VETTERLING, W.T., FLANNERY, B.P., Numerical Recipes in FORTRAN — The Art of Scientific Programming, 2nd edn, Cambridge University Press, Cambridge (1992).
[31] KREFT, A., ZUBER, A., On the physical meaning of the dispersion equation and its solutions for different initial and boundary conditions, Chem. Eng. Sci. **33** (1978) 1471.
[32] SCHWEICH, D., "Transport of linearly reactive solutes in porous media: Basic models and concepts", Migration and Fate of Pollutants in Soils and Subsoils, NATO ASI Series G: Ecological Sciences, Vol. 32, Springer-Verlag, Berlin (1992) 221.
[33] JONSSEN, J.A., Chromatographic Theory and Basic Principles, Dekker, New York (1987).

[34] CHARPENTIER, J.C., MIDOUX, N., Distributions des temps de Séjour dans la phase gazeuse d'un contacteur gaz–liquide, 2ème partie: Application à une colonne à garnissage arrosé fonctionnant à contre-courant, Chi. Ind., Génie Chim. **104** (1971) 1563.
[35] ANVARIPOUR, B., ASHTON, N., ARROWSMITH, A., "Effect of co-solute on VOC-gas stripping in packed columns", Chemical Engineering (Proc. 1st Eur. Congr. Florence, 1997), AIDIC Conf. Series, Vol. 2, Milan (1997) 1371.
[36] HORNER, G.V., "Development and test results of a new random tower packing in metal and plastic", ibid., p. 1341.
[37] BRUNAZZI, E., PAGLIANTI, A., PETARCA, L., Design of absorption columns equipped with structured packings, Chim. Ind. **78** (1996) 459.
[38] SHAH, Y.T., STIEGEL, G.J., SHARMA, M.M., Backmixing in gas–liquid reactors, AIChE J. **24** 3 (1978) 369.
[39] SCHÜGERL, K., LÜBBERT, A., KORTE, T., DIEKMANN, J., Measuring techniques for characterizing gas/liquid reactors, Int. Chem. Eng. **27** (1987) 583.
[40] THYN, J., PECHLAK, B., HOVORKA, J., SVARC, Z., Dynamic characteristics of a system of packed absorption columns, Radioisot. **22** (1981) 1.
[41] TOYE, D., MARCHOT, P., CRINE, M., L'HOMME, G., Modeling of multiphase flow in packed beds by computer assisted tomography, Meas. Sci. Technol. **7** (1996) 436.
[42] KUMAR, S.B., MOSLEMIAN, D., DUDUKOVIC, M.P., Gas holdup measurements in bubble columns using computed tomography, AIChE J. **43** (1997) 1414.
[43] DE LEYE, D., FROMENT, G.L., A rigorous simulation and design of columns for gas absorption and chemical reaction — I. Packed columns, Comput. Chem. Eng. **10** (1986) 493–504.
[44] VILLERMAUX, J., Génie de la réaction chimique, Tec. & Doc. Lavoisier, Paris (1982).
[45] VAN SWAAIJ, W.P.M., CHARPENTIER, J.C., VILLERMAUX, J., Residence time distribution in the liquid phase of trickle flow in packed columns, Chem. Eng. Sci. **24** (1969) 1083.
[46] BRIENS, C.L., MARGARITIS, A., WILD, G., A new stochastic model and measurement errors in residence time distributions of multiphase reactors, Chem. Eng. Sci. **50** (1995) 279.
[47] FURZER, I.A., MICHELL, R.W., Liquid phase dispersion in packed beds with two phase flow, AIChE J. **16** (1970) 380.
[48] BLET, V., et al., "Application of radioactive tracers for the study of ventilation in industrial premises", paper presented at 1st Eur. Congr. on Chemical Engineering, Florence, 1997.
[49] DANCKWERTS, P.V., Continuous flow systems, Chem. Eng. Sci. **2** 1 (1953) 1.
[50] DESSAGNE, J.M., OLANDER, L., BONTHOUX, F., AUBERTIN, G., "Use of residence time distribution for evaluation of ventilation systems", paper presented at Ventilation '94, Stockholm, 1994.

[51] OLANDER, L., DESSAGNE, J.M., BONTHOUX, F., LECLERC, J.P., A study of general ventilation and local exhaust ventilation in industrial premises using residence time distribution theory, Environ. Prog. **14** 3 (1995) 159.
[52] LABORDE, J.C., LAQUERBE, C., FLOQUET, P., PIBOULEAU, L., DOMENECH, S., "Simulation of air flow distribution in rooms by a systemic approach", paper presented at Ventilation '97, Ottawa, 1997.
[53] NIELSEN, P.V., "Air distribution in rooms — Research and design methods", paper presented at Roomvent '94, Cracow, 1994.
[54] VILLAND, M., TRIO-VF — Notice d'utilisation, Rep. STR/LMTL/96-49, Commissariat à l'energie atomique, Grenoble (1996).
[55] ESPI, E., BERNE, P., DUVERNEUIL, P., "Using CFD to understand the air circulation in a ventilated room", paper presented at Eur. Symp. on Computer Aided Process Engineering, Bruges, 1998.
[56] LeCLERC, J.P., DETREZ, C., BERNARD, A., SCHWEICH, D., DTS: Un logiciel d'aide à l'élaboration de modèles d'écoulement dans les réacteurs, Rev. l'Inst. Fr. Pét. **50** 5 (1995) 641.
[57] THERESKA, J., Research and development in radiotracer methodology and technology, Récents progrès en genie des procédés, No. 79, 15 (2001) 335.
[58] THERESKA, J., LeCLERC, J.P., PLASARI, E., VILLERMAUX, J., Tracer experiments and residence-time distributions in the analyses of industrial units: Case studies, Nukleonika **44** 1 (1999) 39–58.
[59] THYN, J., BURDYCH, J., BLAHA, L., ŽITNÝ, R., "Radiotracer applications in wastewater treatment", Applications of Isotopes and Radiation in Conservation of the Environment (Proc. Int. Symp. Karlsruhe, 1992), International Atomic Energy Agency, Vienna (1992) 239.
[60] JI, Z., McCORQUODALE, J.A., ZHOU, S., VITASOVIC, Z., A dynamic solids inventory model for activated sludge systems, Water Environ. Res. **68** (1996) 329–337.
[61] BERNE, P., BLET, V., "Correcting the results of radioactive tracer experiments for the effects of the detection chain", paper presented at Int. Congr. on Tracers and Tracing Methods, Nancy, 2001.
[62] LUX, I., KNOBLINGER, K., Monte Carlo Particle Transport Methods: Neutrons and Photons, CRC Press, Boca Raton, FL (1991).
[63] BLET, V., BERNE, P., CHAUSSY, C., PERRIN, S., SCHWEICH, D., Characterization of a packed column using radioactive tracers, Chem. Eng. Sci. **54** (1999) 91.
[64] LEGOUPIL, S., Tomographie d'émission gamma à partir d'un nombre limité de détecteurs, appliquée à la visualisation d'écoulements, PhD Thesis, University of Caen (1997).
[65] BERNE, P., BLET, V., LEGOUPIL, S., NARP, F., BANDELIER, P., "An attempt at dual-ring SPECT tomography on a packed column", paper presented at Int. Congr. on Tracers and Tracing Methods, Nancy, 2001.
[66] WATKINS, J.W., MARDOCK, E.S., Use of radioactive iodine as a tracer in water-flooding operations, J. Petrol. Technol. **6** 9 (1954) 117–124.

[67] FLAGG, A.H., MYERS, J.P., CAMPBELL, J.L.P., TERRY, J.M., MARDOCK, E.S., Radioactive tracers in oil production problems, J. Petrol. Technol. **7** (1955) 1.
[68] BIRD, J.M., DEMSEY, J.C., How you can follow your flood?, World Oil **143** (1956) 152.
[69] FEARON, R.E., Tritium — Newest tool for tracing reservoir flow, World Oil **145** (1957) 114.
[70] BJØRNSTAD, T., Selection of Tracers for Oil and Gas Reservoir Evaluation, Rep. IFE/KR/E-91/009, Institute for Energy Technology, Kjeller (1991) 43.
[71] ZEMEL, B., Tracers in the Oil Field, Developments in Petroleum Science, Vol. 43, Elsevier Science, Amsterdam (1995).
[72] BJØRNSTAD, T., HAUGEN, O.B., HUNDERE, I.A., Dynamic behavior of radiolabelled water tracer candidates for chalk reservoirs, J. Pet. Sci. Eng. **10** (1994) 223–238.
[73] WOOD, K.N., LAI, F.S., HEACOCK, D.W., Water Tracing Enhances Miscible Pilot, Rep. SPE-19642, Society of Petroleum Engineers, Richardson, TX (1989).
[74] INTERNATIONAL ATOMIC ENERGY AGENCY, Isotope Techniques in the Hydrogeological Assessment of Potential Sites for the Disposal of High-level Radioactive Wastes, Technical Reports Series No. 228, IAEA, Vienna (1983).
[75] BJØRNSTAD, T., MICHELSEN, O.B., ERIKSEN, D.Ø., Safe Application of Radiolabelled Cobalt Hexacyanides as Water Tracers in Oil Reservoirs, Rep. IFE/KR/F-97/037, Institute for Energy Technology, Kjeller (1997) 64 pp.
[76] SYLTE, J.E., HALLENBECK, L.D., THOMAS, L.K., Ekofisk Formation Pilot Waterflood, Rep. SPE-18276, Society of Petroleum Engineers, Richardson, TX (1990).
[77] BJØRNSTAD, T., BØE, E., CARLSEN, H.P., COSGRIFF, T., HAUGERUD, O.S., "Bottomhole tracer injection and sampling", Tracers (Proc. 2nd Workshop Austin, 1994), (BJØRNSTAD, T., POPE, G., Eds), University of Texas at Austin (1994) 147–150.
[78] BJØRNSTAD, T., BRENDSDAHL, E., MICHELSEN, O.B., ROGDE, S.A., Analysis of radiolabelled thiocyanate tracer in oil field brines, Nucl. Instrum. Meth. Phys. Res. A **299** (1990) 629–633.
[79] BJØRNSTAD, T., ROGDE, S.A., An improved gamma spectrometric method for trace analysis of ^{22}Na, Nucl. Instrum. Meth. Phys. Res. A **299** (1990) 634–641.
[80] ABBASZADEH, M., BRIGHAM, W.E., Analysis of well-to-well tracer flow to determine reservoir layering, J. Pet. Technol. **36** (1984) 1753–1762.
[81] ALLISON, S.B., POPE, G.A., SEPEHRNOORI, K., Analysis of field tracers for reservoir description, J. Pet. Sci. Eng. **5** (1991) 173–186.
[82] SOMARUGA, C., Interpretación de Ensayos de Trazadores en Medios Porosos Petroleros, Universidad Nacional del Comahue, Neuquén, Argentina.
[83] SAGEN, J., et al., Reservoir Chemical-Thermal Simulation with Tracers, Rep. SPE-36921, Society of Petroleum Engineers, Richardson, TX (1996).

[84] NAJURIETA, H.L., MAGGIO, G.E., "Empleo de radiotrazadores en la evaluación hidrodinámica de un yacimiento de petróleo viscoso", Exploración y Desarrollo de Hidrocarburos (Proc. 4th Congr. Mar del Plata, 1999), Instituto Argentino del Petróleo y Gas, Buenos Aires (1999).
[85] HUTTRER, G.W., The status of world geothermal power generation 1995–2000, Geothermics **30** 1 (2001) 1.
[86] EINARSSON, S.E., VIDES, A.R., CUELLAR, G., "Disposal of geothermal waste water by reinjection", paper presented at 2nd UN Symp. on Developing Geothermal Resources, San Francisco, CA, 1975.
[87] GULATI, M.S., LIPMAN, S.C., STROBEL, C.J., Tritium tracer survey at The Geysers, Trans. Geothermal Resources Council **2** (1978) 237.
[88] McCABE, W.J., BARRY, B.J., MANNING, M.R., 'Radioactive tracers in geothermal underground water flow studies', Geothermics **12** 2–3 (1983) 83.
[89] VETTER, O.J., ZINNOW, K.P., Evaluation of Well-to-Well Tracers for Geothermal Reservoirs, Rep. LBL-11500, National Technical Information Service, Springfield, VA (1981).
[90] KLEYN, L.E., Vessel for collecting subsurface water samples from geothermal drillholes, Geothermics **2** (1973) 57.
[91] BARRY, B.J., Analysis of Xenon for Geothermal Vapour Phase Tracing, Rep. INS-R-434, Institute of Geological and Nuclear Sciences, Lower Hutt, New Zealand (1990).
[92] McCABE, W.J., BARRY, B.J., BAKER, D.B., Analysis of Geothermal Water Samples for Radioactive Iodide Tracer, Rep. 98/15, Institute of Geological and Nuclear Sciences, Lower Hutt, New Zealand (1998).
[93] OUTTERIDGE, K.D., The Statistics of the Adjustment and Comparison of Counters, Rep. AERE 1/M 32, United Kingdom Atomic Energy Authority, Harwell (1954).
[94] BEVINGTON, P.R., ROBINSON, D.K., Data Reduction and Error Analysis for the Physical Sciences, McGraw-Hill, New York (1992).
[95] STEFANSSON, V., Geothermal injection experience, Geothermics **26** (1997) 99–130.
[96] AXELSSON, G., GUNNLAUGSSON, E., "Long term monitoring of high- and low-enthalpy fields under exploitation", World Geothermal Congress (Proc. Congr. Kokonoe, 2000), International Geothermal Association, Pisa (2000) 226.
[97] PRUESS, K., BODVARSSON, G., Thermal effects of injection in geothermal reservoirs with major vertical fractures, J. Pet. Technol. **36** (1984) 1567–1578.
[98] HORNE, R.N., Reservoir engineering aspects of injection, Geothermics **14** (1985) 449–457.
[99] SVERRISDOTTIR, G., HAUKSDOTTIR, S., AXELSSON, G., ARNASON, A., "Chemical monitoring during injection in the Laugaland geothermal system, N-Iceland", Geochemistry of the Earth's Surface (Proc. 5th Int. Symp. Reykjavik, 1999), Balkema, Rotterdam (1999) 547–550.

[100] UNITED NATIONS UNIVERSITY, Geothermal Training Programme, ICEBOX, 2nd edn (ARASON, T., BJORNSSON, G., compilers), Reykjavik (1994) 66 pp.
[101] BEAR, J., TSANG, C.F., DE MARSILY, G. (Eds), Flow and Contaminant Transport in Fractured Rock, Academic Press, New York (1993) 560 pp.
[102] JAVANDEL, I., DOUGHTY, C., TSANG, C.F., Groundwater Transport — Handbook of Mathematical Models, Water Resources Monograph Series No. 10, American Geophysical Union, Washington, DC (1984) 228 pp.
[103] BJORNSSON, G., AXELSSON, G., FLÓVENZ, Ó.G., "Feasibility study for the Thelamork low-temperature system in N-Iceland", Geothermal Reservoir Engineering (Proc. 19th Workshop Stanford, 1994), Stanford University, CA (1994) 5–13.
[104] AXELSSON, G., BJORNSSON, G., FLOVENZ, O.G., KRISTMANNSDOTTIR, H., SVERRISDOTTIR, G., "Injection experiments in low-temperature geothermal areas in Iceland", World Geothermal Congress (Proc. Congr. Florence, 1995), International Geothermal Association, Pisa (1995) 1991–1996.
[105] HORNE, R.N., "Uncertainty in forecasting breakthrough of fluid transported through fractures", Geostatistical, Sensitivity and Uncertainty Methods for Groundwater Flow and Radionuclide Transport Modeling (Proc. Conf. 1987), Batelle Press, Columbus, OH (1989) 261–274.
[106] HORNE, R.N., RODRIGUEZ, F., Dispersion in tracer flow in fractured geothermal systems, Geophys. Res. Lett. **10** (1983) 289–292.
[107] ROBINSON, B.A., TESTER, J.W., Dispersed fluid flow in fractured reservoirs: An analysis of tracer-determined residence time distributions, J. Geophys. Res. **89** (1984) 1037–1038.
[108] GRISAK, G.E., PICKENS, J.F., Solute transport through fractured media: The effect of matrix diffusion, Water Resour. Res. **16** (1980) 719–730.
[109] NERETNIEKS, I., A note on fracture flow mechanisms in the ground, Water Resour. Res. **19** (1983) 364–370.
[110] CARSLAW, H.W., JAEGER, J.C., Conduction of Heat in Solids, 2nd edn, Claredon Press, Oxford (1959) 403 pp.
[111] BODVARSSON, G., Thermal problems in the siting of injection wells, Geothermics **1** (1972) 63–66.
[112] DELFIN, F.G., Jr., BARRY, B., DACILLO, D.B., MARCELO, E.A., "Analysis and interpretation of ^{125}I tracer test results", paper presented at IAEA Co-ordination Mtg on Isotopic and Geochemical Techniques in Geothermal Exploration and Reservoir Management, Leyte, Philippines, 2001.
[113] MALATE, R.C.M., O'SULLIVAN, M.J., Modelling of chemical and thermal changes in well PN-26 Palinpinon geothermal field, Philippines, Geothermics **20** (1991) 291–318.
[114] AXELSSON, G., et al., "Thermal energy extraction by injection from the Laugaland geothermal system in N-Iceland", World Geothermal Congress (Proc. Congr. Kokonoe, 2000), International Geothermal Association, Pisa (2000) 3027–3032.

[115] AXELSSON, G., FLOVENZ, O.G., HAUKSDOTTIR, S., HJARTARSON, A., LIU, J., Analysis of tracer test data, and injection-induced cooling, in the Laugaland geothermal field, N-Iceland, Geothermics **30** (2001) 697–725.
[116] QUIJANO, J.E., A Revised Conceptual Model and Analysis of Production Data for the Ahuachapan–Chipilapa Geothermal Field in El Salvador, Rep. 1994-10, UNU Geothermal Training Programme, Reykjavik (1994) 30.

BIBLIOGRAPHY

ADAMS, M.C., et al. Hydrofluorocarbons as geothermal vapor-phase tracers, Geothermics **30** (2001) 747–775.

ADAMS, M.C., DAVIS, J., Kinetics of fluorescein decay and its application as a geothermal tracer, Geothermics **20** 1/2 (1991) 53–66.

AXELSSON, G., STEFANSSON, V., "Injection and geothermal reservoir management — Associated benefits", paper presented at Int. Workshop on Direct Use of Geothermal Energy, Ljubljana, 1999.

CHARLTON, J.S., Radioisotope Techniques for Problem Solving in Industrial Process Plants, Leonard Hill (1986).

D'HOOGE, J.A., SHEEL, C.Q., WILLIAMS, B.J., Interwell Radioactive Tracers — An Effective Reservoir Evaluation Tool: West Sumatra Field Results, Rep. SPE-8434, Society of Petroleum Engineers, Richardson, TX (1979).

GÓMEZ, H.R., MAGGIO, G.E., Aportes de los trazadores radiactivos e indicadores isotópicos a la industria petrolera, YPF — Boletín de Informaciones Petroleras **12** (1996) 47.

GÓMEZ, H.R., MAGGIO, G.E., BARÓ, G.B., Hacia una mayor eficiencia en la recuperación secundaria de petróleo, Petrotecnia **37** 2 (1996).

HUTCHINS, R.D., DOVAN, H.T., SANDFORD, B.B., Aqueous Tracers for Oilfield Applications, Rep. SPE-21049, Society of Petroleum Engineers, Richardson, TX (1991).

INTERNATIONAL ATOMIC ENERGY AGENCY, Guidebook on Radioisotope Tracers in Industry, Technical Reports Series No. 316, IAEA, Vienna (1990).

LEVENSPIEL, O., Chemical Reaction Engineering, Wiley, New York (1972).

LICHTENBERGER, G.J., Field Applications of Interwell Tracers for Reservoir Characterization of Enhanced Oil Recovery Pilot Areas, Rep. SPE-21652, Society of Petroleum Engineers, Richardson, TX (1991).

McCABE, W.J., BARRY, B.J., BAKER, D.B., Analysis of Geothermal Water Samples for Radioactive Iodide Tracer, Rep. 98/15, Institute of Geological and Nuclear Sciences Ltd, Lower Hutt, New Zealand (1998).

McCABE, W.J., BARRY, B.J., MANNING, M.R., Radioactive tracers in geothermal underground water flow studies, Geothermics **12** (1983) 83–110.

OUTTERIDGE, K.D., The Statistics of the Adjustment and Comparison of Counters, Rep. AERE 1/M 32, United Kingdom Atomic Energy Authority, Harwell (1954).

ROSE, P.E., APPERSON, K.D., JOHNSON, S., ADAMS, M.C., "Numerical simulation of a tracer test at Dixie Valley, Nevada", paper presented at 22nd Workshop on Geothermal Reservoir Engineering, Stanford, CA, 1997.

ROSE, P.E., BENOIT, W.R., KILBOURN, P.M., The application of the polyaromatic sulfonates as tracers in geothermal reservoirs, Geothermics **30** (2001) 617–640.

ROSE, P.E., BENOIT, D., LEE, S.G., TANDIA, B., KILBOURN, P., "Testing the naphthalene sulfonates as geothermal tracers at Dixie Valley, Ohaaki and Awibengkok", paper presented at 25th Workshop on Geothermal Reservoir Engineering, Stanford, CA, 2000.

ROSE, P.E., GORANSON, C., SALLS, D., KILBOURN, P., "Tracer testing at Steamboat Hills, Nevada using fluorescein and 1,5-naphthalene disulfonate", paper presented at 24th Workshop on Geothermal Reservoir Engineering, Stanford, CA, 1999.

SMART, P.L., LAIDLAW, I.M.S., An evaluation of some fluorescent dyes for water tracing, Water Resour. Res. **13** 1 (1977) 15–33.

THYN, J., et al., Analysis and Diagnostics of Industrial Processes by Radiotracers and Radioisotope Sealed Sources, Vydavatelstvi CVUT, Prague (2000).

VETTER, O.J., ZINNOW, K.P., Evaluation of Well-to-Well Tracers for Geothermal Reservoirs, Rep. LBL-11500, National Technical Information Service, Springfield, VA (1981).

VILLERMAUX, J., Génie de la réaction chimique, Tec. et Doc. Lavoisier, Paris (1993).

WAGNER, O.R., BAKER, L.E., SCOTT, G.R., The Design and Implementation of Multiple Tracer Programs for Multifluid, Multiwell Injection Projects, Rep. SPE-5125, Society of Petroleum Engineers, Richardson, TX (1974).

CONTRIBUTORS TO DRAFTING AND REVIEW

Axelsson, G.	National Energy Authority of Iceland, Iceland
Barry, B.J.	Institute of Geological and Nuclear Sciences, New Zealand
Berne, P.	Commissariat à l'énergie atomique, Centre d'études nucléaires de Grenoble, France
Bjørnstad, T.	Institute for Energy Technology, Norway
Cameron, R.	International Atomic Energy Agency
Charlton, S.	Synetix, Australia
Maggio, G.E.	NOLDOR S.R.L., Argentina
Pang, Z.	International Atomic Energy Agency
Thereska, J.	International Atomic Energy Agency
Vitart, X.	Commissariat à l'énergie atomique, France